

EVIDENCE FOR EARLY-PHASE EXPLOSIVE BASALTIC VOLCANISM AT MT.  
MORNING FROM GLASS-RICH SEDIMENTS IN THE ANDRILL AND-2A CORE AND  
POSSIBLE RESPONSE TO GLACIAL CYCLICITY

Roseanne E. Nyland

A Thesis

Submitted to the Graduate College of Bowling Green  
State University in partial fulfillment of  
the requirements for the degree of

MASTER OF SCIENCE

August 2011

Committee:

Kurt Panter, Advisor

John Farver

Jeffrey Snyder

## ABSTRACT

Kurt Panter, Advisor

Sediments recovered between ~354 and 765 mbsf (~15.9-18.4 Ma) in the ANDRILL AND-2A core contain dispersed accumulations of volcanic glass up to 50% by volume and are used to investigate the petrological evolution and influence of glaciations on volcanism in the McMurdo Sound region of Antarctica. Glass-rich sediments include muddy-to-fine sandstone and stratified diamictite. The glass varies in color, size, vesicularity, crystal content, angularity, and from fresh to moderately altered. Fresh glass with delicate cuspatate forms suggests they were introduced into the basin as ash fall with minimal reworking. Altered glass has low total oxides (< 97 wt.%), low Ca/K ratios (< 2), high Alteration Index (> 40), and are typically more evolved than fresh glass. Pristine basaltic glasses (MgO 3-7 wt.%) are ne-normative (5-30 wt.%) and have restricted average SiO<sub>2</sub> content ( $45.2 \pm 0.8$  wt.%). Overall the glass composition shows an increase in SiO<sub>2</sub> content up-section. Fractional crystallization models indicate differentiation controlled by plagioclase, olivine, clinopyroxene and magnetite ± amphibole and apatite. Trace element concentrations are typical for Erebus Volcanic Province (EVP) volcanism. The data extends known composition of Mount Morning (18.7-11.4 Ma), the only known EVP Early-Middle Miocene source, to a mafic end, revealing a previously unknown phase of explosive, strongly alkaline, basaltic activity. The glass-rich sediments are part of larger sequences that record numerous glacial advances and retreats in the region. Sediments with high glass contents correspond to ice minimums and, geochemically, Ba/LREE ratios correlate to intervals of ice expansion (decreasing values) and contraction (increasing values) at multiple depths. Higher

Ba/LREE may indicate tapping of more volatile-rich magmas. Within a single glacimarine cycle, glass angularity, vesicularity and composition also vary systematically. A model is supported where ice loading and unloading affects the stress state of the crust around a shallow (< 5 km) magma system. During peak glacial periods, the propagation of magma filled fractures is suppressed and volatiles accumulate in response to the fractionation of anhydrous minerals and/or recharge by volatile-rich magmas. Changing stress states during deglaciation allows the volatile enriched magmas to then rise and vesiculate at shallower depths promoting explosive eruptions.

## ACKNOWLEDGMENTS

I would like to recognize several people who have helped me to complete this project. First, I owe many thanks to Kurt Panter, my advisor and friend, for his continuous unfaltering support of this project over the past two years. Without his guidance, patience, encouragement and willingness to always lend an ear, the completion of this project would not have been possible. Thank you for all of your help! I extend my thanks to committee members John Farver and Jeffrey Snyder for their input and help with this project as well.

I would also like to thank Gianfranco Di Vincenzo, Paola Del Carlo, Sergio Rocchi and Massimo Tiepolo for their guidance while working on this project in Italy.

Also, I would like to thank the BGSU Geology Department as a whole. This includes Pat Wilhelm and Bill Butcher for always being willing to help and answer my many questions. I especially want to thank my officemates as well for providing me with some much needed comic relief over the past year!

Finally, I owe very many thanks to my family, close friends and loved ones. I want to especially thank my parents Vivian and Gerald Nyland, my sister Kristina Nyland and my good friend Chris Coy. I have greatly appreciated all of your love and support as I pursue my educational and career goals. I would not have been able to complete this project without any of you. Thank you all!

This thesis was supported by the National Science Foundation under Cooperative Agreement No. 0342484, through sub-award 25-0550-0001-151 to Kurt Panter, BGSU, as part of the ANDRILL U.S. Science Support Program.

## TABLE OF CONTENTS

	Page
INTRODUCTION .....	1
GEOLOGIC BACKGROUND .....	5
AND-2A Core .....	10
METHODS .....	16
Sample Selection .....	16
Determining Physical Properties .....	17
Analytical Techniques .....	18
RESULTS .....	21
Physical Characteristics and Alteration .....	21
Geochemistry .....	29
<i>Major Elements</i> .....	29
<i>Trace and Rare Earth Elements</i> .....	36
DISCUSSION .....	44
Mode of Deposition .....	44
Volcanic Source .....	50
Geochemical Evolution .....	53
Feedback Between Volcanism and Glaciation .....	58
SUMMARY .....	70
REFERENCES .....	74
APPENDICES .....	93
Appendix A .....	93

Appendix B .....	94
Appendix C .....	107

## LIST OF FIGURES

Figure	Page
1 General map of Antarctica showing ANDRILL drillsites .....	3
2 Cross section of the Victoria Land Basin .....	6
3 Comparison plot of ages of Erebus Volcanic Province (EVP) volcanic centers .....	9
4 Depth versus age diagram for AND-2A .....	12
5 Images of representative lithofacies in AND-2A containing glass .....	13
6 ANDRILL SMS Idealized Sequence .....	15
7 Frequency histogram of zones of >15% glass within lithofacies .....	22
8 Photomicrographs of fresh glass grains .....	24
9 Photomicrographs of altered glass grains .....	25
10 TAS diagrams for AND-2A glass .....	26
11 Alteration Index versus Ca/K for AND-2A glass .....	27
12 AI-CCPI alteration box plots for AND-2A glass .....	28
13 Compositional variation diagrams with depth for AND-2A glass .....	34
14 Harker variation diagrams for AND-2A glass and EVP volcanics .....	35
15 TAS diagram for AND-2A glass and EVP volcanics .....	37
16 Zr versus Rb, Th, Y, La, Nb, Sc, Ni for AND-2A glass and EVP volcanics .....	38
17 REE and multi-element diagrams for AND-2A glass and EVP volcanics .....	41
18 Zr versus La <sub>N</sub> /Yb <sub>N</sub> , Eu/Eu*, Sr/Sr*, K/K*, and P/P* for AND-2A glass and EVP volcanics .....	42

19	Comparison plots of 740.89, 742.00, 763.52 and 764.44 with remaining AND-2A glass samples .....	43
20	Frequency histogram of relative rounding of AND-2A glass .....	45
21	Comparison frequency histograms of relative rounding of 740.89, 742.00, 763.52 and 764.44 with upper AND-2A glass samples .....	46
22	Sphericity comparison plots for AND-2A glass .....	47
23	Method of deposition cartoon .....	49
24	Fractional crystallization models for AND-2A glass .....	54
25	Percent volcanic glass versus depth for AND-2A .....	59
26	Ba/La and Ba/Ce versus depth for AND-2A glass .....	63
27	Sequence 32 diagrams .....	64
28	Ice loading and unloading model cartoon .....	69

## LIST OF TABLES

Table	Page
1      Uncertainties of chemical composition from LA-ICP-MS of a representative glass grain .....	20
2      Results from modified point counting for AND-2A glass samples .....	23
3      Representative major and trace elemental compositions for AND-2A glass .....	31

## INTRODUCTION

A better understanding of future global climate change and its effects on the planet and society comes from understanding changes in paleoclimate in the geologic past, as a much wider range of possible climatic behaviors existed in the past than in modern environments (Naish *et al.*, 2001; Shevenell, *et al.*, 2007; Naish *et al.*, 2009). The past climate in Antarctica, which has still not been studied extensively, was extremely different from today's "permanent" icehouse conditions, experiencing a dynamic environment with several fluctuations in climate, glacial advance and retreat, and sea-level change (Harwood *et al.*, 2009; Mackay *et al.*, 2009; Naish *et al.*, 2009; Warny *et al.*, 2009). Understanding how fast, large, and frequent these fluctuations occurred in the past will provide the opportunity to predict how global warming and climate change could affect the planet in the future. The investigation of glacimarine sediments and the volcanic materials within them, found in key Antarctic sedimentary basins have the potential to offer a wealth of information on this subject.

The ANtarctic DRILLing (ANDRILL) project is a multi-national project, developed along the western margin of the West Antarctic rift system bordering the Transantarctic Mountains. The purpose of this project is to collect and examine drill cores from sedimentary basins along the coast of Antarctica in order to build up stratigraphic data that record key events of the glacial and climate history, as well as volcanic and tectonic events in the region (Naish *et al.*, 2007; Harwood *et al.*, 2009). The sediment input into the marine depositional environment close to the Antarctic continent is directly affected by environmental changes in the terrestrial environment, making it an excellent location to use the stratigraphic record as a paleoclimate proxy (Naish *et al.*, 2007; Harwood *et al.*, 2009). So far, two cores have been drilled; the

McMurdo Ice Shelf (MIS) project (AND-1B core) in 2006 and the Southern McMurdo Sound (SMS) project (AND-2A core) in 2007 (Fig 1).

The AND-1B and AND-2A cores contain a significant volcanic component from the Cenozoic Erebus Volcanic Province (LeMasurier and Thomson, 1990). The Erebus Volcanic Province (EVP) consists of several large shield volcanoes and stratovolcanoes surrounding and within the Victoria Land Basin as well as large volcanic fields containing dozens of small cinder cones and their associated lavas (Fig. 1). The composition of most of the Erebus Volcanic Province deposits belong to the basanite-to-phonolite alkaline series (strongly silica-undersaturated), while much fewer deposits belong to the alkali basalt to trachyte alkaline series (moderately silica-undersaturated) or, in rare cases, peralkaline trachytes (silica-oversaturated) (Kyle, 1990; Kyle *et al.*, 1992; Cooper *et al.*, 2007; Del Carlo *et. al.*, 2009; Martin *et al.*, 2009). Volcaniclastic sediments, particularly primary pyroclastic layers, are essential in constraining the timing of volcanic, tectonic, and climatic events but can also be useful in many other ways, including paleocurrent and provenance determination. It is therefore important to examine these volcaniclastic sediments in detail in order to determine the source of the volcanic material and better understand the relationship of the area's volcanic activity and the dynamic climate of the Early - Middle Miocene.

Previous studies in Antarctica and around the world have suggested that climate and volcanism are intimately linked, and that climate changes, more specifically in regards to glacial unloading during a warming climate, may be a factor that can control the volume, explosiveness, and timing of volcanic activity. The relationship between rapid de-glaciation resulting from a rapidly warming climate and increased volcanism/explosiveness of eruptions has been suggested in Iceland (Slater *et al.*, 1998; Sigvaldason, 2002; Maclennan *et al.*, 2002; Stinton *et al.*, 2005),

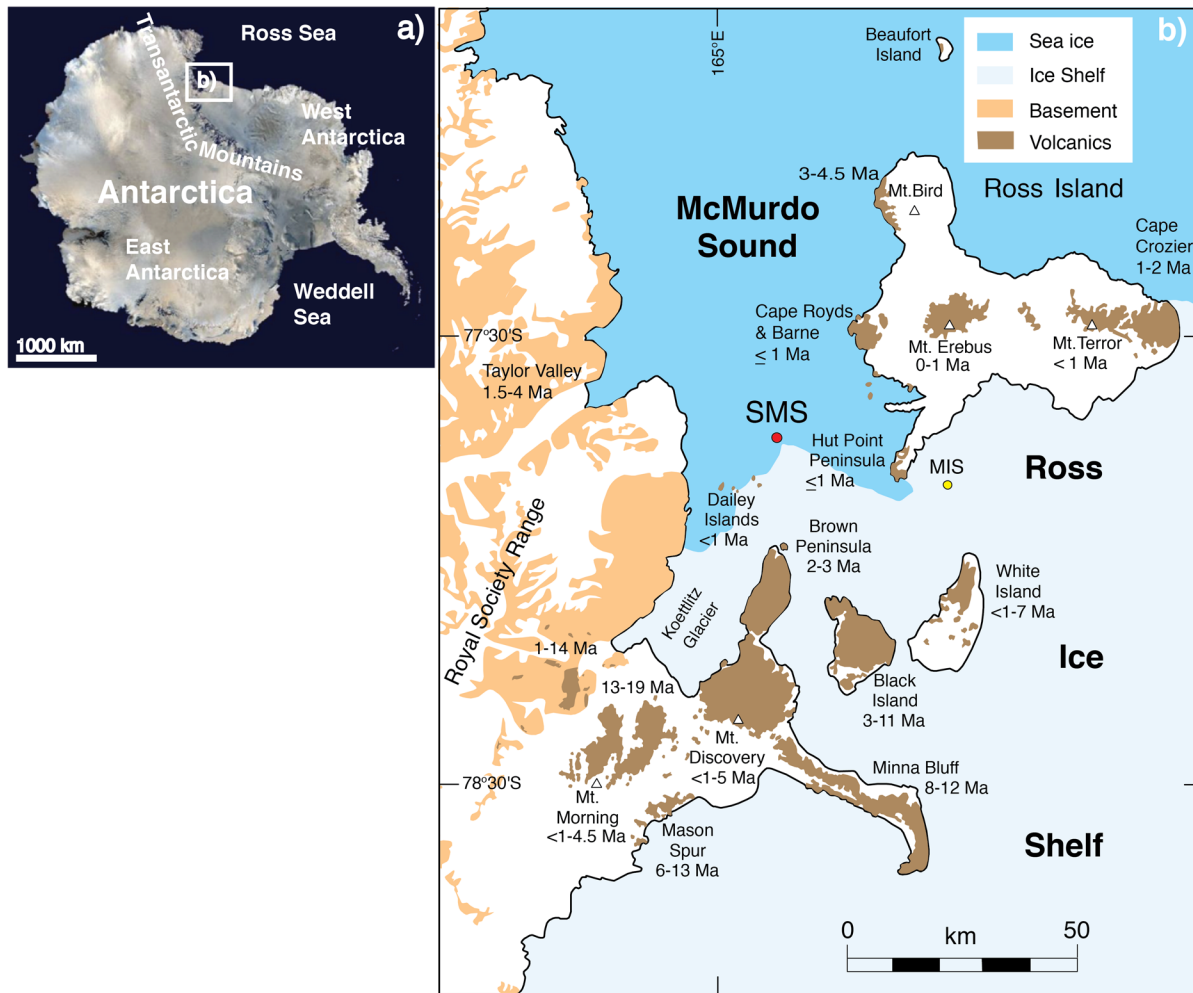


**Figure 1:** a) General map of Antarctica showing the area of the ANDRILL drillsites located along the Transantarctic Mountains near the Ross Sea. b) McMurdo Sound area map showing ANDRILL SMS (AND-2A) and MIS (AND-1B) drillsites relative to deposits of the Erebus Volcanic Province (brown) and basement rocks (orange). Ages are from Kyle (1990 and references there in); additional dates from Wilch *et al.* (1993), Esser *et al.* (2004), Harpel *et al.* (2004), Tauxe *et al.* (2004), Cooper *et al.* (2007) and Fargo *et al.* (2008).

Germany and France (Nowell *et al.*, 2006), Canada (Edwards *et al.*, 2002), and many other areas around the world. In Ireland, isostatic rebound triggered by glacial unloading has been shown to reactivate faults as well (Knight, 1999). It is possible then, that the frequent glacial loading and unloading caused by the dynamic environment in Antarctica during the Early to Middle Miocene could be one factor controlling the input of volcanic material into the AND-2A core. A tentative link between explosive volcanic activity and glaciations in this area has been previously suggested by Lewis *et al.* (2007) based on the occurrence of Middle Miocene ash fall deposits found within the Dry Valleys, but the authors did not evaluate this assertion.

The specific objectives of this study include: (1) to describe volcanic glass recovered from the AND-2A core in twenty-four, 15-cm long segments between ~354 and ~765 meters below sea floor (mbsf), corresponding to an age range of ~15.9-18.4 Ma; (2) to analyze the geochemistry of the volcanic glass found in the AND-2A core using major and trace element composition in order to determine the source(s) of the volcanic material and examine the changes in composition with depth/time in the core; (3) to examine a specific sediment interval of ~638-664 mbsf in detail, corresponding to an age range of ~17.4-17.5 Ma, interpreted to represent a nearly complete glacial cycle of retreat and advance (Fielding *et al.*, 2011; Passchier *et al.*, 2011), in order to investigate feedback mechanisms between ice-sheet unloading and volcanism during the Miocene in the McMurdo Sound area and (4) to prepare glass separates for  $^{40}\text{Ar}/^{39}\text{Ar}$  radioisotopic dating in order to better constrain the current AND-2A age model and aid in correlating possible land source(s) of the volcanic material.

## GEOLOGIC BACKGROUND

Several drilling projects have been conducted in the region, including the Cenozoic Investigations of the Ross Sea project (1986), with more recent drilling in western McMurdo Sound beginning in 1998 with the Cape Roberts Project, where three cores (CRP-1, CRP-2, and CRP-3) were drilled (Cape Roberts Science Team, 2000). The goal of this project was to obtain a stratigraphic record of events associated with the onset and history of the continental glaciation in Antarctica and to date the onset of rifting and the uplift of the Transantarctic Mountains (Florindo *et al.*, 2005). The sedimentary record obtained from these CRP cores extends from ~34 to ~17 Ma.

The first ANDRILL core (AND-1B) was drilled in 2006, and provides a sedimentary record spanning the last ~13 Ma, while the second core (AND-2A) drilled in 2007 extends back to just over 20 Ma. The AND-2A core provides an extended sedimentary record between ~20 and ~14 Ma, including sediments corresponding to the Middle Miocene Climatic Optimum (Warny *et al.*, 2009; Di Vincenzo *et al.*, 2010). The AND-2A core reaches sediments within time intervals that other drill cores have not recovered previously (Fig 2). Piecing together stratigraphic and chronological data from CRP and ANDRILL cores provides a virtually complete history of the past ~34 million years of Antarctica's climate, tectonic, and volcanic past. Seismic reflection surveys have been performed in the McMurdo Sound area in order to help resolve the stratigraphic and tectonic history. Fielding *et al.* (2008b) combined seismic reflection data from several different surveys including those performed specifically for the McMurdo Ice Shelf Project drilling (AND-1B). Internal seismic facies were arranged into packages considered to represent glacial advances and retreats. Once drilling began and the sediment of the AND-1B core was logged, much more detailed information was gained by the

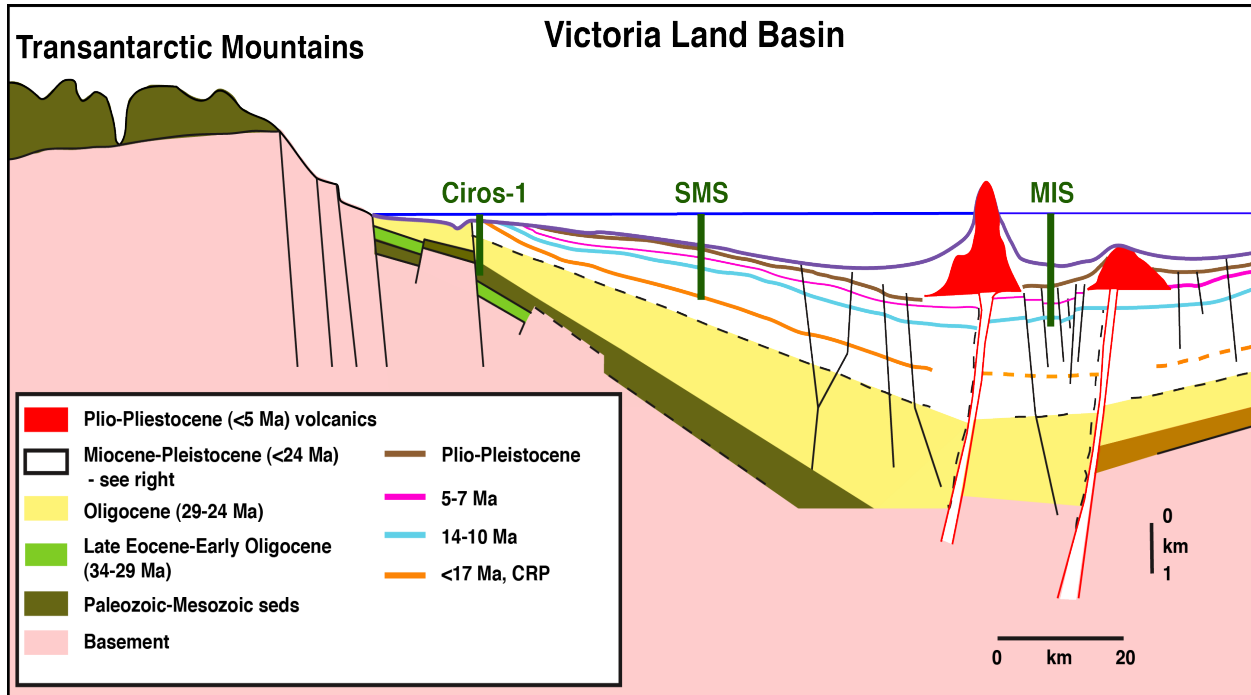


**Figure 2:** Cross section of the Victoria Land Basin, showing locations of the SMS (AND-2A) and MIS (AND-1B) drill cores relative to each other. Modified from Naish *et al.* (2007). Colored lines are key reflectors determined by seismic studies for Miocene-Pleistocene aged sediments. The SMS drill core reaches sediment that had previously not been recovered by earlier drill cores, which encompass an expanded Early to Middle Miocene stratigraphic record in the AND-2A core and includes sediments from the Middle Miocene Climatic Optimum. The CIROS-1 drill core is part of the Ocean Drilling Project drilled in 1986. Together, these three drillcores across the Victoria Land Basin provide a near complete stratigraphic record from ~30 Ma to present.

analysis of the sediment. The AND-1B core was found to contain 58 depositional sequences of successions of subglacial, glacimarine, and marine sediments recording periods of ice-sheet advance followed by a later retreat, constrained in age by a number of geochronological techniques (McKay *et al.*, 2009). These stratigraphic data have then been used to examine past fluctuations in the relatively unstable West Antarctic Ice Sheet (WAIS), and also the more stable East Antarctic Ice Sheet (EAIS) in several studies (McKay *et al.*, 2009; Naish *et al.*, 2009; Talarico and Sandroni, 2009). Local ice variations at the AND-1B core were found to reflect the overall state of the WAIS, being controlled by ocean-induced melt variations, while the sedimentary cycles in the core were found to reflect coastal margin variations of the EAIS (e.g., the outlet glaciers of the Transantarctic Mountains) and offer evidence for major mass balance changes in the WAIS as well (Naish *et al.*, 2009). Understanding the past behavior of the WAIS and EAIS is extremely important, especially considering the possible collapse of the WAIS during the late Pleistocene at a time when temperatures were  $\sim 3^{\circ}\text{C}$  higher than today (McKay *et al.*, 2009). A  $3^{\circ}\text{C}$  increase in average global temperature is predicted by the end of the 21st century (Solomon *et al.*, 2007).

The AND-2A core was drilled adjacent to the Transantarctic Mountains and recovered sediments deposited into the southern Victoria Land Basin in western Antarctica, which developed as part of the West Antarctic rift system (Fig. 1). The accommodation space needed to allow for deposition of sediments in the basin was created by fault and flexure-related subsidence associated with rifting (Wilson, 1999; Fielding *et al.*, 2008b). The Victoria Land Basin contains a 14 km thick sequence of Mesozoic-Cenozoic strata with dominant sediment supply being from the Transantarctic Mountains (Fig. 2), followed volumetrically by volcanic detritus from the EVP. The Transantarctic Mountains are comprised of Late Precambrian to

Cambrian basement metamorphic rocks from the Ross Supergroup, which were intruded by Early Palaeozoic granite from the Granite Harbour Intrusive Complex (Gunn and Warren, 1962; Harrington, 1965). Overlying the basement rocks are the Devonian - Triassic continental sediments from the Beacon Supergroup, which are intruded by the Jurassic Ferrar Supergroup (Gunn and Warren, 1962; Kyle *et al.*, 1981). The development of the EVP that surrounds and lies within the southern portion of the basin (McMurdo Sound) has provided a steady supply of sediments resulting in enhanced sedimentation rates since ~20 Ma (Fielding *et al.*, 2008b; Di Vincenzo *et al.*, 2010). The southwestern portion of the Victoria Land Basin contains the Terror Rift; a sub-basin which developed through the Cenozoic to the Early Neogene and has accumulated approximately 3.5 km of sediments (Henrys *et al.*, 2007). Subsidence of the basin, due to loading from Ross Island volcanics, has occurred since <4.5 Ma (Naish *et al.*, 2007).

Extensive outcrops from the EVP are located near the drillsite (Fig 1). These Cenozoic, alkali volcanic deposits originated from Ross Island, White Island, Black Island, Minna Bluff, and the Mount Discovery-Mount Morning volcanic peninsula (Kyle, 1990; Cooper *et al.*, 2007; Martin *et al.*, 2009). The Volcanic activity in the EVP has been nearly continuous since the Early Miocene and shows a broad age migration towards the northwest, with ages of volcanic deposits on land ranging from ~19 Ma to the present Strombolian-style activity at Mount Erebus (Fig. 3). However, there is some evidence found in drillcores of older volcanic activity back to ~26 Ma (McIntosh, 1998, 2000; Di Vincenzo *et al.*, 2010). Tephra layers and accumulations found in terrestrial deposits, marine cores, and entrained in ice provide evidence for explosive volcanism in the Erebus Volcanic Province, and range in composition from primitive to more evolved volcanism following the basanite-to-phonolite series (Harpel *et al.*, 2004). Most of the deposits from the EVP belong to a silica-undersaturated basanite-to-phonolite alkaline series,

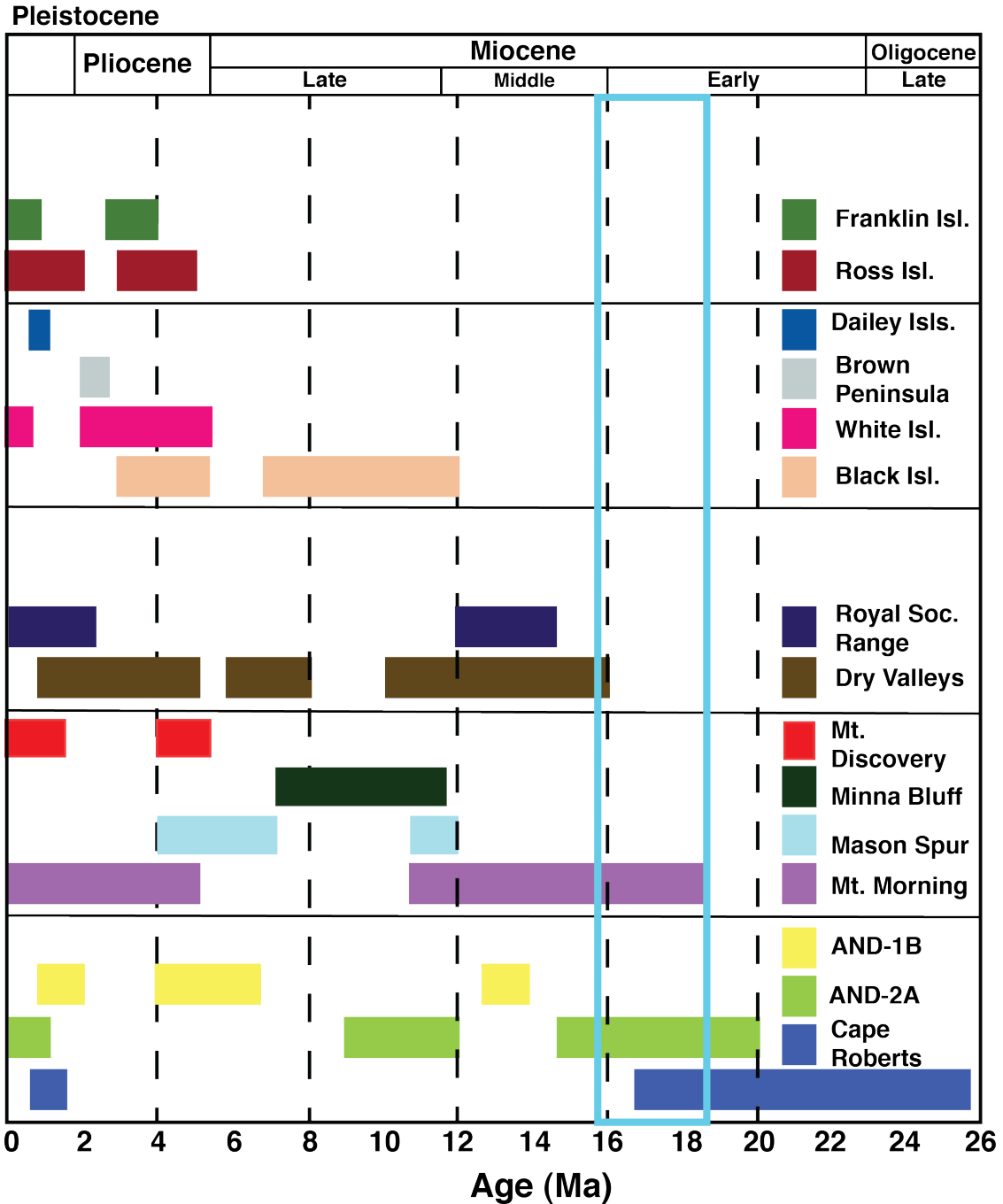


**Figure 3:** Radioisotopic ages (K-Ar and  $^{40}\text{Ar}/^{39}\text{Ar}$  methods) of volcanic centers from the Erebus Volcanic Province are shown, modified from Di Vincenzo *et al.* (2010). Radioisotopic ages derived from the Cape Roberts, ANDRILL MIS, and ANDRILL SMS drilling projects are shown along the bottom. Volcanic activity in the Erebus Volcanic Province is shown to extend back to ~26 Ma based on evidence from drillcores. The box surrounds the approximate time period studied (15.9–18.4 Ma) in AND-2A, with Mt. Morning being the only known eruptive center coeval with AND-2A volcanic deposits

though Mount Morning shows an earlier phase of activity that produced a more silica-oversaturated trachytic-alkaline series (Martin *et al.*, 2009). Mount Morning is the inferred source of Early to Middle Miocene volcanic material recovered from the Cape Roberts (Barrett, 2007), AND-1B (Pompilio *et al.*, 2007) and AND-2A (Panter *et al.*, 2008; Di Vincenzo *et al.*, 2010) cores.

#### AND-2A Core

In 2007, the ANDRILL program completed its second drill hole (AND-2A), having 98% recovery and reaching sediments to a depth of 1,138.54 mbsf in McMurdo Sound. The core consists of many terrigenous clastic lithologies including claystone, siltstone, sandstone, conglomerate, breccia, and diamictites, and also has a significant volcanic component (> 50% volcanic material in many of the lithostratigraphic units; Di Vincenzo *et al.*, 2010). The materials recovered from the AND-2A core consist of Early Miocene to Pleistocene aged sediments and include an expanded Middle Miocene section, which has not been recovered from previous drill cores (Fielding *et al.*, 2011; Passchier *et al.*, 2011). In the Di Vincenzo *et al.* (2010) study, volcanic clasts and primary to moderately re-worked tephra layers from the AND-2A core were dated using the  $^{40}\text{Ar}/^{39}\text{Ar}$  method. The results reveal a nearly continuous stratigraphic record from ~358-1093 mbsf, corresponding to an age range of ~16-20.1 Ma, characterized by a relatively fast and nearly constant mean sedimentation rate of ~19 cm/ka. This study is focused on volcanic glass in the sediments recovered from the Early to Middle Miocene (~765-354 mbsf) where approximate ages for samples (~18.4-15.9 Ma) were determined using the AND-2A age model (Fig. 4).

The sediments in the AND-2A core were originally separated into 14 different lithostratigraphic units, based on packages of lithologies, with an emphasis on diamictite

abundance. A total of 9 sedimentary facies were characterized and interpreted to be deposited in environments that range from open water to shallow marine conditions to proglacial, glacimarine, and subglacial environments (Fielding *et al.*, 2008a). Facies 1, which consists of highly fossiliferous, extensively bioturbated, clast-poor mudstone, was most likely deposited in an open, shallow marine shelf environment with minimal ice influence. Facies 2 and 3 are similar to Facies 1, but are coarser-grained (silty), and contain some evidence of occasional ice influence. Facies 4 and 5 were still most likely deposited in open marine conditions, though they contain much more sand. Facies 4 was deposited in the open marine shoreface or upper offshore area, as indicated by the presence of planar lamination, ripple cross-lamination, cross-bedding, hummocky cross-stratification, and minimal bioturbation. Dispersed gravel seen in Facies 4 indicates some minor ice rafting as well. Facies 5 is muddier and is unstratified, and is also heavily affected by hemipelagic fallout and sediment input from ice rafting, indicating deposition farther offshore. Facies 6 and 7 were likely deposited in open glacimarine conditions. In Facies 6, this is demonstrated by the presence of interlaminated siltstone, sandstone, and diamictite, with dispersed clasts and fine-scale lamination, while Facies 7 is dominated by stratified diamictite with a sandy/muddy matrix. Facies 5-7 (Fig. 5) contain a significant volcanic component in the form of dispersed accumulations of glass within sediment and are a focus of this study. Facies 8 contains massive diamictite, and shows shear structures including box-work fracturing and brecciation, indicating deposition in an ice-proximal glacimarine environment (Fielding *et al.*, 2011). Fielding *et al.* (2011) then arranged these lithofacies into 74 glacial marine cycles (Fig. 6).

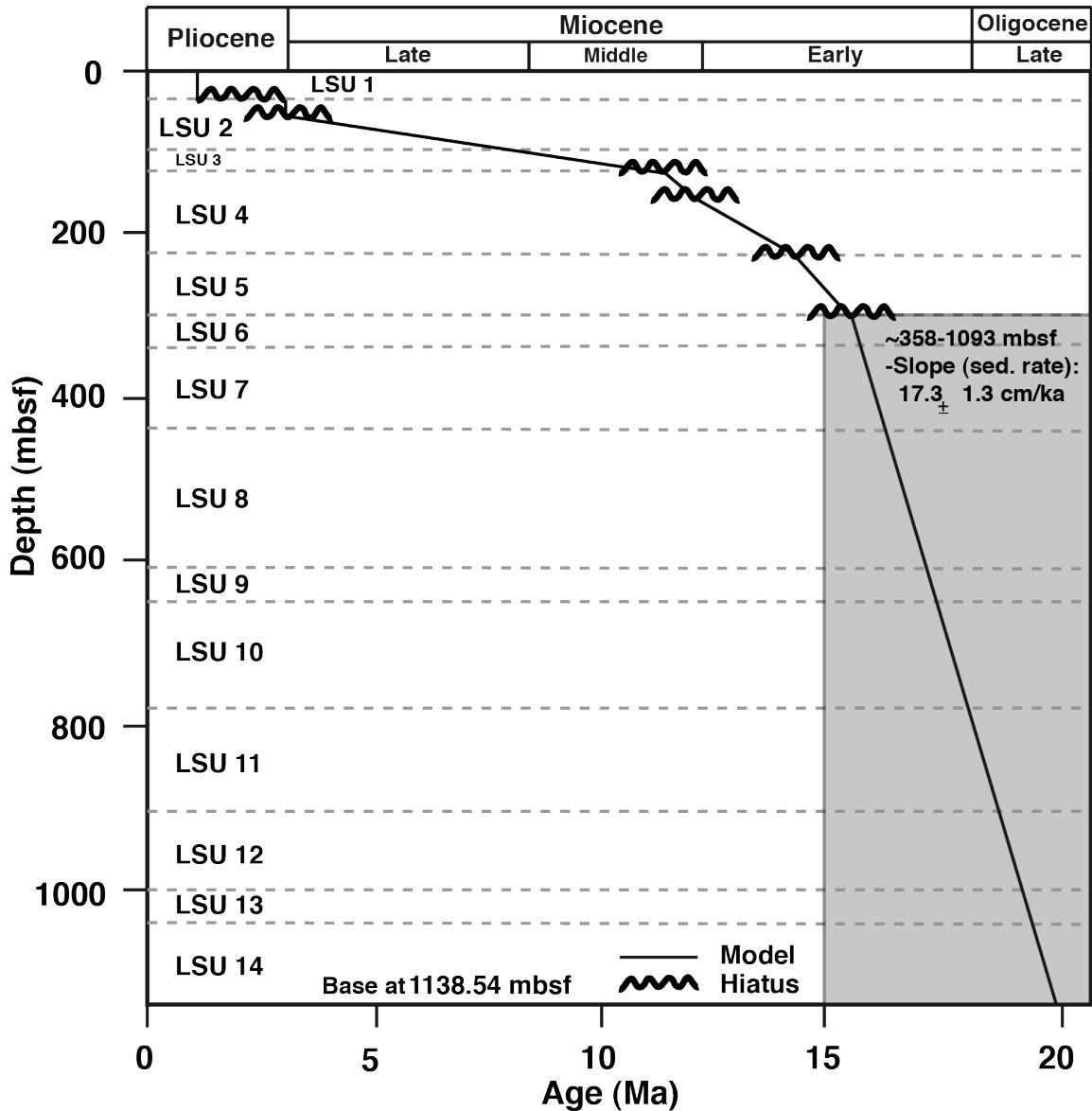


**Figure 4:** Depth versus age diagram for the AND-2A core derived from Sr isotope stratigraphy, biostratigraphy from foraminifera and diatoms, magnetostratigraphy, and  $^{40}\text{Ar}/^{39}\text{Ar}$  radioisotopic ages from primary and moderately reworked tephra and volcanic clasts from the AND-2A core. Modified from Acton *et al.*, (2008); Di Vincenzo *et al.* (2010).

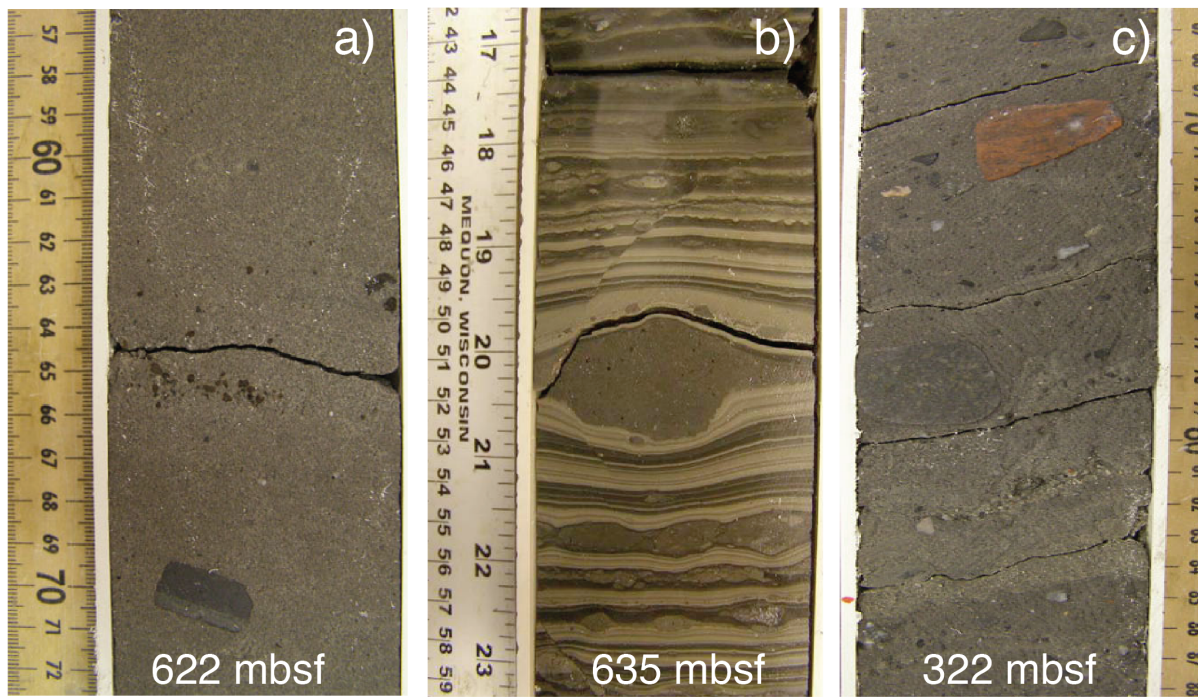


**Figure 5:** Representative lithofacies in the AND-2A core that contain the majority of the accumulations of dispersed glass. a) Lithofacies 5: fine muddy sandstone or mudstone with dispersed clasts; interpreted to represent hemipelagic sedimentation with deposition from icebergs and sea ice. b) lithofacies 6: interlaminated fine sandstone and siltstone with dispersed clasts and diamictite; interpreted to be deposited in a glacimarine environment. c) lithofacies 7: stratified diamictite with dispersed clasts; interpreted to be deposited in a glacimarine environment.

Five different stratigraphic motifs (or sequence styles) were then derived from AND-2A sediments. Differences between motifs result from the diversity and abundance of the different lithofacies, which reflect a variety of environmental conditions from a temperate glacial regime to sub-polar to polar regimes (Fielding *et al.*, 2011; Passchier *et al.*, 2011). Motifs 1 and 2 are indicative of a sub-polar glacial regime with significant melt-water influence, and motif 3 is indicative of a temperate glacial regime, again with significant melt-water influence. Motif 4 is much more lithologically diverse, indicating a temperate glacial regime, with smaller floating glaciers interspersed or distal to the drillsite except during glacial maximum conditions, and motif 5 records distal glacimarine deposition during glacial advance periods, followed by open marine conditions during glacial minimum conditions (Fielding *et al.*, 2011)

Other lithofacies include primary volcanic deposits and moderately reworked volcanic deposits (Panter *et al.*, 2008). The upper lithostratigraphic unit one (LSU 1, 0 to 37.07 mbsf) was found to be the most volcanic-rich unit within the AND-2A core, and thus became an important unit from which information on age, composition, and volcanological and depositional features of these volcanic sediments and tephra layers could be obtained (Del Carlo *et al.*, 2009; Di Vincenzo *et al.*, 2010). The interval between ~640-1093 mbsf (~17.4-19.9 Ma; Early to Middle Miocene) contains seven weakly to strongly reworked tephra concentrations, including a single primary tephra layer at ~640 mbsf (Panter *et al.*, 2008), and dated by Di Vincenzo *et al.* (2010) at 17.4 Ma. High abundances (typically 5% by volume or higher; up to 70%) of *fresh* volcanic glass are found in finer grained sediments such as siltstone and sandstone between ~230-780 mbsf (~15.3-18.5 Ma, Early to Middle Miocene; Panter *et al.*, 2008) and are the focus of this study.

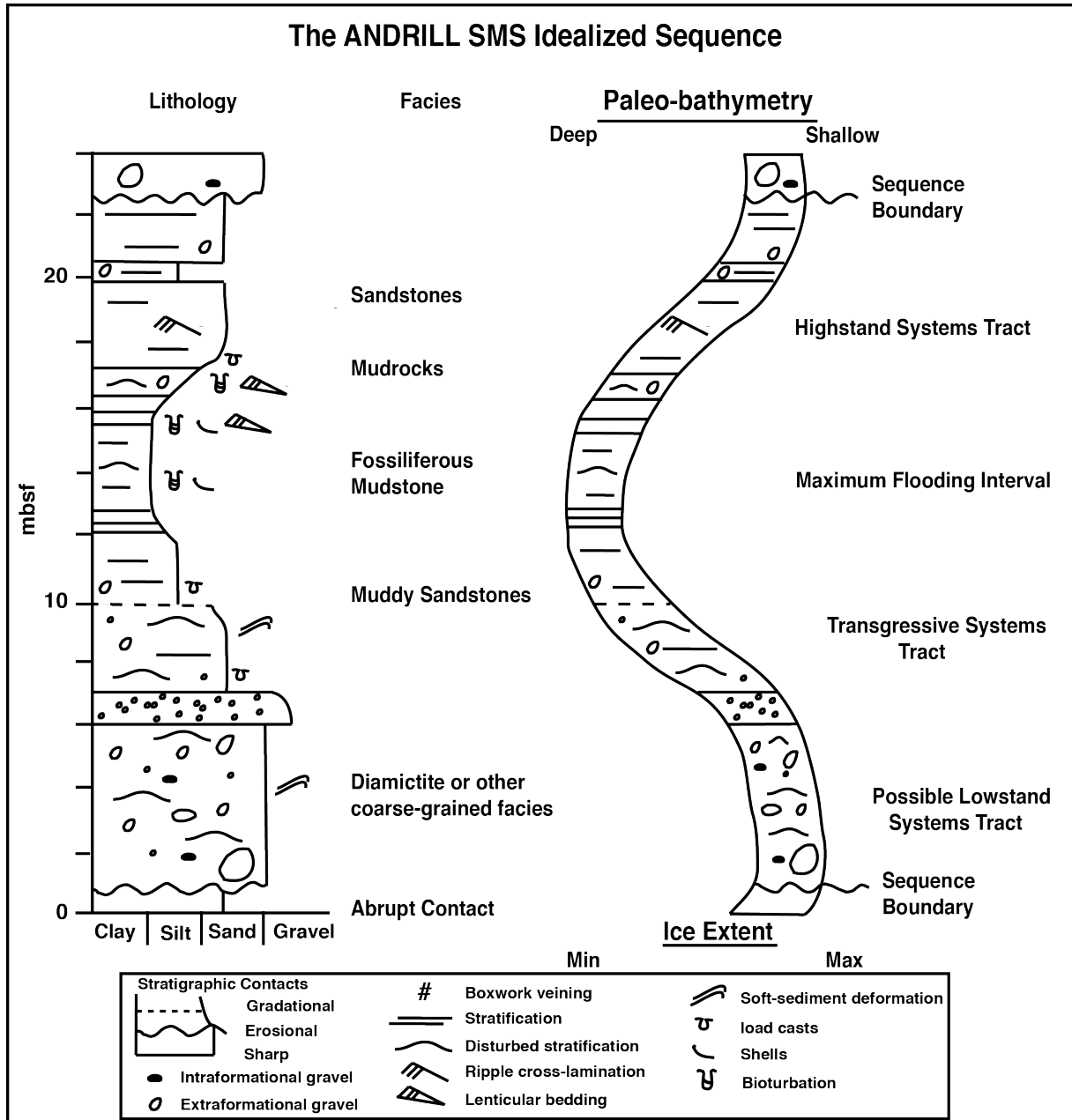


**Figure 6:** Diagram modified from Fielding *et al.* (2011) that shows the SMS Idealized Sequence (complete glacimarine sequence), beginning with an abrupt basal contact overlain by a coarse-grained lithofacies (6-8) representing ice-proximal conditions, then fining upward to sandstone (lithofacies 4-5) representing a transgressive systems tract, and continuing to fine upward into fine, muddy deposits (lithofacies 1-3) representing ice distal conditions. Muddy deposits are overlain by a coarsening upwards into sandstones, interpreted to represent a Highstand Systems Tract, though in some cases may represent a Regressive Systems Tract, which may indicate the onset of the next glaciation. Sequence 32 (~638-664 mbsf), as the most complete glacimarine cycle in the AND-2A, will be examined in detail in this study.

## METHODS

### Sample Selection

Twenty-four samples (15-cm long,  $\frac{1}{4}$  round core samples, 25-30 mm radius) have been studied. Samples were requested from the Antarctic Marine Research Facility at Florida State University and were selected based on several criteria. First, sediment samples were required to contain a significant amount of glass (>15% by volume). The amount of glass was determined by visual estimates of smear slides and core log identification of scoria concentrations during the logging of the core (Panter *et al.*, 2008). Second, glass-rich sediments were selected based on roughly even spacing in depth in order to evaluate changes in composition with time. Third, to specifically test for glacial influence on volcanism, a set of seven samples were selected from a targeted stratigraphic interval that represents a single glacimarine cycle (Sequence 32, Fielding *et al.*, 2011), interpreted to preserve one of the most complete cycles in the core (C. Fielding, personal communication). The objective here was to determine whether or not there are systematic compositional and textural variations with glacial cyclicity. All 24 samples were then described and analyzed using standard petrographic techniques. Characteristics of the samples including size, vesicularity, color, angularity, crystal content, and "freshness" (refers to degree of alteration) of the volcanic glass shards were carefully documented petrographically before microprobe analysis.

For  $^{40}\text{Ar}/^{39}\text{Ar}$  dating, samples were carefully hand-crushed and sieved in order to separate size fractions to assure minimal modification of individual glass fragments. Glass separates were then separated manually using a binocular microscope, cleaned in an ultrasonic bath, and thereafter only the "cleanest" and largest 15-30 grains were chosen for possible dating. Glass from 4 samples could not be separated using the above technique because of their extremely

small grain size (<100 microns). This difficulty was overcome for sample 385.38 mbsf, by first concentrating the glass using a magnetic separator. Then, based on the known density of the glass, the glass was further concentrated using a "heavy liquids" technique (using a sodium metatungstate solution). Though this method produced a high concentration of glass fragments, the glass grains could still not be used due to a very small grain size (<100 microns), which would not be suitable for dating or LA-ICP-MS techniques.

### Determining physical properties

Standard point counting techniques, as outlined by Dickinson (1970), were used to determine relative percentages of brown, colorless and green glass as well as scoria within each of the 22 samples. Characteristics of each glass grain, including degree of rounding and an estimation of vesicularity (vol. %) were also recorded. The degree of rounding was classified into four categories, including angular, sub-angular, sub-rounded, and rounded, which were based on visual estimates using a representative range of glass fragments (Appendix A).

A methodology was also developed to quantify the shapes and sizes of glass grains found in the 7 samples from Sequence 32. Shape and size of 78 particles were measured using digital image techniques in ArcMap<sup>©</sup>. The perimeter of each glass grain was determined by the sum of pixels making up its outer boundary and the area was determined by the sum of pixels within the perimeter. Rounding was then determined quantitatively using the method of Manga *et al.* (2010). For comparison, the shape and size of ash grains from a primary pyroclastic fall deposit on nearby Mount Erebus (Panter and Winter, 2008) were digitally processed and evaluated in the same manner (Appendix B).

### Analytical Techniques

The concentrations of major and minor elements (Na, Mg, Al, Si, P, S, Cl, K, Ca, Ti, Mn, Fe, Sr and Ba) of volcanic glass and minerals were measured using a Cameca SX-100 Electron Microprobe Analyzer at the University of Michigan. A beam current of 10 nA was used, operating at an acceleration voltage of 15 kV, employing a count time of 30s for each element (Na and K corrected by using three 5s counting periods and extrapolating count rate back to zero time) and a beam size of 5  $\mu\text{m}$ . For each of the 24 samples analyzed, 9-19 individual glass grains were probed. Individual glass fragments were selected based on the larger and least altered clasts but insuring that glass representing all varieties (e.g., different colors) was analyzed.

Trace element composition of glass in 20 samples was determined by laser ablation-inductively coupled plasma-mass spectrometry (LA-ICP-MS) at the CNR - Istituto di Geoscienze e Georisorse, U.O. di Pavia. The instrument couples an Nd:YAG laser working at 266 nm with a quadrupole ICP mass spectrometer type DRCE from Perkin Elmer. The laser was operated at 10 Hz with pulse energy on the sample of 0.01 - 0.03 mJ. The spot size was set to 20-30  $\mu\text{m}$ . Data reduction was performed with the ‘Glitter’ software package (van Achterbergh *et al.*, 2001) using NIST SRM 610 as the external standard and  $^{44}\text{Ca}$  as the internal one. Precision and accuracy, assessed during each analytical run on the BCR-2 USGS reference glass, are better than  $\pm 6\%$ . Approximately 5 to 13 individual glass grains were analyzed per sample, and the largest grains were analyzed twice wherever possible. Grains were chosen based on previous composition obtained by electron microprobe, minimal alteration, size, and having an area large enough for laser ablation (away from vesicles and crystals). A suitable spot location for laser ablation was determined by observing the grains in both transmitted and reflected light before analysis. The beam size was then adjusted accordingly from 20-30  $\mu\text{m}$  for each grain.

The full analyses, together with the corresponding major element analyses, are given in Appendix C. This percentage of error determined from the counting statistics varies with the total concentration of any given element and its ionization potential, with a typical analysis from sample 354.05 mbsf shown (Table 1). In general, however, the majority of errors are low, under 5 %. In some cases, where errors are present over 15%, analyses were considered suspect and removed from the dataset.

**Table 1:** Representative analysis of a basaltic glass shard from sample 354.05-K, showing uncertainties for typical chemical composition from LA-ICP-MS results.

Element	Concentration (ppm)	% Error
Li	4.10	25.37
Be	<1.18	39.83
B	22.28	23.43
Sc	21.23	5.18
Ti	20954.38	3.80
V	268.07	3.85
Cr	16.32	16.91
Co	34.24	4.73
Ni	13.83	9.18
Zn	125.85	5.84
Rb	28.32	4.48
Sr	792.52	3.52
Y	22.30	4.30
Zr	199.64	3.80
Nb	50.25	4.08
Cs	0.29	13.10
Ba	441.96	3.64
La	41.44	3.67
Ce	84.25	4.05
Pr	10.40	4.33
Nd	39.41	4.36
Sm	6.28	8.12
Eu	3.09	6.80
Gd	7.46	7.37
Tb	0.88	8.34
Dy	5.24	7.25
Ho	0.99	8.00
Er	1.77	11.30
Tm	0.22	14.81
Yb	2.38	11.76
Lu	0.33	12.69
Hf	4.59	8.28
Ta	2.92	5.48
Pb	2.96	6.76
Th	3.85	5.19
U	1.43	6.62

## RESULTS

### Physical Characteristics and Alteration

The ash recovered from ~354-765 mbsf occurs as accumulations of dispersed glass (2-50 vol. %) and scoria within fine-grained glacimarine sediments and corresponds to an age range of ~15.9-18.4 Ma, based on the age model for the AND-2A core (Di Vincenzo *et al.*, 2010). The glass-rich sediments consist of muddy sandstone, fine sandstone, and stratified diamictite, and occur most frequently in lithofacies 5 to 7 (Fig. 7). The glass varies in color (brown, colorless, green), size (up to 4 mm), vesicularity (0-50 vol. %, including both spherical and stretched vesicles), crystal content (0-20 vol. %, primarily as plagioclase and smaller portions of apatite, clinopyroxene, magnetite, and olivine), angularity, and freshness (Table 2; Fig. 8). The common occurrence of delicate cuspatate forms and the relative freshness of the majority of the glass suggests that they were introduced either directly into the water as fallout or minimally reworked (windblown and/or ice-rafted) before deposition in the Victoria Land Basin.

A significant amount of altered glass (10-20%) exists within samples and typically displays de-vitrified rims and vesicles filled with calcite when examined petrographically (Fig. 9). Chemically, the altered glass has low total oxides (< 97 wt.%), low Ca/K ratios (< 2), high Alteration Index (> 40), and are typically more evolved (Figs. 10a, 11, 12). Visible alteration of mafic glass generally increases down section, a common phenomenon in ashes from marine cores (Schacht *et al.*, 2008). Several factors have combined to make glass in the AND-2A core more susceptible to alteration: 1) a high geothermal gradient (Fielding *et al.*, 2008b; Panter *et al.*, 2008), 2) presence of alkaline formation waters (Fielding *et al.*, 2008b) and 3) the abundance of chemically reactive volcanic material throughout the core (Panter *et al.*, 2008). Glass of trachytic composition is typically more altered relative to basaltic glass (Fig. 10), and therefore

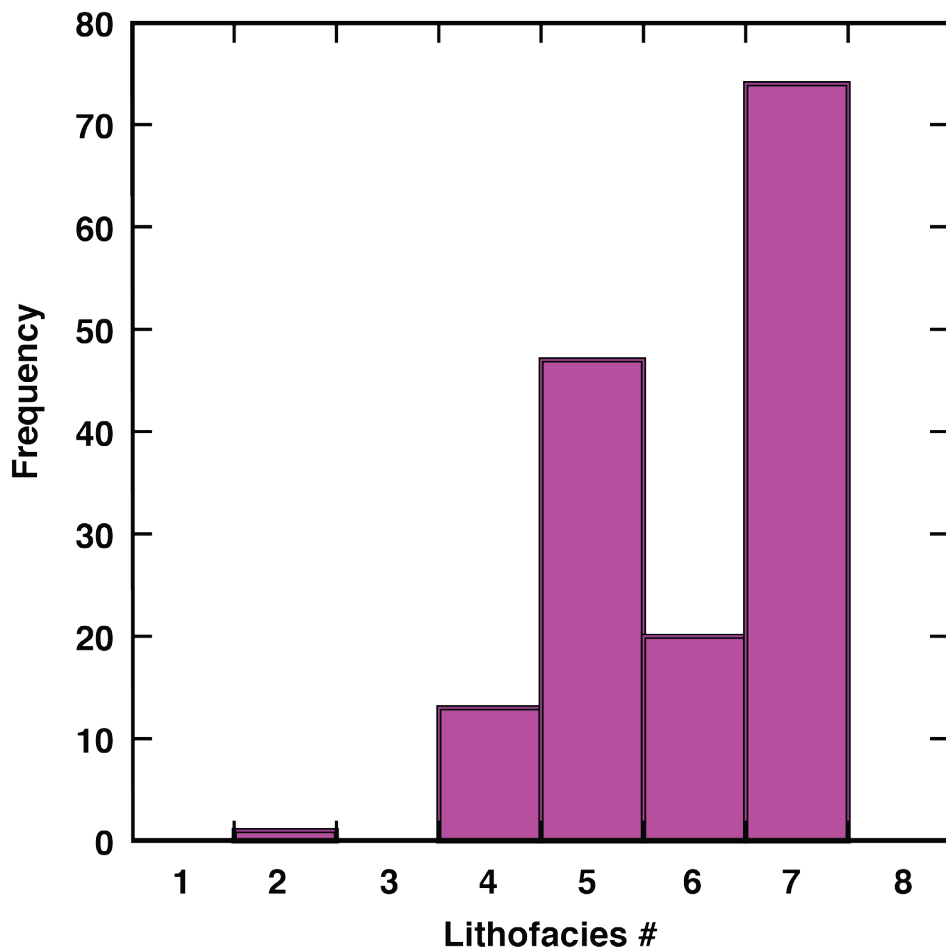


**Figure 7:** Histogram showing the frequency of zones with  $>15\%$  glass (by volume) in non-volcanic sediments. Glass-rich areas most often occur in lithofacies 5-7 (glacially influenced); little/no glass occurs in the ice-distal lithofacies (1-4), and the most ice-proximal lithofacies (8). Volume estimates based on smear slide observations performed by Dr. Brad Field, GNS Science (Panter *et al.*, 2008).

**Table 2:** Results from modified point counting, performed on glass sample layers throughout AND-2A, where BG = Brown Glass, CG = Colorless Glass, GG = Green Glass, AG = Angular Glass, SAG = Sub-Angular Glass, SRG = Sub-Rounded Glass, RG = Rounded Glass, LVG = Low Vesicular Glass, HVG = High Vesicular Glass and R = R-value (sphericity):  $4\pi A/P^2$ , where A = Area and P = Perimeter).

Sample	% Total Glass	% Scoria	% BG	% CG	% GG	% AG	% SAG	% SRG	% RG	% LVG	% HVG	R
354.05	56.86	0.00	82.62	17.38	0.00	15.96	46.81	29.79	7.45	85.82	14.18	-
355.63	28.49	1.34	72.65	26.50	0.85	16.24	23.93	31.62	27.35	74.36	25.64	-
419.56	34.77	1.12	95.10	4.90	0.00	29.41	11.76	15.69	43.14	59.80	40.20	-
446.85	23.58	0.53	78.33	21.67	0.00	6.67	23.33	25.00	45.00	86.67	13.33	-
534.77	25.75	2.51	88.35	11.65	0.00	24.27	24.27	33.01	18.45	67.96	32.04	-
539.22	29.14	0.73	88.15	11.85	0.00	20.74	23.70	24.44	31.11	62.96	37.04	-
577.50	29.21	0.00	64.15	35.85	0.00	5.66	16.98	45.28	32.08	88.68	11.32	-
592.76	11.91	0.00	76.09	21.74	2.17	26.09	15.22	36.96	21.74	65.22	34.78	-
596.77	23.15	0.49	65.63	32.29	0.00	8.33	7.29	43.75	40.63	89.58	10.42	-
640.15	100.00	0.00	100.00	0.00	0.00	23.19	57.25	18.12	1.45	12.32	87.68	-
640.82	23.47	0.00	75.38	24.62	0.00	15.38	23.08	40.00	21.54	75.38	24.62	0.26
642.38	15.02	0.00	73.58	26.42	0.00	18.87	32.08	33.96	15.09	66.04	33.96	0.12
644.25	15.07	0.00	76.29	24.71	0.00	26.37	16.48	20.88	34.07	27.47	48.35	0.13
649.67	20.76	0.00	72.86	25.71	0.00	52.86	22.86	15.71	8.57	42.86	57.14	0.09
650.67	21.77	0.00	85.48	14.52	0.00	40.32	24.19	19.35	16.13	58.06	41.94	0.08
654.85	20.84	2.19	88.00	12.00	0.00	60.00	18.00	14.00	8.00	38.00	62.00	0.02
661.67	23.73	0.00	85.29	14.71	0.00	29.41	23.53	26.47	20.59	64.71	55.76	0.00
721.67	31.83	1.22	64.81	33.33	0.00	26.85	25.00	23.15	25.00	58.33	41.67	-
740.89	24.70	2.39	82.11	16.84	0.00	14.74	22.11	44.21	18.95	72.63	27.37	-
742.00	14.67	0.00	82.93	17.07	0.00	19.51	26.83	36.59	17.07	63.41	36.59	-
763.52	20.47	4.27	69.77	20.93	9.30	16.28	18.60	46.51	18.60	69.77	30.23	-
764.44	28.01	10.02	64.44	20.00	15.56	22.22	17.78	31.11	28.89	71.11	28.89	-

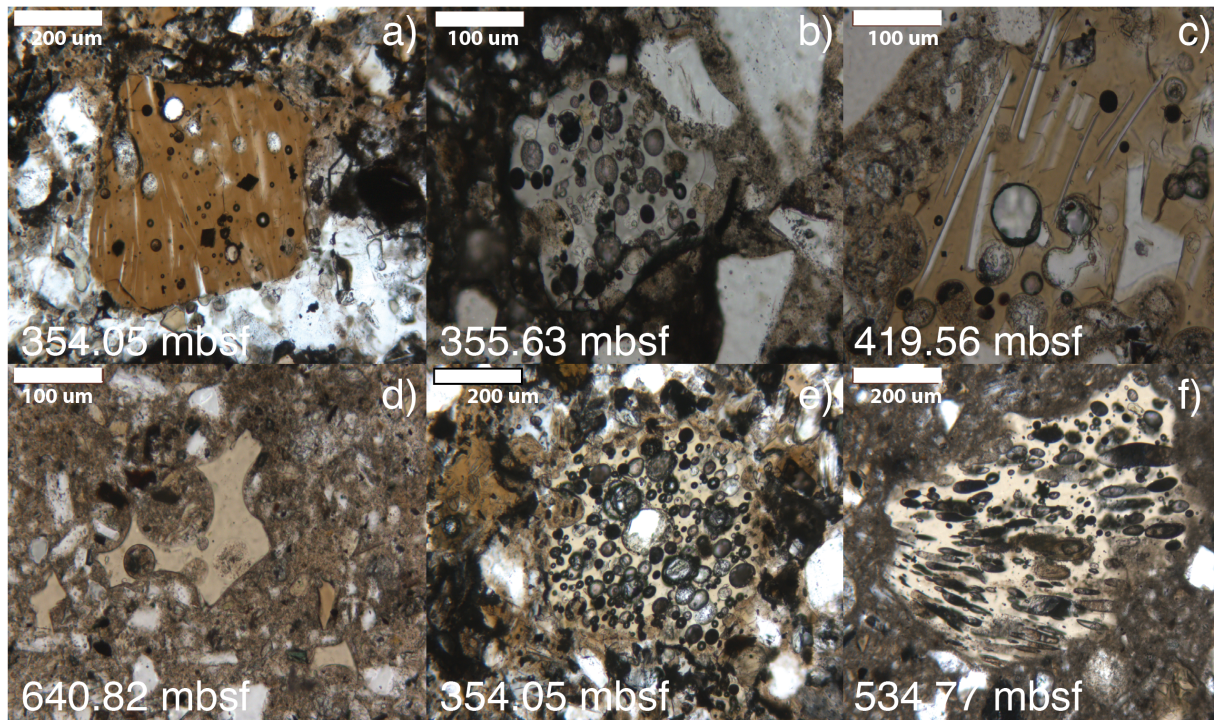


**Figure 8:** Photomicrographs of a variety of different glass types found in AND-2A. a-b) Glass clasts from 354.05 mbsf and 355.63 mbsf show a range of colors (brown and colorless; green glass is also present in some parts of AND-2A). c) Glass clast from 419.56 mbsf is crystal rich. d) Glass clast at 640.82 mbsf shows extremely delicately preserved bubbled walls. e) Glass clast at 354.05 mbsf is highly vesicular. f) Glass clast at 534.77 mbsf has stretched vesicles.

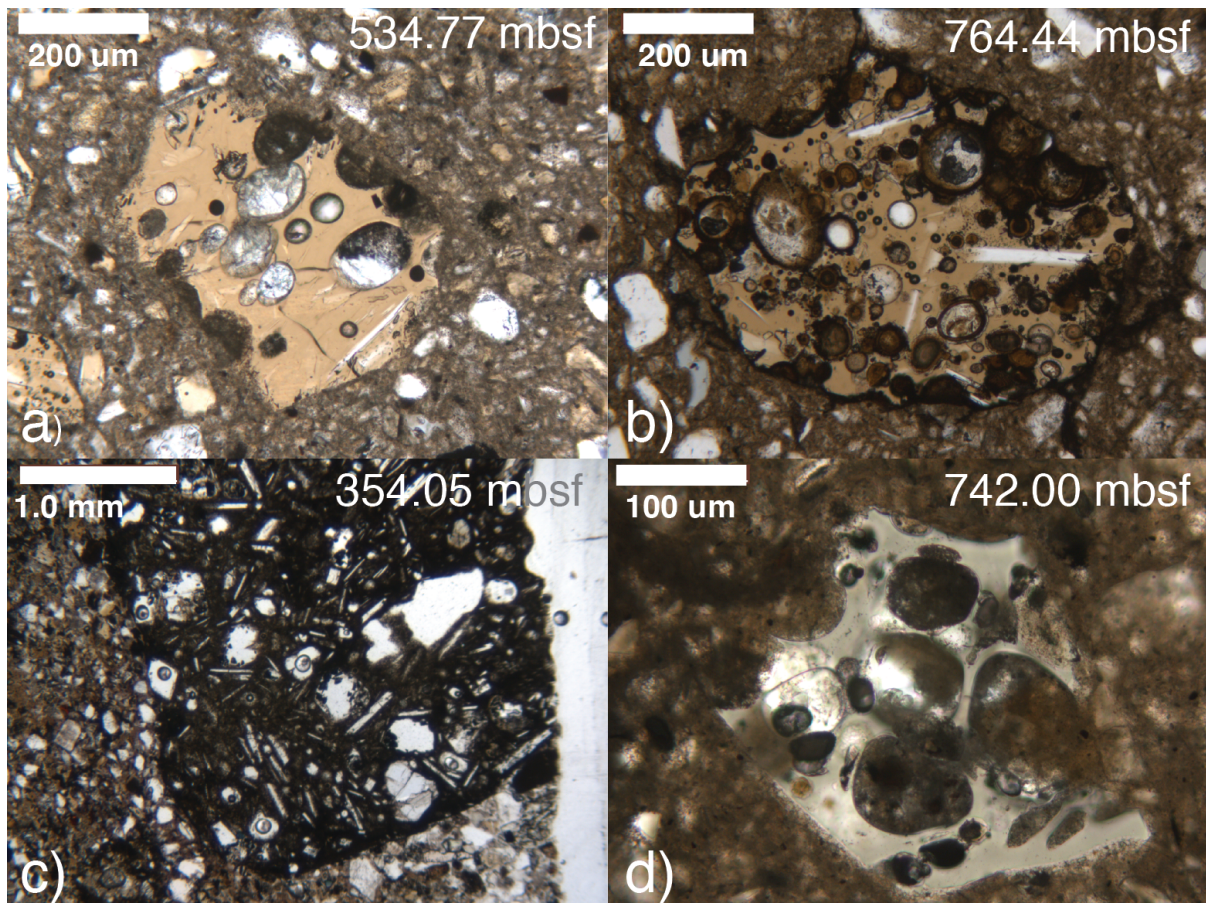


**Figure 9:** Photomicrographs of altered glass grains found within AND-2A. a) Glass clast at 534.77 mbsf displays secondary mineralization of calcite in vesicles and hydration (dark areas) around the rim of the grain, indicating early stages of alteration. b) Glass class at 764.44 mbsf shows similar types of visible alteration, but it is in a much more advanced stage down section. c) Scoria clast at 354.05 mbsf is complete black, indicating high amounts of hydration. Scoria clasts are typically highly altered. d) Colorless glass clast at 742.00 mbsf. Colorless glass was later found to be generally more felsic in composition, and is typically highly altered as a result of dissolution processes.

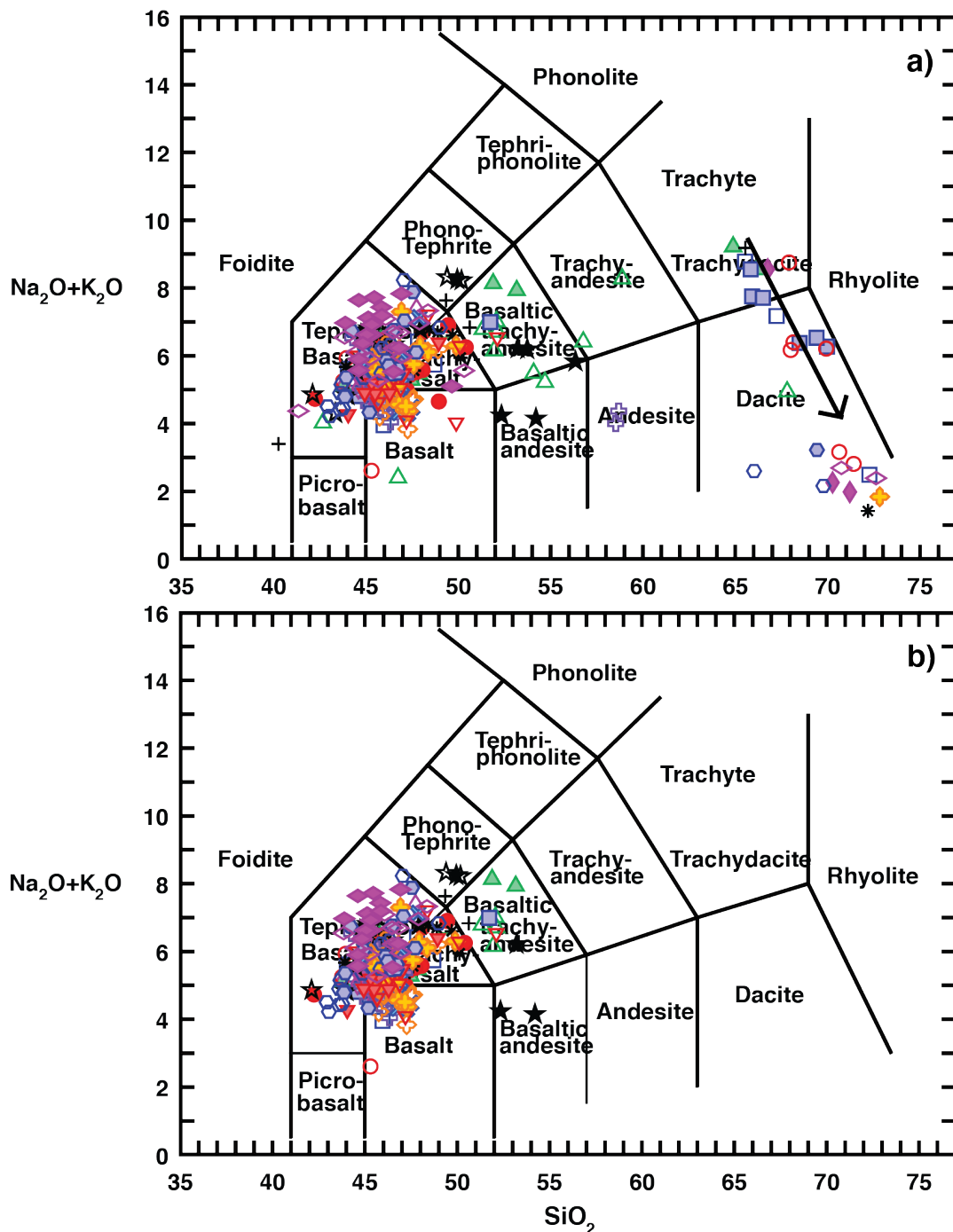


**Figure 10:** Total alkali versus silica (TAS) diagrams after Le Bas *et al.* (1986) for analyzed AND-2A glass shards. a) Shows all AND-2A glass on a TAS diagram. b) Glass with analytical totals lower than 97% (these are interpreted to be altered glass grains) are removed and are mostly felsic. Dacitic glass shards were likely trachytic in composition before experiencing significant alteration in the form of dissolution (leaching out of alkalis) as indicated by arrow.

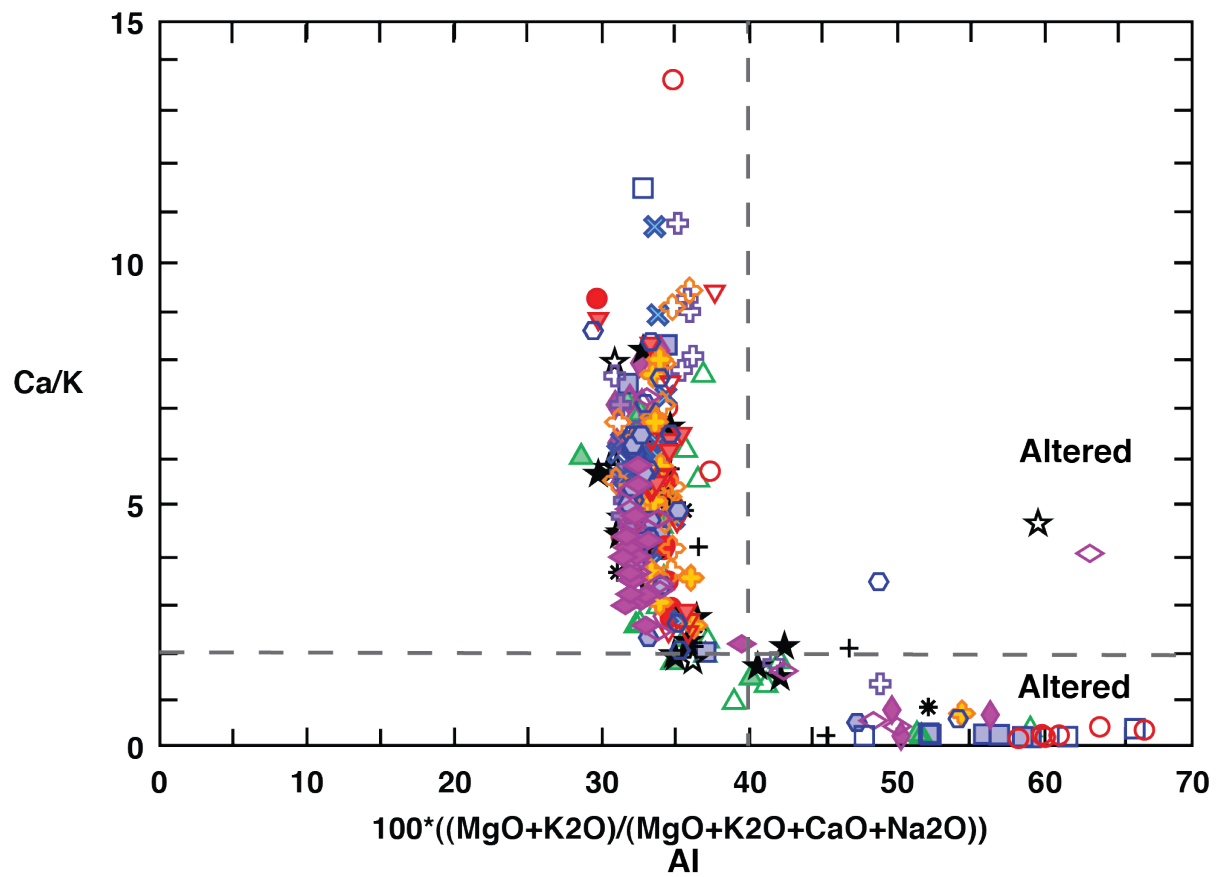


**Figure 11:** Alteration Index versus Ca/K plot. Analyzed Glass shards with low analytical totals (< 97%) were also found to have very low Ca/K ratios (< 1) and overall higher Alteration Index (> 40) and form a distinct grouping away from other glass shards with analytical totals closer to 100%. A combination of these characteristics and low analytical totals allows accurate removal of altered glass grains from the dataset.

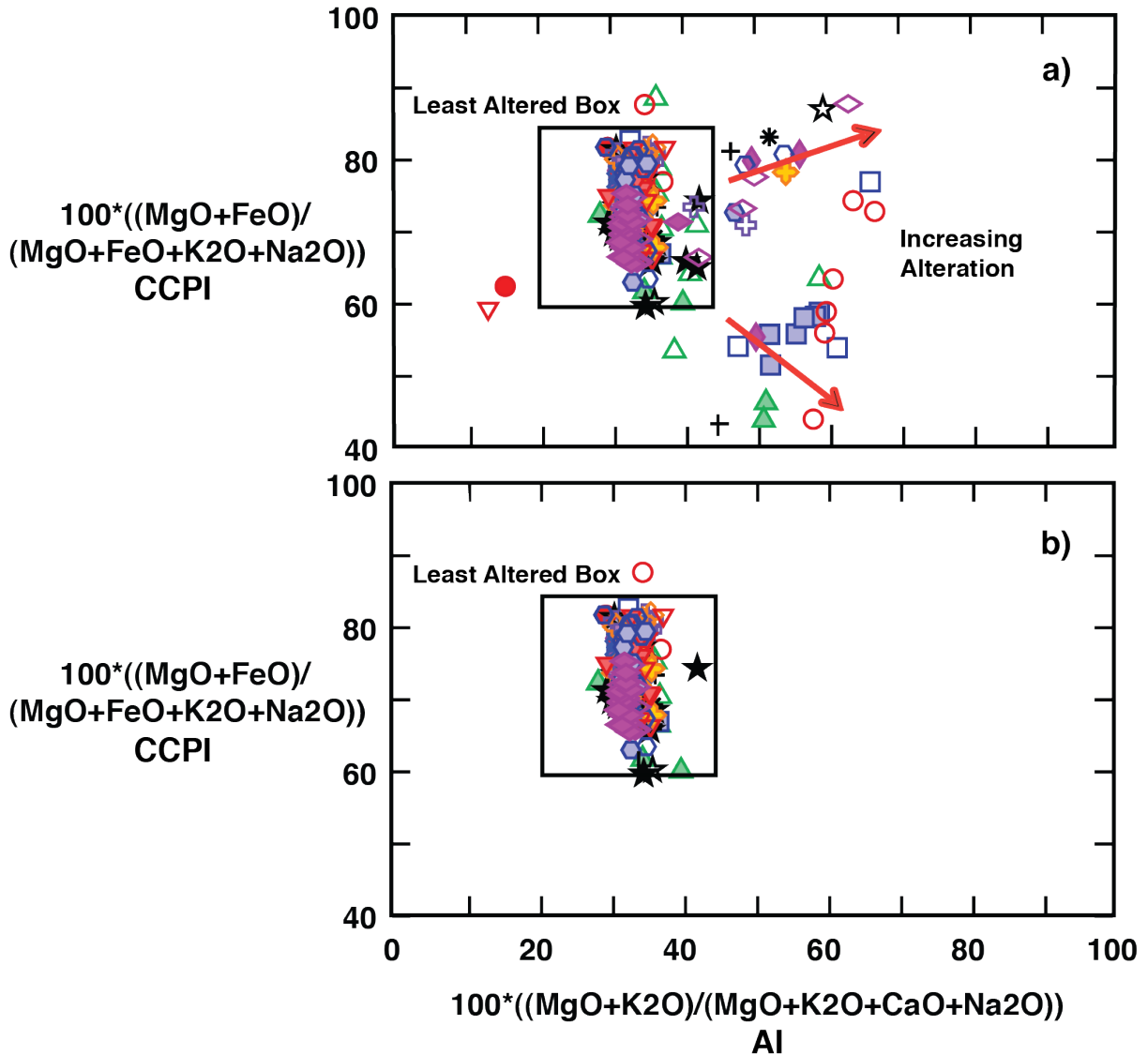


**Figure 12:** AI-CCPI Alteration box plots modified after Large *et al.* (2001), showing magma evolution of presumably unaltered volcanic arc material. Material within each box represents the least altered material. As magma evolves, the CCPI should increase. a) Alteration box plot showing the inclusion of all data. b) Alteration box plot (at same scale) after glass shards with analytical totals < 97%. Remaining glass is within the least altered box. Compositionally the altered glass manifests itself in electron microprobe data with analyses having low total oxides (< 97 wt. %), low Ca/K ratios (< 2) and high Alteration Index (AI > 40).

the geochemistry of felsic glass is not usable to impart information regarding magma source and differentiation processes. Studies find that the dissolution rates of natural glasses are found to decrease with increasing silica content at conditions of the Earth's surface (Petit *et al.*, 1990; Shoji *et al.*, 1993; Wolff-Boenisch *et al.*, 2004). However, the felsic glass present in AND-2A appears to be the most highly altered. Although devitrification of the felsic glass is not observed petrographically, the losses of alkali elements Na and K (Figs. 10-12) and lower analytical totals most likely indicate higher amounts of dissolution. It is also possible that low total oxides in felsic glass may, in part, be related to higher primary volatile content (Burnham and Jahns, 1962).

Many factors can contribute to the level of alteration, including size and morphology of grains, and time. A longer residence time in sediment interacting with fluid compounded with a change to a higher thermal regime will enhance alteration effects (Hajash and Chandler, 1981). However, because basaltic and felsic glass coexist and both occur in a range of sizes, the influence of these factors cannot explain the difference. It is likely that the trachyte glass originated from a more volatile-rich magma. Glass with higher water content is typically altered much more quickly relative to 'dry' compositions (Gifkins *et al.*, 2005), which could explain the loss of the more fluid mobile alkali elements from trachyte glass.

## Geochemistry

### *Major Elements*

The majority of the unaltered glass is mafic in composition with SiO<sub>2</sub> ranging from 41 to 52 wt. % and MgO ranging from 3 to 7 wt. %, and is strongly silica undersaturated with 5-30 wt. % normative nepheline. Basaltic compositions consist of basanite, alkali basalt, tephrite,

hawaiite and potassic trachybasalt, and slightly evolved compositions include phonotephrite, mugearite and shoshonite (Fig. 10). Additionally, two samples are basaltic andesites (Fig. 10). Representative major and trace elemental compositions for glass shards from the AND-2A core are shown (Table 3). The composition of glass shards varies within individual samples but stay mostly within the basaltic compositional spectrum. Such variability is reasonable for basaltic volcanic eruptions. For example, Erlund *et al.* (2009) determined bulk compositions of juvenile tephra erupted from the Parícutin basaltic cinder cone in Mexico, and found that the samples evolved from basaltic andesite (52.7 wt. % SiO<sub>2</sub>) to andesite (61.6 wt. % SiO<sub>2</sub>) over the course of the nine-year eruption at the volcano from 1943 to 1952. Dated tephras were found to have a compositional range from 54.7-58.5 wt. % SiO<sub>2</sub> (Luhr, 2001) and lavas displayed a compositional range of ~55-60 wt. % SiO<sub>2</sub> during the nine-year eruption (Wilcox, 1954). Also, the AND-2A glass samples do display some compositional variations with time (Fig. 13). Overall, average glass compositions for each sample show an overall increase in SiO<sub>2</sub> content up-section from ~765-534 mbsf with a notable shift back to more mafic compositions at ~446 mbsf (Fig. 13a). Also, average glass compositions for each sample show trends in Na<sub>2</sub>O and TiO<sub>2</sub>, but opposite for the middle and lower sample depth intervals. AND-2A glass compositions cluster around 5 wt. % MgO on Harker variation diagrams (Fig. 14). CaO concentrations decrease with decreasing MgO, while P<sub>2</sub>O<sub>5</sub> and Al<sub>2</sub>O<sub>3</sub> increase with decreasing MgO content. TiO<sub>2</sub> content increases, and then decreases with decreasing MgO. The variations in CaO and TiO<sub>2</sub> indicate differentiation that is primarily controlled by the fractionation of olivine, clinopyroxene and magnetite.

Overall, the composition of unaltered AND-2A glass is very similar to the mafic-intermediate (41-48 wt. % SiO<sub>2</sub>) portion of the EVP compositional spectrum (Fig. 14 & 15).

**Table 3:** Representative major and trace elemental compositions for glass shards from the AND-2A core.

Sample	354.05-K	355.63-L	385.38-1	409.46-F	419.56-G	426.28-E	446.85-C	534.77-M
Model Age (Ma)	15.91	15.91	16.07	16.20	16.25	16.28	16.39	16.85
wt% oxide								
SiO <sub>2</sub>	46.73	46.40	45.26	44.85	45.46	44.46	46.45	45.49
TiO <sub>2</sub>	4.03	3.03	3.44	3.91	3.22	4.68	4.79	4.78
Al <sub>2</sub> O <sub>3</sub>	15.41	15.47	14.07	15.85	16.18	14.57	12.43	13.79
FeO	12.52	10.65	12.33	11.66	9.08	12.37	15.09	13.28
MnO	0.24	0.19	0.17	0.21	0.16	0.18	0.31	0.21
MgO	5.21	5.72	6.52	6.46	6.27	5.73	4.13	4.77
CaO	9.39	11.48	12.08	10.98	12.31	10.83	9.41	9.93
Na <sub>2</sub> O	3.91	3.81	3.08	3.44	3.74	3.74	3.62	4.19
K <sub>2</sub> O	1.42	1.74	0.87	1.10	1.61	1.69	1.80	1.90
P <sub>2</sub> O <sub>5</sub>	0.77	0.74	0.67	0.65	0.83	1.29	1.43	0.98
SO <sub>2</sub>	0.03	0.06	0.03	0.02	0.00	0.03	0.00	-0.05
Cl	0.07	0.08	0.05	0.06	0.09	0.09	0.08	0.06
SrO	-0.16	-0.13	-0.15	-0.15	-0.16	-0.19	-0.17	-0.11
BaO	0.04	0.10	-0.04	0.08	0.08	0.06	0.09	0.14
Total	99.60	99.33	98.38	99.11	98.85	99.52	99.45	99.35
Mg-no.	42.57	48.93	48.53	49.70	55.21	45.23	32.82	39.04
ne	2.37	9.16	3.38	4.96	10.65	6.58	0.00	7.58
di	17.22	25.93	27.58	20.79	26.65	22.24	20.68	24.26
ol	6.47	4.56	6.78	7.01	3.08	3.71	1.54	1.84
Q	0.00	0.00	0.00	0.00	0.00	0.00	0.00	0.00
hy	0.00	0.00	0.00	0.00	0.00	0.00	3.59	0.00
Li	4.10	5.54			3.24		9.92	6.08
Be	<1.18	4.66			1.87		<0.00	<0.00
B	22.28	8.48			7.23		22.30	8.07
Sc	21.23	33.47			34.40		29.17	29.91
Ti	20954.38	16343.26			18345.35		27541.30	26827.92
V	268.07	275.04			290.93		243.30	349.43
Cr	16.32	108.95			122.20		<7.37	25.13
Co	34.24	31.38			34.41		32.95	34.16
Ni	13.83	29.38			49.36		<0.94	12.56
Zn	125.85	78.73			88.43		123.91	101.80
Rb	28.32	42.52			36.18		35.42	37.56
Sr	792.52	557.92			790.68		566.20	638.21
Y	22.30	28.55			25.71		40.06	32.48
Zr	199.64	237.20			229.16		289.52	342.22
Nb	50.25	75.88			65.20		61.17	79.81
Cs	0.29	0.53			0.43		0.52	0.31
Ba	441.96	434.80			470.27		613.36	454.94
La	41.44	55.91			52.18		59.45	65.44
Ce	84.25	99.91			100.62		116.09	119.79
Pr	10.40	11.74			11.20		14.62	13.82
Nd	39.41	47.08			48.30		70.59	58.04
Sm	6.28	9.41			8.64		13.96	9.62
Eu	3.09	2.94			2.96		5.06	3.13
Gd	7.46	6.73			6.40		11.92	9.56
Tb	0.88	1.01			1.03		2.06	1.32
Dy	5.24	5.96			5.18		9.10	7.50
Ho	0.99	1.27			0.91		1.77	1.18
Er	1.77	2.51			2.79		4.23	3.90
Trn	0.22	0.40			0.31		0.64	0.49
Yb	2.38	2.66			2.65		4.53	3.38
Lu	0.33	0.43			0.30		0.54	0.39
Hf	4.59	5.68			5.70		6.73	8.15
Ta	2.92	4.06			3.42		3.55	4.60
Pb	2.96	3.16			2.35		3.39	2.43
Th	3.85	6.45			5.05		4.32	6.68
U	1.43	1.77			1.71		1.31	2.21
AI	33.27	32.81	32.76	34.39	32.93	33.73	31.28	32.07
CCPI	76.88	74.68	82.69	79.97	74.15	76.92	78.03	74.76

Model ages were determined using the AND-2A age model from Di Vincenzo *et al.* (2010). Major (wt. %) and trace elements (ppm) are normalized to 100% anhydrous with total Fe as FeO<sup>t</sup> (FeO = 0.9 Fe<sub>2</sub>O<sub>3</sub>). CIPW values for ne, di, ol, hy, and Q are cation normative. Mg-number is the atomic percent Mg<sup>2+</sup>/(Mg<sup>2+</sup> + Fe<sup>2+</sup>). AI is the Ishikawa alteration index from Ishikawa *et al.* (1976) and CCPI is the chlorite-carbonate-pyrite index from Large *et al.* (2001). Trace element data with errors >15% are tagged in yellow.

Representative major and trace elemental compositions for glass shards from the AND-2A core, continued

Sample Model Age (Ma)	539.22-A 16.88	577.50-C 17.08	592.76-I 17.16	596.77-K 17.18	640.82-G 17.41	642.38-A 17.42	644.25-I 17.43	649.67-C 17.45
SiO <sub>2</sub>	46.56	46.84	45.33	46.22	45.72	45.23	45.88	46.07
TiO <sub>2</sub>	3.15	3.04	4.12	3.87	3.29	4.35	4.31	3.84
Al <sub>2</sub> O <sub>3</sub>	15.80	15.78	16.14	14.82	15.39	14.37	14.05	15.63
FeO	9.74	10.89	10.79	12.49	10.57	12.36	13.26	10.71
MnO	0.12	0.19	0.20	0.22	0.18	0.19	0.23	0.14
MgO	6.23	5.99	4.91	5.27	7.33	5.21	4.84	5.82
CaO	11.33	10.25	10.23	10.16	11.46	10.97	9.64	10.59
Na <sub>2</sub> O	3.77	3.76	4.16	3.98	3.50	3.87	3.94	3.60
K <sub>2</sub> O	1.59	1.75	2.23	1.66	1.06	1.89	1.54	1.40
P <sub>2</sub> O <sub>5</sub>	0.72	0.85	1.10	0.82	0.66	1.06	1.24	0.81
SO <sub>2</sub>	0.00	-0.02	-0.04	-0.01	-0.02	-0.04	0.08	0.00
Cl	0.07	0.06	0.15	0.07	0.04	0.08	0.07	0.07
SrO	-0.12	-0.16	-0.12	-0.16	-0.19	-0.14	-0.13	-0.09
BaO	0.09	0.04	-0.03	0.00	0.07	0.09	0.16	-0.03
Total	99.06	99.26	99.17	99.43	99.07	99.49	99.11	98.56
Mg-no.	53.28	49.54	44.76	42.93	55.31	42.90	39.41	49.21
ne	7.56	5.71	10.12	6.41	5.93	8.28	2.68	3.31
di	24.17	19.60	20.08	22.20	23.69	25.41	19.40	20.28
ol	4.81	7.75	2.74	5.08	7.96	2.29	5.15	4.91
Q	0.00	0.00	0.00	0.00	0.00	0.00	0.00	0.00
hy	0.00	0.00	0.00	0.00	0.00	0.00	0.00	0.00
Li	4.08	5.41	8.80	6.77	3.14	7.06		2.37
Be	4.20	4.67	4.48	<0.00	<0.00	<1.79		4.10
B	11.76	20.63	6.66	5.98	8.27	12.77		<8.45
Sc	29.58	26.72	24.59	26.67	31.84	27.14		30.48
Ti	16772.91	16458.45	22043.62	21678.01	18563.02	24365.65		23112.49
V	245.97	237.10	259.58	320.94	293.27	329.65		338.23
Cr	121.41	94.19	48.95	36.60	143.59	60.23		<6.64
Co	31.82	33.71	29.81	37.73	41.10	34.98		43.39
Ni	40.21	38.08	27.40	12.38	72.22	18.92		27.53
Zn	67.99	88.56	83.28	114.67	91.46	113.75		124.01
Rb	38.05	27.30	50.12	30.06	14.73	36.24		31.25
Sr	594.57	648.93	894.15	535.09	682.18	731.76		882.22
Y	23.69	25.93	29.87	27.10	23.89	33.34		30.78
Zr	270.63	239.10	327.92	249.39	218.22	329.89		299.67
Nb	55.79	52.73	85.37	61.69	42.54	72.69		60.48
Cs	0.31	0.28	0.60	0.28	0.27	0.35		0.21
Ba	323.28	487.79	566.54	370.76	238.23	457.45		569.57
La	45.61	48.56	69.23	47.67	37.22	63.14		56.88
Ce	85.25	88.86	122.56	97.65	68.72	119.38		106.89
Pr	9.34	10.03	14.72	10.76	8.42	13.97		12.66
Nd	41.21	43.79	60.32	49.40	35.31	61.98		59.35
Sm	6.76	8.87	11.71	6.30	7.41	11.92		12.37
Eu	1.89	2.80	3.56	3.27	2.14	3.46		4.06
Gd	5.68	7.37	10.48	8.18	7.12	10.90		8.42
Tb	0.93	0.93	1.35	1.15	1.03	1.15		1.04
Dy	4.15	6.14	6.26	6.31	5.05	7.30		7.25
Ho	0.79	1.10	1.28	1.04	0.86	1.46		1.49
Er	2.16	1.77	3.45	3.28	2.75	2.98		3.25
Tm	0.31	0.33	0.44	0.28	0.45	0.46		0.47
Yb	2.05	2.93	3.11	2.65	2.96	1.57		3.18
Lu	0.29	0.31	0.38	0.36	0.24	0.34		0.46
Hf	5.12	5.22	7.80	7.14	6.56	7.92		5.48
Ta	2.82	3.02	4.75	3.52	2.43	4.48		3.91
Pb	2.14	2.01	3.47	2.40	1.90	2.34		3.05
Th	4.11	4.36	7.55	4.56	3.54	6.69		4.72
U	1.22	1.30	1.88	1.35	0.80	1.79		1.20
Al	34.13	35.60	33.14	32.89	35.95	32.35	31.95	33.72
CCPI	74.87	75.39	71.08	75.89	79.69	75.29	76.77	76.80

Representative major and trace elemental compositions for glass shards from the AND-2A core, continued

Sample Model Age (Ma)	650.67-B 17.46	654.85-G 17.48	661.67-D 17.52	721.67-F 18.19	740.89-L 18.29	742.00-T 18.29	763.52-U 18.41	764.44-I 18.41
SiO <sub>2</sub>	45.65	46.63	45.99	45.03	44.50	44.89	45.43	45.66
TiO <sub>2</sub>	4.55	3.26	4.01	3.99	3.11	3.15	3.46	3.32
Al <sub>2</sub> O <sub>3</sub>	14.64	14.27	14.83	15.58	16.73	16.22	16.41	15.91
FeO	12.56	10.26	11.21	11.34	9.10	10.39	10.25	11.12
MnO	0.20	0.15	0.15	0.18	0.17	0.19	0.22	0.27
MgO	4.99	6.75	5.74	6.44	5.89	5.25	4.65	3.80
CaO	9.14	13.12	10.96	10.81	11.33	10.57	8.83	8.15
Na <sub>2</sub> O	3.71	3.14	4.01	3.49	3.84	4.06	4.50	5.11
K <sub>2</sub> O	1.86	1.42	1.72	1.39	1.65	1.65	2.19	2.72
P <sub>2</sub> O <sub>5</sub>	1.05	0.65	1.00	0.73	0.75	0.71	1.10	1.24
SO <sub>2</sub>	-0.01	-0.02	0.00	-0.02	0.06	0.07	0.05	0.06
Cl	0.11	0.06	0.22	0.05	0.06	0.10	0.11	0.16
SrO	-0.10	-0.17	-0.15	-0.21	-0.12	-0.06	-0.11	-0.11
BaO	0.10	0.02	-0.01	-0.06	0.16	0.07	0.15	0.01
Total	98.45	99.55	99.68	98.76	97.24	97.25	97.23	97.41
Mg-no.	41.47	53.99	47.71	50.32	53.58	47.39	44.71	37.85
ne	1.94	6.30	7.97	5.51	11.11	10.47	9.53	14.15
di	17.04	32.40	24.55	21.19	22.76	21.93	15.21	16.35
ol	4.89	3.17	3.17	6.22	4.25	4.72	5.01	4.19
Q	0.00	0.00	0.00	0.00	0.00	0.00	0.00	0.00
hy	0.00	0.00	0.00	0.00	0.00	0.00	0.00	0.00
Li	6.81	6.17	7.79	5.83	3.52	8.57	14.89	5.36
Be	<4.94	<0.00	<0.00	<0.00	<3.33	8.23	<2.87	<0.00
B	14.95	33.06	<3.40	<2.38	21.59	2.40	16.46	9.04
Sc	23.44	28.85	28.72	26.34	26.32	26.86	18.41	10.87
Ti	23241.04	16036.27	23754.71	22209.65	17247.32	17230.16	13233.25	9832.47
V	325.01	259.35	328.27	298.79	249.03	265.24	182.19	106.99
Cr	20.24	137.31	73.07	83.61	95.89	63.45	182.08	17.22
Co	36.04	37.93	40.30	39.00	31.02	32.35	23.59	15.31
Ni	17.99	72.36	29.34	43.48	50.12	27.76	19.15	5.85
Zn	112.85	71.29	104.72	103.33	78.90	86.58	66.99	40.54
Rb	32.95	36.72	32.91	25.33	35.23	34.32	62.17	52.31
Sr	635.31	602.34	858.67	775.71	787.18	686.71	522.72	399.12
Y	32.33	23.65	27.69	26.38	25.40	28.64	27.68	19.93
Zr	339.91	264.47	306.79	266.06	244.02	237.95	335.96	252.26
Nb	67.90	44.33	71.27	55.88	64.42	61.93	64.06	53.51
Cs	0.37	0.53	0.37	0.28	0.40	0.42	1.08	0.68
Ba	406.97	339.92	459.99	319.99	420.55	393.83	434.31	467.10
La	63.05	37.26	61.78	46.48	46.49	46.38	54.30	44.54
Ce	113.70	71.09	122.57	89.12	90.92	84.37	93.06	76.25
Pr	15.42	8.92	15.49	10.03	9.83	9.83	10.77	8.32
Nd	62.85	39.53	56.26	48.39	43.08	41.87	47.24	33.08
Sm	15.86	8.61	10.78	9.21	7.80	9.52	8.58	5.70
Eu	3.72	2.25	4.42	2.77	2.38	2.83	2.31	1.90
Gd	8.63	6.81	8.99	6.40	5.62	5.91	6.40	4.84
Tb	1.41	0.85	1.11	1.02	0.86	0.98	0.89	0.73
Dy	7.52	4.39	6.42	4.99	4.75	4.84	5.01	3.12
Ho	1.25	1.03	1.46	1.08	0.94	0.87	1.16	0.72
Er	4.08	2.29	3.53	2.80	3.01	2.84	3.22	1.67
Tm	0.39	0.25	0.48	0.41	0.47	0.31	0.47	0.27
Yb	3.87	2.04	1.52	2.28	2.07	1.84	2.68	1.83
Lu	0.49	0.32	0.51	0.30	0.41	0.27	0.32	0.29
Hf	6.03	5.29	8.18	6.75	6.15	4.06	6.43	5.15
Ta	4.45	2.52	4.07	3.12	3.29	3.59	3.87	2.68
Pb	2.50		2.98	1.68	2.76	3.23	6.97	5.46
Th	5.18	3.96	4.87	4.23	4.70	5.27	7.24	5.48
U	1.36	1.00	1.40	1.23	1.40	1.51	1.85	1.48
Al	34.76	33.44	33.25	35.40	33.21	32.04	33.90	32.93
CCPI	75.92	78.85	74.75	78.46	73.21	73.26	69.03	65.57

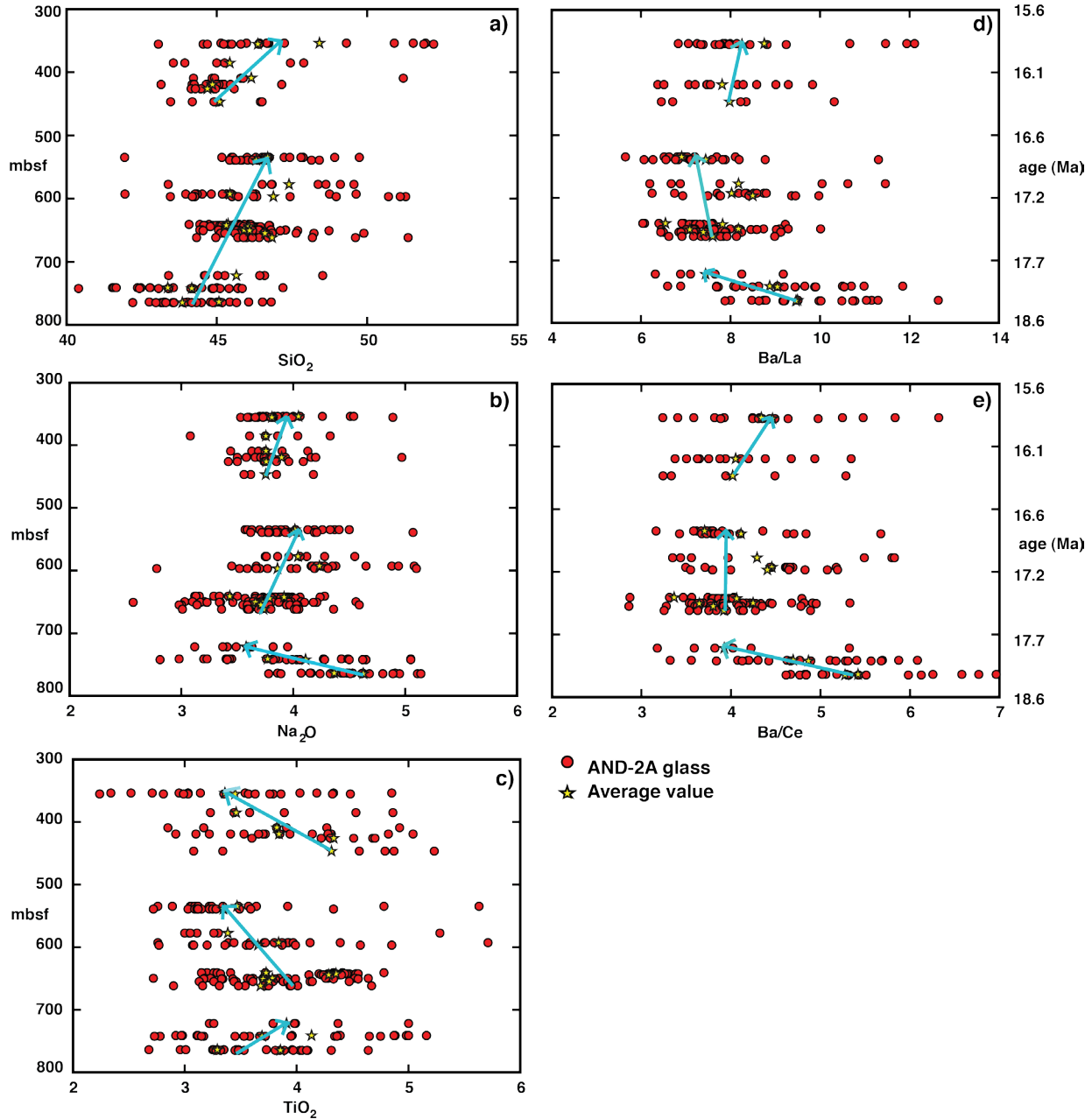


**Figure 13:** Compositional variations with depth (mbsf) for fresh glass shards, filtered for alteration as demonstrated in the previous diagrams with an average value (star) shown for each sample "layer." a)  $\text{SiO}_2$  versus depth. Note that overall, AND-2A glass becomes slightly more felsic up-section, however, there is a jog between 534 and 447 mbsf, where  $\text{SiO}_2$  content reverts back to a slightly more mafic composition and then begins to become more felsic up-section again. b)  $\text{Na}_2\text{O}$  versus depth. c)  $\text{TiO}_2$  versus depth. d)  $\text{Ba/La}$  versus depth. e)  $\text{Ba/Ce}$  versus depth.

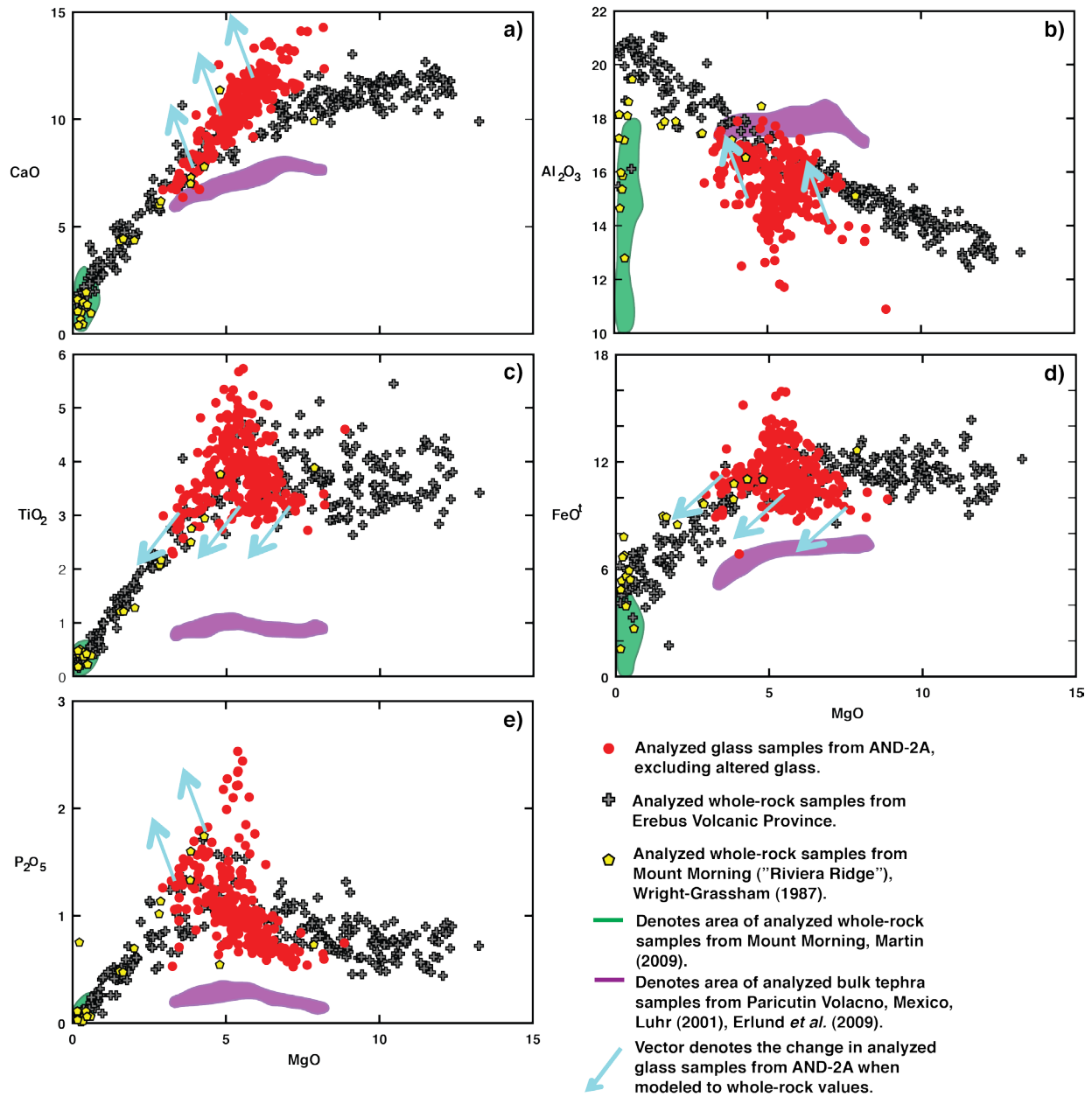


**Figure 14:** Harker variation diagrams for fresh analyzed AND-2A glass shards compared with the Erebus Volcanic Province whole-rock data and whole-rock data from Mount Morning (Martin, 2009) and Mount Morning at "Riviera Ridge" (Wright-Grassham, 1987), and bulk tephra data from Parícutin Volcano, Mexico (Luhr, 2001; Erlund *et al.*, 2009). The vectors denote the change in analyzed glass shard composition in AND-2A when "modeled" to whole-rock composition. The whole-rock composition of the glass was estimated by adding back mineral compositions using mass balance calculations for plagioclase, clinopyroxene, apatite, magnetite, and olivine analyzed from Mount Morning (Wright-Grassham, 1987) and Mount Sidley (Panter, 1995; Panter *et al.*, 1997) found in similar overall whole-rock compositions relative to AND-2A glass. Proportions of these minerals to be added back to AND-2A glass compositions were determined by visual estimation of the volume % of minerals per each grain. Overall, AND-2A glass (especially whole-rock equivalents) is very similar to mafic whole-rock data from the EVP and Mount Morning at "Riviera Ridge." The most striking differences are that AND-2A glass shows higher amounts of CaO and  $\text{P}_2\text{O}_5$  relative to a given MgO content when compared with the EVP and Mount Morning data.

However, there are a few marked differences. AND-2A glass shows higher concentrations of CaO, TiO<sub>2</sub>, and P<sub>2</sub>O<sub>5</sub> and lower concentrations of Al<sub>2</sub>O<sub>3</sub> relative to EVP compositions at the same MgO levels (Fig. 14). The difference is enhanced further for CaO and P<sub>2</sub>O<sub>5</sub> when the composition of the glass is adjusted to approximate whole-rock compositions. Another notable difference is the linear array displayed by CaO with decreasing MgO content of the glass, which contrasts with the curvilinear trend shown by EVP lavas. Mafic compositions from Middle Miocene deposits at Mount Morning's Riviera Ridge (Wright-Grassham, 1987) closely match AND-2A glass and published data from the rest of the EVP as well.

#### *Trace and Rare Earth Elements*

Variations in the trace element compositions of AND-2A glass are shown in Figure 16. Overall, incompatible elements in AND-2A glass, such as Rb, Th, Y, La, and Nb decrease with increasing differentiation, while compatible elements such as Sc and Ni generally decrease with increasing differentiation.

The trace element composition of AND-2A glass is remarkably similar to mafic-intermediate EVP whole rock compositions (41-48 wt. % SiO<sub>2</sub>) and specifically the Early to Middle Miocene mafic samples from Mount Morning's Riviera Ridge (Wright-Grassham, 1987). The only major difference is the markedly lower amounts of Ni in AND-2A glass relative to EVP samples at the same level of Zr concentrations (Fig. 16g). This is most likely an artifact of comparing whole rock and glass compositions, in which whole rock analyses contain olivine ( $K_D$  Ni<sub>olivine</sub> = 32; Adam and Green, 2006), while the glass does not.

The AND-2A glass is light rare earth element (LREE) enriched relative to heavy rare earth elements (HREE) (Fig. 17a) with La<sub>N</sub>/Yb<sub>N</sub> ratios of about 10 or greater, which increase

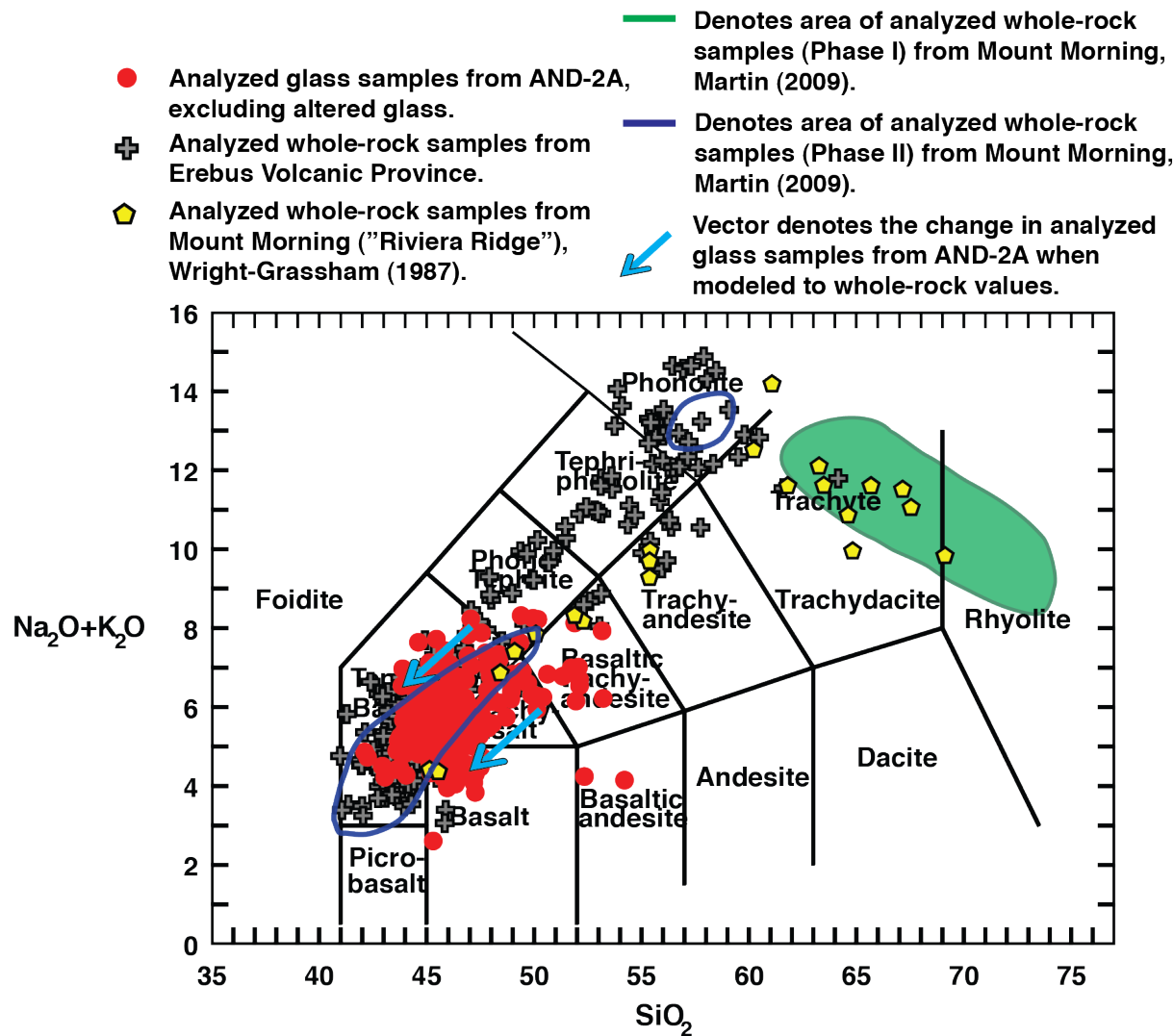


**Figure 15:** Combined alkalis versus silica (TAS) diagram after Le Bas *et al.* (1986) for analyzed AND-2A glass compared with EVP whole-rock data and whole-rock data from Mount Morning (Martin, 2009) and Mount Morning at "Riviera Ridge" (Wright-Grassham, 1987). The vector denotes the change in glass composition in AND-2A when "modeled" to equivalent whole-rock compositions. AND-2A glass does not display evolved compositions such as that seen in Mount Morning whole-rock data, but is very similar to mafic whole-rock data from the EVP and Mount Morning at "Riviera Ridge."

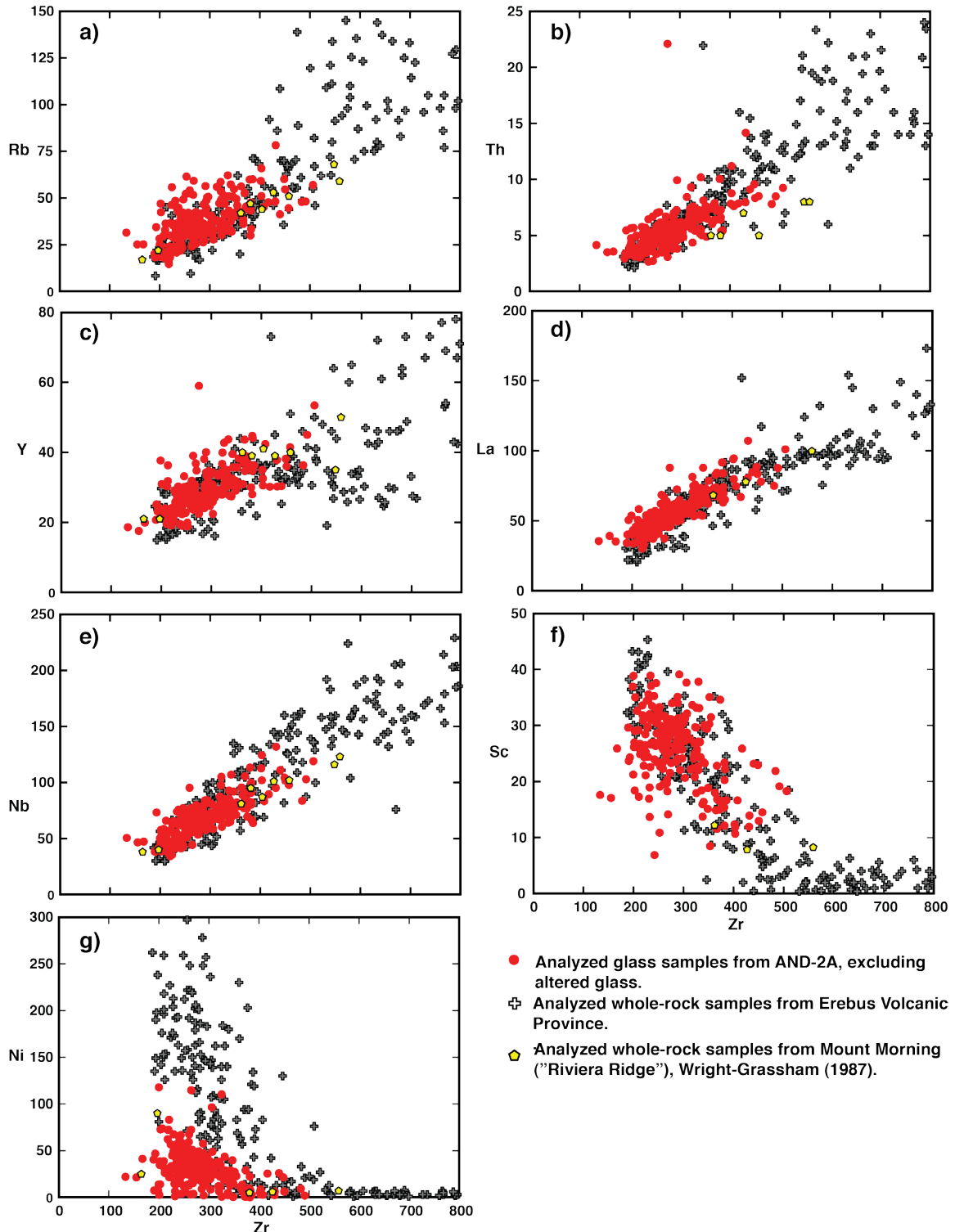


**Figure 16:** Zr versus Rb, Th, Y, La, Nb, Sc, and Ni for AND-2A glass (fresh) compared with whole-rock data from the EVP and mafic whole-rock data from Mount Morning (Wright-Grassham, 1987). Overall, there are remarkable similarities between AND-2A analyzed glass, Mount Morning and EVP data, with the only major difference being that AND-2A and mafic Mount Morning data display greater concentrations of Ni.

with differentiation (Fig. 18a). Also, AND-2A glass display a classic highly incompatible element enriched ‘hump-shaped’ pattern on multi-element plots (Fig. 17b). Also displayed in the patterns are prominent negative anomalies at Pb and K (Fig. 17b). These characteristics are typical of many intraplate ocean island basalts (OIB) and are characteristic of Cenozoic alkaline rocks from the EVP and throughout the rest of the West Antarctic rift system. A less prominent negative anomaly exists for Sr while a slightly positive anomaly exists for P (Fig. 17b), the latter being consistent with higher concentrations of  $P_2O_5$  (Fig. 14e). The slight positive Eu anomaly on the REE diagram and the K, Sr and P anomalies on multi-element plots are evaluated with respect to sample differentiation in Figure 18. Eu/Eu\* ratios are  $\geq 1.0$  (i.e. anomalies that are flat or slightly positive) and remain relatively constant with differentiation (Fig. 18b), while Sr/Sr\* and P/P\* ratios decrease with differentiation (Fig. 18c, e). K/K\* ratios are  $\leq 1$  and remain relatively constant with differentiation (Fig. 18d). Overall, the AND-2A glasses have higher Eu/Eu\* and P/P\* ratios relative to EVP whole-rock data at low Zr concentrations (Fig. 18b, e). A notable compositional difference within the core is found when comparing samples between depths 700 and 800 mbsf with the rest of the core samples. These deeper samples are generally more mafic compared to the upper portion of the core, displaying a distinct decrease in  $Na_2O$  and an increase in  $TiO_2$  up-section (Fig. 13b, c). There is also a decrease in Ba/LREE ratios up-section to  $\sim 500$  mbsf, followed by an increase further up-section (Fig. 13d, e). In addition, the glass deeper in the core shows overall lower concentrations in trace elements and higher Rb/Zr ratios relative to samples from the upper portion of the core (Fig. 19c). It is also important to note that samples between 700 and 800 mbsf have the highest proportions of green glass and scoria relative to the other samples in the core (Table 2). The presence of green glass may be a

visual confirmation of differences in composition while the increase in scoria content may indicate that this earlier activity was also more explosive.

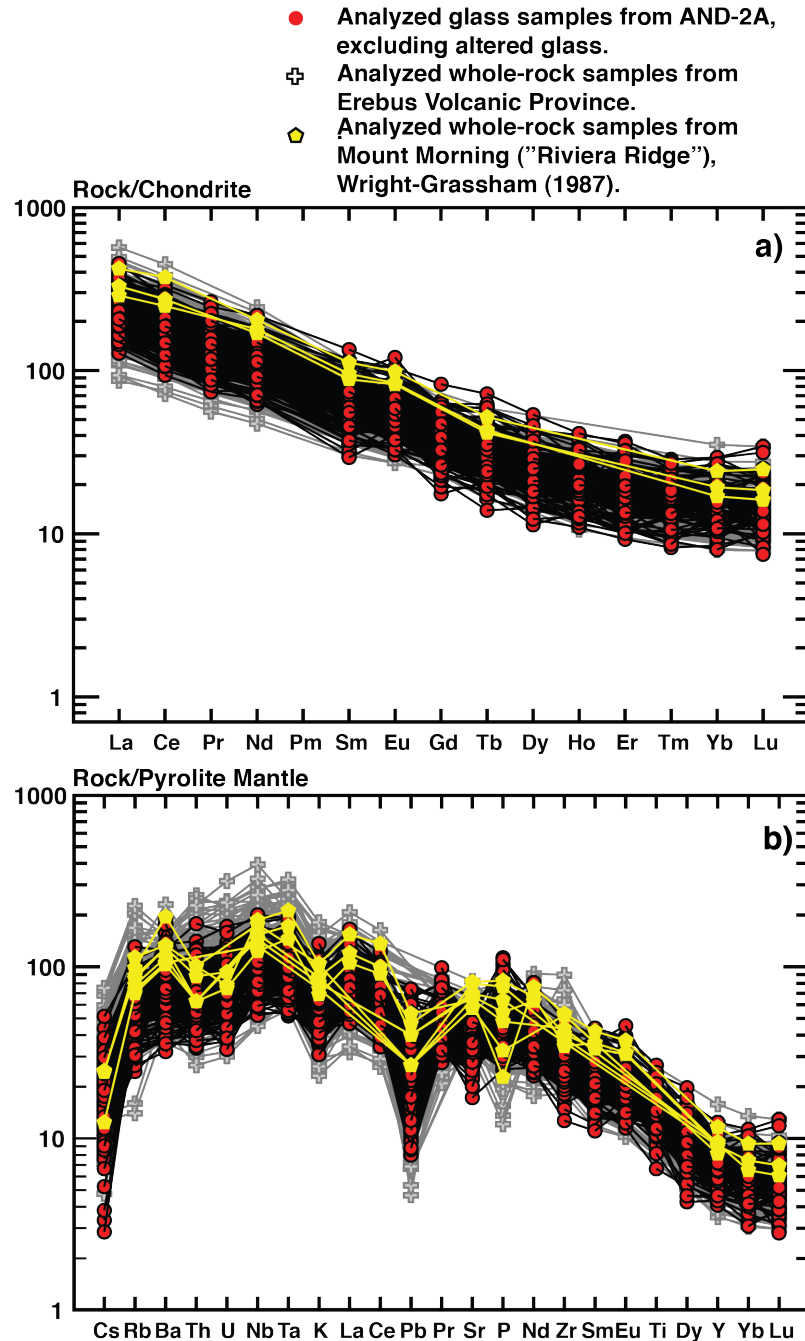


**Figure 17:** REE and Multi-element diagrams. a) REE diagram from Sun and McDonough (1989) normalized to chondrites showing unaltered glass from the AND-2A core compared with whole-rock data from the EVP and mafic whole-rock data from Mount Morning at "Riviera Ridge." More evolved whole-rock compositions from Mount Morning were grouped with the EVP samples. Overall, AND-2A analyzed glass samples and EVP and Mount Morning samples are very similar to each other. Note that EVP whole-rock samples display negative Eu anomalies not seen in AND-2A (or mafic Mount Morning) data. b) Multi-element diagram from McDonough and Sun (1995) normalized to pyrolite mantle for unaltered glass from the AND-2A core compared with whole-rock data from the EVP and mafic whole-rock data from Mount Morning at "Riviera Ridge." More evolved whole-rock compositions from Mount Morning were grouped with the EVP samples. Overall, AND-2A glass shards and mafic whole-rock data from Mount Morning and the EVP are very similar.

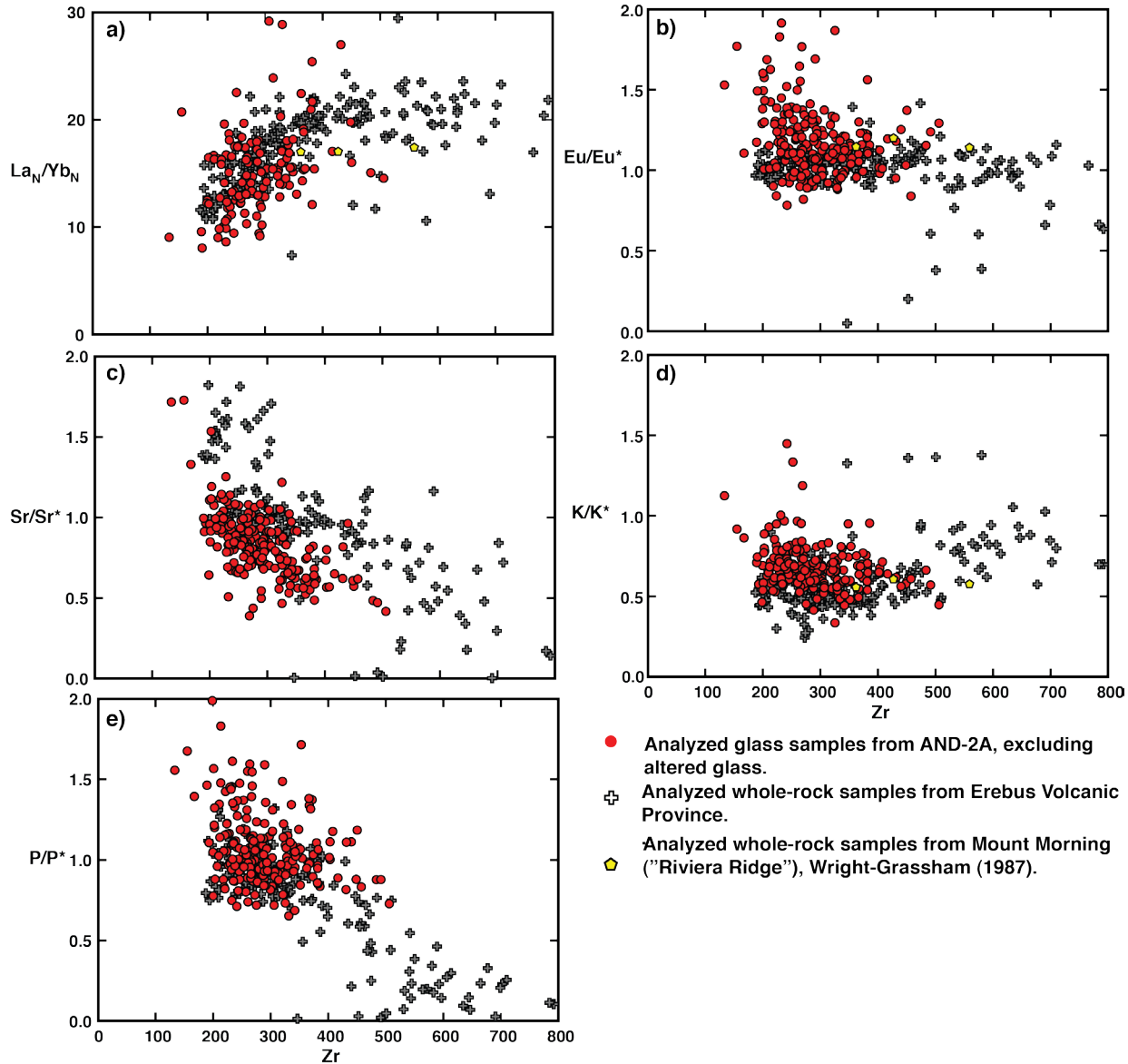


**Figure 18:** The slight positive Eu anomaly on the REE diagram and the K, Sr and P anomalies on multi-element plots are evaluated with respect to sample differentiation. Zr versus  $\text{La}_N/\text{Yb}_N$ ,  $\text{Eu}/\text{Eu}^*$ ,  $\text{Sr}/\text{Sr}^*$ ,  $\text{K}/\text{K}^*$  and  $\text{P}/\text{P}^*$  for glass, compared with whole-rock data from the EVP and mafic whole-rock data from Mount Morning at "Riviera Ridge" (Wright-Grassham, 1987).  $\text{Eu}^*$ ,  $\text{Sr}^*$ ,  $\text{K}^*$ , and  $\text{P}^*$  are normalized values calculated by log interpolation from adjacent REEs. The AND-2A analyzed glass is very similar to whole-rock data from the EVP and whole-rock data from Mount Morning. Major differences include: AND-2A glass contains higher  $\text{Eu}/\text{Eu}^*$  ratios overall (indicating slight positive anomaly on REE diagrams) compared to EVP and Mount Morning data, AND-2A glass contains a lower  $\text{Sr}/\text{Sr}^*$  ratio with a given Zr content relative to EVP whole-rock data (though overall EVP data suggests a more negative Sr anomaly on spider diagrams) and decreases overall as the samples evolve (indicating plagioclase fractionation). AND-2A glass contains a higher  $\text{P}/\text{P}^*$  ratio with a given Zr content relative to EVP whole-rock data indicating a slight positive P anomaly on spider diagram. For the EVP, Mount Morning and AND-2A data,  $\text{K}/\text{K}^*$  ratios are generally less than 1, indicating a slight negative K anomaly on multi-element diagrams, a common feature of alkaline magmas erupted in Antarctica and continental areas of the southwest Pacific.

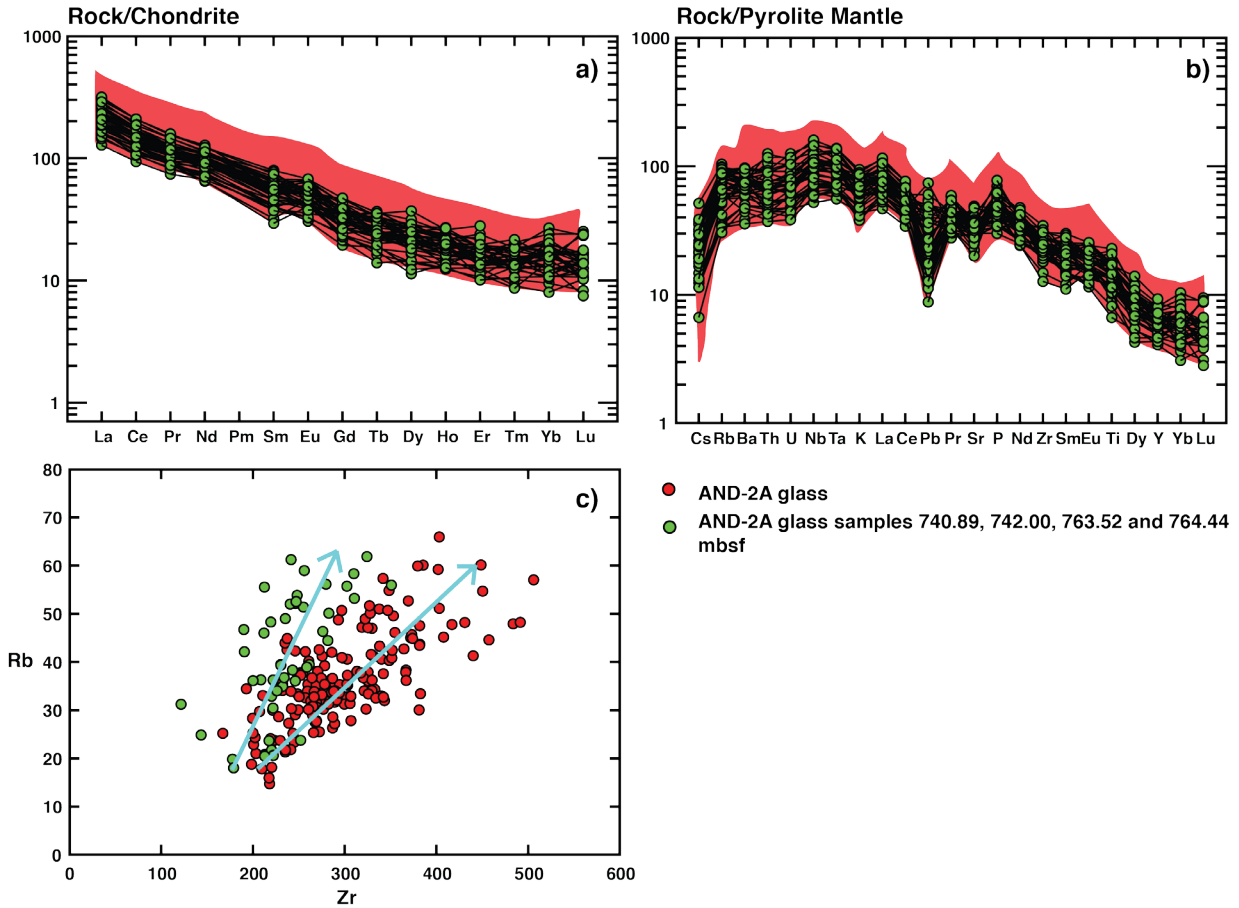
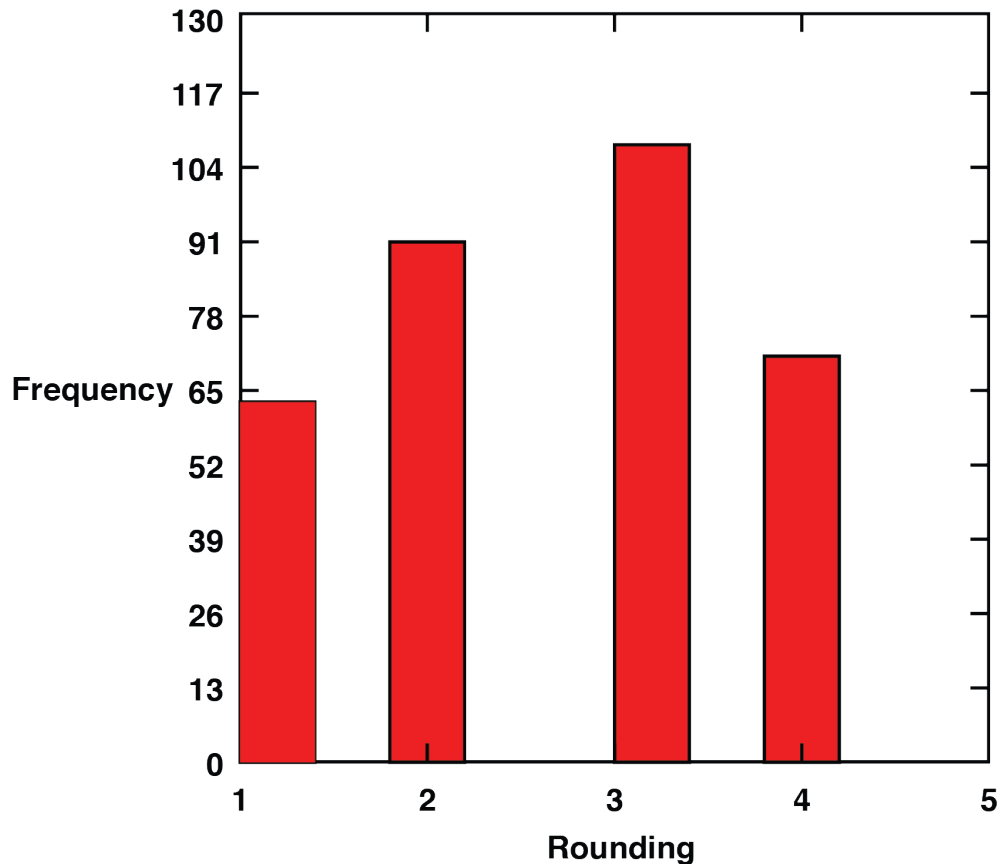


Figure 19: Shows diagrams that highlight compositional differences for samples 740.89, 742.00, 763.52 and 764.44 mbsf compared to the rest of the AND-2A core. a) REE diagram from Sun and McDonough (1989) normalized to chondrites. b) Multi-element diagram from McDonough and Sun (1995) normalized to pyrolite mantle. From these diagrams it is clear that these samples are significantly more mafic than the rest of AND-2A sample layers. c) Zr vs. Rb plot shows that these samples have higher amounts of Rb relative to Zr.

## DISCUSSION

### Mode of Deposition

Since the majority of the glass is found dispersed within sediments and not as primary ash layers, it is necessary to consider possible mechanisms for how the glass was introduced into the basin. The origin of the glass from volcanoes in the EVP is confirmed by their matching geochemistry. Moreover the relatively restricted range in basaltic compositions in all samples strongly suggests that they were derived from very similar if not the same volcanic source with minimal reworking. A primary origin of the glass as fallout from an eruption column is also supported chemically by their mostly unaltered condition and physically by their overall angularity. Based on visible estimates made from a modified point counting technique (Table 2), glass grains show a range in morphology, from highly angular to rounder forms (Fig. 20). It is important to note that the angularity is controlled, to a large extent, by how vesicular a grain is. For example, highly vesicular grains often display extremely well preserved and delicate bubble walls that often occur along the perimeter of the grain, while less vesicular grains typically do not, and thus, are less angular. This can explain why the four samples at greater than 740 mbsf show higher amounts of rounding and a lower percentage of vesicles (Table 2; Fig. 21). In order to investigate this issue in a more quantitative fashion, digital image processing techniques were conducted on 7 samples (78 grains total) within a single glacimarine cycle (Sequence 32; Fielding *et al.*, 2011). All grains in Sequence 32 have rounding (R) values much less than 1, and in many cases display R-values less than 0.1 (Fig. 22). Glass shards from a primary tephra deposit on nearby Mount Erebus that contains a mixture of both blocky grains with low vesicularity and frothy grains with high vesicularity are also shown (Fig. 22; Panter and Winter, 2008). These primary ash fall grains fit well with the low R-values found in AND-2A glass and



**Figure 20:** Frequency histogram showing relative rounding of glass grains for all AND-2A samples studied based on visual estimates (see Appendix A) into angular, sub-angular, sub-rounded and rounded. The highest frequency of grains occurs in the sub-rounded category.

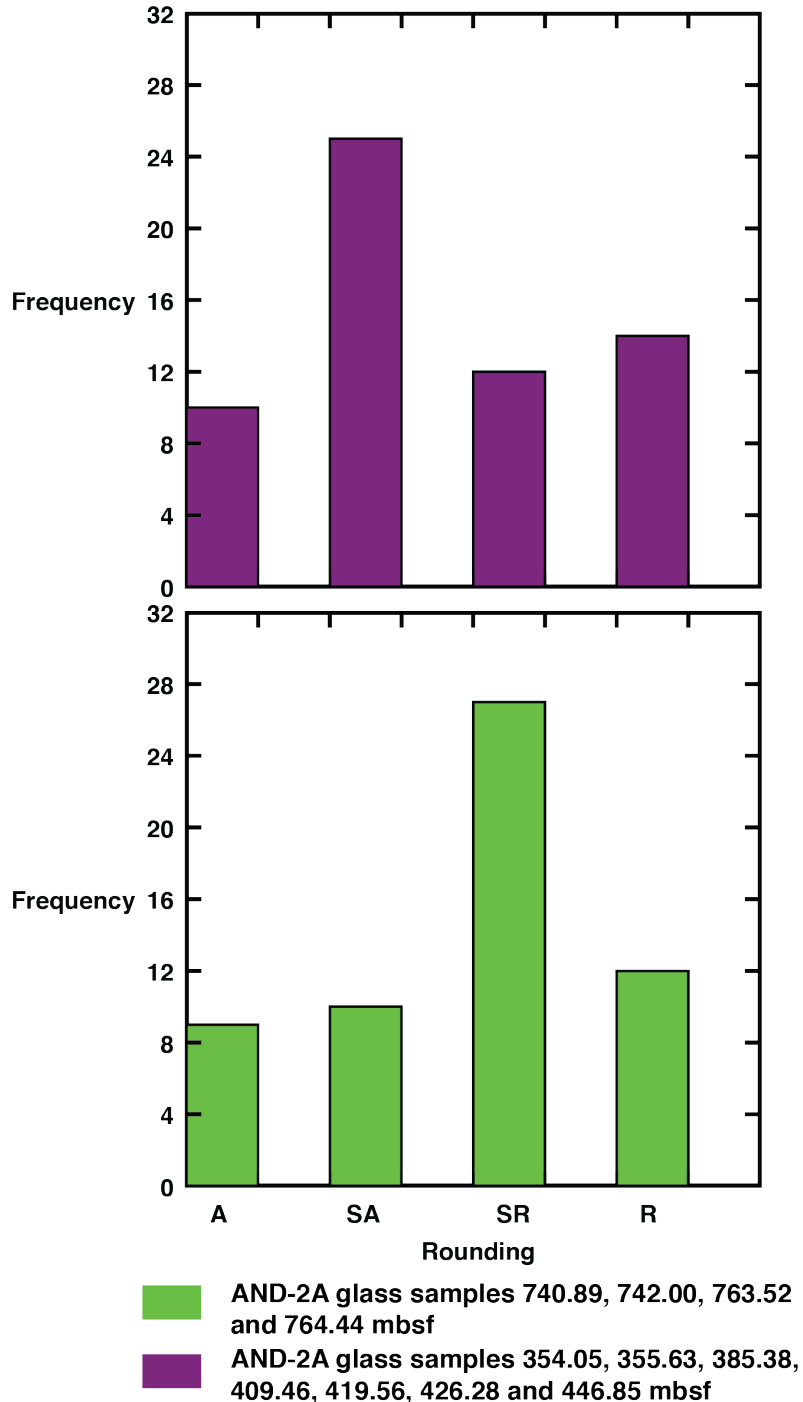


**Figure 21:** Frequency histograms showing variations in the amount of rounding for glass grains throughout the AND-2A core based on visual estimations during modified point counting (see Table 2, Appendix A). a) AND-2A samples 354.05, 355.63, 385.38, 406.46, 419.56, 426.28 and 446.85 mbsf. b) AND-2A samples 740.89, 742.00, 763.52 and 764.44 mbsf. The four samples between 740.89 and 764.44 mbsf have a higher frequency of more rounded grains in comparison with the samples seven samples between 354.05 and 446.85 mbsf.

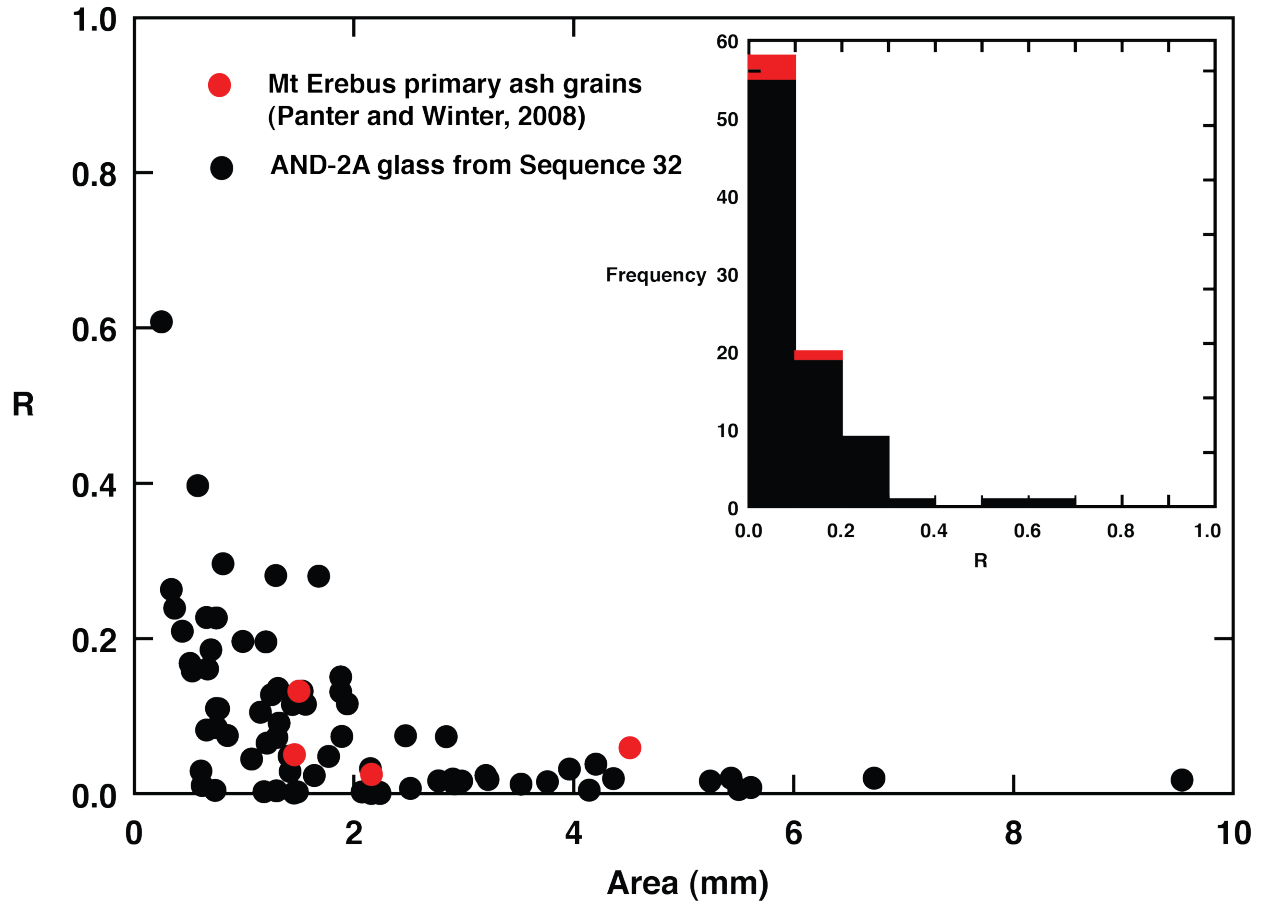


**Figure 22:** Sphericity comparison plots. Area (mm) of glass grains versus R-values ( $4\pi A/P^2$ , where A = Area and P = Perimeter; Manga *et al.*, 2010) for glass grains studied in Sequence 32 (samples 640.82, 642.38, 644.25, 649.67, 650.67, 654.82 and 661.67 mbsf), where 1 is a perfect sphere, determined using digital imaging processing techniques (see Appendix B for tutorial). Sequence 32 glass grains are compared with glass grains from Mt. Erebus primary ash (Panter and Winter, 2008) using the same techniques. Overall the glass grains (including primary glass from Mt. Erebus) have very low R-values indicating that they are highly angular.

provide strong evidence to support the idea that the glass was delivered directly into the water column as ash fall before being incorporated within basin sediments.

Grain size can also be used to help constrain their origins by serving as an indication of how far grains were transported before deposition. Volcanic ash can sometimes travel up to 100's of thousands of kilometers downwind from their source, depending on wind speed, volume of ash erupted, and the height of the eruption column. However, according to Johnston (1997), the size of ash particles decreases exponentially with increasing distance from their source, and the range of grain size of the volcanic glass also decreases. Glass and scoria in AND-2A that are up to several millimeters in diameter could not have been transported very far from their source, as sediments will typically fine downwind into silt size ( $\mu\text{m}$ ) particles when experiencing a long transport of 100's of kilometers or more (Atkins and Dunbar, 2009). Present-day wind and ice-flow directions in this area are from the south (Mullen *et al.*, 1990; Monaghan *et al.*, 2005; Atkins and Dunbar, 2009), which is what is the direction predicted for ice flow in the Early Miocene to Pleistocene (Talarico and Sandroni, 2009; Sandroni and Talarico, 2011). This supports a Miocene source area to the south where the only volcanic source is proto-Mount Morning. It is envisaged that periodic Strombolian-style eruptions, similar to the activity proposed for the origin of englacial ash sourced from Mount Erebus (Esser *et al.*, 2004; Harpel *et al.*, 2004), introduced glass into the atmosphere up to 5 km above the vent. The glass was then dispersed over short distances of 10's of kilometers by winds prevailing from the south and eventually settled onto the Ross Sea (Fig. 23). In many cases, ice rafting and limited submarine transport in the form of small turbidity currents must have occurred before final deposition, as evidenced by the facies associations present from ~259-648 mbsf, consisting of stratified diamictites, mudstones and sandy mudstones. The stratified diamictites, in this case, are formed

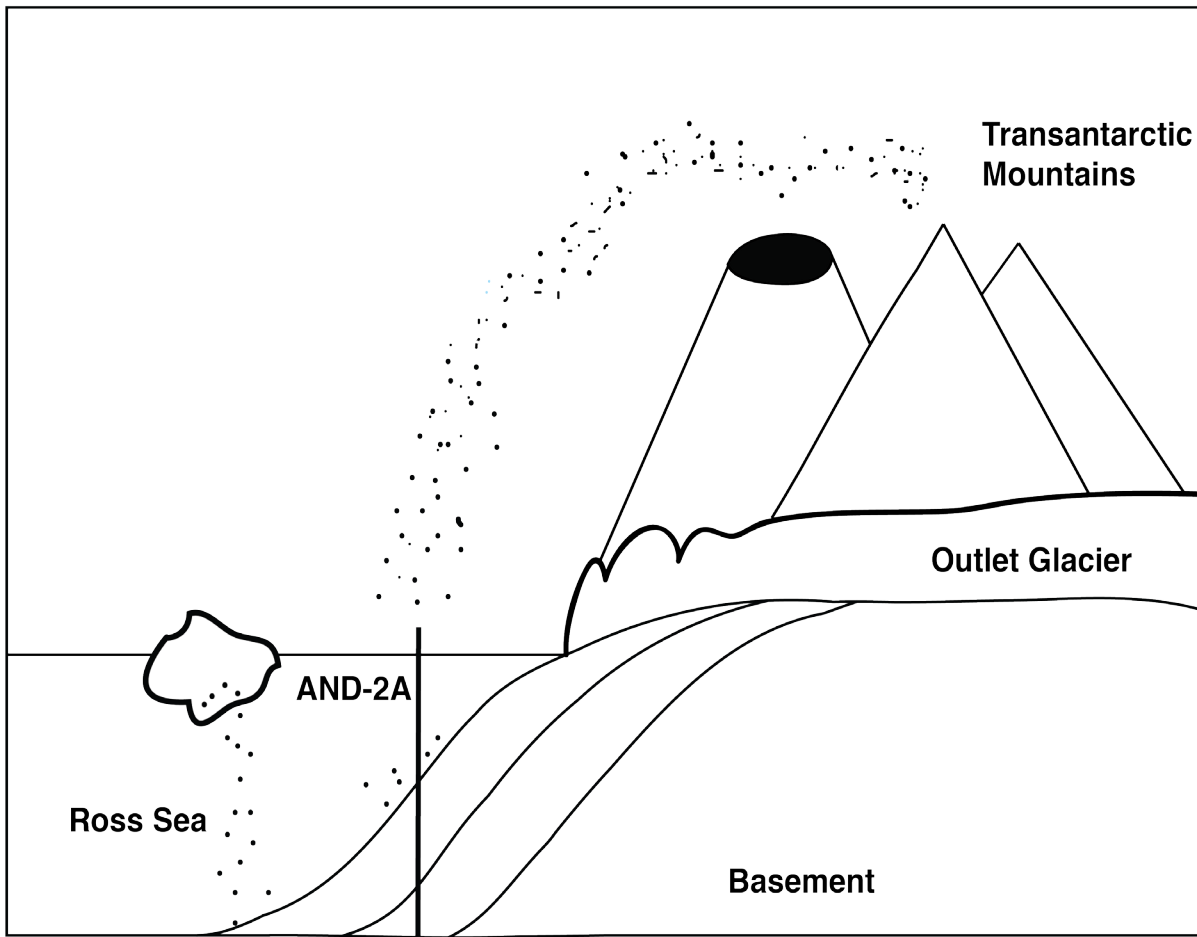


**Figure 23:** Cartoon showing the direct deposition of pyroclastic materials onto the sea floor after eruptions, which are eventually incorporated into sediments. Not to scale.

by a combination of hemipelagic sedimentation with significant input from icebergs and ice rafted debris, along with subglacial and proglacial mass wasting processes (Passchier *et al.*, 2011). Mudstone facies are deposited in a more ice-distal open marine environment containing clusters of clasts, which suggests iceberg rafting, and the presence of sandy mudstones are interpreted to represent sediments deposited from a terrigenous supply of turbid plumes (Passchier *et al.*, 2011). The facies associations present from ~648-786 mbsf, dominated by massive and stratified diamictites, can be formed by a combination of hemipelagic sedimentation with significant input from icebergs and ice rafted debris, which is more significant in massive diamictites, along with subglacial and proglacial mass wasting processes. The presence of intermittent fine sandstones and siltstones throughout this facies association also indicates deposition from suspension settling along with periodic deposition from turbidity currents (Passchier *et al.*, 2011).

In summary, the majority of AND-2A glass analyzed in this study is considered to originate from mildly explosive eruptions and was incorporated with sediment with minimal reworking. The relatively short time period (100's to a few 1000's of years) inferred for such processes (Powell and Molnia, 1989; Powell and Domack, 2002) would not be resolvable within error of  $^{40}\text{Ar}/^{39}\text{Ar}$  dating (Di Vincenzo *et al.*, 2010), and therefore, AND-2A glass accumulations dispersed within sediments are regarded as time-stratigraphic markers.

#### Volcanic Source

Mount Morning is the inferred source of Early to Middle Miocene volcanic material recovered from the Dry Valleys (Lewis *et al.*, 2007), the Cape Roberts drillcores (McIntosh, 1998, 2000; Barrett, 2007), as well as the AND-1B (Pompilio *et al.*, 2007) and AND-2A (Panter

(*et al.*, 2008; Di Vincenzo *et al.*, 2010) cores. Mount Morning is located in the southwest Ross Sea, approximately 85 km southwest of the AND-2A drillsite. Early to Middle Miocene ages from deposits on Mount Morning range from 11.4 to 18.7 Ma (Wright-Grassham, 1987; Kyle and Muncy, 1989; Martin *et al.*, 2009). Older deposits may exist but are not exposed due to either being covered by younger deposits or glaciers. The only other possible volcanic activity of comparable age is found on the Malta Plateau, a major volcanic complex that consists of several major explosive silicic vents along with many basaltic vents (Schmidt-Thome *et al.*, 1990), which is located approximately 200 km north of the drillsite in the Melbourne Volcanic Province. Given the inferred low-column eruption style (Strombolian) and the northward trending paleocurrents for wind and ice, it is highly unlikely that the AND-2A glass came from a source to the north. Yet some AND-2A glass contains recycled material from sources other than those in the EVP. For instance, the compositions of two unaltered glass grains in sample 596.77 are classified as basaltic andesite (Fig. 10). This glass was probably eroded from basalts from the Ferrar large igneous province, which are Jurassic deposits found within the Transantarctic Mountains (Kyle *et al.*, 1981).

A Mount Morning source for the oldest volcanic materials in the EVP would indicate that it has remained intermittently active since the Early Miocene, with documented volcanic activity occurring in two phases; Phase I, ~18.7-11.4 Ma and Phase II, ~6.13-0.02 Ma, with a period of volcanic quiescence occurring between (Martin *et al.*, 2009). Though Mount Morning Phase I volcanism is coeval with AND-2A glass, only 7% of the Phase I volcanic rocks exposed at Mount Morning are mafic and the remainder consist of trachytes and rhyolites (Martin *et al.*, 2009), which contrasts with the mostly mafic glass found in AND-2A core during this same period. If a proto-Mount Morning is the source of AND-2A glass, then the compositional range

of Phase I volcanism is extended to a more mafic end, and thus reveals a previously unknown phase of explosive, strongly alkaline, basaltic volcanism that is compositionally indistinguishable from the younger Phase II activity (Fig. 15).

An example of an eruptive complex whose activity is nearly as long-lived as Mount Morning is the Jemez volcanic field in New Mexico, which has been intermittently active from about 13 Ma to 0.13 Ma (Heiken *et al.*, 1990). It is also similar to Mount Morning in that it has experienced two eruptive phases (Heiken *et al.*, 1990). The Jemez Volcanic Field is located at the intersection of two structural trends: the Rio Grande rift system and the Jemez lineament (Heiken *et al.*, 1990). Basaltic and rhyolitic volcanism in the first phase of activity (~13-7 Ma), was facilitated by rifting of the Rio Grande Rift system which began ~16.5 Ma in the vicinity of the Jemez Mountains. During the early phase of volcanic activity, magma was allowed to vent easily along faults, including the Cañada de Cochiti fault (Heiken *et al.*, 1990). From ~7-4 Ma, the Cañada de Cochiti fault became inactive, coinciding with a significant reduction in volcanic activity, characterized by a cessation in basaltic and rhyolitic volcanism with new eruptions dominated by mixed magmas (Heiken *et al.*, 1990). Following the lull in volcanic activity, renewed volcanism began ~4 Ma and shifted to the east, concurrent with the beginning of tectonic activity at the Pajarito fault zone. Volcanic activity continued at the Jemez Volcanic Field as the Pajarito and Jemez fault zones remained active through the Quaternary (Heiken *et al.*, 1990). Similarly, volcanism in the McMurdo Sound region has been linked to tectonic activity and faulting (Wilson, 1999; Paulsen and Wilson, 2009). Martin et al. (2009) concluded that Mt. Morning's location on the stationary Antarctic plate at the active western boundary between the thinned lithosphere of the West Antarctic Rift System and the thick East Antarctic craton can explain the longevity of volcanism at the Mount Morning eruptive center.

## Geochemical Evolution

The alkaline mafic compositions of AND-2A glass may be related to a single magma lineage by fractional crystallization. In order to test this assertion, basanite sample 740.89-F1 was chosen as a representative parental magma based on its primitive composition. Although none of the basalt compositions for AND-2A glass represent primary mantle melts (*mg*-number  $\geq 68$ ; Ni  $\geq 320$  ppm; Frey *et al.*, 1978), sample 740.89-F1 was chosen as being one of the least evolved basanites, having a moderately high *mg*-number (49), low SiO<sub>2</sub> content (43 wt. %) and Ni content of 41 ppm, respectively. Fractional crystallization models are shown graphically (Fig. 24).

The modeled curves are compatible with the progressive crystallization of olivine, clinopyroxene, plagioclase, and magnetite  $\pm$  amphibole and apatite. The models show that ~60% crystallization is necessary to produce phonotephrites and mugearites from the least evolved basanite compositions (Fig. 24a). The concentrations of Ni and Cr are sensitive to the crystallization of olivine, clinopyroxene and amphibole (Adam and Green, 2006). The fractionation of 35% clinopyroxene, 7% olivine, and possibly small amounts of amphibole (~2%) could explain the depletion in Ni and Cr with differentiation (Fig. 24b, c). Middle REEs, such as Ho (Fig. 24d), are moderately compatible with amphibole based on published K<sub>D</sub> values (K<sub>D</sub> Ho = 1.03; Botazzi *et al.*, 1999), however, Ho concentrations increase with differentiation (Fig. 24d) confirming that little if any amphibole is being fractionated. The concentration of Ti is most sensitive to the crystallization of magnetite. Trends in Ti concentrations can be explained by fractional crystallization models in which Ti behaves incompatibly until magma becomes slightly more evolved (Zr  $\approx$  300 ppm, Fig. 24e), followed by the fractionation of

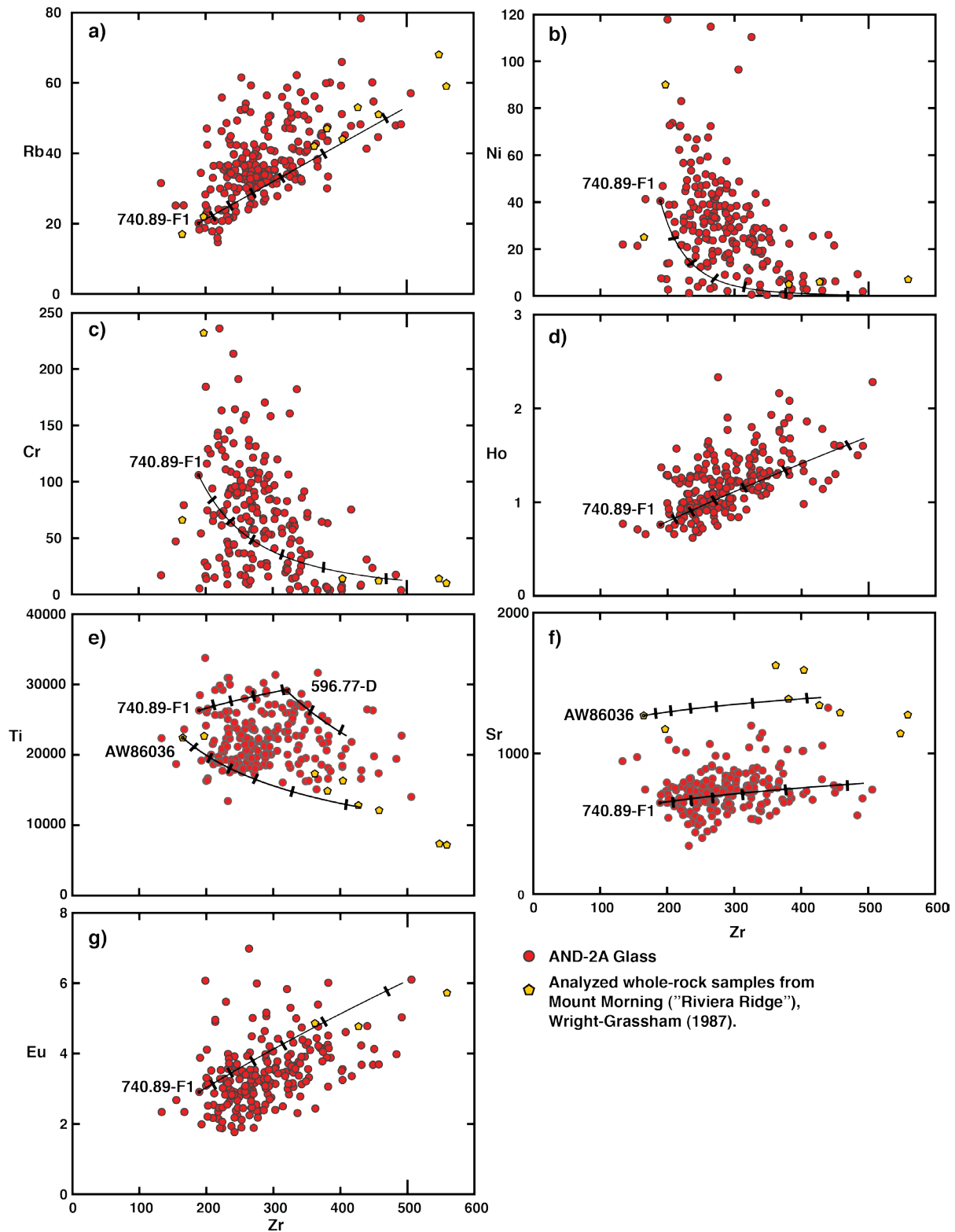


Figure 24.

**Figure 24:** Zr versus Rb, Ni, Cr, Ho, Ti, Sr, Eu diagrams with fractional crystallization (FC) models for AND-2A glass and Mount Morning "Riviera Ridge" whole rock samples. Bulk distribution coefficients ( $D = \sum W_A K_{D(i)}$ , where  $W_A$  is the weight fraction of a mineral A, and  $K_{D(i)}$  is the mineral-liquid partition coefficient for an element i in mineral A) were estimated by the fitting of model fractional crystallization curves to the data arrays and checking the validity of such projections by comparing with published mineral-liquid partition coefficients ( $K_D$  values) determined for basanite and basalt assemblages (Caroff *et al.*, 1993; Botazzi *et al.*, 1999; Adam and Green, 2006) and reasonable proportions for the minerals being fractionated. Tick marks on the model lines represent 10% crystallization increments. Sample 740.89-F1 is the parent basanite used for all models. a) Zr vs. Rb. Incompatible element trends such as this one show that ~60% fractional crystallization must take place to model from the parent to more evolved basanites. b) Zr vs. Ni FC ( $C_L = C_0 \times F^{(D-1)}$ , where  $C_L$  is the concentration of some element in the residual liquid,  $C_0$  is the concentration of the element in the original magma and F is the melt fraction remaining) curve using a bulk distribution for Ni ( $D^{Ni} = 5.8$ ). The decrease in Ni content can be related to the fractionation of olivine. c) Zr vs. Cr FC curve using  $D^{Cr} = 3.2$ . The decrease in Cr is due to the fractionation of clinopyroxene. d) Zr vs. Ho FC model curve using  $D^{Ho} = 0.18$ . The incompatibility of Ho shows that if amphibole is fractionating it is not enough to cause Ho to behave compatibly. e) Zr vs. Ti FC model curve using  $D^{Ti} = 0.8$ , then from parent 596.77-D at  $D^{Ti} = 2$ . The increase followed by decrease in Ti shows that small amounts of magnetite begin to fractionate after 40% fractional crystallization. f) Zr vs. Sr. FC model curve using  $D^{Sr} = 0.8$ . Sr stays flat indicating that it must be buffered by the fractionation of some plagioclase. g) Zr vs. Eu FC model curve using  $D^{Eu} = 0.25$ . Though Eu remains incompatible, a small amount of plagioclase is allowed to crystallize (~10%), consistent with Sr remaining constant.

small portion of magnetite (~5%) from a slightly more evolved basanite (sample 596.77-D, Fig. 24e). Whole rock samples from Mount Morning "Riviera Ridge" (Wright-Grassham, 1987) have the same or lower Ti content relative to AND-2A glass at any given Zr concentration. The least evolved sample with the lowest Zr content, AW86036 (Wright-Grassham, 1987), requires Ti to behave compatibly ( $D^{Ti} = 1.5$ ) to explain evolved basaltic whole rock compositions at Mount Morning (Fig. 24e). Strontium and Eu concentrations in magmas are typically sensitive to plagioclase crystallization ( $K_D Sr = 2.12$ ;  $K_D Eu = 0.22$ ; Caroff *et al.*, 1993). In Figure 24f, Sr content stays relatively constant with increasing Zr content while Eu significantly increases in concentration, behaving incompatibly (Fig. 24g). Models can explain these trends with the crystallization of small amounts of plagioclase (~10% of ~An<sub>57</sub>). A low percentage of plagioclase fractionation can explain the lack of a Eu anomaly on REE diagrams (Fig. 17a, 18b) and the slight negative Sr anomaly shown in Fig. 17b and 18c. Whole-rock samples from Mount Morning at "Riviera Ridge" (Wright-Grassham, 1987) have higher Sr concentrations at any given concentration of Zr but are modeled in the same way ( $D^{Sr} = 0.8$ ). The difference in Sr concentrations may again be related to the comparison of whole-rock and glass compositions, where whole rock analyses would include plagioclase and the glass would not.

Kyle and Muncy (1989) initially recognized two compositional trends in Mount Morning deposits at Gandalf Ridge, which include a benmoreite-Q-trachyte non-peralkaline trend and a peralkaline trend represented by a benmoreite-comenditic trachyte, pantellerite sequence. Major and trace-element data point to benmoreite being derived from an alkali basalt parent, perhaps what is seen in AND-2A by fractional crystallization (Fig. 24). However at Mount Morning, felsic rocks were erupted over most of the 7.3 m.y. recorded history of Phase I volcanism, and are volumetrically more important. Martin *et al.* (2009) suggested that the assimilation of

varying degrees of crustal material, in addition to fractional crystallization, played an important role in the evolution of Phase I volcanism. A small portion of the exposed deposits at Mount Morning's Riviera Ridge (Wright-Grassham, 1987), have very similar compositions as AND-2A glass. However, compositions from nearly all of the much younger Phase II activity (6.13-0.02 Ma) closely match the glass. According to Martin *et al.* (2009), the more evolved compositions (Phase I activity) are likely the result of longer magma residence times, compared to that experienced by Phase II activity.

Significant chemical variations are noted over the depth interval 300 to 800 mbsf (Fig. 13). A systematic change in SiO<sub>2</sub> content exists, with basaltic glass becoming more felsic up section (Fig. 13a). Overall variations in Ba/LREE ratios also exist, which decrease up-section to 534 mbsf, followed by an increase up-section towards 354 mbsf (Fig. 13d, e). The lowest four samples (740.89, 742.00, 763.52 and 764.44) are also significantly more mafic than younger samples at shallower depths, and display a distinct decrease in Na<sub>2</sub>O and increase in TiO<sub>2</sub> up-section, which is not observed within the upper portion of the core (Figs. 13, 19). The increase in SiO<sub>2</sub> content of the basalts up-section could be controlled by changes in the degree of partial melting in the mantle (Dasgupta *et al.*, 2007), which would have to increase with time to explain the trend. The shift back to lower SiO<sub>2</sub> content between ~539 and ~446 mbsf (Fig. 13a), correlates to an interval of time where there is also substantially less glass input (Fig. 25). If the lower glass contents reflect a suppression of volcanic activity during this time period, then the renewed activity at ~16 Ma may be associated with a new phase of partial melting at smaller degrees. However, this time period is considered to be a period of passive thermal subsidence in the Victoria Land Basin and renewed extension forming the Terror Rift and associated volcanism

did not begin until ~13 Ma (Fielding *et al.*, 2008b); therefore, the change in chemistry is not likely due to a change in tectonic regime.

### Feedback Between Volcanism and Glaciation

The lithostratigraphy of the core offers a previously unavailable ice-proximal stratigraphic archive that provides clear evidence of repeated fluctuations in climate, ice expansion/contraction and sea level change over the period of ~20-14 Ma (Fielding *et al.*, 2011; Passchier *et al.*, 2011). This is demonstrated by the presence of fine-scale resolution of glacimarine cycles that record the advance and retreat of glaciers into and out of the Victoria Land Basin, along with the overall distribution of sedimentary packages consistent with dynamic ice sheet activity. Due to the presence of extremely dynamic climate conditions in the McMurdo Sound area during the Early to Middle Miocene, it is possible that glacial unloading during a rapidly warming climate may have had an effect on the volume, timing, and explosiveness of volcanic eruptions. Specific physical and chemical evidence supports the idea that the volcanic ash found in the AND-2A core records a cause-effect relationship between glacial dynamism and volcanic activity.

In Iceland, Slater *et al.* (1998) found that there was an increase in magma eruption rates by a factor of 20 relative to present day eruptions during the end of the last ice age (~11 ka). This increase in eruptive volume was documented in several other volcanic centers around Iceland, and increased eruption rates were found to occur from 1 to 3 kyr after de-glaciation commenced. Slater *et al.* (1998) also provided evidence that lavas erupted during postglacial/interglacial times were depleted in trace element concentrations with respect to the lavas erupted during glacial times. The authors speculate that the relative depletion in trace

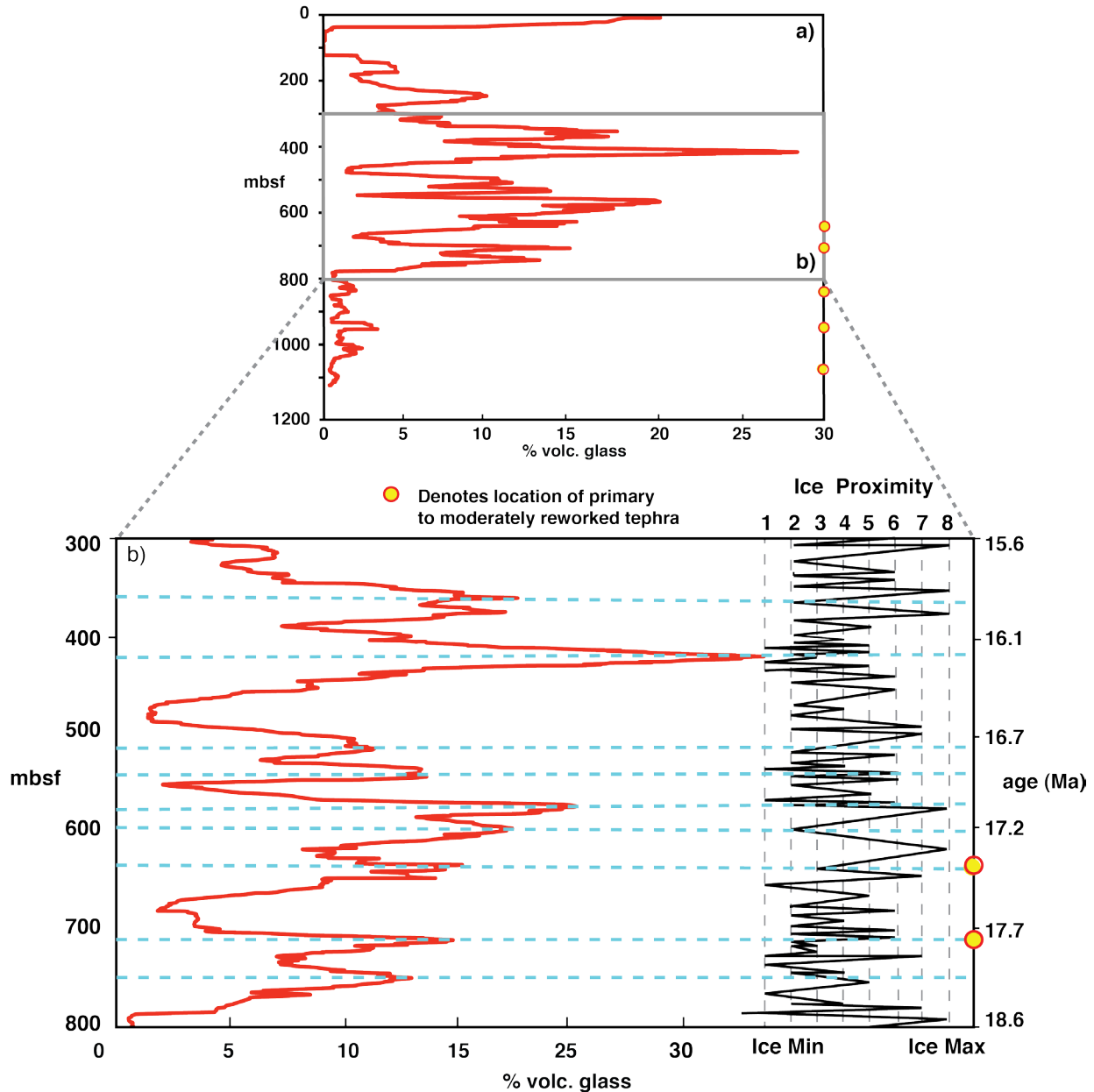


**Figure 25:** a) Variations in the amount of volcanic glass within sediment over the AND-2A core are shown, plotted as a 20-point moving average, based on smear slide data determined by Dr. Brad Field, GNS Science (Panter *et al.*, 2008). There appears to be a systematic variation in the amount of glass with depth throughout the core, occurring as "pulses." b) Shows a blow-up of the study area of the AND-2A core ~300-800 mbsf, where the volcanic "pulses" are correlated to generalized ice volumes determined by Fielding *et al.* (2011). There is generally a correlation between higher volcanic glass content and lower ice proximity, where 1 is the least ice proximal and 8 is the most ice proximal.

elements was most likely caused by an increase in mantle melting at shallower depths that was triggered by pressure release. Sigvaldason (2002) used tephra-chronology and volume estimates to document high production rates at the Dyngjufjöll volcanic center with rapid crustal rebound at the end of the Pleistocene in Iceland. The ice sheet may have been as thick as 1500 meters which would have caused a nearly 400 meter depression of the crust. Sigvaldason (2002) indicates that with melting, crustal rebound could have occurred over as short of a time span as 1000 years, and higher volume eruptions triggered by the pressure release would have been the result of supersaturation and exsolution of volatiles from the magma. Carrivick *et al.* (2009) noted that the combined flexure of the Earth's crust and changes in stress on magma chambers caused by rapid de-glaciation is likely to stimulate volcanic activity. Bigg *et al.* (2008) noted that a significant increase in the amount of ice rafted debris, signifying the destruction of the northern hemisphere ice sheets precedes and accompanies a substantial amount of ash deposits in a marine core in the northwest Pacific, ca. 40 ka, and the authors speculate that the initial rapid decay of the ice sheet may have triggered the large input of volcanic activity. Zielinski *et al.* (1996), after investigating an 110,000-year record of explosive volcanism from the GISP2 ice core in Greenland, found that the largest and most abundant amounts of volcanically produced sulfate occurred between 17 and 6 ka with a greater estimated concentration between 13 and 7 ka. This time period marks the last de-glaciation during the most recent ice age and provides further evidence that climate can be a factor controlling volcanic activity. In another study, Nowell *et al.* (2006) compared oxygen isotope records, which serve as a climate proxy, with the frequency of eruptions in the Quaternary for volcanic centers in Germany and France. The authors found a positive correlation between warming events and the number of volcanic eruptions.

The depth interval of this study (~354-765 mbsf) corresponds to a period of cyclic variations in sea level, glacial proximity to the drillsite, and climate change (Fielding *et al.*, 2011; Passchier *et al.*, 2011). Changes in the ice-sheet extent recorded at the drillsite also would have occurred upstream in the area of Mount Morning; the inferred source for the glass. A first order observation providing a link between glaciation and volcanism is the greater amounts of volcanic glass that correlate with times of ice minimum conditions (Fig. 25). The increase in the amount of volcanic glass may represent an increase in volcanic activity or, alternatively, an increase in erosion of newly exposed land deposits following glacial retreat.

In addition to physical correlations exhibited between glacial processes and volcanism in McMurdo Sound, chemical correlations are also evaluated. The most prominent correlation exists for ratios of Ba to LREEs, where Ba/La and Ba/Ce ratios for volcanic glass increase towards ice minimum conditions and decrease towards ice maximum conditions over several different depth intervals (Fig. 26). Also, the magnitude of change in Ba/LREE ratios appears to match the magnitude of change in ice conditions. For example, a relatively small change in average Ba/LREE ratios (<1) correlates to a lithofacies change of one, interpreted by Fielding *et al.* (2011) to indicate changes in ice proximity, where lithofacies 8 reflects the most ice proximal conditions, and lithofacies 1 reflects the least ice proximal conditions (Fig. 26a, b). Volcanic glass in another section (Fig. 26c) shows the average Ba/LREE ratios increase by approximately 3 towards ice minimum conditions and the ice proximity change by ~5 towards ice minimum conditions.

Aqueous fluids concentrate fluid mobile elements such as Ba, Rb, U, K and Pb in magmatic systems (Brenan *et al.*, 1995; Keppler, 1996). Higher Ba/LREE ratios (typically Ba/La) have been frequently used as an indicate enrichment by slab fluids in arc magmas

(McCulloch and Gamble, 1991; Hawkesworth *et al.*, 1994). Variations in Ba/LREE ratios of AND-2A glass may be caused by variations in the fluid content of the magmas and therefore, a change from lower to higher Ba/LREE ratios may indicate progressive tapping of more fluid-rich magmas during initial glacial retreat.

To further investigate the relationship between volcanic activity and glaciations, glass-rich sediments were selected from a nearly complete glacimarine cycle, ranging from ice proximal to minimal ice conditions and back to ice proximal conditions (Sequence 32; Fielding *et al.*, 2011). Seven samples were analyzed within the sequence collected between ~638 and 664 mbsf. The depth corresponds to a model age range spanning ~140,000 years (~17.39-17.53 Ma). Figure 27 shows that there are some systematic variations within Sequence 32 with regards to chemical and physical parameters. Physical variations include an increase in R-values (i.e. rounding) and a decrease in the amount of vesicular glass (grains with >15% vesicles by volume) from >50% to <30% up section. Chemically, variations include an overall decrease in SiO<sub>2</sub> and K<sub>2</sub>O (not shown) contents up section. An increase in Ba/La, Ba/Ce and K/La (not shown) ratios is projected for the ice minimum in this sequence at ~647 mbsf, where the finest-grained sediments occur (Fielding *et al.*, 2011).

MacLennan *et al.* (2002) observed that subaerial, postglacial lavas in Iceland are generally more mafic than subglacial lavas, consistent with what is seen in Sequence 32. Also, the overall decrease in vesicularity and increase in rounding up-section may be consistent with changes in the magma system in response to deglaciation. For instance, Bindeman *et al.* (2010) found that during and shortly after deglaciation shallow magma chambers that produced pre-Holocene caldera-forming eruptions in Kamchatka reached volatile saturation and erupted more explosively, producing highly vesicular vitroclasts. Eruptive degassing magmas into an

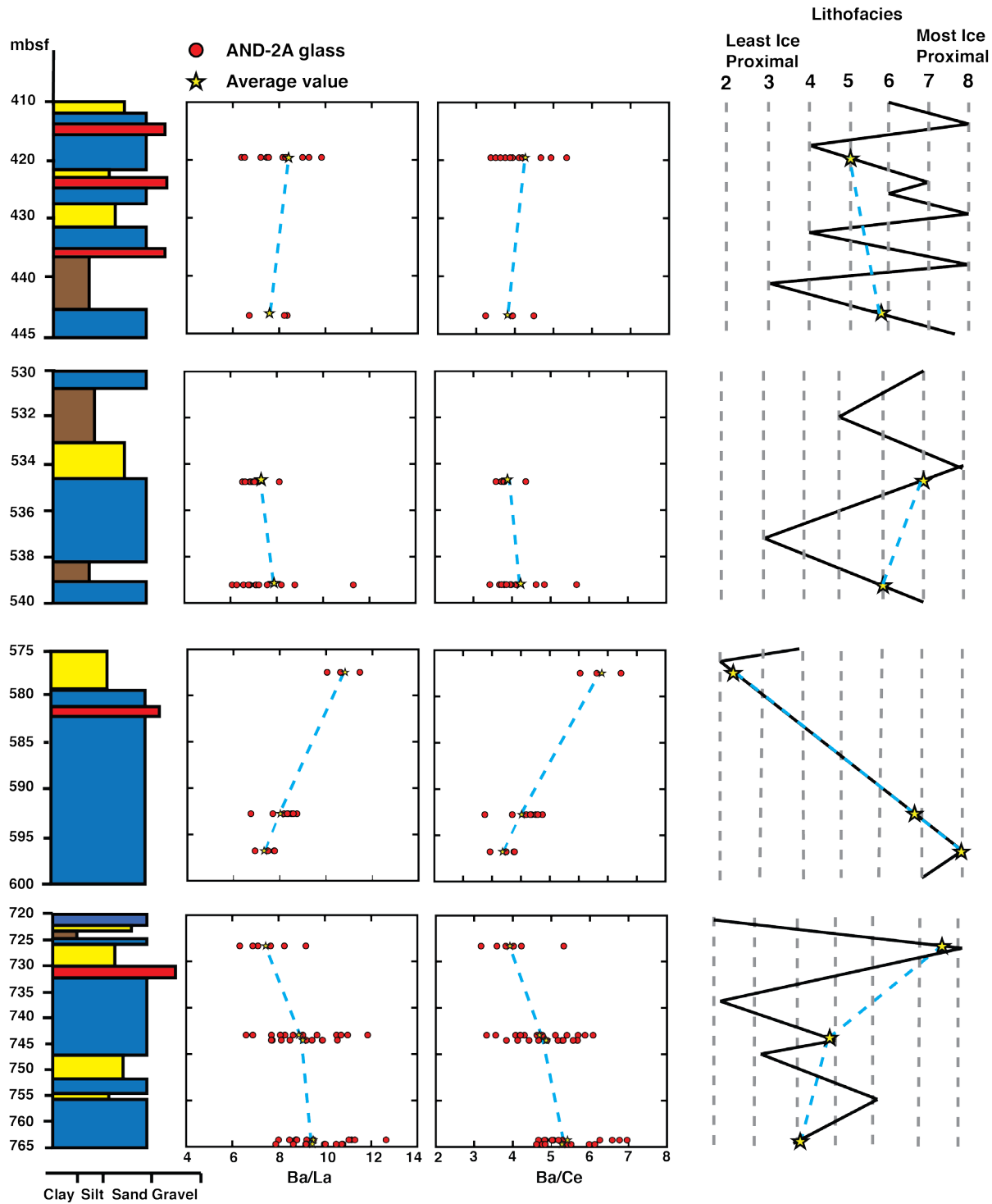


**Figure 26:** Plot of Ba/La and Ba/Ce versus depth for specific stratigraphic intervals for unaltered AND-2A glass limited to grains with 41–48 wt. % SiO<sub>2</sub> and 3–7 wt. % MgO. Also shown are sedimentary columns showing changes in lithology and estimates for ice extent based on the distribution of lithofacies within sediments (Fielding *et al.*, 2011). Ba/LREE ratios of glass grains increase towards ice minimums and decrease towards ice maximum conditions.

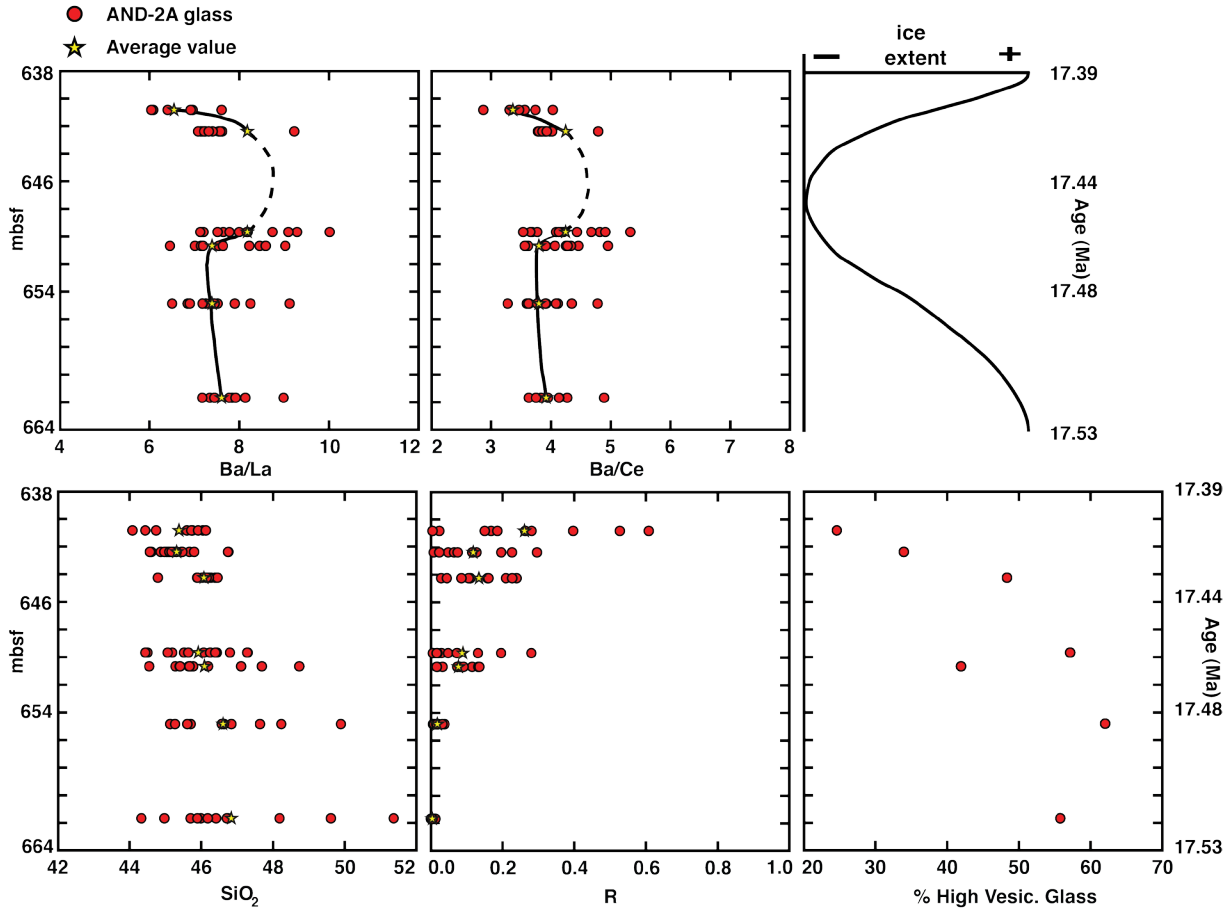


**Figure 27:** Diagram for glass samples studied within Sequence 32, showing changes in R-value, relative percentage of high vesicular glass, SiO<sub>2</sub> content, Ba/LREE ratios and generalized ice proximity curve (interpreted from Fielding *et al.*, 2011). For Ba/La and Ba/Ce versus depth, unaltered AND-2A glass limited to grains with 41–48 wt. % SiO<sub>2</sub> and 3–7 wt. % MgO. Several correlations are noted to exist up-section through Sequence 32: increase in R-values (decrease in angularity), decrease in high vesicular glass, and a slight decrease in SiO<sub>2</sub> content and an increase in Ba/LREE towards ice minimum conditions.

ice-free period would have produced an overall decrease in the vesicularity of vitroclasts. This overall decrease in volatiles in the magma system can also be linked to the level of rounding, which increases up-section in Sequence 32, along with a decrease in vesicularity.

The physical and chemical evidence from AND-2A glass support a glacial influence on volcanism in the McMurdo Sound region. It is likely that there was a significant amount of ice cover on land during glacial intervals in the Early to Middle Miocene, based on evidence from grounded ice present at times throughout the AND-2A core (Passchier *et al.*, 2011). Also it is very likely that the East Antarctic ice sheet was significantly thicker over the Mount Morning area when ice maximums occurred at the drillsite. Thus, a strong possibility remains that rapid melting of the East Antarctic Ice Sheet during warming events, resulting in significant isostatic changes in the vicinity of Mount Morning, could have influenced the rate and/or explosivity of eruptions at Mount Morning. Unloading of the crust during de-glaciation could allow magma systems to produce more eruptions either by increasing the tapping of magma chambers due the change of the stress state in the crust due to the removal of an ice sheet (Gudmundsson, 1986), or by accentuated decompression due to the effect of ice unloading, which can produce a significant increase in mantle melting (Jull and McKenzie, 1996). Also, glacial loading/unloading could have caused volatile saturation in shallow magma chambers to increase the proportion of explosive versus effusive eruptions (Bindeman *et al.*, 2010) and/or triggering higher volume eruptions (Sigvaldason, 2002). However, most of these models are based on volcanism in Iceland. Though the tectonic setting of Iceland and the Victoria Land Basin are different, the lithosphere of the Victoria Land Basin has been warmed and thinned from extension processes, though not to the same extent of Iceland (Wilson, 1999). However, according to Wilson *et al.* (2003), geophysical data shows that the EVP has formed on top of lithosphere that is relatively

weak, and in some locations has an elastic lithosphere thickness of only ~7.5 km. These data along with seismic reflection data (Bannister, 1993; Melluish *et al.*, 1995; Bannister and Naish, 2002; Horgan *et al.*, 2003; Horgan *et al.*, 2005; Henrys *et al.*, 2006; Naish *et al.*, 2006; Henrys *et al.*, 2007) show that deep flexural moats exist around Ross Island due to loading of volcanic edifices. Stern and ten Brink (1989) found the flexural rigidity of the Ross Embayment in Antarctica to be  $4 \times 10^{22}$  Nm, which controls how abrupt vertical movement decays away from the edge of a load (ice sheet), with an average elastic lithosphere thickness of 19.5 km. Gudmundsson (1986) found that the flexural rigidity for the Reykjanes Peninsula, Iceland, is on the order of  $8.8 \times 10^{19}$  Nm. The elastic lithosphere of Iceland is known to range from 1-6 km (Kaban *et al.*, 2002). The lower the value of flexural rigidity of the lithosphere, the more local the isostatic effects will be under given a load, whereas the higher the value of flexural rigidity, the more regional the isostatic effects will be under given a load (Stern, 1989). The flexural rigidity of the lithosphere in Iceland is significantly less than that in the Ross Embayment, and therefore is affected by isostatic processes to a greater magnitude than what is seen in Antarctica, experiencing shorter crustal response times (100's to a few 1000's of years) to de-glaciations.

For these reasons, a model is proposed in which ice loading and un-loading induces stress on the earth's crust, which can then impact shallow upper crustal magma systems. Induced stress on the crust caused by an ice sheet load will change from compressive to tensile at a certain depth depending on the size of the ice sheet, though the exact depth depends on the properties of the layers in the crust and upper mantle and the lateral extent and thickness of the ice sheet (Geyer and Bindeman, 2011). A large Icelandic ice sheet (e.g., 100 km in diameter) may induce compressive stress through the entire crust and into the mantle, creating stress conditions that discourage volcanic eruptions, while a smaller ice sheet (e.g., 20 km in diameter) may induce

tensile stress in the crust (Andrew and Gudmundsson, 2007). At a depth in which the stress state in the crust changes from tensile to compressive, magmas rising along faults and fractures will likely stall and not propagate to the surface, forming shallow, sill-like magma conduits (Andrew and Gudmundsson, 2007, Geyer and Bindeman, 2011). Andrew and Gudmundsson (2007) also suggest that the induced tensile stress caused by the presence of a smaller ice sheet could increase the extent of a relatively deep (~20 km) magma system by inducing increased melt fracturing, thereby increasing the magma content which may promote rise and eruption of more primitive compositions, due to the reservoir extending to greater depths in the mantle, and larger eruptive volumes during de-glaciations. Pinel and Jaupart (2000, 2005) show that also the load induced by the volcanic edifice itself may have caused magmas propagating towards the surface within narrow conduits to become arrested at certain depths in the shallow upper crust where the stress regime changes from tensile to compressive.

A model is envisaged by which a shallow (~5 km depth) magma system underlying proto-Mount Morning during periods of maximum ice thickness (~400-600 meters) and extent (~100 km in diameter) produced compressive stresses, which may have extended through the entire upper crust, that caused magmas to stagnate (Fig 28a). During these periods, which may last ~1000's to 10's of thousands of years, stored magmas accumulated volatiles by the fractionation of anhydrous minerals (clinopyroxene, olivine, and plagioclase) and/or by recharge from new volatile-rich magmas depth (Fig 28a). The accumulation of volatiles during the glacial period produces magmas with higher Ba/LREE ratios. With melting and the retreat of glacial ice (Fig. 28b) the thinning ice sheet will continue to induce compressive stress in the crust but the depth at which the stress regime changes to tensile will be more shallow (Andrew and Gudmundsson, 2007). The exact depth where the stress regime changes from compressive to

tension depends on the exact dimensions of the ice sheet and layer properties of the crust and upper mantle (Geyer and Bindeman, 2010). Rising magma due to lower pressures may allow for the exsolution of volatiles and vesiculation of magma at shallower depths (Andrew and Gudmundsson, 2007; Geyer and Bindeman, 2011). However, the propagating conduits will be prohibited from reaching the surface, as they will become arrested at a neutral surface where the stress regime changes from tensile to compressive (Andrew and Gudmundsson, 2007; Fig. 28b). As the ice sheet continues to thin (Fig. 28c), the tensional stress regime in the crust will resume, and vesiculation of volatile-rich magma may occur at very shallow depths, eventually driving more explosive eruptions as evidenced by highly vesicular vitroclast input in AND-2A. Moving into ice-free conditions, the degassing of magmas with continued eruptions will eventually lead to less explosive eruptions, resulting in less vesicular vitroclasts and more mafic magmas with less volatiles and lower Ba/LREE ratios.

The significant volume difference between felsic and mafic deposits at Mount Morning erupted during Early to Middle Miocene time (Martin *et al.*, 2009) could be related to the presence of an ice sheet covering parts of the volcanic system. Magmas experiencing prolonged stagnation in the crust would promote higher degrees of crystal fractionation and crustal assimilation. During a rapid climate warming event following a glacial period, changes in the stress state of the crust during de-glaciation could allow some magmas to quickly reach the surface, resulting in more primitive compositions (Gudmundsson, 1986), as evidenced by mafic AND-2A glass input.

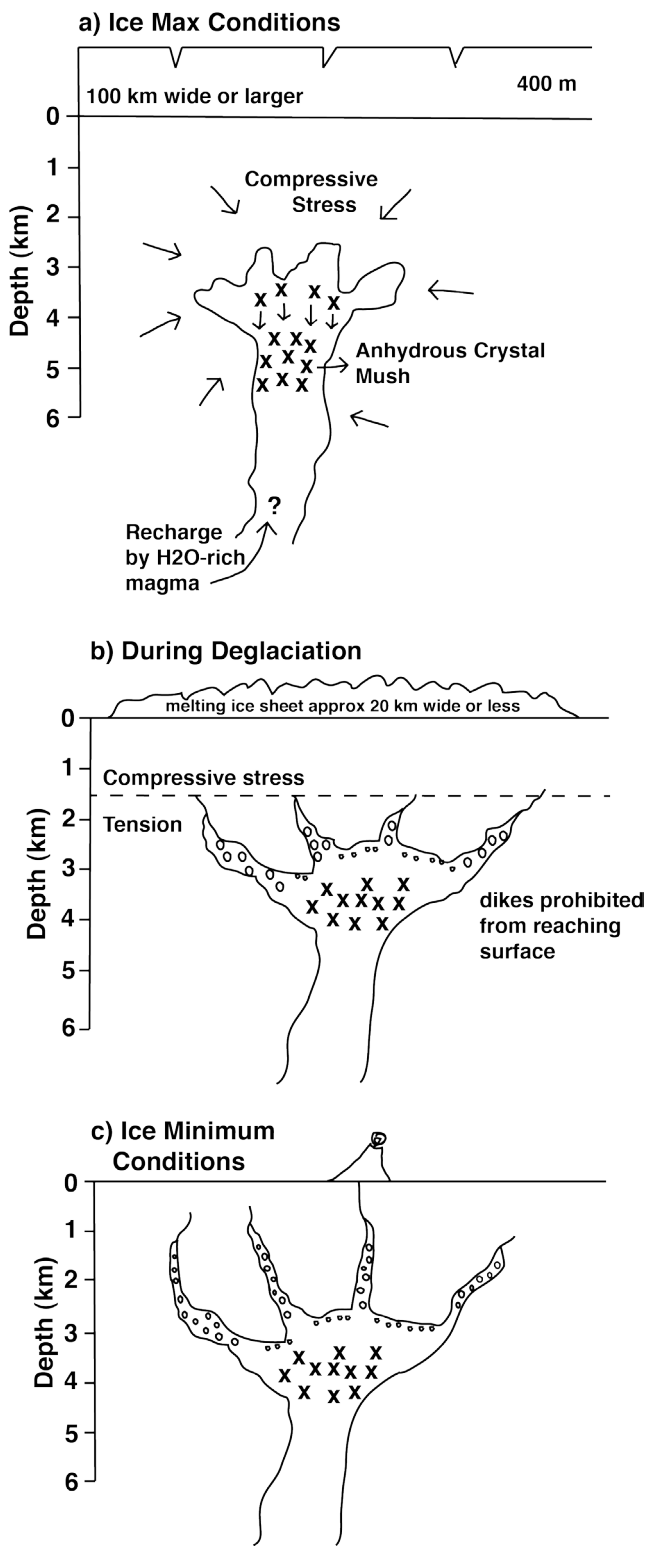


**Figure 28:** Cartoon of model in which ice loading and unloading affects stress states of earth's crust and stress states within and around shallow magma chambers. Not to scale. a) Model for glacial periods (ice maximums). Volcanism and propagation of dikes may be suppressed as a large ice sheet induces compressive stress through entire crust, allowing for accumulation of volatile-rich magmas due to differentiation of magma during long residence times. b) Model for initial de-glaciation. Thinning ice sheets will still induce compressive stress in the crust but to a much shallower depth, where the stress regime will change to tensile. Due to accumulation of volatiles during the glacial period, vesiculation of magma will be able to occur at shallow depths, allowing fractures to propagate. However, fractures will be prohibited from propagating towards the surface at the neutral surface where the stress regime changes from tensile to compressive. Volcanism will continue to be suppressed leading to further differentiation and accumulation of more volatiles. c) Model for ice-free periods. As the ice sheet continues to thin, tensional stress regime in the crust will resume, and vesiculation of volatile-rich magma may occur at very shallow depths, eventually driving more explosive eruptions as supported by volcanic glass input in AND-2A.

## SUMMARY

In this study, dispersed accumulations of primarily *fresh* volcanic glass within glacimarine sediments in the AND-2A core in southern McMurdo Sound, Antarctica, between ~354 and ~765 mbsf (corresponding to ~15.9 to ~18.4 Ma) were examined, resulting in several key findings:

- Dispersed glass accumulations in AND-2A vary from 2-50 vol. % within sediments. These glass-rich sediments include muddy to fine sandstone and stratified diamictite. The glass varies in color, size, vesicularity, crystal content, angularity, and from fresh to moderately altered.
- The common occurrence of delicate cuspatate forms in AND-2A, low R-values (sphericity) of selected glass grains and the large amount of fresh glass present suggest they were introduced into the atmosphere from periodic small-scale Strombolian-style eruptions near McMurdo Sound, Antarctica, and were then transported a relatively short distance and introduced directly into the water as ashfall with minimal reworking. Thus, AND-2A glass accumulations can be interpreted as near-primary time-stratigraphic markers.
- A majority of the glass dispersed within sediments is fresh and unaltered, with altered glass consisting of ~10-20% of the samples. Altered glass can be distinguished visually due to the presence of devitrified rims and vesicles filled with calcite. Chemically, altered glass has low analytical totals (<97 wt. % oxides), low Ca/K ratios (<2) and high AI (>40). Based on chemical evidence, glasses with felsic compositions were found to display signs of significant amounts of alteration in the form of dissolution of alkali elements.

- Based on major and trace element data, unaltered AND-2A glass was found to be chiefly mafic, with SiO<sub>2</sub> ranging from 41 to 52 wt. % and MgO ranging from 3 to 7 wt. %, and are strongly silica undersaturated. Basaltic compositions consist of basanite, alkali basalt, tephrite, hawaiite and potassie trachybasalt, and slightly evolved compositions include phonotephrite, mugearite and shoshonite. The composition of glass shards varies within individual samples but stay mostly within the basaltic compositional spectrum.
- AND-2A glass is sourced from the EVP, which is confirmed by the geochemical similarities between the glass and mafic-intermediate EVP samples. AND-2A glass is also very similar to mafic-intermediate samples from Mount Morning. These observations are supported by the relatively restricted basaltic compositions of the glass through the core and within individual samples, which suggests that the glass was derived from a similar source with minimal reworking before deposition, supported chemically by their unaltered condition and physically by their high angularity. The compositions of AND-2A glass may be related to a single magma lineage by fractional crystallization of the minerals olivine, clinopyroxene, plagioclase, magnetite ± amphibole and apatite, as confirmed by fractional crystallization models.
- AND-2A glass is coeval with Phase I volcanism at Mount Morning based on the current age model for the core, and is likely the source of AND-2A glass due to its proximity to the core. AND-2A glass then extends the known compositional range of Phase I volcanism at Mount Morning to a significantly more mafic end

revealing a previously unknown phase of explosive, strongly alkaline, basaltic volcanism.

- AND-2A glass found within stratigraphic sequences interpreted to represent glacimarine cycles recording transitions from ice proximal, to ice minimum, back to ice proximal conditions during the extremely dynamic Early to Middle Miocene climate contain physical and chemical evidence that provides new insight into the possibility of glacial loading and unloading of the lithosphere during de-glaciation, which can influence the rate and explosivity of eruptions in the vicinity of Mount Morning. Physical evidence shows a first-order correlation between high percentages of glass input during relative ice minimum conditions and chemical evidence shows that Ba/LREE ratios increase towards ice minimum conditions and decrease towards ice maximum conditions, which may correspond to the accumulation of volatiles in magmas during glacial periods.
- A model in which ice loading and unloading affects the stress state of the earth's crust and thus, the state of stress within and around shallow magma chambers is supported. Due to the presence of a thick ice sheet at Mount Morning during glacial periods, volcanism and the propagation of dikes may be suppressed as the ice sheet induces compressive stress through the entire crust, allowing for the accumulation of volatile-rich magmas due to differentiation of the magma during long residence times. When the ice sheet begins to thin during de-glaciation, the ice sheet will still induce compressive stress in the crust but to a much shallower depth, where the stress regime will change to tensile. Due to the accumulation of volatiles during the glacial period, vesiculation of magma will be able to occur at

shallow depths, allowing fractures to propagate. However, fractures will be prohibited from propagating towards the surface at the neutral surface where the stress regime changes from tensile to compressive. Volcanism will continue to be suppressed leading to further differentiation and the accumulation of more volatiles. As the ice sheet continues to thin, the tensional stress regime in the crust will resume, and vesiculation of volatile-rich magma may occur at very shallow depths, eventually driving more explosive eruptions as supported by volcanic glass input in AND-2A.

## REFERENCES

- Acton, G., Crampton, J., Di Vincenzo, G., Fielding, C. R., Florindo, F., Hannah, M., Harwood, D. M., Ishman, S., Johnson, K., Jovane, L., Levy, R. H., Lum, B., Marcano, M. C., Mukasa, S., Ohneiser, C., Olney, M. P. Riesselman, C., Sagnotti, L., Stefano, C., Strada, E., Taviani, M., Tuzzi, E., Verosub, K. L., Wilson, G. S., Zattin, M. & the ANDRILL-SMS Science Team. (2009). Preliminary integrated chronostratigraphy of the AND-2A core, ANDRILL Sourthern McMurdo Sound Project, Antarctica. *Terra Antarctica* **15**, 211-220.
- Adam, J. & Green, T. (2006). Trace element partitioning between mica- and amphibole-bearing garnet lherzolite and hydrous basanitic melt: 1. Experimental results and the investigation of controls on partitioning behavior. *Contributions to Mineralogy and Petrology* **152**, 1-17.
- Andrew, E. B. & Gudmundsson, A. (2007). Distribution, structure, and formation of Holocene lava sheilds in Iceland. *Journal of Volcanology and Geothermal Research* **168**, 137-154.
- Atkins, C. & Dunbar, G. (2009). Aeolian sediment flux from sea ice into Southern McMurdoSound, Antarctica. *Global and Planetary Change* **69**, 133-141.
- Bannister, S. (1993). Seismic investigation of the Victoria Land Basin under Ross Island. New Zealand Programme 1992/93, Event K101. *Institute of Geological and Nuclear Sciences (GNS Science)*, Science report **93/14**, 16 p.

Bannister, S. & Naish, T. R. (2002). ANDRILL site investigations, New Harbour and McMurdo Ice Shelf, Southern McMurdo Sound, Antarctica. *Institute of Geological and Nuclear Sciences (GNS Science)*, Science report **2002/01**, 24 p.

Barrett, P. (2007). Cenozoic climate and sea level history from glacimarine strata off the Victoria Land coast, Cape Roberts Project, Antarctica. In: Hambrey, K., Christoffersen, P., Glasser, N. & Hubbart, B. (eds) *Glacial Processes and Products*. New York: Blackwell, pp. 259-287.

Bigg, G. R., Clark, C. D. & Hughes, A. L. C. (2008). A last glacial ice sheet on the Pacific Russian coast and catastrophic change arising from coupled ice-volcanic interaction. *Earth and Planetary Science Letters* **265**, 559-570.

Bindeman, I., Leonov, V., Izbekov, P., Ponomareva, V., Watts, K., Shipley, N., Perepelov, A., Bazanova, L., Jicha, B., Singer, B., Schmitt, A., Portnyagin, M. & Chen, C. (2010). Large-volume silicic volcanism in Kamchatka: Ar-Ar and U-Pb ages, isotopic, and geochemical characteristics of major pre-Holocene caldera-forming eruptions. *Journal of Volcanology and Geothermal Research* **189**, 57-80.

Botazzi, P., Tiepolo, M., Vannucci, R., Zanetti, A., Brumm, R., Foley, S. F. & Oberti, R. (1999). Distinct site preferences for heavy and light REE in amphibole and the prediction of Amph/LDREE. *Contributions to Mineralogy and Petrology* **137**, 36-45.

Brenan, J. M., Shaw, H. F., Ryerson, F. J. & Phinney, D. L. (1995). Mineral-aqueous fluid

partitioning of trace elements at 900°C and 2.0 GPa: Constraints on the trace element chemistry of mantle and deep crustal fluids. *Geochimica et Cosmochimica Acta* **59**, 3331-3350.

Burnham, C. & Jahns, R. (1962). A method for determining the solubility of water in silicate melts. *American Journal of Science* **260**, 721-745.

Cape Roberts Science Team. (2000). Introduction. In: Ricci, C. (ed) Studies from the Cape Roberts Project, Ross Sea, Antarctica. *Initial Report on CRP-3* **7**, 3-18.

Caroff, M., Maury, R. C., Leterrier, J., Joron, J. L., Cotten, J. & Guille, G. (1993). Trace element behavior in the alkali basalt-comenditic trachyte series from Mururoa, Atoll, French Polynesia. *Lithos* **30**, 1-22.

Carrivick, J., Russell, A., Rushmer, E., Tweed, F., Marren, P., Deeming, H. & Lowe, O. J. (2009). Geomorphological evidence towards a de-glacial control on volcanism. *Earth Surface Processes and Landforms* **34**, 1164-1178.

Cooper, A., Adam, L., Coulter, R., Eby, G. & McIntosh, W. (2007). Geology, geochronology and geochemistry of a basanitic volcano, White Island, Ross Sea, Antarctica. *Journal of Volcanology and Geothermal Research* **165**, 189-216.

Dasgupta, R., Hirschmann, M. M. & Smith, N. D. (2007). Partial melting experiments of peridotite + CO<sub>2</sub> at 3 GPa and genesis of alkalic ocean island basalts. *Journal of Petrology* **48**,

2093-2124.

Del Carlo, P., Panter, K., Bassett, K., Bracciali, L., Di Vincenzo, G. & Rocchi, S. (2009). The upper lithostratigraphic unit of ANDRILL AND-2A core (Southern McMurdo Sound, Antarctica): local Pleistocene volcanic sources, paleoenvironmental implications and subsidence in the southern Victoria Land Basin. *Global and Planetary Change*, doi:10.1016/j.gloplacha.2009.09.002.

Dickenson, W. (1970). Interpreting detrital modes of graywacke and arkose. *Journal of Sedimentary Petrology* **40**, 695-707.

Di Vincenzo, G., Bracciali, L., Del Carlo, P., Panter, K. & Rocchi, S. (2010).  $^{40}\text{Ar}$ - $^{39}\text{Ar}$  dating of volcanogenic products from the AND-2A core (ANDRILL Southern McMurdo Sound Project, Antarctica): correlations with the Erebus Volcanic Province and implications for the age model of the core. *Bull Volcanol*, doi:10.1007/s00445-009-0337-z.

Edwards, B., Russell, J. & Anderson, R. (2002). Subglacial, phonolitic volcanism at Hoodoo Mountain volcano, northern Canadian Cordillera. *Bull Volcanol* **64**, 254-272.

Esser, R. P., Kyle, P. R. & McIntosh, W. C. (2004).  $^{40}\text{Ar}$ / $^{39}\text{Ar}$  dating of the eruptive history of Mount Erebus, Antarctica: volcano evolution. *Bull Volcanol* **66**, 671-686.

Erlund, E. J., Cashman, K. V., Wallace, P. J., Pioli, L., Rosi, M., Johnson, E. & Delgado

Granados, H. (2009). Compositional evolution of magma from Parícutin Volcano, Mexico: The tephra record. *Journal of Volcanology and Geothermal Research*, doi:10.1016/j.jvolgeores.2009.09.015.

Fargo, A., McIntosh, W., Dunbar, N., & Wilch, T. (2008).  $^{40}\text{Ar}/^{39}\text{Ar}$  geochronology of Minna Bluff, Antarctica: Timing of mid-Miocene glacial erosional events within the Ross Embayment. *Eos Trans AGU* **89**, Fall Meet Suppl. V13C-2127.

Fielding, C., Atkins, C., Bassett, K., Browne, G., Dunbar, G., Field, B., Frand, T., Krissek, L., Panter, K., Passchier, S., Pekar, S., Sandroni, S., Talarico, F. & the ANDRILL-SMS Science Team. (2008a). Sedimentology and stratigraphy of the AND-2A Core, ANDRILL Southern McMurdo Sound Project, Antarctica. *Terra Antarctica* **15**, 77-112.

Fielding, C., Browne, G., Field, B., Florindo, F., Harwood, D., Krissek, L., Levy, R., Panter, K., Passchier, S. & Pekar, S. (2011). Sequence stratigraphy of the ANDRILL AND-2A drillcore, Antarctica: a long-term, ice-proximal record of Early to mid-Miocene climate, sea-level and glacial dynamism. *Palaeogeography, Palaeoclimatology, Palaeoecology* **305**, 337-351.

Fielding, C., Whittaker, J., Henrys, S., Stuart, A., Wilson, T., Terry, J., Naish, T. & Timothy, R. (2008b). Seismic facies and stratigraphy of the Cenozoic succession in McMurdo Sound, Antarctica: Implications for tectonic, climatic and glacial history. *Palaeogeography, Palaeoclimatology, Palaeoecology* **260**, 8-29.

Florindo, F., Wilson, G., Roberta, A., Sagnotti, L. & Verosub, K. (2005). Magnetostratigraphic chronology of a late Eocene to early Miocene glacimarine succession from the Victoria Land Basin, Ross Sea, Antarctica. *Global and Planetary Change* **45**, 207-236.

Frey, F. A., Green, D. H, & Roy, S. D. (1978). Integrated models of basalt petrogenesis: a study of quartz tholeiites to olivine melilites from south eastern Australia utilizing geochemical and experimental petrological data. *Journal of Petrology* **19**, 463-513.

Geyer, A. & Bindeman, I. (2011). Glacial influence on caldera-forming eruptions. *Journal of Volcanology and Geothermal Research* **202**, 127-142.

Gifkins, C., Herrmann, W., & Large, R. (2005). *Altered Volcanic Rocks: A guide to description and interpretation*. Hobart: Centre for Ore Deposit Research.

Gudmundsson, A. (1986). Mechanical aspects of postglacial volcanism and tectonics of the Reykjanes Peninsula, southwest Iceland. *Journal of Geophysical Research* **91**, 12711-12721.

Gunn, B. & Warren, G. (1962). Geology of Victoria Land between the Mawson and Mulock glaciers, Antarctica. *New Zealand Geological Survey* **71**.

Hajash, A. & Chandler, G. (1981). An experimental investigation of high-temperature interactions between seawater and nrhyolite, andesite, basalt and peridotite. *Contributions to Mineralogy and Petrology* **78**, 240-254.

Harpel, C. J., Kyle, P. R., Esser, R. P., McIntosh, W. C. & Caldwell, D. A. (2004).  $^{40}\text{Ar}/^{39}\text{Ar}$  dating of the eruptive history of Mount Erebus, Antarctica: Summit flows, tephra, and caldera collapse. *Bull Volcanol* **66**, 687-702.

Harrington, H. (1965). Geology and morphology of Antarctica. Biogeography and ecology in Antarctica. *Monographs in Population Biology* **15**, 1-71.

Harwood, D., Florindo, F., Talarico, F., Levy, R., Kuhn, G., Naish, T., Niessen, F., Powell, R., Pyne, A. & Wilson, G. (2009). Antarctic drilling recovers stratigraphic records from the continental margin. *Eos* **90**, 90-91.

Hawkesworth, C. J., Gallagher, K., Herdt, J. M. & McDermott, F. (1994). Destructive plate margin magmatism: Geochemistry and melt generation. *Lithos* **33**, 169-188.

Heiken, G., Goff, F., Gardner, J., Baldridge, W., Hulen, J., Nielson, D and Vaniman, D. (1990). The Valles/Toledo Caldera Complex, Jemez Volcanic field, New Mexico. *Annual Review of Earth and Planetary Sciences* **18**, 27-53.

Henderson, P. (1984). About rare earth elements. In: Henderson, P. (ed.) *Rare Earth Element Geochemistry*. New York: Elsevier, pp. 1-50.

Henrys, S., Naish, T., Wilson, G., Gorman, A., Clifford, A., Johnston, L. & Blakemore, H.

(2006). ANDRILL 2005 site investigation/seismic surveys, McMurdo and Southern McMurdo Ice Shelf, McMurdo Sound, Antarctica. *The Institute of Geological and Nuclear Sciences (GNS Science)*, Science report **2006/13**, 42 p.

Henrys, S., Wilson, T., Whittaker, J., Fielding, C., Hall, J. & Naish, T. (2007). Tectonic history of Mid-Miocene to present southern Victoria Land Basin, inferred from seismic stratigraphy, in McMurdo Sound, Antarctica. In: Cooper, A. & Raymond, C. (eds) Antarctica: A keystone in a changing world - online proceedings for the Tenth International Symposium on Antarctic Earth Sciences. *USGS Open-file Report 2007-1047*, Short Research Paper **049**, doi:10.3133/of2007-1047.srp049.

Horgan, H., Bannister, S., Naish, T., Wilson, G., Pyne, A., Atkins, C. & Finnemore, M. (2003). ANDRILL site investigations/seismic surveys, McMurdo and Southern McMurdo Ice Shelf, McMurdo Sound, Antarctica. *Institute of Geological and Nuclear Sciences (GNS Science)*, Science report **2003/05**, 47 p.

Horgan, H., Naish, T., Bannister, S., Balfour, N. & Wilson, G. (2005). Seismic stratigraphy of the Ross Island Flexural Moat under the McMurdo-Ross Ice Shelf, Antarctica, and a prognosis for stratigraphic drilling. *Global and Planetary Change* **45**, 83-97.

Ishikawa, Y., Sawaguchi, T., Iwaya, S. & Horiuchi, M. (1976). Delineation of prospecting targets for Kuroko deposits based on modes of volcanism of underlying dacite and alteration halos. *Mining Geology* **26**, 105-117.

Johnston, D. M. (1997). Physical and social impacts of past and future volcanic eruptions in New Zealand. Ph.D. thesis, University of Canterbury, Christchurch, 288 p.

Jull, M. & McKenzie, D. (1996). The effect of deglaciation on mantle melting beneath Iceland, *Journal of Geophysical Research* **101**, 815-828.

Kaban, K., Flóvenz, Ó. G. & Pálmasón, G. (2002). Nature of the crust-mantle transition zone and the thermal state of the upper mantle beneath Iceland from gravity modeling. *Geophysical Journal International* **149**, 281-299.

Keppler, H. (1996). Constraints from partitioning experiments on the composition of subduction zone fluids. *Nature* **380**, 237-244.

Knight, J. (1999). Geological evidence for neotectonic activity during deglaciation of the southern Sperrin Mountains, Northern Ireland. *Journal of Quaternary Science* **14**, 45-57.

Kyle, P. (1990). Erebus Volcanic Province. In: LeMasurier, W. & Thomson, J. (eds) *Volcanoes of the Antarctic Plate and Southern Ocean*. Washington, D.C.: American Geophysical Union, pp. 97-108.

Kyle, P., Elliot, D. & Sutter, J. (1981). Jurassic Ferrar Supergroup tholeiites from the Transantarctic Mountains, Antarctica, and their relationship to the initial fragmentation of

Gondwana. In: Cresswell, M. & Vella, P. (eds) *Gondwana Five, Fifth International Gondwana Symposium*, pp. 283-287.

Kyle, P., Moore, J. & Thirlwall, M. (1992). Petrologic evolution of anorthoclase phonolite lavas at Mount Erebus, Ross Island, Antarctica. *Journal of Petrology* **33**, 849–875.

Kyle, P. & Muncy, H. (1989). Geology and geochronology of McMurdo Volcanic Group rocks in the vicinity of Lake Morning, McMurdo Sound, Antarctica. *Antarctic Science* **1**, 345-350.

Large, R., Gemmell, J. & Paulick, H. (2001). The alteration box plot - a simple approach to understanding the relationship between alteration mineralogy and lithogeochemistry associated with volcanic hosted massive sulfide deposits. *Economic Geology* **96**, 957-971.

Le Bas, M., Maitre, M., Streckeisen, A. & Zanettin, B. (1986). A chemical classification of volcanic rocks based on the total alkali-silica diagram. *Journal of Petrology* **27**, 745-750.

LeMasurier, W. & Thomson, J. (eds) (1990). *Volcanoes of the Antarctic Plate and Southern Oceans*. Washington, D.C.: American Geophysical Union.

Lewis, A., Marchan, D., Ashworth, A., Hemming, S. & Machlus, M. (2007). Major middle Miocene global climate change: Evidence from East Antarctica and the Transantarctic Mountains. *GSA Bulletin* **119**, 1449-1461.

Luhr, J. F. (2001). Glass inclusions and melt volatile contents at Parícutin volcano, Mexico. *Contributions to Mineralogy and Petrology* **142**, 261-283.

MacLennan, J., Jull, M., McKenzie, D., Slater, L. & Grönvold, K. (2002). The link between volcanism and deglaciation in Iceland. *Geochemistry, Geophysics, Geosystems* **3**, doi:10.1029/2001GC000282.

Manga, M., Patel, A. & Dufek, J. (2010). Rounding of pumice clasts during transport; field measurements and laboratory studies. *Bull Volcanol*, doi:10.1007/s00445-010-0411-6.

Martin, A. (2009). Mount Morning, Antarctica: geochemistry, geochronology, petrology, volcanology, and oxygen fugacity of the rifted Antarctic lithosphere. PhD thesis, University of Otago, Dunedin, New Zealand, 413 p.

Martin, A., Cooper, Alan F. & Dunlap, J. (2009). Geochronology of Mount Morning Antarctica: two-phase evolution of a long-lived trachyte-basanite-phonolite eruptive center. *Bull Volcanol*, doi:10.1007/s00445-009-0319-1.

Matsui, Y., Onuma, N., Nagasawa, H., Higuchi, H. & Banno, S. (1977). Crystal structure control in trace element partition between crystal and magma. *Tectonics* **100**, 315-324.

McCulloch, M. T. & Gamble, J. A. (1991). Geochemical and geodynamical constraints on

subduction zone magmatism. *Earth and Planetary Science Letters* **102**, 358–374.

McDonough, W. & Sun, S. (1995). The composition of the Earth. *Chemical Geology* **120**, 223-253.

McIntosh, W. (1998).  $^{40}\text{Ar}/^{39}\text{Ar}$  geochronology of volcanic clasts and pumice in CRP-1 core, Cape Roberts, Antarctica. *Terra Antarctica* **5**, 683-690.

McIntosh, W. (2000).  $^{40}\text{Ar}/^{39}\text{Ar}$  geochronology of tephra and volcanic clasts in CRP-2A Victoria Land Basin, Antarctica. *Terra Antarctica* **7**, 621-630.

McKay, R., Browne, G., Carter, L., Cowan, E., Dunbar, G., Krissek, L., Naish, T., Powell, R., Reed, J., Talarico, F. & Wilch, T. (2009). The stratigraphic signature of the late Cenozoic Antarctic Ice Sheets in the Ross Embayment. *GSA Bulletin* **129**, 1537-1561.

Melluish, A., Henrys, S., Bannister, S. & Davey, F. J. (1995). Seismic profiling adjacent to Ross Island: Constraints on late Cenozoic stratigraphy and tectonics. *Terra Antarctica* **2**, 127-136.

Monaghan, A., Bromwich, D., Powers, J., & Manning, K. (2005). The climate of the McMurdo, Antarctica region as represented by one year of forecasts from the Antarctic Mesoscale Prediction System. *Journal of Climate* **18**, 1174–1189.

Mullen, A., Sinclair, M. & Hatherton, T. (1990). *Antarctica: the Ross Sea Region*. Wellington:

Department of Scientific and Industrial Research.

Naish, T. R., Levy, R. H., Powell, R. P. & the ANDRILL MIS Science and Operations Team.

2006. *ANDRILL McMurdo Ice Shelf Scientific Logistical Implementation Plan*. ANDRILL

Contribution 7, University of Nebraska, Lincoln, 117 p.

Naish, T., Woolfe, K., Barrett, P., Wilson, G., Atkins, C., Bohaty, S., Bücker, C., Claps, M., Davey, F., Dunbar, G., Dunn, A., Fielding, C., Florindo, F., Hannah, M., Harwood, D., Henrys, S., Krissek, L., Lavelle, M., van der Meer, J., McIntosh, W., Niessen, F., Passchier, S., Powell, R., Roberts, A., Sagnotti, L., Scherer, R., Strong, C., Franco, P., Talarico, F., Verosub, K., Villa, G., Watkins, D., Webb, P. & Wonik, T. (2001). Orbitally induced oscillations in the East Antarctic ice sheet at the Oligocene/Miocene boundary. *Nature* **413**, 207-216.

Naish, T., Powell, R., Levy, R. & the ANDRILL-SMS Science Team. (2007). Background to the ANDRILL McMurdo Ice Shelf Project, Antarctica. *Terra Antarctica* **14**, 121-130.

Naish, T., Powell, R., Wilson, G., Scherer, R., Talarico, F., Krissek, L., Niessen, F., Pompilio, M., Wilson, T., Carter, L., DeConto, R., Huybers, P., McKay, R., Pollard, D., Ross, J., Winter, D., Barrett, P., Browne, G., Cody, R., Cowan, E., Crampton, J., Dunbar, G., Dunbar, N., Florindo, F., Gebhardt, C., Graham, I., Hannah, M., Hansraj, D., Harwood, D., Helling, D., Henrys, S., Hinnov, L., Kuhn, G., Kyle, P., Laufer, A., Maffioli, P., Magens, D., Mandernack, K., McIntosh, W., Millan, C., Morin, R., Ohneiser, C., Paulsen, T., Persico, D., Raine, I., Reed, J., Riesselman, C., Sagnotti, L., Schmitt, D., Sjunneskog, C., Strong, P., Taviani, M., Vogel, S.,

Wilch, T. & Williams, T. (2009). Obliquity-paced Pliocene West Antarctic Ice Sheet oscillations. *Nature* **458**, 322-328.

Nowell, D., Jones, M. & Pyle, D. (2006). Episodic Quaternary volcanism in France and Germany. *Journal of Quaternary Science* **21**, 645-675.

Panter, K. (1995). Geology, geochemistry and petrogenesis of the Mount Sidley volcano, Marie Byrd Land, Antarctica. PhD thesis, New Mexico Institute of Mining and Technology, Socorro, NM, 118 p.

Panter, K., Kyle, P. & Smellie, J. (1997). Petrogenesis of a phonolitic-trachyte succession at Mount Sidley, Marie Byrd Land, Antarctica. *Journal of Petrology* **38**, 1225-1253.

Panter K., Talarico F., Bassett K., Del Carlo P., Field B., Frank T., Hoffmann S., Kuhn G., Reichelt L., Sandroni S., Taviani M., Bracciali L., Cornamusini G., von Eynatten H., Rocchi S. & the ANDRILL-SMS Science Team. (2008). Petrologic and Geochemical Composition of the AND-2A Core, ANDRILL Southern McMurdo Sound Project, Antarctica. *Terra Antarctica* **15**, 147-192.

Panter, K & Winter, B. (2008). Geology of the Side Crater of the Erebus Volcano, Antarctica. *Journal of Volcanology and Geothermal Research* **177**, 578-588.

Passchier, S., Browne, G., Field, B., Fielding, C., Florindo, F., Harwood, D., Krissek, L., Pekar,

S. & Panter, K. (2011). Early and middle Miocene Antarctic glacial history from the sedimentary facies distribution in the AND-2A drill hole, Ross Sea, Antarctica. *GSA Bulletin*, doi:10.1130/B30334.1.

Paulsen, T. S. & Wilson T. J. (2009). Structure and age of volcanic fissures on Mount Morning: A new constraint on Neogene to contemporary stress in the West Antarctic Rift, southern Victoria Land, Antarctica. *GSA Bulletin* **121**, 1071-1088.

Petit, J., Della, M., Dran, J., Magonthier, M., Mando, P. & Paccagnella A. (1990). Hydrated-layer formation during dissolution of complex silicate glasses and minerals. *Geochimica et Cosmochimica Acta* **54**, 1941–1955.

Pinel, V. & Jaupart, C. (2000). The effect of edifice load on magma ascent beneath a volcano. *Philosophical Transactions of the Royal Society of London A* **358**, 1515-1532.

Pinel, V. & Jaupart, C. (2005). Some consequences of volcanic edifice destruction for eruption conditions. *Journal of Volcanology and Geothermal Research* **145**, 68-80.

Pompilio, M., Dunbar, N., Gebhardt, A., Helling, D., Kuhn, G., Kyle, P., McKay, R., Talarico, F., Tulaczyk, S., Vogel, S., Wilch, T. & the ANRILL-MIS Science Team. (2007). Petrology and geochemistry of the AND-1B core, ANDRILL McMurdo Ice Shelf Project, Antarctica. *Terra Antarctica* **14**, 255-288.

Powell, R. & Domack, E. (2002). Modern glaciomarine environments. In Menzies, M. (ed.) *Modern and Past Glacial Environments*. Oxford: Butterworth-Heinemann, pp. 361-389.

Powell, R. D. & Molnia, B. F. (1989). Glacimarine sedimentary processes, facies and morphology of the south-southwest Alaska shelf and fjords. *Marine Geology* **85**, 359-390.

Sandroni, S. & Talarico, F. (2011). The record of Miocene climatic events in AND-2A drill core (Antarctica): Insights from provenance analyses of basement clasts. *Global and Planetary Change* **75**, 31-46.

Schacht, U., Wallmann, K., Kutterolf, S. & Schmidt, M. (2009). Volcanogenic sediment-seawater interactions and the geochemistry of pore waters. *Chemical Geology* **249**, 321-338.

Schmidt-Thomé, M., Mueller, P. & Tessensohn, F. (1990). Malta Plateau. In: LeMasurier, W. & Thomson, J. (eds) *Volcanoes of the Antarctic Plate and Southern Ocean*. Washington, D.C.: American Geophysical Union, pp. 53-39.

Shevenell, A. & Kennett, J. (2007). Cenozoic Antarctic cryosphere evolution: Tales from deep sea sedimentary records. *Deep Sea Research II* **54**, 2308-2324.

Shoji S., Nanzyo M., Shirato Y. & Ito T. (1993). Chemical kinetics of weathering in young andisols from northeastern Japan using soil age normalized to 10°C. *Soil Science* **155**, 53–60.

Sigvaldason, G. (2002). Volcanic and tectonic processes coinciding with glaciation and crustal rebound: an early Holocene rhyolitic eruption in the Dyngjufjöll volcanic centre and the formation of the Askja caldera, north Iceland. *Bull Volcanol* **64**, 192-205.

Slater, L., McKenzie, D. & Grönvöld, K. (1998). Deglaciation effects on mantle melting under Iceland: results from the northern volcanic zone. *Earth and Planetary Science Letters* **164**, 151-164.

Solomon, S., D. Qin, M., Manning, Z., Chen, M., Marquis, K., Averyt, M., Tignor & Miller, H. (eds) (2007). IPCC. In: *Climate Change 2007: The Physical Science Basis. Contribution of Working Group I to the Fourth Assessment Report of the Intergovernmental Panel on Climate Change*. Cambridge: Cambridge University Press, Cambridge, pp. 707-709.

Stern, T. A. & ten Brink, U. S. (1989). Flexural uplift of the Transantarctic Mountains. *Journal of Geophysical Research* **94**, 10315-10330.

Stinton, J. Grönvold, K. & Sæmundsson, K. (2005). Postglacial eruptive history of the western volcanic zone, Iceland. *Geochemistry Geophysics Geosystems* **6**, doi:10.1029/2005GC001021.

Sun, S. & McDonough, W. (1989). Chemical and isotopic systematics of ocean basalts: Implications for mantle composition processes. In Saunders, A. and Norry, M. (eds.) Magmatism in the Ocean Basins. *Geological Society of London Special Publications* **42**, 313-345.

Talarico, F. & Sandroni, S. (2009). Provenance signatures of the Antarctic ice sheets in the Ross Embayment during the Late Miocene to Early Pliocene: The ANDRILL AND-1B core record. *Global and Planetary Change*, doi:10.1016/j.globch.2009.09.002.

Tauxe L., Gans P. & Mankinen E. A. (2004). Paleomagnetism and  $^{40}\text{Ar}/^{39}\text{Ar}$  Ages from Volcanics Extruded during the Matuyama and Brunhes Chrons near McMurdo Sound, Antarctica. *Geochemistry Geophysics Geosystems* **5** Q06H12, doi:10.1029/2003GC000656.

van Achterbergh E., Ryan C. & Jackson S. (2001). Data reduction software for LA-ICP-MS. In: Sylvester P, editor. Laser Ablation-ICPMS in the Earth Science. *Mineralogical Association of Canada. Short course series* **29**, 239-243.

Warny, S., Askin, R., Hannah, M., Mohr, B., Raine, J., Harwood, D., Florindo, F. & the SMS Science Team. 2009. Palynomorphs from a sediment core reveal a sudden remarkably warm Antarctica during the Middle Miocene. *Geology* **37**, 955-958.

Wilch, T. I., Lux, D. R., Denton, G. H. & McIntosh, W. C. (1993). Minimal Pliocene-Pleistocene uplift of the dry valley sector of the Transantarctic Mountains: A key parameter in ice-sheet reconstructions. *Geology* **21**, 841- 44.

Wilcox, R. E. (1954). Petrology of Parícutin Volcano, Mexico. *US Geological Survey Bulletin* **96SC**, 281-353.

Wilson, G. S., Naish, T., Jordon, T., Damaske, D., Ali, M., Horgan, H., Balfour, N., Watts, A., Bannister, S. & the ANDRILL Site Survey Team. (2003). Using flexural modeling and geophyscial data to define Neogene stratigraphic drilling targets in moat basins beneath the McMurdo Ice Shelf. *Geophysical Research Abstracts* **5**, article number 05682.

Wilson, T. (1999). Cenozoic structural segmentation of the Transantarctic Mountains rift flank in southern Victoria Land. *Global and Planetary Change* **23**, 105-127.

Wolff-Boenisch, D., Gislason, S., Oelkers, E. & Putnis, C. (2004). The dissolution rates of natural glasses as a function of their composition at pH 4 and 10.6, and temperatures from 25 to 74°C. *Geochimica et Cosmochimica Acta* **68**, 4843–4858.

Wright-Grassham, A. (1987). Volcanic geology, mineralogy, and petrogenesis of the Discovery Volcanic Subprovince, southern Victoria Land, Antarctica. PhD Thesis. New Mexico Institute of Mining and Technology, Socorro, NM. 460 p.

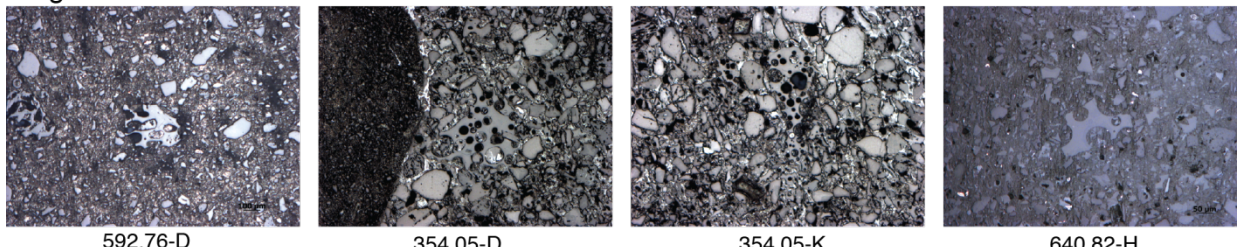
Zielinski, G., Mayewski, P., Meeker, L., Whitlow, S. & Twickler, M. (1996). 110,000-yr record of explosive volcanism from the GISP2 (Greenland) ice core. *Quaternary Research* **45**, 109-118.

## APPENDICES

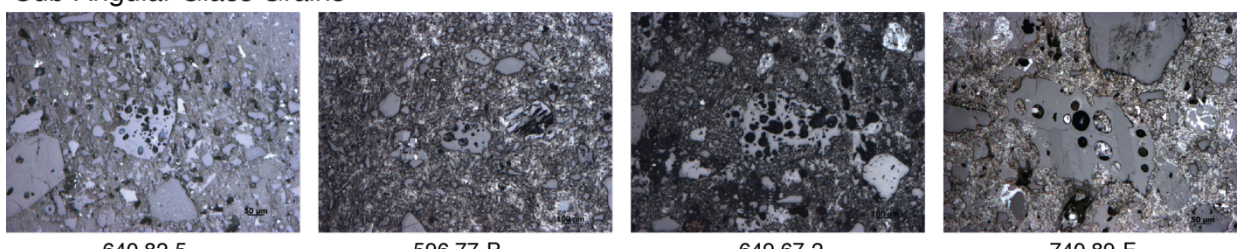
### Appendix A

Examples of angular, sub-angular, sub-rounded, and rounded glass grains found in the AND-2A core that were used as a visual aid in order to determine relative rounding of glass grains while completing modified point counting of samples.

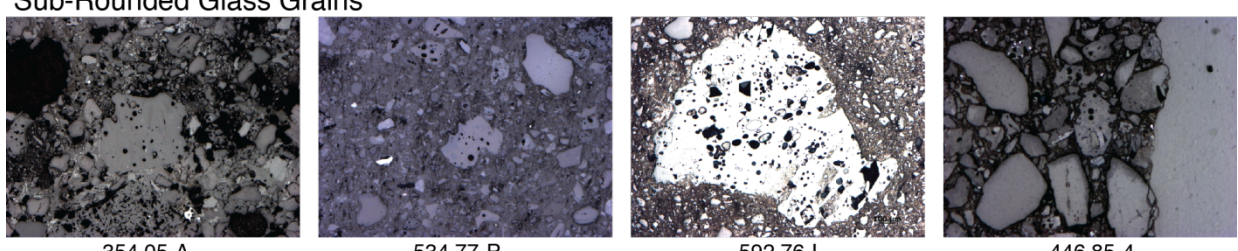
**Angular Glass Grains**



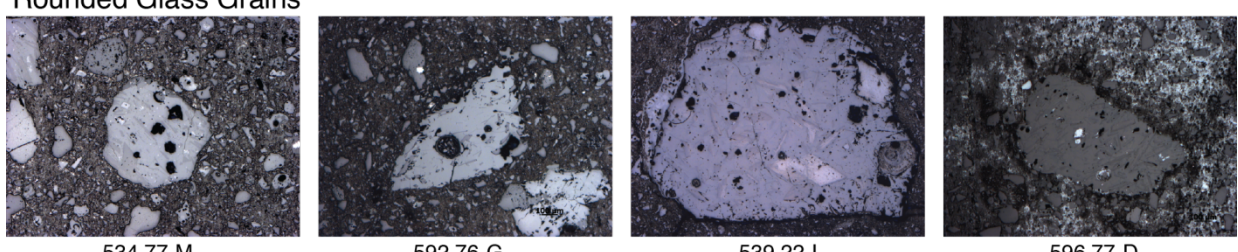
**Sub-Angular Glass Grains**



**Sub-Rounded Glass Grains**



**Rounded Glass Grains**



## Appendix B

Tutorial of digital image processing techniques used to determine R-values in this study.

Digital image processing techniques in ArcMap<sup>©</sup> were used to quantify the shape and size of 78 glass grains found in the 7 samples from Sequence 32 in the AND-2A core. First, layers were created for each of the 3 bands (R, G, B) for each color image of an individual glass grain in ArcCatalog<sup>©</sup> (Fig. 1).

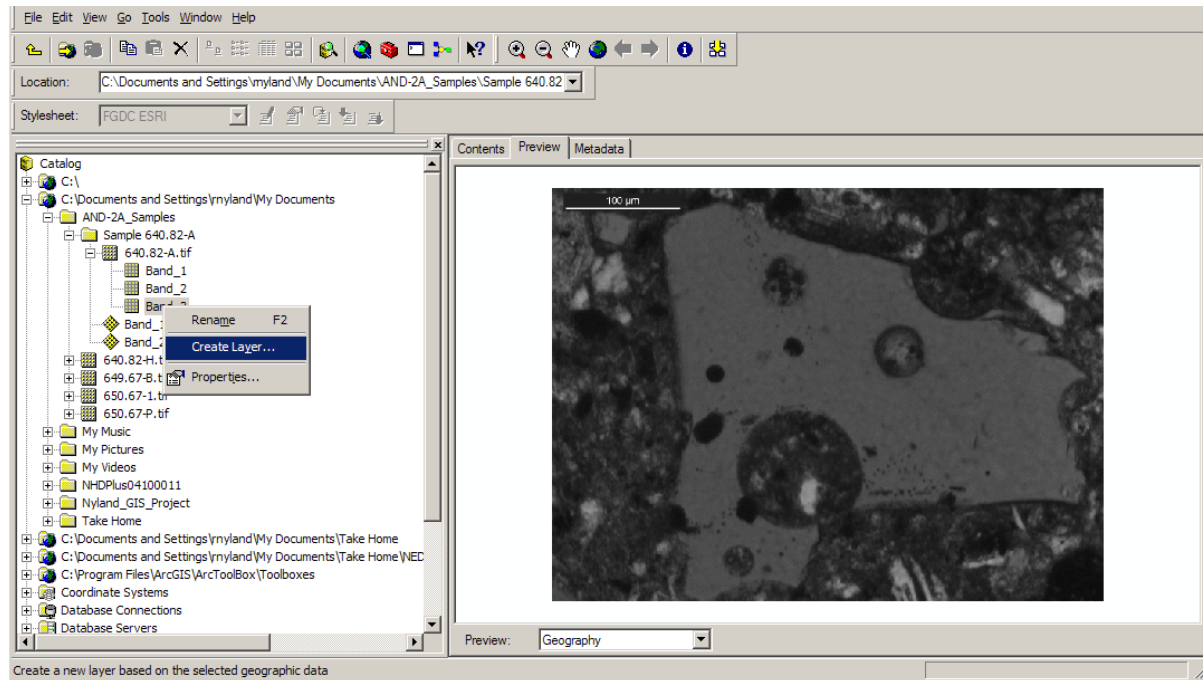


**Figure 1**

The three band layers were then loaded into ArcMap© (Fig. 2).

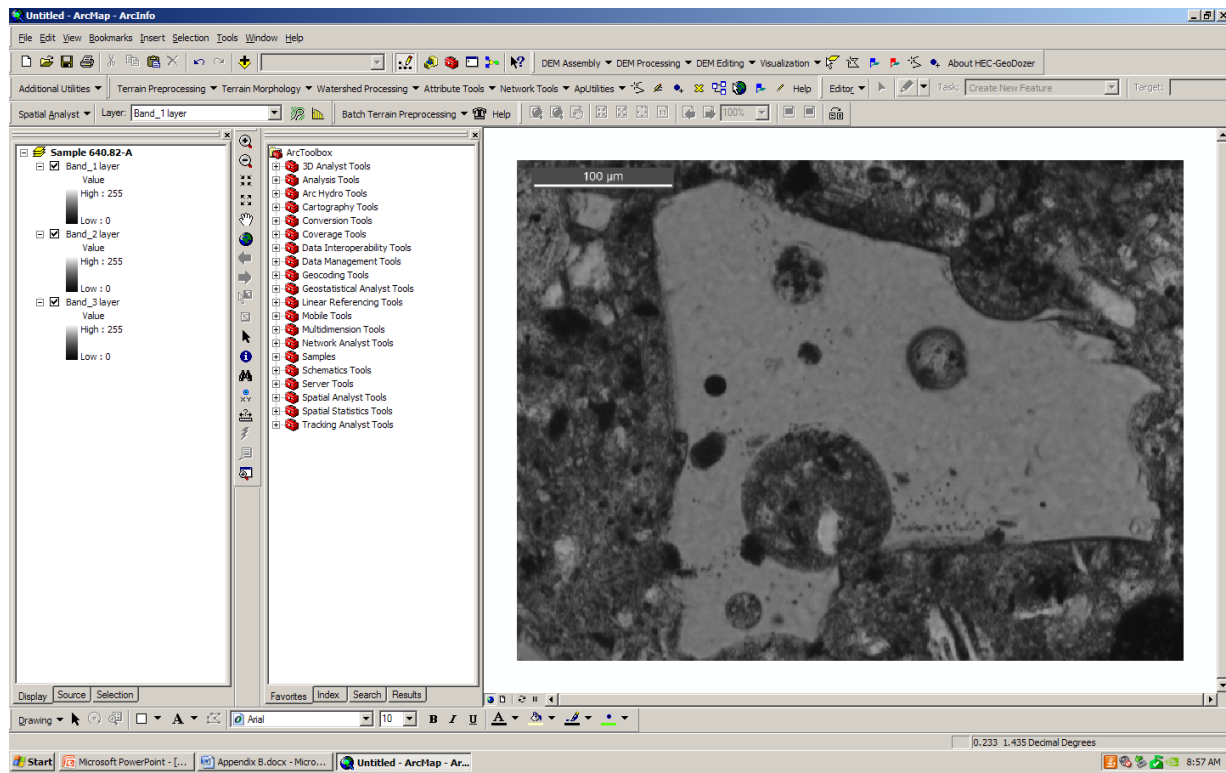


Figure 2

Using the model builder tool in ArcToolbox®, the following model was built to digitally process the color images of the glass grains (Fig. 3).

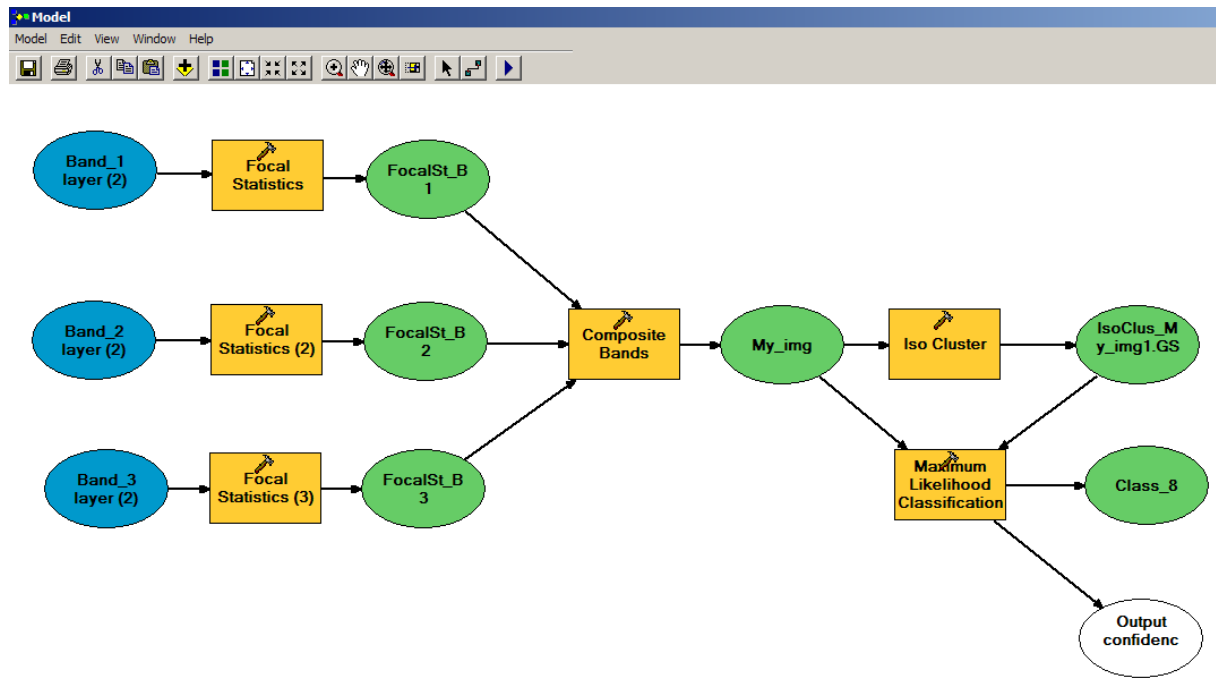


Figure 3

Each of the band layers for an individual grain was input into the model, and focal statistics were calculated for each band layer (Fig. 4). The focal statistics tool calculates a statistic on a raster file over a specific neighborhood. In this case, the statistics were calculated using the median of the cells in the neighborhood.

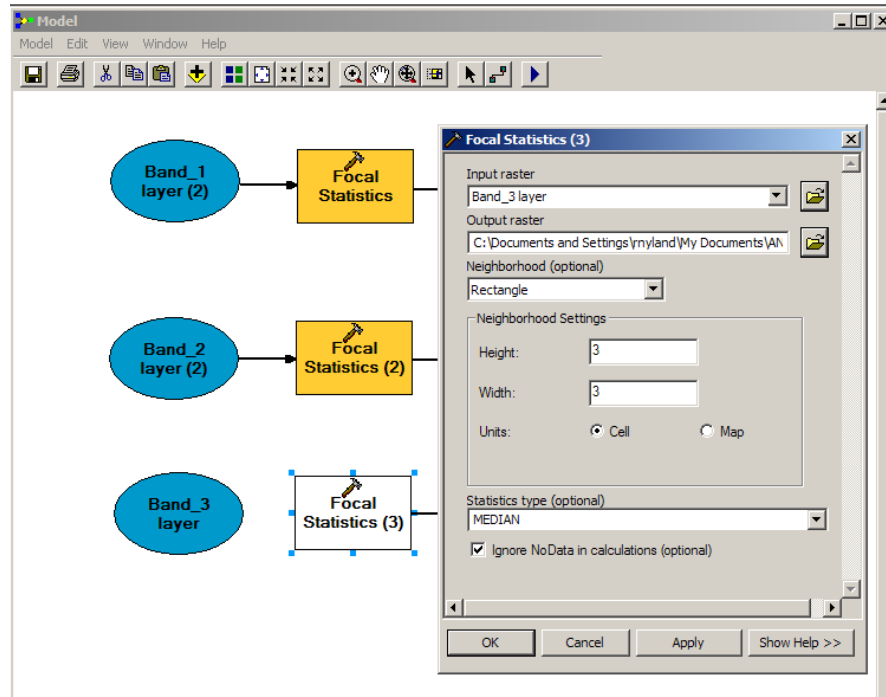
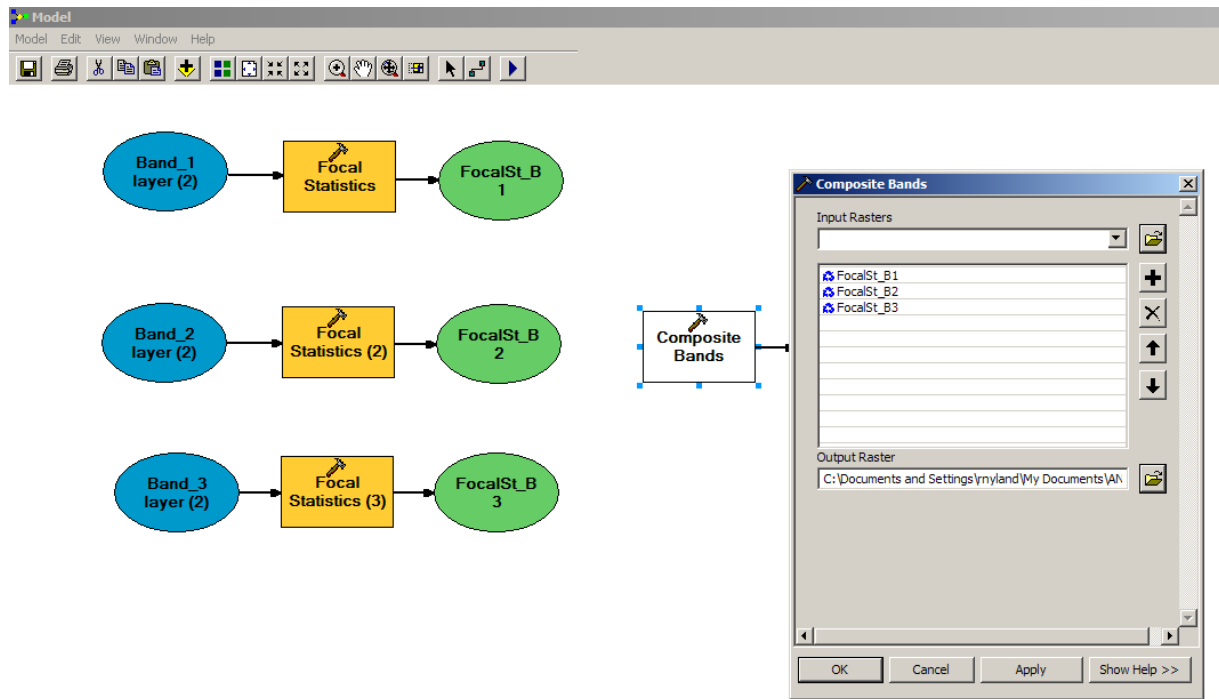


Figure 4

After focal statistics were run on each band, the results were used to composite the 3 bands into a single raster dataset (Fig. 5).



**Figure 5**

The isodata clustering algorithm was then performed on the resulting composite image. This function uses the natural groupings of cells in multidimensional attribute space. In this case the cells were grouped into 8 classes (Fig. 6).

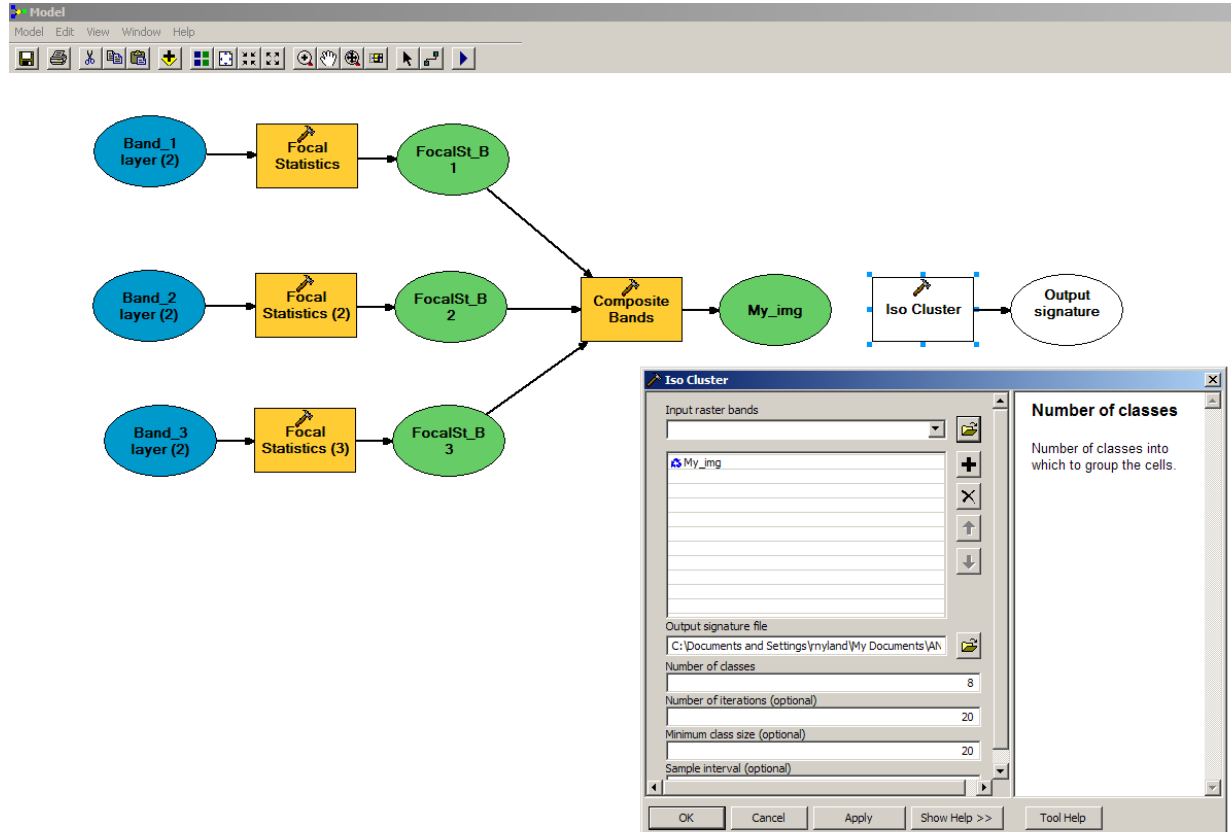


**Figure 6**

Then, the composite image was classified using maximum likelihood classification, using the composite raster dataset and isodata clustering result (Fig. 7).

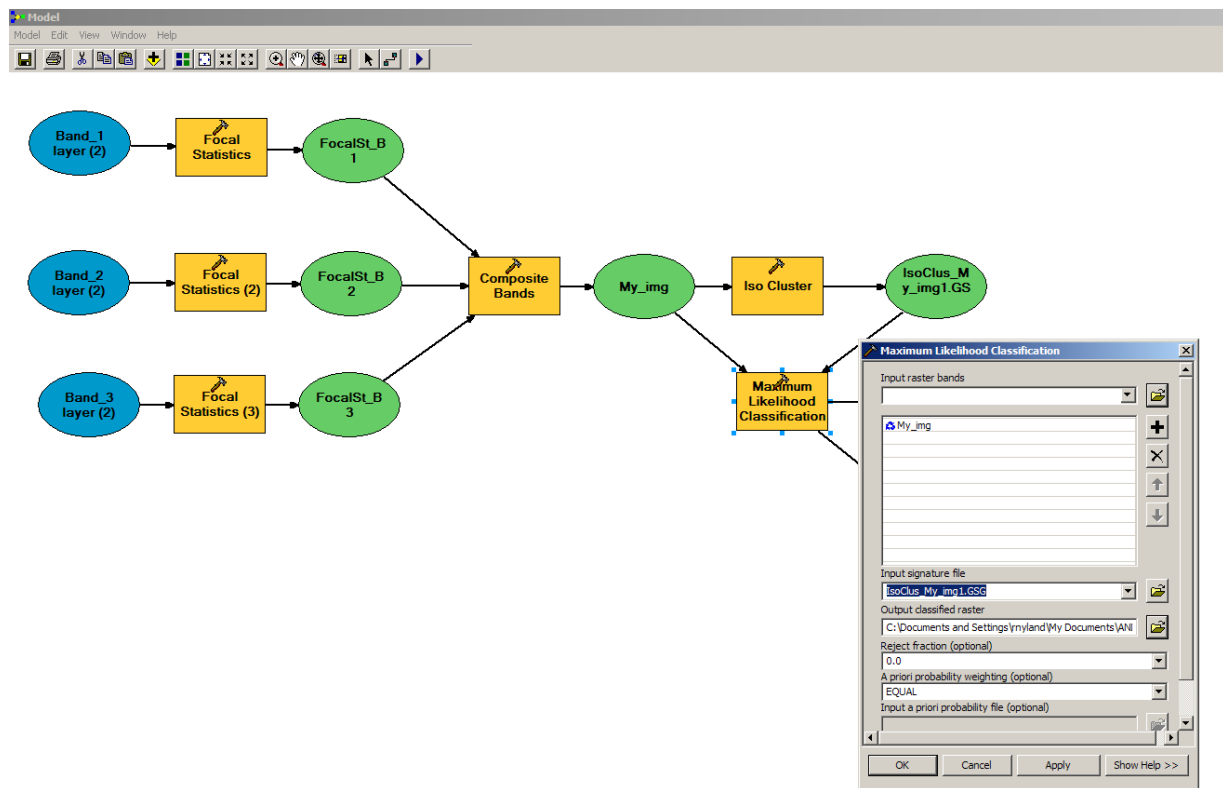


**Figure 7**

A classified image resulted from running the entire model (Fig. 8).

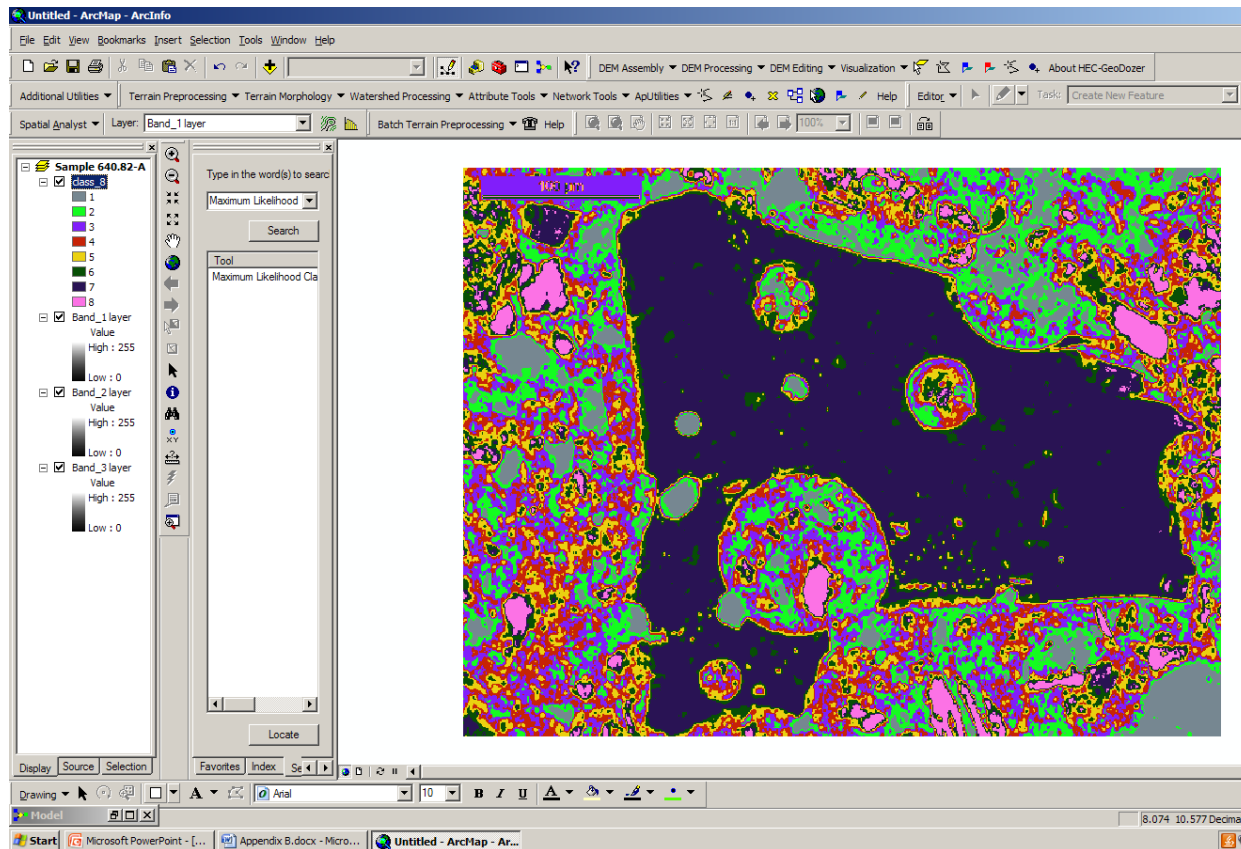


Figure 8

After the composite image was classified, manual reclassification was used as needed in order to correctly classify the image (Fig. 9).

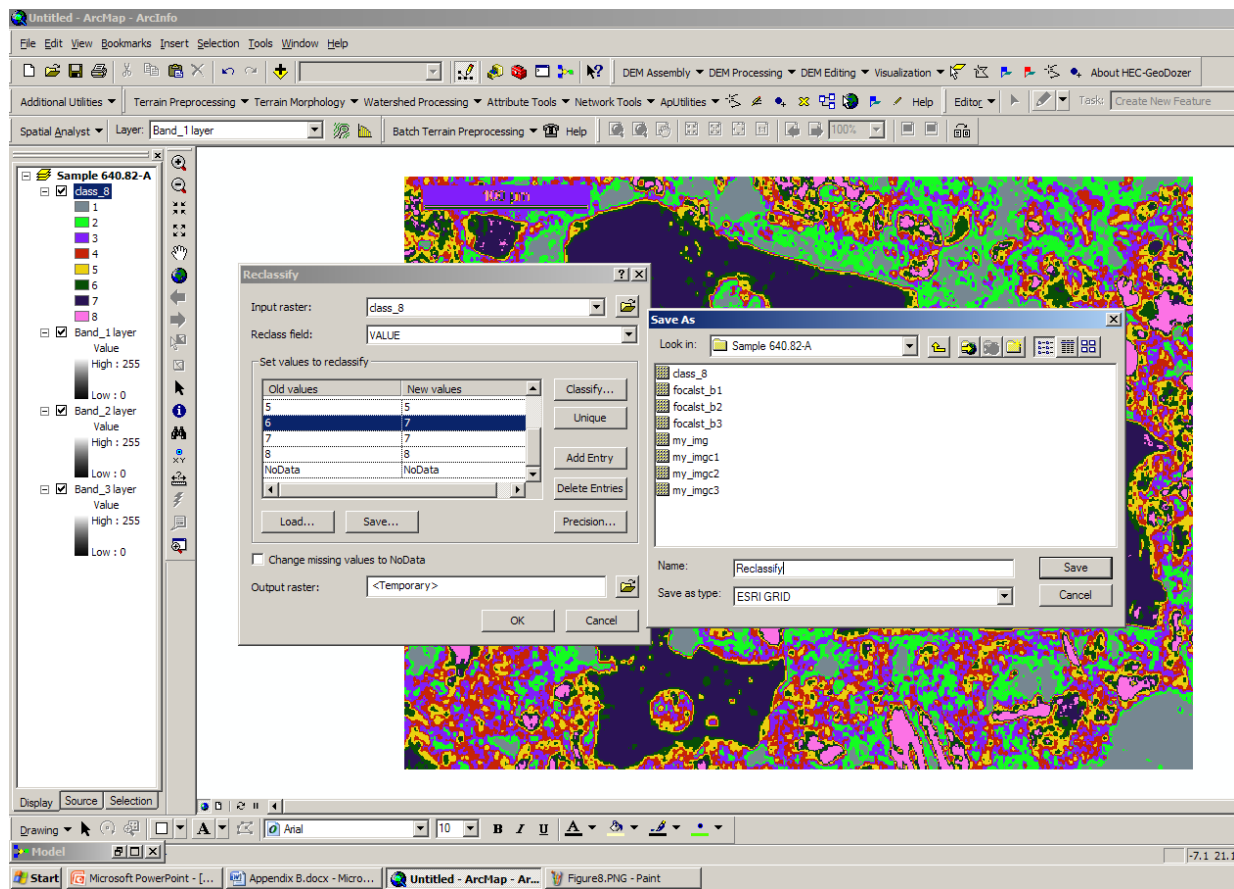


Figure 9

Once satisfied with the classification, the resulting classification scheme for each individual grain (Fig. 10) was then converted from raster data to polygon (vector) data (Fig. 11), and a shapefile was created for each individual glass grain (Fig. 12).

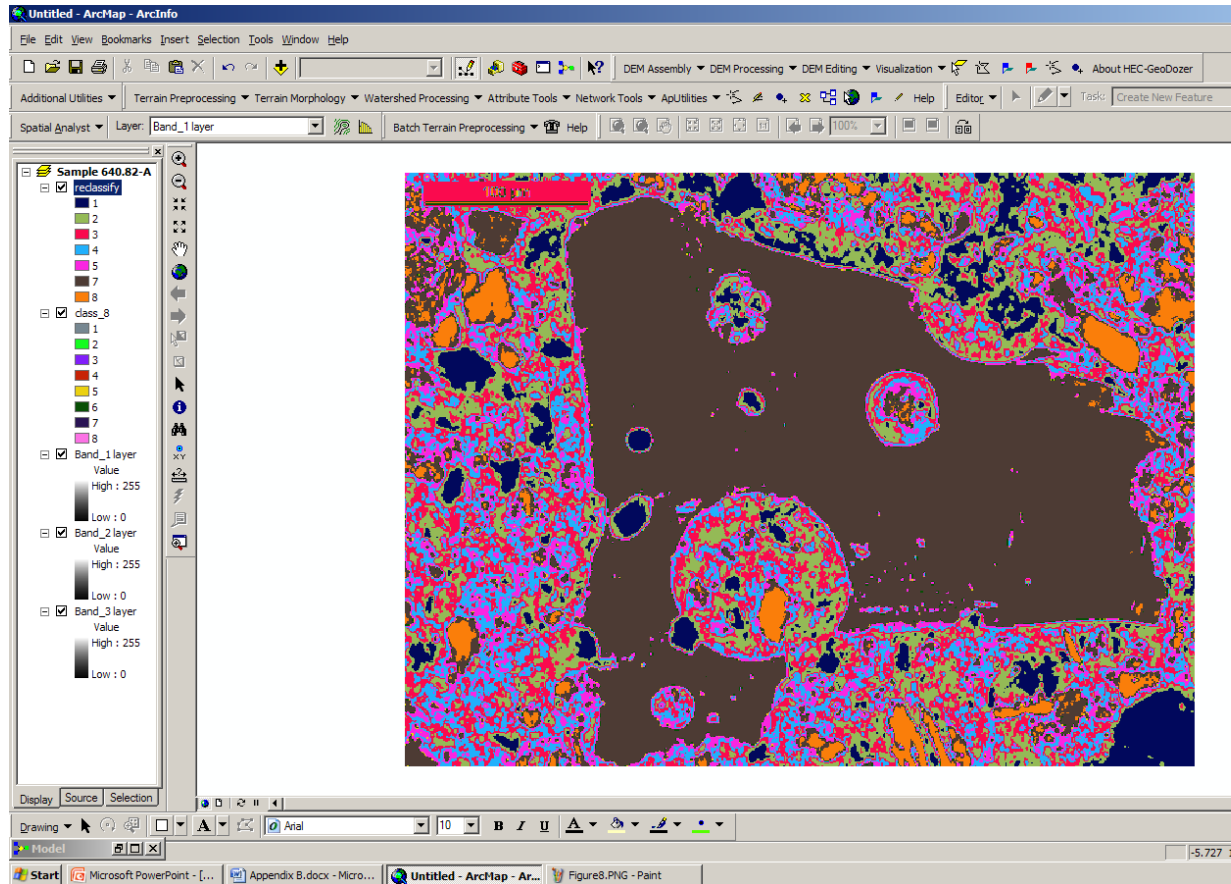


Figure 10

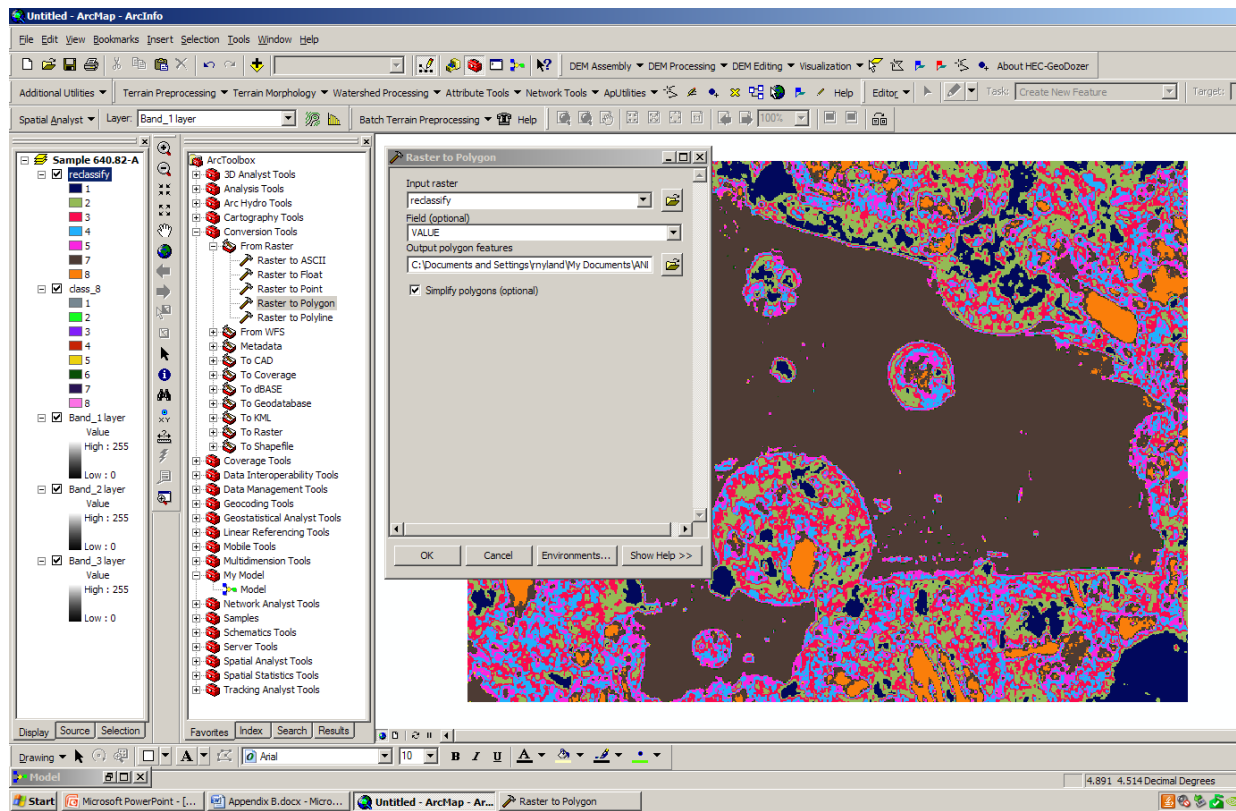


Figure 11

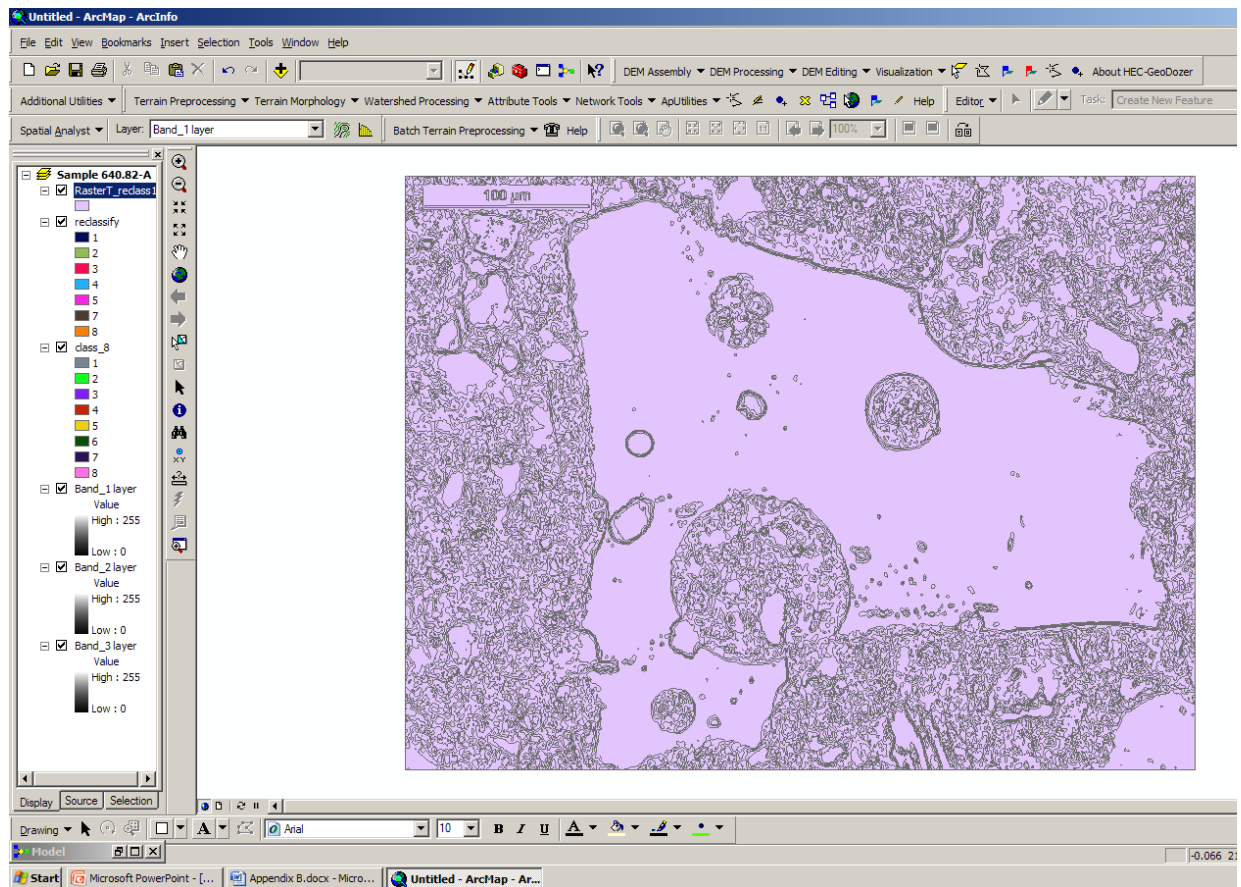


Figure 12

The perimeter of each grain, defined as the sum of the pixels making up its outer boundary, was determined by calculating the geometry of the resulting polygons from the classified image directly in ArcMap<sup>©</sup>. The area of each grain, defined as the sum of the pixels within the perimeter, was also determined by calculating the geometry of the resulting polygons from the classified image directly in ArcMap<sup>©</sup> (Fig. 13).

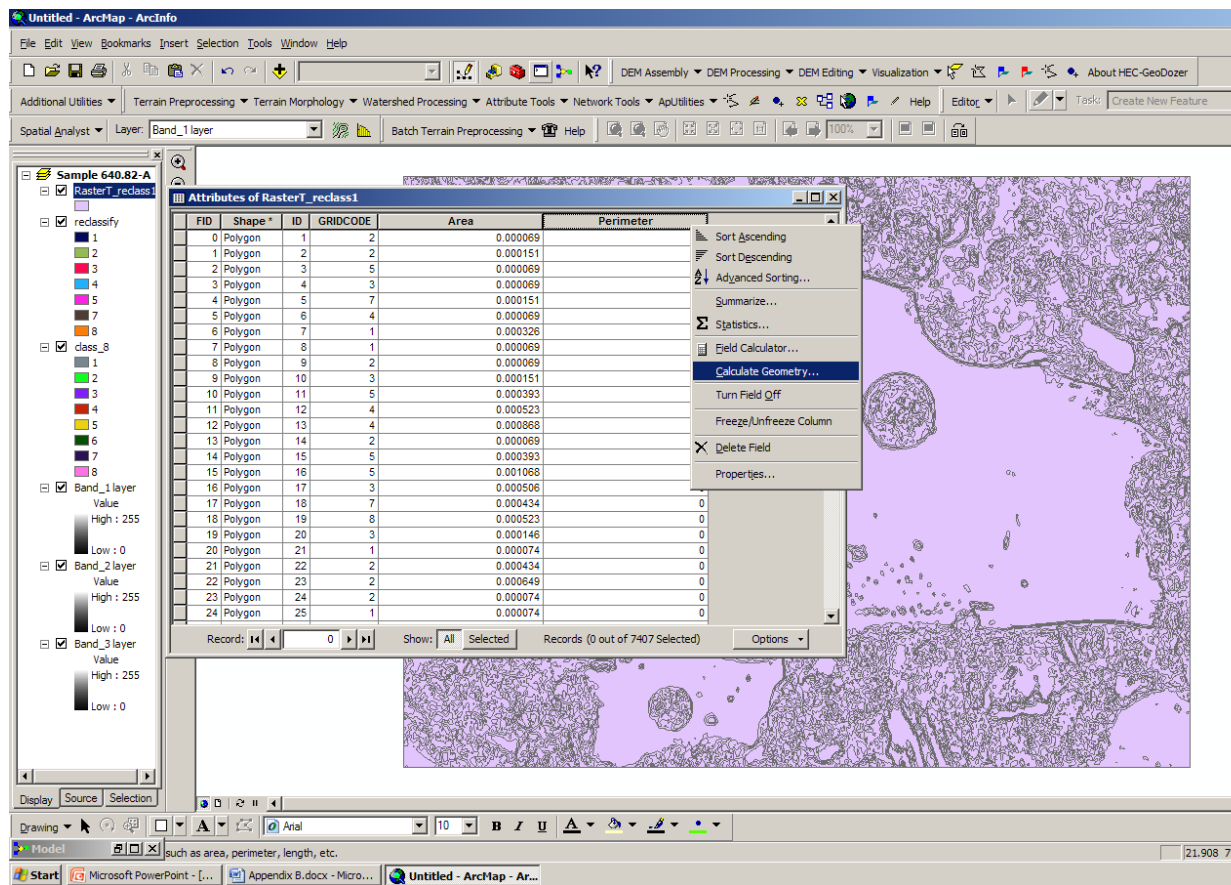


Figure 13

Rounding was then determined quantitatively ( $4\pi A/P^2$ ) following Manga *et al.* (2010). For comparison, the shape and size of ash grains from a primary pyroclastic fall deposit on nearby Mount Erebus (Panter and Winter, 2008) were digitally processed and evaluated in the same manner.

## Appendix C

Full dataset of major and trace elemental compositions of glass shards from the AND-2A core

Sample	354.05-A	354.05-A2	354.05-Q	<b>354.05-1</b>	354.05-K	354.05-E	354.05-O	<b>354.05-N</b>
Model Age (Ma)	15.91	15.91	15.91	<b>15.91</b>	15.91	15.91	15.91	<b>15.91</b>
wt% oxide								
SiO <sub>2</sub>	49.31	49.31	45.99	<b>47.40</b>	46.73	51.53	51.53	<b>58.60</b>
TiO <sub>2</sub>	3.03	3.03	4.85	<b>3.40</b>	4.03	2.71	2.34	<b>1.35</b>
Al <sub>2</sub> O <sub>3</sub>	16.21	16.21	15.06	<b>10.45</b>	15.41	15.63	16.83	<b>16.87</b>
FeO	11.46	11.46	13.14	<b>7.68</b>	12.52	10.58	11.28	<b>7.94</b>
MnO	0.27	0.27	0.26	<b>0.13</b>	0.24	0.27	0.25	<b>0.21</b>
MgO	3.96	3.96	4.98	<b>10.96</b>	5.21	3.34	3.24	<b>1.57</b>
CaO	7.48	7.48	9.70	<b>18.64</b>	9.39	6.65	6.81	<b>4.26</b>
Na <sub>2</sub> O	4.51	4.51	3.83	<b>1.73</b>	3.91	4.06	4.54	<b>4.35</b>
K <sub>2</sub> O	2.16	2.16	1.45	<b>0.67</b>	1.42	2.95	2.24	<b>3.92</b>
P <sub>2</sub> O <sub>5</sub>	1.47	1.47	0.73	<b>0.36</b>	0.77	1.26	1.33	<b>0.46</b>
SO <sub>2</sub>	0.00	0.00	0.07	<b>-0.05</b>	0.03	0.06	0.00	<b>0.00</b>
Cl	0.11	0.11	0.08	<b>0.03</b>	0.07	0.12	0.12	<b>0.16</b>
SrO	-0.15	-0.15	-0.13	<b>-0.17</b>	-0.16	-0.12	-0.12	<b>-0.14</b>
BaO	0.09	0.09	-0.01	<b>0.05</b>	0.04	0.01	0.10	<b>0.07</b>
Total	99.91	99.91	100.02	<b>101.27</b>	99.60	99.05	100.48	<b>99.61</b>
Mg-no.								
ne	38.10	38.10	40.30	<b>71.81</b>	42.57	36.04	33.84	<b>26.08</b>
di	0.23	0.23	2.71	<b>6.28</b>	2.37	0.00	0.00	<b>0.00</b>
ol	7.98	7.98	19.31	<b>56.21</b>	17.22	7.44	4.96	<b>2.60</b>
Q	8.66	8.66	3.79	<b>1.27</b>	6.47	0.00	3.68	<b>0.00</b>
hy	0.00	0.00	0.00	<b>0.00</b>	0.00	0.55	0.00	<b>5.80</b>
ppm								
Li	8.13	12.04			4.10	11.11	11.14	
Be	2.62	<0.00			<1.18	5.53	<0.00	
B	12.64	15.33			22.28	23.03	12.73	
Sc	17.95	20.25			21.23	15.11	18.28	
Ti	14316.22	17116.76			20954.38	14807.61	15886.50	
V	89.12	105.23			268.07	98.81	79.19	
Cr	4.31	<2.71			16.32	4.22	<3.40	
Co	14.97	18.66			34.24	15.19	15.75	
Ni	0.65	0.13			13.83	0.42	<0.33	
Zn	134.09	153.43			125.85	172.19	210.47	
Rb	37.91	43.66			28.32	54.83	57.04	
Sr	683.39	721.89			792.52	710.78	741.80	
Y	42.73	44.72			22.30	31.92	53.40	
Zr	325.49	381.91			199.64	348.39	505.95	
Nb	85.01	99.71			50.25	77.57	119.06	
Cs	0.40	0.39			0.29	0.47	0.57	
Ba	518.56	591.50			441.96	800.44	732.52	
La	75.89	83.80			41.44	69.83	100.98	
Ce	160.14	173.68			84.25	146.15	204.36	
Pr	20.28	20.15			10.40	16.23	25.05	
Nd	84.57	87.24			39.41	64.18	101.02	
Sm	16.42	17.78			6.28	14.61	16.28	
Eu	5.30	6.01			3.09	4.25	6.10	
Gd	12.82	12.72			7.46	9.93	12.79	
Tb	1.71	1.74			0.88	1.28	2.17	
Dy	9.60	10.90			5.24	6.74	11.01	
Ho	1.80	2.08			0.99	1.17	2.28	
Er	4.28	4.22			1.77	3.81	6.10	
Tm	0.61	0.46			0.22	0.50	0.73	
Yb	4.25	4.97			2.38	3.31	4.98	
Lu	0.49	0.55			0.33	0.48	0.87	
Hf	7.39	9.10			4.59	7.84	11.80	
Ta	4.58	5.49			2.92	3.96	7.09	
Pb	10.03	9.89			2.96	6.65	3.66	
Th	5.79	6.62			3.85	6.58	9.25	
U	1.70	2.25			1.43	2.36	2.81	
AI	33.81	33.81	32.20	<b>36.34</b>	33.27	37.02	32.54	<b>38.94</b>
CCPI	69.80	69.80	77.43	<b>88.61</b>	76.88	66.49	68.17	<b>53.47</b>

Model ages determined using the AND-2A age model from Di Vincenzo *et al.* (2010). Major (wt. %) and trace elements (ppm) are normalized to 100% anhydrous with total Fe as FeO<sup>t</sup> (FeO = 0.9 Fe<sub>2</sub>O<sub>3</sub>). CIPW values for ne, di, ol, hy, and Q are cation normative. Mg-number is the atomic percent Mg<sup>2+</sup>/(Mg<sup>2+</sup> + Fe<sup>2+</sup>). AI is the Ishikawa alteration index from Ishikawa *et al.* (1976) and CCPI is the chlorite-carbonate-pyrite index from Large *et al.* (2001). Altered major element data was determined by relatively low totals (<97%), high alteration index (>40), low Ca/K ratios, visual characteristics, relatively low Na<sub>2</sub>O content (<3 wt%), or some combination thereof, and are marked in bold. Trace element data with errors >15% are tagged in yellow.

Full dataset of major and trace elemental compositions of glass shards from the AND-2A core, continued

Sample Model Age (Ma)	354.05-D 15.91	354.05-C 15.91	354.05-H 15.91	354.05-I 15.91	354.05-M 15.91	354.05-L 15.91	354.05-B 15.91	354.05-2 15.91
SiO <sub>2</sub>	47.25	50.90	46.68	51.94	46.66	46.42	<b>40.58</b>	<b>52.06</b>
TiO <sub>2</sub>	4.18	2.52	3.14	2.95	3.03	3.54	<b>2.79</b>	<b>3.17</b>
Al <sub>2</sub> O <sub>3</sub>	15.21	15.92	15.49	15.49	15.78	16.35	<b>22.23</b>	<b>15.25</b>
FeO	12.07	11.16	9.58	10.77	9.01	10.48	<b>8.70</b>	<b>8.90</b>
MnO	0.23	0.32	0.17	0.25	0.18	0.23	<b>0.16</b>	<b>0.18</b>
MgO	4.64	3.52	6.86	3.46	6.39	6.44	<b>6.34</b>	<b>2.49</b>
CaO	8.88	6.24	11.18	7.15	12.29	10.45	<b>9.69</b>	<b>7.60</b>
Na <sub>2</sub> O	3.94	3.76	3.70	4.00	3.86	3.73	<b>2.97</b>	<b>2.95</b>
K <sub>2</sub> O	1.53	2.39	1.69	2.70	1.62	1.42	<b>1.05</b>	<b>2.54</b>
P <sub>2</sub> O <sub>5</sub>	0.80	1.26	0.69	0.95	0.74	0.68	<b>0.58</b>	<b>1.12</b>
SO <sub>2</sub>	0.04	-0.02	0.01	0.03	0.00	-0.03	<b>0.02</b>	<b>0.04</b>
Cl	0.09	0.11	0.09	0.11	0.11	0.07	<b>0.14</b>	<b>0.27</b>
SrO	-0.12	-0.20	-0.17	-0.14	-0.16	-0.11	<b>-0.21</b>	<b>-0.15</b>
BaO	0.07	0.11	0.02	0.04	0.13	0.15	<b>0.10</b>	<b>0.03</b>
Total	98.81	97.99	99.13	99.70	99.63	99.80	<b>95.14</b>	<b>96.43</b>
Mg-no.	40.68	35.96	56.08	36.40	55.86	52.31	<b>56.53</b>	<b>33.26</b>
ne	0.02	0.00	7.60	0.00	10.19	5.14	<b>6.92</b>	<b>0.00</b>
di	16.01	2.64	24.35	10.48	28.12	18.99	<b>0.05</b>	<b>8.09</b>
ol	4.90	0.00	5.90	0.00	3.10	7.10	<b>14.32</b>	<b>0.00</b>
Q	0.00	2.28	0.00	1.27	0.00	0.00	<b>0.00</b>	<b>10.23</b>
hy	0.00	14.77	0.00	8.16	0.00	0.00	<b>0.00</b>	<b>3.24</b>
Li	5.62	7.74	7.53	10.35	7.22			
Be	2.76	3.33	<0.00	<0.00	<3.26			
B	14.04	22.13	<3.91	69.51	20.36			
Sc	18.93	14.88	31.23	16.63	31.70			
Ti	22409.16	11953.25	17211.75	15129.67	17341.34			
V	229.49	63.38	268.28	122.96	275.13			
Cr	8.86	<2.26	191.08	4.01	159.22			
Co	28.75	11.96	36.97	16.72	35.51			
Ni	1.25	<0.19	57.75	2.96	59.34			
Zn	145.38	146.67	99.32	155.24	81.65			
Rb	34.06	42.71	33.37	60.07	35.35			
Sr	782.73	753.93	700.54	680.32	748.86			
Y	23.02	37.02	22.74	36.21	28.37			
Zr	232.29	364.66	248.75	385.49	259.99			
Nb	55.29	88.75	64.96	63.79	62.93			
Cs	0.42	0.41	0.24	0.45	0.34			
Ba	533.01	565.33	397.21	788.31	421.60			
La	44.65	71.74	49.70	65.09	53.84			
Ce	91.37	148.07	101.24	124.73	97.58			
Pr	10.68	17.50	12.00	15.11	11.27			
Nd	47.42	70.75	46.60	64.95	46.79			
Sm	9.29	13.12	8.80	10.97	8.44			
Eu	3.57	4.44	2.76	3.88	2.91			
Gd	6.12	10.70	6.54	9.60	8.01			
Tb	0.96	1.41	1.16	1.41	1.31			
Dy	5.45	8.06	5.66	7.04	6.49			
Ho	1.21	1.31	0.76	1.46	1.61			
Er	1.99	4.20	2.01	3.55	<b>2.82</b>			
Tm	0.46	0.51	<b>0.29</b>	0.51	<b>0.21</b>			
Yb	2.56	3.60	2.85	3.03	<b>3.58</b>			
Lu	<b>0.21</b>	0.35	<b>0.31</b>	0.45	<b>0.18</b>			
Hf	5.90	7.19	5.22	8.25	6.71			
Ta	2.85	4.79	3.72	3.53	3.40			
Pb	3.98	3.08	2.44	<b>18.00</b>				
Th	4.03	6.04	4.16	5.45	5.97			
U	1.36	2.13	1.26	1.47	1.70			
Al	32.49	37.14	36.47	35.60	33.18	35.67	<b>36.86</b>	<b>32.30</b>
CCPI	75.34	70.49	75.31	67.98	73.76	76.70	<b>78.92</b>	<b>67.47</b>

Full dataset of major and trace elemental compositions of glass shards from the AND-2A core, continued

Sample Model Age (Ma)	354.05-F 15.91	354.05-G 15.91	354.05-J 15.91	355.63-A 15.91	355.63-B 15.91	355.63-C 15.91	355.63-D 15.91	355.63-E 15.91
SiO <sub>2</sub>	45.14	<b>52.25</b>	<b>54.77</b>	<b>61.07</b>	52.21	46.41	<b>62.12</b>	43.06
TiO <sub>2</sub>	4.33	<b>2.79</b>	<b>1.97</b>	<b>0.84</b>	2.24	3.57	<b>0.53</b>	4.32
Al <sub>2</sub> O <sub>3</sub>	16.12	<b>14.92</b>	<b>15.66</b>	<b>12.81</b>	16.45	14.81	<b>13.91</b>	15.28
FeO	11.14	<b>9.62</b>	<b>9.30</b>	<b>8.30</b>	8.76	12.77	<b>7.31</b>	10.14
MnO	0.19	<b>0.12</b>	<b>0.19</b>	<b>0.25</b>	0.21	0.17	<b>0.24</b>	0.19
MgO	4.84	<b>3.14</b>	<b>2.22</b>	<b>0.31</b>	3.20	4.90	<b>0.06</b>	6.29
CaO	9.39	<b>6.67</b>	<b>5.26</b>	<b>1.46</b>	6.68	9.14	<b>1.14</b>	13.39
Na <sub>2</sub> O	4.26	<b>2.04</b>	<b>2.92</b>	<b>1.29</b>	3.99	3.61	<b>3.57</b>	3.53
K <sub>2</sub> O	2.25	<b>3.18</b>	<b>3.49</b>	<b>3.65</b>	3.94	1.67	<b>4.97</b>	1.57
P <sub>2</sub> O <sub>5</sub>	0.99	<b>0.80</b>	<b>0.70</b>	<b>0.08</b>	0.52	0.74	<b>0.04</b>	0.65
SO <sub>2</sub>	0.02	<b>-0.02</b>	<b>0.01</b>	<b>0.04</b>	0.07	0.11	<b>0.03</b>	0.06
Cl	0.13	<b>0.09</b>	<b>0.12</b>	<b>0.27</b>	0.05	0.05	<b>0.21</b>	0.07
SrO	-0.16	<b>-0.14</b>	<b>-0.11</b>	<b>-0.12</b>	-0.11	-0.13	<b>-0.11</b>	-0.13
BaO	0.04	<b>0.16</b>	<b>0.33</b>	<b>0.00</b>	0.17	0.05	<b>0.01</b>	0.06
Total	98.66	<b>95.61</b>	<b>96.82</b>	<b>90.24</b>	98.38	97.85	<b>94.02</b>	98.49
Mg-no.	43.64	<b>36.75</b>	<b>29.86</b>	<b>6.15</b>	39.43	40.63	<b>1.42</b>	52.53
ne	9.67	<b>0.00</b>	<b>0.00</b>	<b>0.00</b>	0.80	1.49	<b>0.00</b>	14.97
di	17.83	<b>4.94</b>	<b>1.86</b>	<b>0.00</b>	11.74	17.60	<b>0.00</b>	33.35
ol	3.50	<b>0.00</b>	<b>0.00</b>	<b>0.00</b>	4.61	7.40	<b>0.00</b>	0.75
Q	0.00	<b>11.44</b>	<b>9.55</b>	<b>34.75</b>	0.00	0.00	<b>16.35</b>	0.00
hy	0.00	<b>9.21</b>	<b>10.50</b>	<b>9.30</b>	0.00	0.00	<b>7.42</b>	0.00
Li	6.24				3.61			7.82
Be	2.93				4.05			<0.00
B	24.03				7.53			6.80
Sc	22.33				13.67			33.10
Ti	23144.09				11646.54			22758.66
V	294.94				150.29			350.32
Cr	19.53				17.92			63.47
Co	34.93				21.53			43.68
Ni	12.01				6.61			43.56
Zn	105.81				77.06			96.98
Rb	47.19				35.45			41.18
Sr	770.39				343.67			807.39
Y	28.93				22.78			33.64
Zr	318.95				232.39			331.49
Nb	87.39				42.08			78.98
Cs	0.38				0.34			0.49
Ba	520.24				1049.41			481.09
La	63.90				41.93			62.85
Ce	122.65				77.59			113.39
Pr	13.82				9.48			13.43
Nd	57.60				38.67			55.97
Sm	12.68				6.70			11.45
Eu	3.48				3.99			3.66
Gd	7.83				6.07			8.99
Tb	1.18				0.89			1.22
Dy	6.00				4.86			6.62
Ho	1.21				1.02			1.53
Er	2.92				2.68			3.08
Tm	0.42				0.36			0.43
Yb	2.96				1.80			2.82
Lu	0.35				0.36			0.50
Hf	6.46				4.89			8.03
Ta	4.63				2.63			4.49
Pb	4.27				4.00			4.44
Th	6.83				3.99			6.89
U	2.07				1.12			1.57
AI	34.19	<b>42.04</b>	<b>41.08</b>	<b>58.99</b>	40.09	34.03	<b>51.63</b>	31.71
CCPI	71.02	<b>70.94</b>	<b>64.26</b>	<b>63.55</b>	60.11	77.00	<b>46.33</b>	76.33

Full dataset of major and trace elemental compositions of glass shards from the AND-2A core, continued

Sample Model Age (Ma)	355.63-F 15.91	355.63-I 15.91	355.63-K 15.91	355.63-L 15.91	355.63-L2 15.91	<b>355.63-N 15.91</b>	355.63-P 15.91	355.63-R 15.91
SiO <sub>2</sub>	45.40	45.24	45.50	46.40	46.40	<b>61.48</b>	44.55	44.69
TiO <sub>2</sub>	3.63	3.35	3.79	3.03	3.03	<b>0.52</b>	4.48	3.76
Al <sub>2</sub> O <sub>3</sub>	15.49	16.26	15.48	15.47	15.47	<b>14.52</b>	14.51	15.46
FeO	10.36	9.55	10.07	10.65	10.65	<b>7.04</b>	13.24	10.61
MnO	0.17	0.19	0.20	0.19	0.19	<b>0.22</b>	0.23	0.20
MgO	5.91	6.04	5.59	5.72	5.72	<b>0.17</b>	5.46	6.16
CaO	11.64	11.72	11.42	11.48	11.48	<b>1.52</b>	9.86	12.00
Na <sub>2</sub> O	3.68	3.60	3.82	3.81	3.81	<b>3.79</b>	3.59	3.73
K <sub>2</sub> O	1.61	1.44	1.77	1.74	1.74	<b>5.43</b>	1.54	1.45
P <sub>2</sub> O <sub>5</sub>	0.78	0.64	0.88	0.74	0.74	<b>0.07</b>	1.41	0.74
SO <sub>2</sub>	0.06	0.04	0.05	0.06	0.06	<b>0.02</b>	0.11	-0.03
Cl	0.08	0.07	0.08	0.08	0.08	<b>0.15</b>	0.09	0.08
SrO	-0.11	-0.14	-0.09	-0.13	-0.13	<b>-0.13</b>	-0.13	-0.15
BaO	0.10	0.09	0.12	0.10	0.10	<b>-0.02</b>	0.02	0.13
Total	98.80	98.08	98.68	99.33	99.33	<b>94.76</b>	98.96	98.83
Mg-no.	50.43	53.00	49.75	48.93	48.93	<b>4.06</b>	42.35	50.86
ne	8.51	8.27	8.92	9.16	9.16	<b>0.00</b>	2.52	10.26
di	25.68	24.47	25.24	25.93	25.93	<b>0.51</b>	17.04	27.22
ol	3.23	3.76	2.31	4.56	4.56	<b>0.00</b>	6.85	3.11
Q	0.00	0.00	0.00	0.00	0.00	<b>11.88</b>	0.00	0.00
hy	0.00	0.00	0.00	0.00	0.00	<b>6.96</b>	0.00	0.00
Li	5.46	4.68	7.18	5.54	4.92		3.56	
Be	<0.00	2.27	<2.76	4.66	<1.90		<0.00	
B	5.24	6.38	108.74	8.48	3.95		6.59	
Sc	25.64	29.20	25.66	33.47	32.91		25.18	
Ti	18339.15	18300.72	15918.06	16343.26	16428.33		23673.27	
V	279.78	271.62	217.94	275.04	281.37		266.04	
Cr	53.23	154.77	158.17	108.95	106.59		23.33	
Co	33.49	35.46	25.36	31.38	33.44		33.14	
Ni	35.38	51.85	23.46	29.38	36.88		15.12	
Zn	76.44	72.49	71.22	78.73	73.45		87.23	
Rb	33.94	32.59	50.69	42.52	42.30		30.27	
Sr	704.21	719.25	598.12	557.92	542.03		698.68	
Y	27.79	25.03	24.70	28.55	30.15		30.58	
Zr	259.52	257.03	296.87	237.20	246.04		267.97	
Nb	64.10	65.41	62.81	75.88	77.06		65.06	
Cs	0.46	0.22	0.60	0.53	0.46		0.42	
Ba	399.58	358.25	443.62	434.80	441.66		457.17	
La	50.14	48.49	50.31	55.91	57.00		54.20	
Ce	90.12	92.23	89.19	99.91	98.34		106.10	
Pr	10.75	10.98	10.42	11.74	11.52		12.79	
Nd	46.22	44.06	43.05	47.08	46.72		55.45	
Sm	8.46	9.66	8.19	9.41	9.27		9.97	
Eu	2.84	2.98	2.75	2.94	2.67		3.11	
Gd	7.91	6.09	6.44	6.73	8.45		9.53	
Tb	1.14	1.18	0.92	1.01	1.04		1.12	
Dy	5.61	6.15	5.60	5.96	6.50		7.15	
Ho	0.97	1.03	1.04	1.27	1.30		1.06	
Er	2.83	3.15	2.65	2.51	2.63		3.90	
Tm	0.43	0.39	0.37	0.40	0.45		0.40	
Yb	1.96	2.85	2.64	2.66	3.06		3.77	
Lu	0.32	0.23	0.39	0.43	0.32		0.29	
Hf	6.33	5.11	6.90	5.68	4.73		6.09	
Ta	3.48	3.54	3.58	4.06	4.15		3.65	
Pb	3.07	2.17	24.39	3.16	3.26		1.98	
Th	5.58	4.99	5.91	6.45	6.70		4.58	
U	1.50	1.39	1.54	1.77	1.62		1.07	
Al	32.93	32.80	32.57	32.81	32.81	<b>51.27</b>	34.20	32.59
CCPI	75.48	75.57	73.69	74.68	74.68	<b>43.85</b>	78.47	76.41

Full dataset of major and trace elemental compositions of glass shards from the AND-2A core, continued

Sample Model Age (Ma)	355.63-S 15.91	355.63-U 15.91	355.63-B1 15.91	385.38-A 16.07	385.38-C 16.07	<b>385.38-D 16.07</b>	385.38-1 16.07	<b>385.38-F 16.07</b>
SiO <sub>2</sub>	45.23	51.88	45.80	47.89	43.94	<b>63.73</b>	45.26	<b>64.42</b>
TiO <sub>2</sub>	3.86	2.99	2.81	3.58	4.53	<b>0.74</b>	3.44	<b>0.70</b>
Al <sub>2</sub> O <sub>3</sub>	15.50	15.59	17.37	14.16	14.70	<b>13.19</b>	14.07	<b>12.29</b>
FeO	10.52	10.18	9.38	11.26	12.36	<b>8.15</b>	12.33	<b>10.29</b>
MnO	0.13	0.31	0.15	0.24	0.21	<b>0.33</b>	0.17	<b>0.45</b>
MgO	5.86	2.94	4.69	4.81	5.63	<b>0.25</b>	6.52	<b>0.08</b>
CaO	11.47	6.71	12.36	9.31	10.89	<b>1.16</b>	12.08	<b>1.17</b>
Na <sub>2</sub> O	3.80	4.89	3.66	3.86	3.75	<b>2.14</b>	3.08	<b>4.07</b>
K <sub>2</sub> O	1.74	3.24	1.72	1.88	1.57	<b>5.03</b>	0.87	<b>4.71</b>
P <sub>2</sub> O <sub>5</sub>	0.77	1.26	0.63	1.34	1.28	<b>0.07</b>	0.67	<b>0.13</b>
SO <sub>2</sub>	-0.03	0.04	0.01	0.07	0.01	<b>0.04</b>	0.03	<b>0.07</b>
Cl	0.07	0.05	0.07	0.05	0.06	<b>0.20</b>	0.05	<b>0.31</b>
SrO	-0.12	-0.12	-0.13	-0.16	-0.13	<b>-0.11</b>	-0.15	<b>-0.07</b>
BaO	0.13	0.09	0.16	0.49	-0.09	<b>-0.07</b>	-0.04	<b>-0.05</b>
Total	98.94	100.01	98.67	98.79	98.70	<b>94.85</b>	98.38	<b>98.58</b>
Mg-no.	49.84	33.98	47.15	43.25	44.82	<b>5.24</b>	48.53	<b>1.38</b>
ne	9.63	1.64	10.37	0.00	7.14	<b>0.00</b>	3.38	<b>0.00</b>
di	25.70	11.29	25.40	17.84	22.11	<b>0.00</b>	27.58	<b>3.00</b>
ol	2.66	3.91	1.74	4.68	4.05	<b>0.00</b>	6.78	<b>0.00</b>
Q	0.00	0.00	0.00	0.00	0.00	<b>25.58</b>	0.00	<b>14.68</b>
hy	0.00	0.00	0.00	0.79	0.00	<b>8.84</b>	0.00	<b>10.26</b>
Li	3.15	3.24						
Be	6.67	10.47						
B	10.72	<2.68						
Sc	31.71	14.12						
Ti	22202.31	16499.05						
V	304.49	112.94						
Cr	96.90	<3.23						
Co	35.51	15.27						
Ni	34.06	3.80						
Zn	90.98	119.40						
Rb	32.75	35.18						
Sr	756.13	461.27						
Y	29.93	36.84						
Zr	302.50	269.07						
Nb	72.91	59.52						
Cs	0.30	0.27						
Ba	403.13	589.66						
La	54.93	63.78						
Ce	103.76	127.14						
Pr	12.35	16.23						
Nd	52.09	69.21						
Sm	10.04	13.06						
Eu	3.52	5.01						
Gd	7.42	9.53						
Tb	1.06	1.54						
Dy	6.99	8.24						
Ho	1.23	1.50						
Er	3.50	3.61						
Tm	0.49	0.43						
Yb	2.77	2.77						
Lu	0.29	0.43						
Hf	7.04	6.47						
Ta	4.23	3.35						
Pb	4.32	3.27						
Th	5.18	4.91						
U	1.45	1.08						
Al	33.24	34.75	28.59	33.70	32.96	61.57	32.76	47.76
CCPI	74.73	61.74	72.36	73.68	77.18	53.96	82.69	54.14

Full dataset of major and trace elemental compositions of glass shards from the AND-2A core, continued

Sample Model Age (Ma)	385.38-2 16.07	<b>385.38-3 16.07</b>	385.38-1 16.07	385.38-4 16.07	385.38-5 16.07	409.46-A 16.20	409.46-F 16.20	<b>409.46-G 16.20</b>
SiO <sub>2</sub>	43.56	<b>28.25</b>	47.45	45.00	66.51	45.80	44.85	<b>65.57</b>
TiO <sub>2</sub>	4.86	<b>29.93</b>	3.23	3.89	0.69	4.27	3.91	<b>0.62</b>
Al <sub>2</sub> O <sub>3</sub>	13.91	<b>4.35</b>	15.92	14.92	12.69	15.24	15.85	<b>11.04</b>
FeO	13.41	<b>1.78</b>	11.20	11.20	8.20	12.25	11.66	<b>8.91</b>
MnO	0.23	<b>0.29</b>	0.21	0.16	0.33	0.17	0.21	<b>0.34</b>
MgO	5.30	<b>0.08</b>	4.37	6.05	0.13	4.92	6.46	<b>0.07</b>
CaO	11.10	<b>21.94</b>	8.61	12.14	0.95	8.73	10.98	<b>0.84</b>
Na <sub>2</sub> O	4.04	<b>0.07</b>	4.33	3.61	0.26	4.13	3.44	<b>2.10</b>
K <sub>2</sub> O	1.57	<b>0.00</b>	2.09	1.55	2.23	1.67	1.10	<b>4.17</b>
P <sub>2</sub> O <sub>5</sub>	0.98	<b>0.06</b>	1.81	0.73	0.06	0.94	0.65	<b>0.06</b>
SO <sub>2</sub>	-0.03	<b>-0.58</b>	0.00	0.00	0.02	-0.02	0.02	<b>0.03</b>
Cl	0.13	<b>0.00</b>	0.08	0.06	0.17	0.09	0.06	<b>0.40</b>
SrO	-0.17	<b>-0.24</b>	-0.11	-0.17	-0.09	-0.13	-0.15	<b>-0.12</b>
BaO	0.05	<b>0.11</b>	0.07	0.12	-0.01	-0.06	0.08	<b>0.01</b>
Total	98.94	<b>86.04</b>	99.27	99.27	92.13	97.99	99.11	<b>94.03</b>
Mg-no.	41.35	<b>7.09</b>	41.04	49.05	2.67	41.71	49.70	<b>1.28</b>
ne	10.80	<b>0.00</b>	2.54	9.57	0.00	3.70	4.96	<b>0.00</b>
di	27.43	<b>0.00</b>	10.57	28.78	0.00	15.65	20.79	<b>0.00</b>
ol	1.76	<b>0.00</b>	7.72	2.58	0.00	5.55	7.01	<b>0.00</b>
Q	0.00	<b>2.19</b>	0.00	0.00	53.65	0.00	0.00	<b>31.68</b>
hy	0.00	<b>0.28</b>	0.00	0.00	9.22	0.00	0.00	<b>10.24</b>
Li								
Be								
B								
Sc								
Ti								
V								
Cr								
Co								
Ni								
Zn								
Rb								
Sr								
Y								
Zr								
Nb								
Cs								
Ba								
La								
Ce								
Pr								
Nd								
Sm								
Eu								
Gd								
Tb								
Dy								
Ho								
Er								
Tm								
Yb								
Lu								
Hf								
Ta								
Pb								
Th								
U								
Al	31.23	0.35	33.30	32.54	66.12	33.85	34.39	59.02
CCPI	76.93	96.11	70.82	76.97	76.98	74.75	79.97	58.87

Full dataset of major and trace elemental compositions of glass shards from the AND-2A core, continued

Sample Model Age (Ma)	409.46-K 16.20	409.46-C 16.20	409.46-D 16.20	409.46-L 16.20	409.46-E 16.20	409.46-B 16.20	409.46-1 16.20	409.46-I 16.20
SiO <sub>2</sub>	51.20	<b>63.94</b>	<b>65.84</b>	44.23	<b>64.04</b>	<b>65.17</b>	44.93	45.88
TiO <sub>2</sub>	2.85	<b>0.75</b>	<b>0.72</b>	4.92	<b>0.75</b>	<b>0.78</b>	3.82	3.17
Al <sub>2</sub> O <sub>3</sub>	15.62	<b>12.94</b>	<b>11.24</b>	13.39	<b>12.80</b>	<b>12.63</b>	15.99	15.99
FeO	10.75	<b>8.94</b>	<b>9.06</b>	14.08	<b>9.64</b>	<b>9.61</b>	11.46	9.66
MnO	0.22	<b>0.32</b>	<b>0.31</b>	0.20	<b>0.43</b>	<b>0.37</b>	0.17	0.17
MgO	3.44	<b>0.16</b>	<b>0.07</b>	5.46	<b>0.17</b>	<b>0.13</b>	6.25	6.12
CaO	7.21	<b>1.45</b>	<b>0.99</b>	10.64	<b>1.48</b>	<b>1.48</b>	10.79	11.88
Na <sub>2</sub> O	3.90	<b>3.40</b>	<b>2.16</b>	3.63	<b>2.67</b>	<b>2.98</b>	3.69	3.75
K <sub>2</sub> O	3.09	<b>5.15</b>	<b>4.37</b>	1.18	<b>5.08</b>	<b>4.73</b>	1.15	1.54
P <sub>2</sub> O <sub>5</sub>	0.70	<b>0.07</b>	<b>0.11</b>	1.36	<b>0.11</b>	<b>0.12</b>	0.58	0.79
SO <sub>2</sub>	0.09	<b>0.10</b>	<b>0.09</b>	0.00	<b>0.08</b>	<b>0.09</b>	0.03	-0.04
Cl	0.05	<b>0.15</b>	<b>0.40</b>	0.05	<b>0.15</b>	<b>0.20</b>	0.06	0.11
SrO	-0.18	<b>-0.11</b>	<b>-0.11</b>	-0.16	<b>-0.07</b>	<b>-0.10</b>	-0.16	-0.13
BaO	0.07	<b>0.03</b>	<b>0.03</b>	0.00	<b>-0.01</b>	<b>0.03</b>	0.05	0.08
Total	99.01	<b>97.29</b>	<b>95.27</b>	98.97	<b>97.31</b>	<b>98.22</b>	98.81	98.97
Mg-no.	36.35	<b>3.05</b>	<b>1.42</b>	40.85	<b>2.96</b>	<b>2.30</b>	49.30	53.05
ne	0.00	<b>0.00</b>	<b>0.00</b>	2.88	<b>0.00</b>	<b>0.00</b>	6.63	9.11
di	12.43	<b>1.62</b>	<b>0.00</b>	22.34	<b>0.00</b>	<b>0.00</b>	21.19	25.48
ol	2.16	<b>0.00</b>	<b>0.00</b>	4.68	<b>0.00</b>	<b>0.00</b>	6.39	4.00
Q	0.00	<b>16.67</b>	<b>30.34</b>	0.00	<b>20.30</b>	<b>21.01</b>	0.00	0.00
hy	4.60	<b>8.70</b>	<b>9.97</b>	0.00	<b>10.94</b>	<b>10.48</b>	0.00	0.00
Li								
Be								
B								
Sc								
Ti								
V								
Cr								
Co								
Ni								
Zn								
Rb								
Sr								
Y								
Zr								
Nb								
Cs								
Ba								
La								
Ce								
Pr								
Nd								
Sm								
Eu								
Gd								
Tb								
Dy								
Ho								
Er								
Tm								
Yb								
Lu								
Hf								
Ta								
Pb								
Th								
U								
Al	37.03	52.26	58.53	31.76	55.85	52.18	33.82	32.89
CCPI	66.98	51.56	58.34	80.22	55.85	55.84	78.53	74.88

Full dataset of major and trace elemental compositions of glass shards from the AND-2A core, continued

Sample Model Age (Ma)	409.46-2 16.20	419.56-A 16.25	419.56-B1 16.25	419.56-C1 16.25	419.56-D1 16.25	419.56-A1 16.25	419.56-N 16.25	419.56-S 16.25
SiO <sub>2</sub>	<b>65.25</b>	45.18	45.01	45.25	45.00	44.19	47.16	44.68
TiO <sub>2</sub>	<b>0.71</b>	3.53	3.72	3.70	2.92	3.94	3.10	4.14
Al <sub>2</sub> O <sub>3</sub>	<b>12.58</b>	16.55	15.05	15.75	16.25	15.22	16.48	14.94
FeO	<b>8.74</b>	10.10	11.71	9.54	8.89	10.42	10.91	12.38
MnO	<b>0.29</b>	0.13	0.20	0.18	0.11	0.15	0.25	0.20
MgO	<b>0.11</b>	6.09	5.80	6.17	6.40	6.00	4.17	5.03
CaO	<b>1.17</b>	11.66	11.52	11.78	13.25	12.31	7.74	10.54
Na <sub>2</sub> O	<b>2.13</b>	3.70	3.93	3.74	3.76	3.50	4.97	4.16
K <sub>2</sub> O	<b>4.25</b>	1.51	1.60	1.83	1.54	1.51	2.40	1.62
P <sub>2</sub> O <sub>5</sub>	<b>0.05</b>	0.80	0.81	0.97	0.64	0.80	1.60	1.15
SO <sub>2</sub>	<b>0.04</b>	-0.01	0.01	-0.03	0.00	0.00	-0.01	-0.02
Cl	<b>0.19</b>	0.06	0.05	0.09	0.11	0.08	0.10	0.11
SrO	<b>-0.10</b>	-0.12	-0.14	-0.10	-0.15	-0.12	-0.08	-0.11
BaO	<b>-0.01</b>	0.12	0.10	0.13	0.09	0.04	0.20	0.12
Total	<b>95.40</b>	99.32	99.38	98.99	98.81	98.05	98.99	98.92
Mg-no.	<b>2.25</b>	51.81	46.92	53.56	56.21	50.67	40.54	42.02
ne	<b>0.00</b>	9.01	10.87	10.12	14.11	9.71	7.94	9.00
di	<b>0.00</b>	23.01	26.79	25.27	31.09	28.28	9.96	22.41
ol	<b>0.00</b>	4.37	3.87	3.42	2.16	2.12	7.54	3.70
Q	<b>29.75</b>	0.00	0.00	0.00	0.00	0.00	0.00	0.00
hy	<b>9.49</b>	0.00	0.00	0.00	0.00	0.00	0.00	0.00
Li	6.08	4.58		7.78	5.24	5.80	3.70	
Be	<4.34	7.15		<0.00	<0.00	15.72	7.97	
B	<9.12	9.35		21.04	34.71	11.46	32.68	
Sc	35.10	39.09		37.03	25.88	14.99	31.48	
Ti	21281.59	21355.14		17494.16	15550.28	16371.01	25987.38	
V	326.55	335.66		294.80	248.01	123.80	313.24	
Cr	91.74	103.44		91.25	79.28	<4.97	35.73	
Co	37.27	38.96		39.64	26.35	22.49	36.95	
Ni	45.82	30.88		56.81	41.28	0.77	22.87	
Zn	79.64	89.12		81.46	66.69	120.34	114.50	
Rb	32.93	33.60		43.95	25.21	45.05	46.11	
Sr	842.41	592.24		771.96	742.62	672.10	744.82	
Y	30.78	30.49		27.55	19.95	37.08	38.25	
Zr	287.93	291.50		235.04	167.20	371.88	354.74	
Nb	70.08	70.66		63.62	47.26	84.81	78.51	
Cs	0.20	0.25		0.47	0.32	0.45	0.16	
Ba	423.27	417.86		456.96	292.06	509.95	448.24	
La	51.88	55.93		46.47	35.25	72.14	70.31	
Ce	103.02	106.10		85.53	69.59	139.85	132.79	
Pr	11.76	12.13		10.09	7.07	15.68	15.61	
Nd	48.01	48.12		40.70	35.39	65.74	63.03	
Sm	8.12	8.69		8.47	7.99	10.56	12.80	
Eu	2.55	2.85		2.80	2.34	4.16	4.10	
Gd	9.23	8.56		5.50	5.24	11.41	10.62	
Tb	0.89	1.09		0.94	0.84	1.61	1.69	
Dy	6.64	6.87		5.38	3.85	6.53	10.72	
Ho	0.94	1.03		1.26	0.66	1.67	1.93	
Er	3.87	3.86		3.43	1.67	2.98	3.52	
Tm	<b>0.34</b>	<b>0.43</b>		0.39	<b>0.16</b>	0.63	<b>0.31</b>	
Yb	1.69	3.32		2.83	0.94	2.24	3.86	
Lu	<b>0.43</b>	0.57		<b>0.17</b>	<b>0.22</b>	0.56	<b>0.42</b>	
Hf	6.72	5.78		5.57	3.79	7.67	10.39	
Ta	4.14	3.76		3.65	2.49	4.68	4.68	
Pb	2.43	2.31		3.11	2.08	3.40	2.96	
Th	6.42	5.50		5.42	3.57	6.39	6.49	
U	1.18	1.44		1.84	0.97	1.66	2.06	
Al	56.92	33.09	32.39	34.00	31.81	32.21	34.07	31.17
CCPI	58.12	75.64	76.01	73.83	74.28	76.63	67.19	75.07

Full dataset of major and trace elemental compositions of glass shards from the AND-2A core, continued

Sample Model Age (Ma)	419.56-Y 16.25	419.56-K 16.25	419.56-J 16.25	419.56-H 16.25	419.56-G 16.25	419.56-E 16.25	419.56-B 16.25	419.56-G1 16.25
SiO <sub>2</sub>	44.66	44.18	43.15	44.25	45.46	45.07	44.65	44.99
TiO <sub>2</sub>	4.31	3.41	4.82	4.28	3.22	3.66	5.04	3.85
Al <sub>2</sub> O <sub>3</sub>	14.75	15.63	14.81	15.41	16.18	15.85	15.16	15.42
FeO	12.48	10.07	12.81	12.30	9.08	9.67	12.26	10.54
MnO	0.14	0.16	0.17	0.16	0.16	0.14	0.20	0.16
MgO	5.11	6.20	5.74	5.80	6.27	5.94	4.60	6.09
CaO	10.27	13.35	10.91	10.75	12.31	11.52	9.77	12.53
Na <sub>2</sub> O	4.20	3.66	3.71	3.78	3.74	3.81	4.20	3.58
K <sub>2</sub> O	1.77	1.81	1.41	1.26	1.61	1.70	1.99	1.45
P <sub>2</sub> O <sub>5</sub>	1.16	0.78	1.01	1.24	0.83	0.90	1.00	0.68
SO <sub>2</sub>	0.01	0.00	0.06	0.03	0.00	0.00	0.04	0.05
Cl	0.10	0.11	0.04	0.08	0.09	0.07	0.07	0.06
SrO	-0.11	-0.14	-0.15	-0.14	-0.16	-0.11	-0.12	-0.15
BaO	0.17	0.07	0.09	0.08	0.08	0.10	0.12	0.11
Total	99.02	99.27	98.58	99.27	98.85	98.32	98.99	99.36
Mg-no.	42.18	52.33	44.43	45.69	55.21	52.26	40.11	50.73
ne	9.27	15.27	8.06	5.92	10.65	9.80	8.79	9.75
di	22.23	32.41	22.93	19.42	26.65	24.54	20.68	29.08
ol	3.53	1.39	3.73	5.88	3.08	3.29	1.99	1.84
Q	0.00	0.00	0.00	0.00	0.00	0.00	0.00	0.00
hy	0.00	0.00	0.00	0.00	0.00	0.00	0.00	0.00
Li	<1.96	4.57	3.38	7.47	3.24	5.90	7.49	
Be	13.28	14.74	9.02	3.71	1.87	4.24	<3.47	
B	73.24	30.19	18.85	13.29	7.23	20.95	27.83	
Sc	24.12	34.40	28.53	24.34	34.40	30.80	29.29	
Ti	21791.99	18431.05	26851.32	23728.33	18345.35	19767.06	26698.51	
V	264.15	299.17	379.35	305.13	290.93	286.37	294.03	
Cr	53.09	74.04	57.70	72.05	122.20	104.13	<7.32	
Co	32.70	39.59	47.59	37.34	34.41	34.13	30.43	
Ni	22.38	44.67	35.52	21.67	49.36	44.96	9.08	
Zn	122.79	79.70	116.08	110.75	88.43	89.01	104.37	
Rb	40.83	35.39	27.81	29.99	36.18	39.21	36.50	
Sr	698.69	763.35	652.59	764.41	790.68	712.76	754.27	
Y	33.74	29.06	27.71	23.68	25.71	25.91	38.10	
Zr	297.73	226.59	269.31	221.58	229.16	278.17	285.64	
Nb	69.51	65.36	61.93	57.81	65.20	71.99	73.84	
Cs	0.25	0.37	0.24	0.26	0.43	0.33	0.22	
Ba	425.56	455.13	332.80	361.92	470.27	432.55	487.56	
La	59.02	48.99	51.10	48.41	52.18	57.29	56.79	
Ce	113.45	92.19	95.00	99.83	100.62	111.62	111.22	
Pr	14.86	11.42	11.52	11.75	11.20	12.25	13.90	
Nd	52.34	43.19	50.77	48.96	48.30	52.20	61.62	
Sm	12.04	8.56	10.89	8.93	8.64	10.18	11.04	
Eu	4.08	3.29	3.30	3.53	2.96	3.29	3.16	
Gd	11.12	8.59	9.11	7.67	6.40	7.59	9.74	
Tb	1.60	1.11	1.32	1.21	1.03	1.09	1.56	
Dy	6.96	7.19	6.60	5.90	5.18	6.08	7.47	
Ho	1.05	1.22	1.09	0.99	0.91	1.23	1.31	
Er	2.06	1.93	2.74	2.93	2.79	1.97	3.63	
Tm	0.27	0.41	0.19	0.29	0.31	0.39	0.38	
Yb	1.75	3.51	2.81	2.73	2.65	3.13	3.70	
Lu	0.22	0.41	0.32	0.21	0.30	0.44	0.43	
Hf	5.36	5.24	6.14	6.20	5.70	6.11	6.91	
Ta	4.16	3.74	3.62	3.37	3.42	4.06	4.57	
Pb	3.00	2.20	2.40	1.77	2.35	2.53	3.39	
Th	5.66	5.25	4.94	4.03	5.05	5.21	4.50	
U	1.72	1.30	1.35	1.11	1.71	1.64	1.41	
Al	32.21	32.02	32.85	32.72	32.93	33.26	32.08	31.88
CCPI	74.65	74.84	78.37	78.21	74.15	73.89	73.15	76.78

Full dataset of major and trace elemental compositions of glass shards from the AND-2A core, continued

Sample Model Age (Ma)	426.28-A 16.28	426.28-E 16.28	426.28-F 16.28	426.28-G 16.28	426.28-1 16.28	<b>426.28-2 16.28</b>	426.28-H 16.28	426.28-3 16.28
SiO <sub>2</sub>	45.58	44.46	44.15	44.48	44.91	<b>63.74</b>	65.49	63.55
TiO <sub>2</sub>	4.31	4.68	4.70	4.51	3.60	<b>0.76</b>	0.80	0.72
Al <sub>2</sub> O <sub>3</sub>	13.78	14.57	14.75	15.61	15.63	<b>12.79</b>	10.95	12.74
FeO	13.37	12.37	12.38	12.51	11.14	<b>8.17</b>	10.50	8.80
MnO	0.27	0.18	0.25	0.19	0.20	<b>0.35</b>	0.44	0.42
MgO	5.02	5.73	5.34	5.06	6.47	<b>0.18</b>	0.14	0.18
CaO	10.02	10.83	10.55	10.18	11.41	<b>1.41</b>	1.18	1.65
Na <sub>2</sub> O	3.85	3.74	3.96	4.09	3.42	<b>0.15</b>	3.73	0.41
K <sub>2</sub> O	1.18	1.69	1.41	1.35	1.16	<b>1.83</b>	4.82	1.85
P <sub>2</sub> O <sub>5</sub>	1.58	1.29	1.28	1.50	0.76	<b>0.14</b>	0.05	0.12
SO <sub>2</sub>	0.02	0.03	0.03	-0.02	0.02	<b>0.08</b>	0.14	0.07
Cl	0.04	0.09	0.07	0.08	0.06	<b>0.14</b>	0.30	0.15
SrO	-0.15	-0.19	-0.16	-0.14	-0.17	<b>-0.16</b>	-0.12	-0.18
BaO	0.14	0.06	-0.04	0.09	0.00	<b>-0.02</b>	-0.01	-0.06
Total	99.00	99.52	98.66	99.48	98.59	<b>89.57</b>	98.41	90.42
Mg-no.	40.11	45.23	43.49	41.89	50.87	<b>3.84</b>	2.31	3.48
ne	0.63	6.58	6.40	5.42	5.74	<b>0.00</b>	0.00	0.00
di	18.54	22.24	21.04	16.60	22.60	<b>0.00</b>	4.63	0.00
ol	6.05	3.71	3.49	5.05	6.60	<b>0.00</b>	0.00	0.00
Q	0.00	0.00	0.00	0.00	0.00	<b>53.73</b>	17.68	49.91
hy	0.00	0.00	0.00	0.00	0.00	<b>9.41</b>	10.11	10.70
Li								
Be								
B								
Sc								
Ti								
V								
Cr								
Co								
Ni								
Zn								
Rb								
Sr								
Y								
Zr								
Nb								
Cs								
Ba								
La								
Ce								
Pr								
Nd								
Sm								
Eu								
Gd								
Tb								
Dy								
Ho								
Er								
Tm								
Yb								
Lu								
Hf								
Ta								
Pb								
Th								
U								
Al	30.89	33.73	31.77	30.97	33.96	<b>56.28</b>	50.30	49.58
CCPI	78.53	76.92	76.74	76.36	79.35	<b>80.80</b>	55.44	79.93

Full dataset of major and trace elemental compositions of glass shards from the AND-2A core, continued

Sample Model Age (Ma)	426.28-C 16.28	426.28-4 16.28	446.85-A 16.39	446.85-1 16.39	446.85-B 16.39	<b>446.85-H 16.39</b>	<b>446.85-E 16.39</b>	446.85-2 16.39
SiO <sub>2</sub>	44.96	44.29	44.19	45.05	43.47	<b>66.60</b>	<b>64.82</b>	44.91
TiO <sub>2</sub>	4.30	4.22	5.23	3.34	4.87	<b>0.69</b>	<b>0.58</b>	4.56
Al <sub>2</sub> O <sub>3</sub>	14.31	14.98	14.54	15.38	13.53	<b>11.55</b>	<b>13.52</b>	10.80
FeO	11.93	12.18	13.38	9.72	13.99	<b>8.86</b>	<b>7.98</b>	9.84
MnO	0.22	0.17	0.26	0.17	0.25	<b>0.28</b>	<b>0.30</b>	0.15
MgO	6.04	5.78	5.16	7.21	5.72	<b>0.06</b>	<b>0.17</b>	8.78
CaO	11.53	10.65	10.40	13.14	10.16	<b>0.91</b>	<b>1.24</b>	16.75
Na <sub>2</sub> O	3.50	3.75	4.18	3.56	3.85	<b>1.96</b>	<b>1.90</b>	1.60
K <sub>2</sub> O	1.21	1.55	1.75	1.56	1.40	<b>4.25</b>	<b>4.50</b>	1.01
P <sub>2</sub> O <sub>5</sub>	0.75	1.13	1.43	0.70	2.09	<b>0.09</b>	<b>0.10</b>	0.74
SO <sub>2</sub>	0.01	0.01	-0.03	0.02	-0.01	<b>0.08</b>	<b>0.07</b>	-0.01
Cl	0.06	0.05	0.09	0.14	0.07	<b>0.23</b>	<b>0.17</b>	0.06
SrO	-0.19	-0.17	-0.16	-0.15	-0.12	<b>-0.07</b>	<b>-0.10</b>	-0.19
BaO	0.05	0.08	0.06	-0.02	-0.03	<b>-0.07</b>	<b>-0.10</b>	0.02
Total	98.68	98.66	100.46	99.80	99.24	<b>95.42</b>	<b>95.15</b>	99.01
Mg-no.	47.46	45.83	40.76	56.94	42.17	<b>1.21</b>	<b>3.66</b>	61.41
ne	5.43	7.00	8.42	12.56	3.78	<b>0.00</b>	<b>0.00</b>	3.18
di	26.66	21.25	21.36	31.28	17.39	<b>0.00</b>	<b>0.00</b>	48.31
ol	3.35	5.25	2.78	3.57	7.11	<b>0.00</b>	<b>0.00</b>	0.49
Q	0.00	0.00	0.00	0.00	0.00	<b>32.92</b>	<b>30.01</b>	0.00
hy	0.00	0.00	0.00	0.00	0.00	<b>9.61</b>	<b>8.85</b>	0.00
Li		6.66	1.65	6.26				12.89
Be		<2.74	<3.20	<0.00				<3.94
B		49.89	<5.80	<6.40				44.38
Sc		27.88	32.61	24.86				29.63
Ti		29347.12	17799.78	27919.92				26071.10
V		311.81	276.32	256.64				364.31
Cr		<5.95	125.11	15.00				160.64
Co		36.85	32.90	34.58				51.79
Ni		8.40	73.71	<0.48				110.32
Zn		125.15	81.05	118.26				176.71
Rb		35.18	29.72	20.85				36.11
Sr		744.61	761.87	1024.22				1197.11
Y		34.28	23.95	36.30				34.27
Zr		303.35	207.24	213.35				325.41
Nb		80.70	58.48	53.44				76.21
Cs		0.34	0.44	0.19				0.45
Ba		393.61	382.50	479.87				404.29
La		58.67	45.81	58.33				62.63
Ce		121.43	85.17	121.76				121.25
Pr		14.46	9.89	14.13				13.31
Nd		62.53	40.74	70.04				58.20
Sm		14.05	6.86	11.18				9.74
Eu		3.61	3.52	4.90				4.54
Gd		9.25	5.94	9.90				5.68
Tb		1.66	0.83	1.84				1.20
Dy		6.65	4.48	7.55				6.71
Ho		1.42	0.65	1.57				1.37
Er		3.11	1.41	2.70				3.97
Tm		0.47	0.28	0.29				0.34
Yb		2.73	1.85	2.29				2.16
Lu		0.42	0.09	0.38				0.47
Hf		8.42	5.00	5.43				6.95
Ta		4.28	3.86	2.84				4.14
Pb			3.39	1.66				30.63
Th			5.73	5.68	3.80			6.65
U			1.68	1.60	1.02			2.28
Al	32.55	33.71	32.16	34.43	33.70	60.04	59.82	34.78
CCPI	79.23	77.22	75.80	76.80	78.95	58.94	56.00	87.72

Full dataset of major and trace elemental compositions of glass shards from the AND-2A core, continued

Sample Model Age (Ma)	446.85-D 16.39	446.85-3 16.39	446.85-C 16.39	446.85-N 16.39	446.85-4 16.39	446.85-F 16.39	534.77-L 16.85	534.77-F 16.85
SiO <sub>2</sub>	<b>66.94</b>	<b>64.01</b>	46.45	<b>64.06</b>	46.51	<b>65.30</b>	46.75	41.94
TiO <sub>2</sub>	<b>0.72</b>	<b>0.68</b>	4.79	<b>0.77</b>	3.08	<b>0.73</b>	3.11	5.63
Al <sub>2</sub> O <sub>3</sub>	<b>13.97</b>	<b>12.75</b>	12.43	<b>10.79</b>	15.44	<b>12.81</b>	15.49	11.74
FeO	<b>6.67</b>	<b>8.36</b>	15.09	<b>10.62</b>	10.27	<b>8.06</b>	9.82	15.82
MnO	0.24	0.33	0.31	0.44	0.19	0.31	0.17	0.25
MgO	<b>0.22</b>	<b>0.13</b>	4.13	<b>0.12</b>	7.25	<b>0.09</b>	6.02	5.36
CaO	<b>1.01</b>	<b>1.10</b>	9.41	<b>1.19</b>	11.42	<b>1.18</b>	11.19	11.47
Na <sub>2</sub> O	<b>3.16</b>	<b>0.36</b>	3.62	<b>1.73</b>	3.56	<b>0.30</b>	3.57	3.70
K <sub>2</sub> O	<b>5.59</b>	<b>2.80</b>	1.80	<b>4.44</b>	1.67	<b>2.51</b>	1.87	1.03
P <sub>2</sub> O <sub>5</sub>	<b>0.06</b>	<b>0.11</b>	1.43	<b>0.05</b>	0.69	<b>0.15</b>	0.68	2.33
SO <sub>2</sub>	<b>0.02</b>	<b>0.06</b>	0.00	<b>0.09</b>	-0.03	<b>0.07</b>	0.01	-0.01
Cl	0.11	0.18	0.08	0.33	0.06	0.16	0.08	0.04
SrO	-0.07	-0.12	-0.17	-0.12	-0.14	-0.11	-0.12	-0.13
BaO	<b>0.06</b>	<b>-0.02</b>	0.09	<b>-0.04</b>	-0.03	<b>0.03</b>	0.00	0.17
Total	<b>98.69</b>	<b>90.72</b>	99.45	<b>94.45</b>	99.94	<b>91.58</b>	98.64	99.35
Mg-no.	<b>5.55</b>	<b>2.64</b>	32.82	<b>2.02</b>	55.76	<b>1.87</b>	52.21	37.66
ne	<b>0.00</b>	<b>0.00</b>	0.00	<b>0.00</b>	8.05	<b>0.00</b>	6.80	4.25
di	<b>0.00</b>	<b>0.00</b>	20.68	<b>0.00</b>	24.65	<b>0.00</b>	24.59	24.29
ol	<b>0.00</b>	<b>0.00</b>	1.54	<b>0.00</b>	7.44	<b>0.00</b>	4.56	4.06
Q	<b>21.21</b>	<b>48.26</b>	0.00	<b>29.17</b>	0.00	<b>51.17</b>	0.00	0.00
hy	<b>5.86</b>	<b>9.69</b>	3.59	<b>12.98</b>	0.00	<b>8.74</b>	0.00	0.00
Li			9.92				5.62	4.29
Be			<0.00				4.16	<3.04
B			22.30				<2.95	3.68
Sc			29.17				29.69	36.94
Ti			27541.30				17424.17	32158.49
V			243.30				261.69	367.82
Cr			<7.37				106.39	28.36
Co			32.95				35.40	40.39
Ni			<0.94				34.65	7.19
Zn			123.91				90.42	120.92
Rb			35.42				30.22	18.78
Sr			566.20				730.05	733.62
Y			40.06				29.60	37.69
Zr			289.52				323.34	198.59
Nb			61.17				60.36	42.28
Cs			0.52				0.24	0.27
Ba			613.36				364.42	1264.59
La			59.45				53.31	53.71
Ce			116.09				95.99	106.90
Pr			14.62				11.64	14.86
Nd			70.59				48.87	70.18
Sm			13.96				9.58	16.65
Eu			5.06				2.84	6.07
Gd			11.92				6.81	12.44
Tb			2.06				1.14	1.59
Dy			9.10				6.57	8.41
Ho			1.77				1.29	1.29
Er			4.23				3.44	3.26
Tm			0.64				0.46	0.46
Yb			4.53				2.50	3.15
Lu			0.54				0.39	0.42
Hf			6.73				7.36	5.57
Ta			3.55				3.39	2.63
Pb			3.39				2.00	1.53
Th			4.32				5.59	3.28
U			1.31				1.67	1.07
Al	58.22	66.67	31.28	61.06	37.31	63.61	34.83	29.66
CCPI	44.08	72.88	78.03	63.53	77.00	74.31	74.45	81.72

Full dataset of major and trace elemental compositions of glass shards from the AND-2A core, continued

Sample Model Age (Ma)	534.77-1 16.85	534.7-A 16.85	534.77-A2 16.85	534.77-B 16.85	534.77-K 16.85	534.77-J 16.85	534.77-I 16.85	534.77-M 16.85
SiO <sub>2</sub>	<b>48.73</b>	47.87	47.87	46.51	47.80	46.59	49.74	45.49
TiO <sub>2</sub>	<b>2.08</b>	3.64	3.64	2.89	3.05	3.06	2.76	4.78
Al <sub>2</sub> O <sub>3</sub>	<b>23.22</b>	15.48	15.48	15.66	16.13	15.82	16.33	13.79
FeO	<b>5.67</b>	10.69	10.69	9.95	10.99	9.76	10.95	13.28
MnO	<b>0.07</b>	0.20	0.20	0.21	0.23	0.14	0.20	0.21
MgO	<b>2.07</b>	4.92	4.92	6.24	5.38	6.03	3.91	4.77
CaO	<b>12.57</b>	9.06	9.06	11.25	9.63	11.08	6.86	9.93
Na <sub>2</sub> O	<b>3.74</b>	4.50	4.50	3.59	4.02	3.93	4.26	4.19
K <sub>2</sub> O	<b>0.91</b>	2.21	2.21	1.41	1.56	1.72	1.99	1.90
P <sub>2</sub> O <sub>5</sub>	<b>0.50</b>	0.94	0.94	0.83	0.66	0.79	1.67	0.98
SO <sub>2</sub>	<b>-0.01</b>	-0.05	-0.05	0.01	-0.01	0.00	0.01	-0.05
Cl	<b>0.06</b>	0.12	0.12	0.07	0.08	0.07	0.11	0.06
SrO	<b>-0.04</b>	-0.12	-0.12	-0.17	-0.10	-0.13	-0.08	-0.11
BaO	<b>0.06</b>	-0.03	-0.03	0.01	0.02	-0.07	0.04	0.14
Total	<b>99.63</b>	99.42	99.42	98.48	99.44	98.78	98.75	99.35
Mg-no.	<b>39.42</b>	45.07	45.07	52.79	46.62	52.42	38.90	39.04
ne	<b>2.54</b>	6.95	6.95	5.43	4.11	8.50	0.00	7.58
di	<b>11.43</b>	18.77	18.77	22.69	17.84	23.64	2.95	24.26
ol	<b>0.00</b>	4.00	4.00	6.52	7.27	4.90	0.43	1.84
Q	<b>0.00</b>	0.00	0.00	0.00	0.00	0.00	0.00	0.00
hy	<b>0.00</b>	0.00	0.00	0.00	0.00	0.00	13.60	0.00
Li	5.82	8.87	7.13	12.76	7.05	6.47	6.08	
Be	<2.36	1.95	<0.00	<0.00	<2.70	5.66	<0.00	
B	5.85	11.04	5.15	9.84	2.95	<1.69	8.07	
Sc	23.34	25.86	27.96	20.31	29.72	11.55	29.91	
Ti	19302.40	20258.72	17151.52	17586.26	17132.12	14548.66	26827.92	
V	227.68	244.20	252.26	227.48	247.66	77.73	349.43	
Cr	63.23	75.30	109.88	64.72	108.07	3.84	25.13	
Co	28.96	30.49	35.98	34.98	33.40	16.73	34.16	
Ni	22.29	25.54	48.35	19.20	49.21	<0.41	12.56	
Zn	76.96	89.12	76.93	92.51	74.97	116.68	101.80	
Rb	43.44	47.77	31.12	29.95	31.78	38.33	37.56	
Sr	657.12	670.01	735.20	760.76	717.94	903.15	638.21	
Y	28.04	30.18	25.44	26.06	24.23	34.67	32.48	
Zr	381.61	416.90	271.99	267.33	279.93	366.90	342.22	
Nb	82.49	89.45	61.41	60.22	60.71	90.96	79.81	
Cs	0.35	0.53	0.32	0.16	0.27	0.33	0.31	
Ba	428.91	462.73	348.27	384.16	361.49	567.17	454.94	
La	62.99	66.99	50.67	47.38	50.23	73.74	65.44	
Ce	118.58	126.16	91.65	88.18	95.96	145.33	119.79	
Pr	13.63	14.83	10.83	10.06	11.49	16.83	13.82	
Nd	54.77	57.40	48.74	39.56	46.34	70.26	58.04	
Sm	8.94	9.73	8.08	7.21	8.96	12.10	9.62	
Eu	3.06	3.36	3.20	2.46	2.38	4.77	3.13	
Gd	7.84	7.61	6.57	5.54	7.38	10.41	9.56	
Tb	1.19	1.12	0.94	0.91	0.92	1.22	1.32	
Dy	5.94	6.68	4.70	4.96	4.73	6.66	7.50	
Ho	1.29	1.22	1.06	1.04	0.99	1.77	1.18	
Er	2.18	2.67	2.37	2.39	2.64	2.07	3.90	
Tm	0.32	0.48	0.37	0.42	0.50	0.49	0.49	
Yb	1.78	2.82	2.64	0.95	1.29	3.45	3.38	
Lu	0.30	0.35	0.49	0.25	0.35	0.46	0.39	
Hf	8.52	8.88	5.71	6.19	5.87	5.16	8.15	
Ta	4.74	5.12	3.62	3.49	3.50	5.12	4.60	
Pb	3.11	3.97	2.26	2.13	2.19	2.88	2.43	
Th	7.26	7.86	5.24	4.93	5.40	7.70	6.68	
U	2.30	2.06	1.29	1.22	1.50	1.95	2.21	
Al	15.44	34.46	34.46	34.01	33.72	34.05	34.67	32.07
CCPI	62.45	69.92	69.92	76.41	74.58	73.68	70.38	74.76

Full dataset of major and trace elemental compositions of glass shards from the AND-2A core, continued

Sample Model Age (Ma)	534.77-Q 16.85	534.77-P 16.85	534.77-O 16.85	534.77-C 16.85	534.77-H 16.85	534.77-2 16.85	534.77-D 16.85	534.77-3 16.85
SiO <sub>2</sub>	46.30	47.24	47.43	46.61	48.92	46.01	45.17	45.54
TiO <sub>2</sub>	3.34	3.22	2.89	3.09	3.24	3.48	3.57	3.92
Al <sub>2</sub> O <sub>3</sub>	15.69	15.54	15.86	15.76	15.00	15.45	15.83	14.93
FeO	10.17	10.08	11.41	9.86	11.38	11.47	10.85	11.77
MnO	0.18	0.18	0.18	0.14	0.20	0.18	0.19	0.19
MgO	5.72	5.78	5.10	6.25	4.06	5.15	6.27	5.18
CaO	10.62	10.75	8.81	11.56	8.19	9.58	11.42	10.01
Na <sub>2</sub> O	3.89	3.84	4.37	3.63	4.33	4.13	3.63	4.41
K <sub>2</sub> O	1.71	1.68	1.77	1.74	2.57	1.96	1.42	2.05
P <sub>2</sub> O <sub>5</sub>	0.73	0.68	0.86	0.75	1.04	1.05	0.79	1.14
SO <sub>2</sub>	-0.02	-0.02	0.03	-0.02	-0.01	-0.04	-0.03	0.01
Cl	0.07	0.09	0.08	0.07	0.09	0.07	0.08	0.08
SrO	-0.12	-0.10	-0.13	-0.12	-0.11	-0.10	-0.15	-0.15
BaO	-0.02	-0.04	0.11	0.02	0.10	0.08	-0.05	0.02
Total	98.25	98.92	98.75	99.33	98.99	98.47	98.97	99.11
Mg-no.	50.09	50.53	44.32	53.08	38.88	44.47	50.73	43.98
ne	7.28	5.93	5.84	7.78	3.59	7.38	7.81	10.66
di	22.43	23.15	15.90	24.81	16.21	18.64	23.25	22.09
ol	4.59	4.56	8.36	4.92	5.16	6.02	5.57	3.89
Q	0.00	0.00	0.00	0.00	0.00	0.00	0.00	0.00
hy	0.00	0.00	0.00	0.00	0.00	0.00	0.00	0.00
Li	6.06	3.03	7.38	4.58	7.52			
Be	8.00	7.58	<0.00	6.04	<0.00			
B	28.68	5.98	14.08	4.21	6.82			
Sc	24.31	28.56	16.36	30.59	21.86			
Ti	18789.08	16800.97	14279.11	18066.05	17750.01			
V	269.52	238.86	157.24	266.63	172.73			
Cr	82.84	80.17	47.72	122.96	17.44			
Co	33.16	30.79	27.83	39.05	26.05			
Ni	38.23	41.36	24.85	47.55	9.30			
Zn	77.52	87.30	93.17	78.58	104.12			
Rb	34.01	30.64	40.59	31.64	47.92			
Sr	773.32	690.91	588.62	772.53	559.56			
Y	27.88	24.34	27.45	26.10	36.34			
Zr	321.26	269.20	340.15	288.76	483.61			
Nb	66.64	60.60	64.91	66.86	83.64			
Cs	0.41	0.43	0.39	0.28	0.49			
Ba	379.90	345.35	355.70	384.82	423.80			
La	58.29	49.48	53.66	53.42	74.96			
Ce	102.01	92.56	99.29	101.63	133.96			
Pr	12.06	11.03	11.67	11.21	15.67			
Nd	54.54	42.32	44.73	48.98	68.04			
Sm	10.64	10.38	7.40	8.50	11.46			
Eu	3.00	2.95	2.78	3.01	3.98			
Gd	6.99	6.93	6.65	7.17	9.71			
Tb	0.93	1.21	0.88	0.91	1.40			
Dy	6.49	5.97	6.09	6.01	9.00			
Ho	1.15	0.85	1.07	1.31	1.50			
Er	2.50	2.30	2.82	1.93	3.83			
Tm	0.34	0.46	0.40	0.27	0.49			
Yb	2.39	2.72	2.18	2.12	3.57			
Lu	0.30	0.45	0.30	0.37	0.46			
Hf	6.56	8.30	8.45	6.41	10.51			
Ta	3.50	4.26	3.81	3.85	5.76			
Pb	3.55	2.41	5.46	2.29	3.42			
Th	5.73	5.30	5.60	5.38	7.81			
U	1.25	1.04	1.60	1.59	2.12			
Al	33.87	33.83	34.25	34.47	34.64	34.17	33.81	33.41
CCPI	73.95	74.20	72.91	75.01	69.10	73.18	77.25	72.40

Full dataset of major and trace elemental compositions of glass shards from the AND-2A core, continued

Sample Model Age (Ma)	534.77-N 16.85	539.22-A 16.88	539.22-B 16.88	539.22-C 16.88	539.22-D 16.88	539.22-F 16.88	539.22-H 16.88	539.22-I 16.88
SiO <sub>2</sub>	46.70	46.56	46.38	45.84	46.65	46.03	45.59	45.43
TiO <sub>2</sub>	3.12	3.15	3.22	3.25	3.28	3.12	3.59	4.33
Al <sub>2</sub> O <sub>3</sub>	15.67	15.80	15.96	15.26	16.47	16.22	15.95	14.87
FeO	9.81	9.74	9.89	11.13	9.69	9.90	11.59	11.84
MnO	0.18	0.12	0.16	0.19	0.15	0.19	0.21	0.21
MgO	6.00	6.23	5.85	5.60	5.34	6.14	5.65	5.10
CaO	11.29	11.33	11.27	10.12	10.71	11.62	10.19	10.28
Na <sub>2</sub> O	3.78	3.77	3.95	3.87	3.93	3.72	3.85	4.19
K <sub>2</sub> O	1.71	1.59	1.53	1.40	1.59	1.49	1.51	2.04
P <sub>2</sub> O <sub>5</sub>	0.80	0.72	0.75	0.90	0.82	0.83	0.91	0.98
SO <sub>2</sub>	-0.04	0.00	0.02	-0.02	-0.01	0.00	0.00	-0.04
Cl	0.07	0.07	0.07	0.07	0.09	0.07	0.08	0.08
SrO	-0.12	-0.12	-0.11	-0.12	-0.10	-0.09	-0.10	-0.13
BaO	0.03	0.09	0.14	0.12	0.06	0.16	0.08	0.17
Total	98.99	99.06	99.06	97.61	98.67	99.40	99.11	99.34
Mg-no.	52.18	53.28	51.33	47.27	49.55	52.51	46.53	43.46
ne	7.58	7.56	8.35	5.05	6.16	8.02	6.11	9.58
di	24.27	24.17	23.97	19.91	20.40	23.37	18.52	23.37
ol	4.54	4.81	4.15	6.84	4.08	5.25	6.94	2.31
Q	0.00	0.00	0.00	0.00	0.00	0.00	0.00	0.00
hy	0.00	0.00	0.00	0.00	0.00	0.00	0.00	0.00
Li	6.41	4.08	4.20	3.54	3.99	4.60	3.02	<0.85
Be	<5.47	4.20	<4.06	4.36	<4.49	<5.16	<4.06	<4.61
B	21.42	11.76	12.67	4.83	23.67	14.54	28.84	33.78
Sc	27.16	29.58	26.63	28.58	23.26	30.70	30.11	37.79
Ti	17390.85	16772.91	13674.88	14101.35	14916.80	16196.40	18245.87	21895.54
V	250.00	245.97	192.62	185.31	195.87	221.53	234.25	303.60
Cr	118.03	121.41	94.35	87.73	76.72	131.48	67.47	65.53
Co	32.18	31.82	22.51	21.34	20.00	25.58	25.97	25.97
Ni	35.86	40.21	30.24	23.36	19.00	38.16	16.59	28.94
Zn	100.20	67.99	38.17	47.02	32.41	44.89	41.13	42.50
Rb	26.31	38.05	44.89	29.07	41.22	36.65	33.70	46.99
Sr	791.67	594.57	506.44	489.20	508.95	588.85	625.94	532.66
Y	27.29	23.69	19.58	22.94	22.51	23.88	26.38	32.19
Zr	286.83	270.63	237.38	246.13	275.42	274.53	285.73	329.81
Nb	63.94	55.79	46.35	43.86	53.39	61.73	58.49	77.85
Cs	0.42	0.31	0.40	0.22	0.40	0.20	0.24	0.42
Ba	363.96	323.28	307.26	239.70	325.16	324.72	402.42	431.01
La	51.73	45.61	37.50	39.49	45.70	51.79	55.70	63.10
Ce	95.92	85.25	66.45	69.98	79.30	88.36	101.04	109.07
Pr	11.03	9.34	7.90	7.99	9.06	10.18	11.07	11.02
Nd	46.86	41.21	30.56	35.35	36.85	42.01	47.54	50.00
Sm	10.01	6.76	5.38	7.83	6.98	8.43	9.20	11.66
Eu	3.14	1.89	1.94	2.25	2.37	2.55	2.39	3.05
Gd	7.59	5.68	3.61	6.54	5.58	6.79	6.76	9.60
Tb	0.85	0.93	0.78	0.87	0.86	1.09	0.96	1.14
Dy	6.30	4.15	3.10	3.98	5.21	5.14	5.99	5.19
Ho	1.12	0.79	0.62	0.68	0.94	0.75	0.89	1.52
Er	2.67	2.16	1.53	2.12	1.71	1.72	3.16	3.43
Tm	0.26	0.31	0.21	0.31	0.25	0.32	0.27	0.31
Yb	2.31	2.05	1.44	1.40	1.84	1.59	2.23	3.24
Lu	0.34	0.29	0.25	0.23	0.23	0.33	0.36	0.54
Hf	5.55	5.12	3.82	3.32	5.48	4.72	6.10	6.98
Ta	3.34	2.82	1.91	2.19	2.49	2.74	3.43	3.63
Pb	6.28	2.14	3.10	1.20	2.33	1.46	2.30	2.10
Th	5.12	4.11	2.67	2.74	3.09	3.75	3.81	5.44
U	1.38	1.22	0.87	0.75	0.92	1.17	1.08	1.10
Al	33.83	34.13	32.66	33.33	32.12	33.23	33.78	33.06
CCPI	74.23	74.87	74.16	76.07	73.14	75.47	76.26	73.13

Full dataset of major and trace elemental compositions of glass shards from the AND-2A core, continued

Sample Model Age (Ma)	539.22-I2 16.88	539.22-J 16.88	<b>539.22-M 16.88</b>	539.22-P 16.88	<b>539.22-Q 16.88</b>	539.22-M1 16.88	539.22-N1 16.88	539.22-C1 16.88
SiO <sub>2</sub>	45.43	45.79	<b>61.07</b>	48.15	<b>-0.05</b>	46.19	45.64	46.36
TiO <sub>2</sub>	4.33	3.49	<b>0.52</b>	2.72	<b>-0.02</b>	3.03	3.09	3.11
Al <sub>2</sub> O <sub>3</sub>	14.87	16.05	<b>13.90</b>	15.73	<b>0.03</b>	15.95	16.07	16.30
FeO	11.84	11.26	<b>6.93</b>	10.76	<b>9.82</b>	9.62	9.44	10.90
MnO	0.21	0.16	<b>0.21</b>	0.25	<b>0.53</b>	0.18	0.22	0.22
MgO	5.10	5.97	<b>0.11</b>	4.03	<b>14.64</b>	6.08	6.08	5.81
CaO	10.28	10.55	<b>1.18</b>	6.57	<b>28.17</b>	11.02	10.80	9.06
Na <sub>2</sub> O	4.19	3.62	<b>4.56</b>	5.07	<b>0.15</b>	3.79	3.78	4.21
K <sub>2</sub> O	2.04	1.53	<b>4.62</b>	2.56	<b>0.02</b>	1.43	1.56	1.83
P <sub>2</sub> O <sub>5</sub>	0.98	0.75	<b>0.07</b>	1.75	<b>0.08</b>	0.78	0.76	0.92
SO <sub>2</sub>	-0.04	-0.03	<b>-0.03</b>	0.00	<b>-0.01</b>	-0.03	-0.03	-0.03
Cl	0.08	0.07	<b>0.11</b>	0.14	<b>0.03</b>	0.08	0.11	0.07
SrO	-0.13	-0.14	<b>-0.12</b>	-0.13	<b>-0.46</b>	-0.11	-0.12	-0.11
BaO	0.17	0.14	<b>0.02</b>	0.20	<b>0.08</b>	0.13	0.10	0.16
Total	99.34	99.22	<b>93.15</b>	97.80	<b>52.99</b>	98.13	97.51	98.80
Mg-no.	43.46	48.61	<b>2.70</b>	40.05	<b>72.69</b>	52.98	53.46	48.70
ne	9.58	5.72	<b>0.00</b>	5.03	<b>0.00</b>	6.62	7.55	7.21
di	23.37	19.73	<b>1.38</b>	7.00	<b>0.00</b>	22.17	21.57	15.19
ol	2.31	6.95	<b>0.00</b>	9.33	<b>0.00</b>	5.62	5.58	8.91
Q	0.00	0.00	<b>11.41</b>	0.00	<b>0.00</b>	0.00	0.00	0.00
hy	0.00	0.00	<b>6.23</b>	0.00	<b>0.00</b>	0.00	0.00	0.00
Li	10.28	8.07		5.72		<3.22	<1.61	6.69
Be	16.68	<0.00		<8.64		<9.30	<12.32	2.42
B	44.60	66.72		17.57		<6.82	23.20	15.11
Sc	33.17	25.16		8.46		19.06	29.23	17.27
Ti	21406.87	19226.09		10540.12		11466.63	14897.75	13351.55
V	287.72	262.63		54.51		166.98	206.66	168.83
Cr	61.18	57.64		<8.73		67.36	105.92	65.13
Co	22.18	39.59		10.80		20.32	23.68	28.62
Ni	21.85	42.22		<1.20		39.05	32.34	31.53
Zn	58.93	132.40		46.25		42.39	45.67	57.47
Rb	47.11	25.51		49.56		37.83	35.30	33.04
Sr	534.35	656.22		557.97		510.11	638.42	624.35
Y	32.97	26.97		31.16		18.87	27.03	19.59
Zr	325.36	272.48		353.04		252.66	294.56	210.77
Nb	80.69	65.76		82.19		50.93	61.68	50.23
Cs	0.41	0.17		0.53		0.34	0.31	0.31
Ba	408.62	369.84		619.32		359.53	350.53	461.79
La	62.31	48.76		78.56		40.97	51.76	40.85
Ce	107.06	99.18		131.69		74.30	90.82	81.40
Pr	12.01	12.49		14.92		8.50	10.03	9.29
Nd	51.01	55.78		52.99		28.94	45.01	38.21
Sm	9.69	13.35		10.66		7.27	7.43	7.91
Eu	3.14	3.53		3.32		2.12	2.70	2.54
Gd	7.90	5.42		8.96		6.29	5.35	5.74
Tb	1.30	1.25		1.37		0.66	0.87	0.89
Dy	6.33	5.84		5.80		5.25	5.78	4.23
Ho	1.31	1.36		1.15		<b>0.54</b>	0.84	0.76
Er	2.91	<b>2.82</b>		<b>1.54</b>		3.14	3.60	1.75
Tm	<b>0.25</b>	0.55		0.40		<b>0.37</b>	<b>0.34</b>	0.24
Yb	<b>3.19</b>	1.40		2.29		<0.35	2.79	1.76
Lu	<b>0.26</b>	0.26		<b>0.22</b>		<b>0.13</b>	<b>0.28</b>	0.25
Hf	5.87	4.03		5.02		4.00	5.50	4.90
Ta	3.84	3.72		3.64		2.93	3.17	2.72
Pb	2.00	2.41		3.52		4.23	2.21	6.70
Th	4.37	4.66		4.89		3.34	3.82	3.86
U	1.22	1.69		1.10		0.94	0.78	1.32
Al	33.06	34.61	<b>45.16</b>	36.16	<b>34.10</b>	33.64	34.37	36.52
CCPI	73.13	76.99	<b>43.42</b>	65.98	<b>99.33</b>	75.07	74.37	73.45

Full dataset of major and trace elemental compositions of glass shards from the AND-2A core, continued

Sample Model Age (Ma)	539.22-S1 16.88	577.50-A 17.08	577.50-F 17.08	577.50-G 17.08	577.50-B 17.08	577.50-C 17.08	577.50-I 17.08	577.50-J 17.08
SiO <sub>2</sub>	48.41	<b>25.09</b>	48.37	48.63	43.39	46.84	46.82	46.51
TiO <sub>2</sub>	3.12	<b>1.42</b>	3.30	3.26	5.28	3.04	3.11	3.04
Al <sub>2</sub> O <sub>3</sub>	15.29	<b>12.86</b>	16.02	15.38	12.48	15.78	15.46	15.91
FeO	10.16	<b>11.30</b>	10.59	11.71	14.11	10.89	11.01	10.85
MnO	0.25	<b>0.13</b>	0.22	0.27	0.23	0.19	0.17	0.19
MgO	3.42	<b>3.41</b>	4.28	4.53	4.86	5.99	5.63	5.69
CaO	6.89	<b>4.08</b>	7.93	8.66	10.63	10.25	9.57	10.10
Na <sub>2</sub> O	4.04	<b>1.72</b>	4.28	4.55	3.75	3.76	3.96	3.86
K <sub>2</sub> O	2.79	<b>1.68</b>	2.41	2.23	1.92	1.75	1.60	1.70
P <sub>2</sub> O <sub>5</sub>	1.27	<b>0.61</b>	1.53	1.20	2.15	0.85	1.03	0.96
SO <sub>2</sub>	0.00	<b>0.11</b>	-0.03	-0.02	-0.02	-0.02	0.03	0.02
Cl	0.13	<b>0.60</b>	0.11	0.10	0.07	0.06	0.08	0.08
SrO	-0.12	<b>-0.29</b>	-0.17	-0.11	-0.14	-0.16	-0.12	-0.18
BaO	0.19	<b>0.01</b>	0.00	0.07	0.03	0.04	0.11	0.12
Total	95.83	<b>62.73</b>	98.85	100.44	98.72	99.26	98.46	98.85
Mg-no.	37.48	<b>34.96</b>	41.86	40.79	38.03	49.54	47.70	48.32
ne	0.00	<b>7.85</b>	1.26	5.32	4.83	5.71	3.90	5.73
di	8.92	<b>0.00</b>	9.73	16.14	22.50	19.60	17.19	18.45
ol	2.72	<b>23.22</b>	6.95	6.39	2.52	7.75	7.99	7.60
Q	0.00	<b>0.00</b>	0.00	0.00	0.00	0.00	0.00	0.00
hy	4.12	<b>0.00</b>	0.00	0.00	0.00	0.00	0.00	0.00
Li	5.24		7.13	9.64	6.42	5.41	13.48	8.32
Be	<1.87		<2.53	4.01	2.97	4.67	<0.00	<0.00
B	10.57		18.36	<4.46	15.60	20.63	6.07	8.59
Sc	15.96		12.97	18.83	22.80	26.72	24.82	26.78
Ti	15137.62		18141.01	15790.96	28839.82	16458.45	18662.62	17358.06
V	103.59		162.81	157.38	297.58	237.10	235.93	237.81
Cr	7.40		<5.03	34.91	<4.97	94.19	65.32	94.74
Co	15.54		24.60	24.52	34.94	33.71	33.86	34.90
Ni	2.24		6.25	14.88	13.56	38.08	32.27	39.01
Zn	111.82		120.79	107.33	138.34	88.56	95.32	99.66
Rb	50.99		54.68	40.31	37.87	27.30	28.97	31.88
Sr	601.40		720.87	655.10	793.68	648.93	743.44	699.10
Y	32.31		36.01	29.08	43.63	25.93	27.98	26.74
Zr	337.72		450.39	348.66	366.51	239.10	265.02	263.10
Nb	92.76		101.62	79.48	77.97	52.73	65.23	58.80
Cs	0.41		0.55	0.28	0.39	0.28	0.36	0.32
Ba	574.46		517.24	440.42	643.74	487.79	629.00	573.33
La	73.40		83.47	64.03	82.88	48.56	54.89	53.98
Ce	145.51		154.48	123.75	162.23	88.86	108.49	98.42
Pr	16.46		17.50	13.40	21.40	10.03	12.21	11.43
Nd	62.27		72.40	57.69	85.94	43.79	51.39	53.04
Sm	12.16		11.10	8.80	17.84	8.87	8.01	10.34
Eu	3.77		4.13	3.21	5.39	2.80	4.03	3.08
Gd	9.49		7.64	8.73	12.56	7.37	7.87	7.70
Tb	1.12		1.32	1.18	2.05	0.93	0.99	0.97
Dy	7.45		7.48	6.43	10.60	6.14	6.49	5.87
Ho	1.34		1.30	1.28	2.16	1.10	0.94	1.25
Er	3.35		3.40	3.19	4.49	1.77	2.52	3.21
Tm	0.44		0.66	0.47	0.51	0.33	<b>0.30</b>	<b>0.24</b>
Yb	2.92		3.74	2.53	3.11	2.93	<b>2.51</b>	1.97
Lu	0.46		0.51	0.40	0.39	<b>0.31</b>	<b>0.32</b>	0.42
Hf	7.47		9.40	8.59	8.43	5.22	6.95	5.03
Ta	4.77		5.69	4.03	5.23	3.02	3.64	3.36
Pb	5.66		4.52	3.34	2.87	2.01	3.55	2.59
Th	7.27		8.34	6.61	6.35	4.36	5.31	5.49
U	2.07		2.16	1.87	1.60	1.30	1.31	1.30
Al	36.22		46.78	35.37	33.85	32.04	35.60	34.60
CCPI	66.54		81.22	68.96	70.56	76.98	75.39	74.85

Full dataset of major and trace elemental compositions of glass shards from the AND-2A core, continued

Sample Model Age (Ma)	577.50-2 17.08	577.50-3 17.08	577.50-H 17.08	592.76-A 17.16	592.76-B 17.16	592.76-I 17.16	592.76-I2 17.16	592.76-J 17.16
SiO <sub>2</sub>	<b>63.26</b>	49.56	49.11	43.97	44.52	45.33	45.33	45.19
TiO <sub>2</sub>	<b>0.71</b>	3.00	3.05	3.71	3.80	4.12	4.12	3.93
Al <sub>2</sub> O <sub>3</sub>	<b>13.67</b>	14.65	15.85	15.93	15.00	16.14	16.14	16.00
FeO	<b>6.79</b>	12.58	10.82	10.14	10.97	10.79	10.79	10.12
MnO	<b>0.32</b>	0.28	0.25	0.19	0.18	0.20	0.20	0.18
MgO	<b>0.23</b>	3.57	4.10	5.06	5.52	4.91	4.91	5.17
CaO	<b>1.21</b>	7.86	7.59	11.74	11.97	10.23	10.23	11.47
Na <sub>2</sub> O	<b>0.16</b>	4.12	4.06	4.38	4.20	4.16	4.16	4.65
K <sub>2</sub> O	<b>1.26</b>	1.82	2.54	2.24	1.73	2.23	2.23	2.16
P <sub>2</sub> O <sub>5</sub>	<b>0.03</b>	1.44	1.43	0.94	0.97	1.10	1.10	1.20
SO <sub>2</sub>	<b>0.05</b>	0.05	-0.02	-0.04	-0.04	-0.04	-0.04	-0.04
Cl	<b>0.12</b>	0.10	0.12	0.14	0.11	0.15	0.15	0.14
SrO	<b>-0.14</b>	-0.12	-0.12	-0.10	-0.13	-0.12	-0.12	-0.06
BaO	<b>-0.01</b>	0.04	0.14	0.10	0.15	-0.03	-0.03	0.14
Total	<b>87.67</b>	98.96	98.91	98.39	98.94	99.17	99.17	100.25
Mg-no.	<b>5.69</b>	33.62	40.34	47.07	47.30	44.76	44.76	47.67
ne	<b>0.00</b>	0.00	0.00	17.69	13.93	10.12	10.12	16.12
di	<b>0.00</b>	11.06	8.75	28.33	29.26	20.08	20.08	26.05
ol	<b>0.00</b>	0.00	5.78	0.00	1.28	2.74	2.74	0.89
Q	<b>57.89</b>	0.02	0.00	0.00	0.00	0.00	0.00	0.00
hy	<b>7.29</b>	11.11	2.94	0.00	0.00	0.00	0.00	0.00
Li		7.10	5.03	6.44	8.80	5.25	7.14	
Be		<0.00	<0.00	13.92	4.48	4.54	3.12	
B		10.11	4.31	15.34	6.66	5.18	8.77	
Sc		10.68	24.98	29.94	24.59	25.67	29.38	
Ti		15725.10	20041.16	20503.51	22043.62	21721.52	21977.90	
V		133.22	264.70	307.37	259.58	249.44	272.95	
Cr		7.32	27.72	57.03	48.95	34.49	91.45	
Co		18.83	28.78	30.81	29.81	32.53	31.45	
Ni		8.54	24.55	30.60	27.40	24.29	39.73	
Zn		117.72	88.41	94.24	83.28	96.85	80.75	
Rb		51.11	48.93	37.67	50.12	51.68	50.70	
Sr		709.74	1042.04	790.42	894.15	875.09	1028.64	
Y		32.55	28.43	25.74	29.87	30.22	31.91	
Zr		403.16	322.33	254.27	327.92	327.02	347.02	
Nb		102.00	83.44	68.19	85.37	84.18	91.90	
Cs		0.54	0.63	0.38	0.60	0.55	0.60	
Ba		532.42	581.31	456.21	566.54	568.64	607.40	
La		79.77	66.47	54.58	69.23	66.77	72.94	
Ce		154.88	123.91	98.99	122.56	122.81	136.47	
Pr		17.28	14.40	11.07	14.72	14.21	15.88	
Nd		72.66	54.64	46.97	60.32	56.05	63.55	
Sm		13.87	12.87	10.96	11.71	11.08	13.15	
Eu		3.25	3.72	3.50	3.56	3.64	3.91	
Gd		7.41	7.75	8.50	10.48	7.76	8.67	
Tb		1.20	1.40	1.07	1.35	1.21	1.41	
Dy		6.58	6.08	6.20	6.26	6.16	7.18	
Ho		1.33	1.17	1.34	1.28	1.13	1.09	
Er		3.76	2.74	2.73	3.45	2.77	2.84	
Tm		<b>0.30</b>	0.29	<b>0.28</b>	0.44	0.39	0.49	
Yb		<b>3.61</b>	3.16	<b>2.83</b>	3.11	2.36	3.36	
Lu		<b>0.29</b>	0.33	<b>0.40</b>	0.38	0.27	0.43	
Hf		8.66	7.76	6.22	7.80	6.91	6.82	
Ta		5.08	4.32	3.91	4.75	4.62	5.31	
Pb		4.32	2.80	2.84	3.47	3.14	3.58	
Th		8.77	7.29	7.01	7.55	7.59	8.13	
U		2.78	1.94	1.75	1.88	1.81	2.53	
AI	52.11	31.05	36.33	31.16	30.96	33.14	33.14	31.24
CCPI	83.25	73.12	69.36	69.68	73.56	71.08	71.08	69.18

Full dataset of major and trace elemental compositions of glass shards from the AND-2A core, continued

Sample Model Age (Ma)	592.76-C 17.16	592.76-K 17.16	592.76-L 17.16	592.76-H 17.16	592.76-M 17.16	592.76-O 17.16	592.76-D 17.16	592.76-E 17.16
SiO <sub>2</sub>	44.35	44.28	46.30	45.50	45.46	48.75	49.63	46.21
TiO <sub>2</sub>	3.92	3.87	3.58	3.39	4.39	3.44	2.76	3.72
Al <sub>2</sub> O <sub>3</sub>	15.93	15.91	15.86	15.04	14.99	16.81	17.34	15.88
FeO	9.66	9.88	10.27	11.42	11.43	8.91	9.04	9.49
MnO	0.22	0.19	0.11	0.17	0.25	0.23	0.19	0.16
MgO	5.58	5.28	5.13	6.09	4.50	3.43	3.44	5.68
CaO	11.75	11.56	11.24	11.27	10.30	7.38	6.93	11.01
Na <sub>2</sub> O	4.88	4.17	4.35	3.45	4.25	5.08	4.94	4.28
K <sub>2</sub> O	1.70	2.37	1.98	1.52	2.46	3.24	3.28	1.81
P <sub>2</sub> O <sub>5</sub>	0.99	1.02	0.78	0.82	1.15	1.42	1.36	0.94
SO <sub>2</sub>	-0.04	-0.02	-0.06	0.10	-0.12	0.04	-0.04	-0.04
Cl	0.31	0.11	0.11	0.05	0.09	0.19	0.17	0.09
SrO	-0.13	-0.10	-0.10	-0.11	-0.10	-0.05	-0.10	-0.15
BaO	0.02	0.12	-0.03	-0.03	0.05	0.16	0.13	0.06
Total	99.12	98.63	99.50	98.67	99.09	99.01	99.07	99.14
Mg-no.	50.76	48.78	47.10	48.73	41.25	40.74	40.43	51.63
ne	18.48	15.91	12.37	6.18	10.90	8.49	6.40	10.54
di	28.31	26.73	26.28	24.05	23.59	11.19	8.08	23.84
ol	0.97	1.05	1.15	6.14	0.62	2.98	5.32	2.88
Q	0.00	0.00	0.00	0.00	0.00	0.00	0.00	0.00
hy	0.00	0.00	0.00	0.00	0.00	0.00	0.00	0.00
Li	4.83			6.42	10.80	6.59		6.31
Be	4.52			4.15	2.22	2.07		4.36
B	<2.22			228.88	8.58	17.10		9.05
Sc	28.94			31.50	22.93	16.53		28.73
Ti	21562.09			18937.73	24594.91	16671.02		17665.80
V	279.69			274.97	296.28	142.96		224.97
Cr	91.04			131.91	23.57	6.88		102.23
Co	31.97			48.05	29.21	16.64		27.26
Ni	38.38			114.73	21.51	6.71		38.27
Zn	88.47			96.83	111.90	71.53		82.23
Rb	42.56			30.81	60.13	59.89		35.35
Sr	982.81			647.53	773.74	1027.57		881.08
Y	27.28			26.80	38.17	30.01		27.50
Zr	272.27			264.50	448.62	379.63		278.16
Nb	79.78			59.13	104.34	113.31		69.86
Cs	0.41			0.48	0.65	0.59		0.28
Ba	528.02			329.43	552.75	806.27		440.68
La	61.51			48.79	88.45	91.64		57.22
Ce	113.32			88.79	158.19	155.77		99.35
Pr	13.76			11.16	17.66	17.79		11.03
Nd	54.11			45.72	73.49	70.35		49.98
Sm	10.09			8.52	12.62	12.02		8.89
Eu	3.17			3.13	3.68	3.89		3.23
Gd	8.77			7.20	9.42	7.83		6.39
Tb	1.15			1.04	1.45	1.21		1.20
Dy	6.50			5.95	7.05	6.77		5.79
Ho	1.07			1.05	1.61	1.34		1.10
Er	2.68			2.42	3.53	3.27		2.72
Tm	0.38			0.39	0.51	0.44		0.31
Yb	3.05			3.10	3.21	3.14		2.79
Lu	0.31			0.25	0.43	0.46		0.29
Hf	6.15			5.92	9.13	7.74		6.28
Ta	4.01			3.40	5.89	5.75		4.07
Pb	3.02			6.02	4.13	3.42		3.03
Th	6.69			4.48	9.57	10.05		6.00
U				1.56	2.52	2.48		1.38
Al	30.47	32.73	31.31	34.06	32.35	34.88	36.16	32.89
CCPI	69.85	69.86	70.85	77.92	70.35	59.74	60.28	71.36

Full dataset of major and trace elemental compositions of glass shards from the AND-2A core, continued

Sample Model Age (Ma)	592.76-F 17.16	592.76-G 17.16	<b>592.76-N 17.16</b>	596.77-A 17.18	596.77-B 17.18	596.77-D 17.18	596.77-D2 17.18	596.77-N 17.18
SiO <sub>2</sub>	44.82	41.95	<b>42.42</b>	46.33	51.28	44.27	44.27	43.46
TiO <sub>2</sub>	3.97	5.71	<b>2.99</b>	3.07	2.77	4.85	4.85	4.57
Al <sub>2</sub> O <sub>3</sub>	15.94	11.67	<b>10.55</b>	15.82	16.30	13.40	13.40	14.46
FeO	9.97	15.84	<b>14.71</b>	10.48	8.77	13.78	13.78	13.12
MnO	0.18	0.26	<b>0.23</b>	0.23	0.23	0.20	0.20	0.27
MgO	5.62	5.52	<b>14.21</b>	6.51	3.21	5.00	5.00	5.87
CaO	11.72	11.37	<b>7.69</b>	11.52	6.57	10.49	10.49	10.45
Na <sub>2</sub> O	4.21	3.67	<b>2.91</b>	3.52	3.70	3.67	3.67	3.77
K <sub>2</sub> O	1.89	1.19	<b>1.39</b>	1.45	2.52	1.90	1.90	1.06
P <sub>2</sub> O <sub>5</sub>	0.96	2.43	<b>0.77</b>	0.72	1.02	1.98	1.98	1.74
SO <sub>2</sub>	-0.06	-0.03	<b>0.02</b>	0.06	0.10	-0.03	-0.03	0.06
Cl	0.10	0.05	<b>0.07</b>	0.07	0.12	0.10	0.10	0.08
SrO	-0.13	-0.15	<b>-0.21</b>	-0.18	-0.17	-0.19	-0.19	-0.15
BaO	0.14	0.24	<b>0.03</b>	0.05	0.04	0.06	0.06	0.12
Total	99.33	99.71	<b>97.76</b>	99.62	96.46	99.46	99.46	98.88
Mg-no.	50.12	38.31	<b>63.28</b>	52.56	39.51	39.29	39.29	44.36
ne	13.85	4.26	<b>6.93</b>	6.62	0.00	3.92	3.92	3.67
di	26.43	23.67	<b>17.31</b>	23.60	4.63	20.22	20.22	17.31
ol	1.79	4.40	<b>30.45</b>	6.76	0.00	4.29	4.29	7.27
Q	0.00	0.00	<b>0.00</b>	0.00	4.54	0.00	0.00	0.00
hy	0.00	0.00	<b>0.00</b>	0.00	8.18	0.00	0.00	0.00
Li			3.33	9.75	7.31	3.20		
Be			<5.03	<0.00	20.37	<0.00		
B			<5.33	32.52	30.87	8.20		
Sc			26.95	12.12	24.05	27.66		
Ti			15892.64	12242.22	28459.82	24179.25		
V			246.79	87.59	324.98	274.20		
Cr			134.19	4.79	23.34	27.71		
Co			34.82	9.22	27.81	34.10		
Ni			46.55	<0.62	6.31	2.11		
Zn			89.11	108.31	177.46	148.16		
Rb			33.90	47.53	36.72	34.01		
Sr			555.13	729.76	722.58	660.59		
Y			22.34	34.71	34.34	34.30		
Zr			241.55	381.76	320.35	289.54		
Nb			48.61	90.93	80.98	84.09		
Cs			0.58	0.46	0.07	0.62		
Ba			327.12	737.93	563.95	542.67		
La			42.18	74.00	81.34	72.42		
Ce			81.86	142.16	158.87	143.13		
Pr			8.92	16.47	18.48	16.40		
Nd			38.02	65.95	72.85	71.72		
Sm			7.74	8.26	14.85	12.50		
Eu			2.91	4.51	5.83	5.16		
Gd			4.43	9.45	11.99	12.10		
Tb			0.91	1.06	1.00	1.40		
Dy			4.25	5.42	13.32	6.43		
Ho			0.99	1.52	<b>1.32</b>	1.90		
Er			2.14	4.48	<b>4.59</b>	<b>2.81</b>		
Tm			<b>0.38</b>	0.61	<b>0.52</b>	0.36		
Yb			2.71	2.45	1.10	1.86		
Lu			<b>0.16</b>	0.38	<b>0.65</b>	0.45		
Hf			4.53	8.53	<b>6.11</b>	<b>4.95</b>		
Ta			2.90	4.97	4.23	3.66		
Pb				<b>14.78</b>	3.60	4.28		
Th				4.39	7.28	7.37	7.00	
U				1.52	1.87	2.80	1.49	
Al	32.03	30.84	59.55	34.60	35.80	32.75	32.75	
CCPI	71.91	81.48	87.08	77.40	65.82	77.12	77.12	79.70

Full dataset of major and trace elemental compositions of glass shards from the AND-2A core, continued

Sample Model Age (Ma)	596.77-R 17.18	596.77-S 17.18	596.77-O 17.18	596.77-P 17.18	<b>596.77-M 17.18</b>	596.77-T 17.18	596.77-K 17.18	<b>596.77-G 17.18</b>
SiO <sub>2</sub>	47.44	50.71	45.51	51.10	<b>51.79</b>	45.72	46.22	<b>54.14</b>
TiO <sub>2</sub>	3.55	3.20	3.99	2.77	<b>2.70</b>	3.58	3.87	<b>2.17</b>
Al <sub>2</sub> O <sub>3</sub>	16.62	17.33	14.73	16.23	<b>16.14</b>	15.80	14.82	<b>16.45</b>
FeO	10.26	6.64	11.78	8.77	<b>8.85</b>	11.45	12.49	<b>8.28</b>
MnO	0.27	0.15	0.21	0.23	<b>0.27</b>	0.19	0.22	<b>0.21</b>
MgO	4.55	3.90	5.35	3.28	<b>3.14</b>	5.65	5.27	<b>2.61</b>
CaO	8.28	9.88	10.09	6.64	<b>6.36</b>	10.50	10.16	<b>5.66</b>
Na <sub>2</sub> O	4.19	2.78	3.59	1.47	<b>2.97</b>	4.31	3.98	<b>2.51</b>
K <sub>2</sub> O	2.59	1.46	1.59	2.68	<b>3.22</b>	1.51	1.66	<b>3.32</b>
P <sub>2</sub> O <sub>5</sub>	1.19	0.84	1.70	1.10	<b>0.94</b>	0.99	0.82	<b>0.73</b>
SO <sub>2</sub>	-0.02	0.08	0.09	0.00	<b>0.02</b>	0.08	-0.01	<b>0.00</b>
Cl	0.12	0.12	0.06	0.10	<b>0.09</b>	0.44	0.07	<b>0.11</b>
SrO	-0.14	-0.12	-0.11	-0.12	<b>-0.11</b>	-0.18	-0.16	<b>-0.14</b>
BaO	0.12	0.13	0.01	0.08	<b>0.16</b>	0.02	0.00	<b>0.09</b>
Total	99.02	97.11	98.58	94.34	<b>96.53</b>	100.04	99.43	<b>96.15</b>
Mg-no.	44.15	51.13	44.74	40.01	<b>38.75</b>	46.79	42.93	<b>35.98</b>
ne	4.58	0.00	0.75	0.00	<b>0.00</b>	9.55	6.41	<b>0.00</b>
di	11.65	9.83	16.05	0.00	<b>3.49</b>	21.15	22.20	<b>0.00</b>
ol	5.78	0.00	6.54	0.00	<b>0.00</b>	5.64	5.08	<b>0.00</b>
Q	0.00	6.89	0.00	15.78	<b>6.45</b>	0.00	0.00	<b>11.34</b>
hy	0.00	6.30	0.00	11.13	<b>9.05</b>	0.00	0.00	<b>10.22</b>
Li	1.91		<0.64				6.77	
Be	<0.00		<3.68				<0.00	
B	29.66		47.43				5.98	
Sc	24.30		11.93				26.67	
Ti	15625.85		13696.32				21678.01	
V	223.08		99.17				320.94	
Cr	54.15		7.58				36.60	
Co	27.31		10.19				37.73	
Ni	46.85		2.37				12.38	
Zn	88.18		138.42				114.67	
Rb	34.43		48.20				30.06	
Sr	713.20		815.73				535.09	
Y	23.15		37.82				27.10	
Zr	192.87		430.96				249.39	
Nb	73.22		95.16				61.69	
Cs	0.35		0.57				0.28	
Ba	424.47		754.03				370.76	
La	50.46		80.51				47.67	
Ce	91.32		156.18				97.65	
Pr	11.29		18.41				10.76	
Nd	38.69		75.01				49.40	
Sm	8.62		13.88				6.30	
Eu	1.99		4.23				3.27	
Gd	3.24		13.34				8.18	
Tb	0.84		1.20				1.15	
Dy	3.99		8.39				6.31	
Ho	0.93		1.78				1.04	
Er	1.57		4.67				3.28	
Tm	0.41		0.58				0.28	
Yb	3.28		2.77				2.65	
Lu	0.27		0.57				0.36	
Hf	4.36		7.89				7.14	
Ta	3.66		6.79				3.52	
Pb	2.54		4.50				2.40	
Th	5.46		7.96				4.56	
U	1.94		2.48				1.35	
Al	36.41	29.72	33.65	42.34	40.53	32.57	32.89	42.07
CCPI	68.61	71.27	76.81	74.36	65.98	74.61	75.89	65.11

Full dataset of major and trace elemental compositions of glass shards from the AND-2A core, continued

Sample Model Age (Ma)	596.77-H 17.18	596.77-F 17.18	640.82-A 17.41	640.82-1 17.41	640.82-B 17.41	640.82-2 17.41	640.82-G 17.41	640.82-H 17.41
SiO <sub>2</sub>	48.97	44.19	45.75	45.60	44.44	46.05	45.72	45.91
TiO <sub>2</sub>	3.08	3.36	3.20	3.26	4.33	3.41	3.29	3.15
Al <sub>2</sub> O <sub>3</sub>	17.05	16.82	15.72	15.28	13.58	15.69	15.39	15.41
FeO	8.91	9.76	10.90	11.13	13.60	11.09	10.57	11.14
MnO	0.19	0.19	0.15	0.21	0.22	0.21	0.18	0.17
MgO	3.33	5.95	7.24	7.12	5.60	6.94	7.33	7.09
CaO	6.95	11.40	11.57	11.55	10.53	11.50	11.46	11.58
Na <sub>2</sub> O	5.10	4.03	3.29	3.12	3.66	3.42	3.50	3.16
K <sub>2</sub> O	3.15	1.62	1.04	1.19	1.32	1.23	1.06	0.89
P <sub>2</sub> O <sub>5</sub>	1.31	0.71	0.58	0.52	1.83	0.62	0.66	0.58
SO <sub>2</sub>	0.02	0.04	0.03	0.03	0.01	0.01	-0.02	0.05
Cl	0.19	0.07	0.03	0.07	0.06	0.05	0.04	0.02
SrO	-0.14	-0.20	-0.19	-0.15	-0.15	-0.11	-0.19	-0.17
BaO	0.10	0.08	0.01	0.01	0.21	0.06	0.07	0.04
Total	98.21	98.01	99.32	98.92	99.24	100.15	99.07	99.02
Mg-no.	39.97	52.07	54.22	53.30	42.35	52.76	55.31	53.18
ne	7.38	13.18	5.01	4.63	2.59	5.71	5.93	3.10
di	9.41	23.46	22.96	24.09	19.39	23.34	23.69	23.03
ol	3.64	4.12	8.61	8.24	7.08	7.51	7.96	8.85
Q	0.00	0.00	0.00	0.00	0.00	0.00	0.00	0.00
hy	0.00	0.00	0.00	0.00	0.00	0.00	0.00	0.00
Li	1.81			1.38		2.79	3.14	4.77
Be	9.95			<2.10		<0.00	<0.00	<0.00
B	36.13			32.27		24.96	8.27	48.95
Sc	11.85			35.01		26.46	31.84	33.57
Ti	17423.05			18988.95		16460.48	18563.02	18202.46
V	135.14			289.64		254.38	293.27	275.80
Cr	3.86			128.95		163.28	143.59	140.59
Co	16.09			45.37		39.58	41.10	42.81
Ni	3.24			72.74		56.67	72.22	62.28
Zn	80.01			86.05		84.57	91.46	84.19
Rb	65.93			21.02		23.76	14.73	15.96
Sr	1017.97			685.12		595.61	682.18	651.06
Y	30.57			21.62		21.75	23.89	22.72
Zr	403.13			203.35		223.62	218.22	217.60
Nb	124.33			38.43		35.36	42.54	36.66
Cs	0.73			0.14		0.16	0.27	0.19
Ba	893.41			234.87		248.99	238.23	211.44
La	94.52			33.76		32.75	37.22	34.77
Ce	175.98			65.95		61.77	68.72	63.82
Pr	18.22			8.19		7.72	8.42	8.37
Nd	71.15			32.37		34.05	35.31	39.58
Sm	11.64			6.26		6.82	7.41	9.72
Eu	3.56			3.25		1.88	2.14	2.35
Gd	8.06			7.69		6.85	7.12	5.18
Tb	0.83			0.70		0.66	1.03	1.30
Dy	6.87			5.83		4.99	5.05	5.02
Ho	0.98			0.87		0.85	0.86	1.20
Er	3.83			3.23		1.77	2.75	2.72
Tm	0.39			0.12		0.30	0.45	0.34
Yb	2.87			1.96		1.36	2.96	1.77
Lu	0.34			0.27		0.29	0.24	0.22
Hf	6.86			5.72		3.96	6.56	5.83
Ta	7.30			1.97		1.99	2.43	2.28
Pb	7.43			4.08		5.44	1.90	1.82
Th	11.20			3.82		3.19	3.54	3.41
U	3.49			1.04		0.84	0.80	0.81
Al	34.97	32.89	35.79	36.15	32.80	35.39	35.95	35.15
CCPI	59.74	73.54	80.72	80.91	79.40	79.52	79.69	81.81

Full dataset of major and trace elemental compositions of glass shards from the AND-2A core, continued

Sample Model Age (Ma)	640.82-3 17.41	640.82-4 17.41	<b>640.82-E 17.41</b>	<b>640.82-D 17.41</b>	640.82-5 17.41	642.38-A 17.42	642.38-B 17.42	642.38-X 17.42
SiO <sub>2</sub>	44.08	44.74	<b>54.96</b>	<b>54.31</b>	46.13	45.23	45.02	45.45
TiO <sub>2</sub>	4.41	4.78	<b>2.02</b>	<b>2.56</b>	3.72	4.35	4.53	4.47
Al <sub>2</sub> O <sub>3</sub>	15.38	12.59	<b>15.60</b>	<b>14.55</b>	14.93	14.37	13.96	14.30
FeO	9.43	14.00	<b>8.84</b>	<b>8.11</b>	10.72	12.36	12.17	12.24
MnO	0.13	0.23	<b>0.21</b>	<b>0.16</b>	0.17	0.19	0.21	0.20
MgO	5.75	5.19	<b>2.26</b>	<b>2.57</b>	6.29	5.21	5.03	5.04
CaO	12.28	10.96	<b>5.20</b>	<b>5.16</b>	12.32	10.97	10.62	10.99
Na <sub>2</sub> O	4.28	3.34	<b>1.49</b>	<b>1.03</b>	3.13	3.87	3.79	3.89
K <sub>2</sub> O	2.25	1.19	<b>2.51</b>	<b>3.34</b>	1.66	1.89	1.98	1.80
P <sub>2</sub> O <sub>5</sub>	1.57	2.08	<b>0.82</b>	<b>0.76</b>	0.68	1.06	0.95	0.95
SO <sub>2</sub>	-0.03	-0.01	<b>0.04</b>	<b>0.02</b>	-0.06	-0.04	-0.02	0.01
Cl	0.19	0.06	<b>0.10</b>	<b>0.06</b>	0.08	0.08	0.09	0.10
SrO	-0.09	-0.18	<b>-0.11</b>	<b>-0.13</b>	-0.12	-0.14	-0.15	-0.15
BaO	0.15	0.10	<b>0.17</b>	<b>0.25</b>	0.16	0.09	-0.01	0.06
Total	99.78	99.08	<b>94.11</b>	<b>92.74</b>	99.81	99.49	98.18	99.33
Mg-no.	52.12	39.81	<b>31.29</b>	<b>36.13</b>	51.12	42.90	42.43	42.32
ne	16.52	0.00	<b>0.00</b>	<b>0.00</b>	5.68	8.28	7.29	7.61
di	27.69	20.66	<b>0.00</b>	<b>0.00</b>	28.16	25.41	25.72	26.14
ol	1.55	1.18	<b>0.00</b>	<b>0.00</b>	3.16	2.29	1.28	1.24
Q	0.00	0.00	<b>22.82</b>	<b>23.17</b>	0.00	0.00	0.00	0.00
hy	0.00	5.25	<b>11.08</b>	<b>8.81</b>	0.00	0.00	0.00	0.00
Li	1.19				2.93	7.06		6.24
Be	<1.92				<1.83	<1.79		<2.26
B	26.69				27.37	12.77		10.40
Sc	23.17				35.54	27.14		27.03
Ti	24079.86				19168.95	24365.65		22635.45
V	267.66				306.64	329.65		291.86
Cr	31.00				110.92	60.23		60.30
Co	31.02				40.21	34.98		32.73
Ni	26.05				67.54	18.92		28.91
Zn	86.79				91.19	113.75		96.67
Rb	41.29				23.71	36.24		34.32
Sr	1323.57				745.46	731.76		834.25
Y	30.34				23.66	33.34		33.16
Zr	440.04				229.79	329.89		332.82
Nb	111.07				52.48	72.69		70.61
Cs	0.75				0.38	0.35		0.48
Ba	511.82				303.74	457.45		441.39
La	84.73				43.93	63.14		61.49
Ce	178.26				81.16	119.38		110.94
Pr	20.33				9.47	13.97		14.23
Nd	74.45				38.96	61.98		56.93
Sm	13.74				7.62	11.92		10.75
Eu	4.78				3.12	3.46		3.57
Gd	9.91				7.34	10.90		12.37
Tb	1.15				0.96	1.15		1.47
Dy	7.01				6.18	7.30		7.21
Ho	1.23				0.93	1.46		1.71
Er	<b>2.81</b>				<b>1.40</b>	2.98		3.84
Tm	<b>0.29</b>				<b>0.40</b>	0.46		0.41
Yb	<b>2.78</b>				<b>1.89</b>	1.57		<b>2.46</b>
Lu	<b>0.32</b>				<b>0.16</b>	0.34		<b>0.34</b>
Hf	10.07				3.40	7.92		6.85
Ta	5.42				2.91	4.48		4.62
Pb	3.58				1.98	2.34		2.09
Th	9.12				4.03	6.69		6.55
U	2.61				1.32	1.79		1.38
Al	32.59	30.85	41.58	48.85	33.97	32.35	32.73	31.50
CCPI	69.91	80.91	73.50	70.96	77.99	75.29	74.88	75.22

Full dataset of major and trace elemental compositions of glass shards from the AND-2A core, continued

Sample Model Age (Ma)	642.38-W 17.42	642.38-V 17.42	642.38-S 17.42	642.38-S2 17.42	642.38-R 17.42	642.38-Q 17.42	642.38-P 17.42	642.38-U 17.42
SiO <sub>2</sub>	44.61	45.67	44.57	44.57	45.07	45.47	46.76	44.87
TiO <sub>2</sub>	4.53	4.35	4.53	4.53	4.45	4.55	4.28	4.41
Al <sub>2</sub> O <sub>3</sub>	14.14	14.52	14.36	14.36	14.52	14.59	13.60	14.18
FeO	12.37	11.99	12.11	12.11	12.18	12.40	12.98	12.03
MnO	0.20	0.22	0.20	0.20	0.14	0.23	0.22	0.16
MgO	4.98	5.07	5.17	5.17	5.08	5.08	4.87	4.86
CaO	10.63	10.68	11.04	11.04	10.65	10.64	9.72	10.27
Na <sub>2</sub> O	3.92	3.95	3.91	3.91	3.90	3.99	3.82	3.84
K <sub>2</sub> O	1.96	1.78	1.63	1.63	2.04	1.99	1.56	2.02
P <sub>2</sub> O <sub>5</sub>	1.01	1.11	0.99	0.99	1.00	0.95	1.37	1.09
SO <sub>2</sub>	0.03	-0.03	0.03	0.03	0.01	0.00	-0.01	0.00
Cl	0.11	0.07	0.09	0.09	0.07	0.07	0.07	0.10
SrO	-0.16	-0.13	-0.15	-0.15	-0.14	-0.12	-0.17	-0.13
BaO	-0.10	0.13	0.04	0.04	0.21	0.13	0.14	0.11
Total	98.24	99.37	98.52	98.52	99.18	99.96	99.22	97.83
Mg-no.	41.80	43.00	43.22	43.22	42.65	42.23	40.09	41.88
ne	8.78	6.60	8.26	8.26	8.59	8.59	0.14	6.89
di	25.45	23.70	25.85	25.85	24.68	24.75	19.61	23.47
ol	1.49	2.27	1.43	1.43	1.83	1.81	4.83	1.92
Q	0.00	0.00	0.00	0.00	0.00	0.00	0.00	0.00
hy	0.00	0.00	0.00	0.00	0.00	0.00	0.00	0.00
Li	7.10		2.34	10.95	9.17	5.80	2.83	
Be	9.19		<0.00	<0.00	<0.00	<0.00	6.47	
B	13.04		37.34	<5.18	<2.84	15.72	20.89	
Sc	27.22		22.02	30.25	27.58	24.67	26.72	
Ti	22018.41		26070.77	25617.77	23952.22	23902.12	24539.54	
V	283.10		354.66	333.22	322.22	309.12	259.75	
Cr	40.92		57.61	68.73	58.37	45.11	<4.13	
Co	30.84		34.64	35.05	35.14	34.19	34.08	
Ni	22.21		22.64	27.28	24.62	23.87	<0.34	
Zn	114.93		131.57	141.07	123.89	127.55	106.42	
Rb	35.43		34.08	40.84	38.05	33.36	20.81	
Sr	792.15		757.82	768.24	728.01	718.02	738.15	
Y	30.82		35.05	35.76	33.39	30.92	31.84	
Zr	302.55		329.71	351.37	313.37	325.83	213.26	
Nb	69.73		75.65	78.14	77.85	73.38	48.88	
Cs	0.40		0.31	0.40	0.32	0.54	0.30	
Ba	415.87		469.82	476.48	457.91	448.92	1036.43	
La	58.23		61.70	67.31	60.74	62.19	48.12	
Ce	109.87		120.45	124.01	117.03	118.13	94.41	
Pr	13.00		14.23	15.33	14.40	14.06	11.95	
Nd	58.03		58.16	68.08	62.82	59.21	54.62	
Sm	11.58		12.26	13.08	12.04	11.98	8.96	
Eu	3.56		4.31	4.32	3.45	3.99	4.96	
Gd	10.24		11.10	9.82	10.90	7.06	9.71	
Tb	0.73		1.02	1.14	1.41	1.37	1.36	
Dy	6.88		6.27	9.11	8.30	7.25	5.80	
Ho	1.34		1.64	1.45	1.15	1.22	1.35	
Er	2.92		4.06	3.02	3.08	4.16	3.30	
Tm	0.60		0.38	0.16	0.30	0.34	0.38	
Yb	1.96		3.98	3.83	2.83	2.46	3.02	
Lu	0.23		0.66	0.37	0.30	0.41	0.27	
Hf	7.82		7.39	8.92	8.22	10.67	5.55	
Ta	3.93		4.29	4.90	4.50	4.23	2.85	
Pb	3.04		2.40	3.25	2.89	2.36	2.16	
Th	6.19		6.27	7.63	6.05	6.82	4.98	
U	1.56		1.41	2.10	1.83	1.36	0.85	
Al	32.32		31.91	31.28	31.28	32.56	32.22	32.78
CCPI	74.69		74.87	75.71	75.71	74.41	76.82	74.26

Full dataset of major and trace elemental compositions of glass shards from the AND-2A core, continued

Sample Model Age (Ma)	642.38-M 17.42	642.38-N 17.42	642.38-L 17.42	642.38-K 17.42	642.38-J 17.42	642.38-I 17.42	644.25-A 17.43	644.25-D 17.43
SiO <sub>2</sub>	45.80	44.97	45.31	45.11	45.17	46.74	44.79	46.14
TiO <sub>2</sub>	4.34	4.41	4.20	4.31	4.43	3.32	4.11	4.38
Al <sub>2</sub> O <sub>3</sub>	13.84	14.21	14.79	14.06	14.40	15.62	14.16	14.70
FeO	13.54	12.47	11.80	11.98	12.25	10.68	12.53	12.18
MnO	0.25	0.16	0.20	0.18	0.20	0.25	0.19	0.22
MgO	5.01	5.04	4.81	5.10	4.90	5.20	5.40	4.88
CaO	9.85	10.65	10.11	10.92	10.52	10.58	10.77	9.97
Na <sub>2</sub> O	3.73	3.89	3.96	3.94	4.24	4.06	3.81	3.78
K <sub>2</sub> O	1.16	1.88	1.85	1.88	1.84	1.84	1.52	1.86
P <sub>2</sub> O <sub>5</sub>	1.35	1.02	1.07	0.89	0.97	1.04	1.39	1.04
SO <sub>2</sub>	0.06	-0.03	-0.02	-0.04	-0.04	-0.01	0.03	-0.08
Cl	0.05	0.11	0.07	0.08	0.09	0.09	0.08	0.12
SrO	-0.12	-0.16	-0.14	-0.15	-0.11	-0.11	-0.14	-0.10
BaO	0.14	0.07	0.09	0.05	0.08	0.01	0.05	0.01
Total	98.98	98.70	98.08	98.30	98.93	99.34	98.69	99.08
Mg-no.	39.76	41.88	42.10	43.13	41.62	46.49	43.45	41.68
ne	0.00	7.93	6.36	8.91	9.67	7.40	5.73	3.61
di	18.52	24.96	21.48	27.25	25.35	21.60	22.41	20.46
ol	5.56	2.14	2.85	1.13	1.38	4.47	4.80	3.28
Q	0.00	0.00	0.00	0.00	0.00	0.00	0.00	0.00
hy	0.78	0.00	0.00	0.00	0.00	0.00	0.00	0.00
Li	<0.38		9.47	3.78	4.13	6.85		
Be	<2.13		2.32	1.86	<0.00	7.33		
B	<4.87		22.72	14.29	17.98	10.98		
Sc	26.14		22.68	26.28	18.40	23.51		
Ti	24272.78		23975.91	23578.19	15792.57	18124.54		
V	262.63		293.61	303.57	198.30	227.70		
Cr	13.70		14.08	54.64	25.05	65.87		
Co	32.90		33.56	34.49	22.21	29.01		
Ni	2.71		21.48	28.75	14.00	38.69		
Zn	113.16		127.07	110.89	72.79	95.55		
Rb	22.86		41.57	36.60	24.34	41.99		
Sr	711.73		817.46	806.71	1095.16	725.37		
Y	30.95		31.94	30.40	21.67	24.07		
Zr	200.86		328.89	286.79	202.42	286.00		
Nb	45.80		81.11	71.86	52.52	79.05		
Cs	0.08		0.34	0.51	0.22	0.32		
Ba	917.15		502.34	430.67	392.38	454.92		
La	40.79		66.34	58.17	42.53	62.15		
Ce	92.18		125.00	111.54	81.89	115.70		
Pr	11.74		14.49	13.18	9.77	13.37		
Nd	48.01		64.35	55.75	41.79	51.77		
Sm	7.97		13.01	9.89	6.87	9.25		
Eu	4.11		3.16	3.47	3.14	3.28		
Gd	8.88		9.05	6.88	5.41	6.31		
Tb	1.13		1.36	0.98	0.75	1.04		
Dy	7.13		6.81	6.32	4.05	5.20		
Ho	1.28		1.50	1.14	0.72	0.98		
Er	3.71		3.16	3.01	2.58	2.24		
Tm	0.44		0.48	0.46	0.30	0.33		
Yb	1.94		2.79	3.22	1.79	2.59		
Lu	0.43		0.40	0.35	0.25	0.33		
Hf	6.40		6.27	5.57	5.35	7.17		
Ta	2.78		4.73	3.66	2.90	4.41		
Pb	1.98		3.40	2.53	1.99	3.25		
Th	3.98		7.07	5.84	4.33	6.73		
U	0.67		1.94	1.73	1.21	1.70		
Al	31.26	32.23	32.11	31.94	31.35	32.50	32.17	32.90
CCPI	79.12	75.19	74.10	74.60	73.82	72.89	77.10	75.16

Full dataset of major and trace elemental compositions of glass shards from the AND-2A core, continued

Sample Model Age (Ma)	644.25-1 17.43	644.25-2 17.43	644.25-3 17.43	644.25-I 17.43	644.25-C 17.43	644.25-G 17.43	644.25-F 17.43	644.25-4 17.43
SiO <sub>2</sub>	46.40	46.17	46.03	45.88	46.20	46.39	46.27	46.45
TiO <sub>2</sub>	4.32	4.26	4.35	4.31	4.36	4.39	4.28	4.40
Al <sub>2</sub> O <sub>3</sub>	13.90	14.10	13.57	14.05	13.67	13.87	14.03	14.02
FeO	13.19	13.48	13.25	13.26	13.13	13.25	12.93	13.25
MnO	0.23	0.24	0.22	0.23	0.24	0.27	0.19	0.22
MgO	5.04	5.05	4.86	4.84	4.82	4.95	5.07	4.91
CaO	9.63	9.91	9.72	9.64	9.58	10.00	9.64	9.92
Na <sub>2</sub> O	3.69	3.74	3.66	3.94	3.71	3.76	3.77	4.00
K <sub>2</sub> O	1.36	1.72	1.60	1.54	1.64	1.32	1.27	1.36
P <sub>2</sub> O <sub>5</sub>	1.24	1.37	1.27	1.24	1.42	1.34	1.35	1.34
SO <sub>2</sub>	0.03	0.05	0.03	0.08	0.06	0.07	0.05	0.01
Cl	0.08	0.07	0.07	0.07	0.07	0.07	0.09	0.07
SrO	-0.11	-0.14	-0.11	-0.13	-0.10	-0.13	-0.10	-0.11
BaO	0.09	0.12	0.20	0.16	0.10	0.17	0.20	0.14
Total	99.09	100.14	98.73	99.11	98.89	99.71	99.04	99.97
Mg-no.	40.51	40.03	39.55	39.41	39.55	39.97	41.14	39.80
ne	0.00	2.33	0.46	2.68	0.00	0.00	0.00	1.69
di	18.37	19.20	19.90	19.40	18.54	19.48	17.65	19.68
ol	4.25	5.92	4.94	5.15	5.14	5.01	4.45	4.80
Q	0.00	0.00	0.00	0.00	0.00	0.00	0.00	0.00
hy	2.14	0.00	0.00	0.00	0.04	0.14	2.01	0.00
Li								
Be								
B								
Sc								
Ti								
V								
Cr								
Co								
Ni								
Zn								
Rb								
Sr								
Y								
Zr								
Nb								
Cs								
Ba								
La								
Ce								
Pr								
Nd								
Sm								
Eu								
Gd								
Tb								
Dy								
Ho								
Er								
Tm								
Yb								
Lu								
Hf								
Ta								
Pb								
Th								
U								
Al	32.44	33.15	32.57	31.95	32.70	31.27	32.11	31.06
CCPI	78.31	77.22	77.51	76.77	77.03	78.19	78.12	77.22

Full dataset of major and trace elemental compositions of glass shards from the AND-2A core, continued

Sample Model Age (Ma)	644.25-J 17.43	644.25-5 17.43	644.25-6 17.43	649.67-A-1 17.45	649.67-A-2 17.45	649.67-C 17.45	649.67-B 17.45	649.67-D 17.45
SiO <sub>2</sub>	46.21	45.89	46.15	44.50	44.44	46.07	46.25	45.19
TiO <sub>2</sub>	4.11	4.22	4.24	4.28	4.26	3.84	3.70	3.61
Al <sub>2</sub> O <sub>3</sub>	13.95	13.95	14.10	15.16	15.26	15.63	15.40	15.70
FeO	13.31	13.28	13.04	11.52	11.50	10.71	10.60	10.13
MnO	0.21	0.19	0.19	0.21	0.25	0.14	0.12	0.13
MgO	4.76	4.99	4.88	5.31	5.33	5.82	5.74	6.07
CaO	9.34	9.70	9.78	10.85	10.71	10.59	10.74	11.22
Na <sub>2</sub> O	3.81	3.57	4.02	3.98	4.07	3.60	3.64	3.81
K <sub>2</sub> O	1.51	1.46	1.46	1.87	1.96	1.40	1.49	1.98
P <sub>2</sub> O <sub>5</sub>	1.44	1.39	1.29	0.98	0.98	0.81	0.88	1.02
SO <sub>2</sub>	0.07	0.08	0.03	-0.06	-0.02	0.00	-0.02	-0.06
Cl	0.07	0.06	0.06	0.09	0.08	0.07	0.09	0.06
SrO	-0.17	-0.13	-0.11	-0.14	-0.11	-0.09	-0.09	-0.12
BaO	0.13	0.13	0.06	0.03	0.13	-0.03	0.10	0.00
Total	98.74	98.76	99.19	98.57	98.82	98.56	98.62	98.74
Mg-no.	38.92	40.11	40.03	45.09	45.25	49.21	49.14	51.68
ne	0.00	0.00	2.67	10.00	11.05	3.31	3.84	10.02
di	16.87	17.62	19.59	24.00	23.74	20.28	21.40	23.51
ol	6.35	5.06	4.97	2.30	2.51	4.91	4.54	4.02
Q	0.00	0.00	0.00	0.00	0.00	0.00	0.00	0.00
hy	0.24	1.77	0.00	0.00	0.00	0.00	0.00	0.00
Li				5.17	10.61	2.37	5.25	5.35
Be				<0.00	7.21	4.10	5.20	<0.00
B				34.84	29.61	<8.45	109.67	45.61
Sc				35.05	34.60	30.48	28.02	30.91
Ti				24064.30	25501.60	23112.49	20076.99	20783.23
V				324.69	351.46	338.23	287.75	296.38
Cr				72.25	64.44	<6.64	109.84	107.11
Co				37.25	42.24	43.39	34.87	34.55
Ni				24.60	28.94	27.53	31.94	43.16
Zn				111.46	130.36	124.01	104.68	94.66
Rb				42.44	45.68	31.25	30.78	33.82
Sr				818.91	856.45	882.22	791.24	905.08
Y				30.30	35.28	30.78	27.64	29.29
Zr				351.72	373.18	299.67	265.50	266.88
Nb				71.16	76.77	60.48	57.42	62.61
Cs				0.43	0.33	0.21	0.32	0.40
Ba				475.17	512.76	569.57	434.38	435.17
La				62.20	71.63	56.88	54.32	55.92
Ce				112.80	122.93	106.89	106.33	105.33
Pr				12.42	14.53	12.66	13.14	13.22
Nd				51.62	62.53	59.35	56.83	47.11
Sm				10.09	11.15	12.37	11.24	10.81
Eu				3.56	3.78	4.06	3.54	3.25
Gd				8.87	7.90	8.42	8.59	7.11
Tb				1.31	1.16	1.04	1.44	1.01
Dy				6.76	6.58	7.25	5.99	5.68
Ho				1.33	1.55	1.49	1.06	1.10
Er				4.11	3.38	3.25	2.63	2.24
Tm				0.39	0.48	0.47	0.34	0.37
Yb				2.12	2.77	3.18	2.24	2.47
Lu				0.42	0.33	0.46	0.29	0.26
Hf				8.00	7.87	5.48	6.44	4.75
Ta				4.50	4.04	3.91	3.72	3.69
Pb				3.01	2.54	3.05	2.39	1.89
Th				7.03	7.21	4.72	5.49	5.32
U				1.80	1.65	1.20	1.54	1.35
Al	32.28	32.71	31.48	32.62	33.04	33.72	33.46	34.88
CCPI	77.28	78.43	76.57	74.23	73.60	76.80	76.15	73.67

Full dataset of major and trace elemental compositions of glass shards from the AND-2A core, continued

Sample Model Age (Ma)	649.67-E 17.45	649.67-F 17.45	649.67-1 17.45	649.67-G 17.45	649.67-2 17.45	649.67-H 17.45	649.67-L 17.45	649.67-J 17.45
SiO <sub>2</sub>	45.06	47.29	47.28	45.52	45.64	46.80	46.43	46.39
TiO <sub>2</sub>	4.64	3.56	2.72	3.73	3.92	3.18	3.23	4.52
Al <sub>2</sub> O <sub>3</sub>	14.16	16.76	13.99	16.21	15.06	14.00	13.85	14.12
FeO	12.45	10.50	9.31	9.77	11.31	10.01	10.42	12.37
MnO	0.26	0.18	0.16	0.18	0.21	0.11	0.23	0.18
MgO	5.36	4.28	7.65	6.24	5.80	6.73	7.04	4.62
CaO	10.42	7.98	14.09	11.47	10.77	12.62	13.09	9.55
Na <sub>2</sub> O	3.73	4.56	3.21	3.89	3.71	3.03	3.10	3.95
K <sub>2</sub> O	1.51	2.57	1.09	1.59	1.56	1.45	1.22	2.11
P <sub>2</sub> O <sub>5</sub>	1.27	1.11	0.54	0.84	0.99	0.61	0.62	1.06
SO <sub>2</sub>	-0.03	-0.01	0.03	-0.02	0.03	-0.02	-0.01	0.00
Cl	0.07	0.12	0.06	0.06	0.09	0.05	0.06	0.09
SrO	-0.13	-0.04	-0.13	-0.13	-0.14	-0.12	-0.14	-0.12
BaO	0.14	0.06	0.00	0.05	0.05	0.00	0.00	0.04
Total	98.91	98.93	100.00	99.38	98.99	98.44	99.15	98.86
Mg-no.	43.41	42.11	59.42	53.24	47.77	54.53	54.66	39.99
ne	3.52	6.97	7.65	9.60	5.45	4.22	5.66	4.12
di	21.33	11.90	36.57	23.55	22.11	31.28	32.90	21.21
ol	3.69	5.29	3.62	4.12	4.72	3.60	4.01	2.28
Q	0.00	0.00	0.00	0.00	0.00	0.00	0.00	0.00
hy	0.00	0.00	0.00	0.00	0.00	0.00	0.00	0.00
Li	8.20	5.39	6.19	4.12	11.49	3.26	6.06	5.20
Be	1.44	1.31	<4.22	<1.39	15.09	<1.94	6.14	2.25
B	108.17	57.10	48.91	70.39	19.72	29.36	<9.47	28.23
Sc	31.12	13.72	38.85	32.63	31.28	30.85	31.55	22.05
Ti	23491.88	19446.13	16159.97	21212.89	22416.94	16866.56	17680.67	22346.25
V	318.20	164.77	288.55	299.05	326.78	274.30	308.84	281.13
Cr	45.39	<2.52	184.23	115.76	56.48	132.39	164.32	15.89
Co	32.91	24.06	44.65	34.56	31.38	37.15	35.88	28.83
Ni	29.48	4.86	117.80	46.92	26.99	72.58	66.72	13.97
Zn	122.70	80.03	100.72	89.68	141.24	106.52	113.30	106.42
Rb	33.21	43.27	25.26	32.82	27.19	24.10	25.20	48.73
Sr	751.39	1110.45	648.50	867.45	780.87	677.20	611.04	836.79
Y	58.98	30.63	23.79	26.90	29.54	21.37	25.61	27.09
Zr	275.34	338.14	200.11	250.34	289.13	219.13	243.63	293.27
Nb	58.11	85.21	49.50	57.24	62.77	45.49	49.69	60.95
Cs	0.44	0.45	0.43	0.33	0.40	0.20	0.30	0.33
Ba	718.85	626.22	327.98	462.49	434.70	307.34	287.01	520.89
La	87.84	67.42	40.15	50.84	57.85	42.66	40.26	59.60
Ce	194.82	130.01	73.94	94.19	115.18	84.06	81.17	111.36
Pr	23.25	15.03	8.98	11.20	13.38	9.95	10.39	13.57
Nd	101.74	62.92	40.91	46.58	64.25	41.08	43.06	55.07
Sm	20.55	12.43	7.77	9.64	11.97	8.01	10.45	9.43
Eu	5.99	3.37	3.31	3.48	3.85	2.46	3.57	3.54
Gd	16.94	8.80	5.14	7.50	10.12	6.54	6.22	7.93
Tb	2.69	1.27	0.73	1.33	1.28	1.01	1.06	0.97
Dy	13.63	6.59	6.33	5.35	7.14	4.81	5.69	5.79
Ho	2.33	1.28	1.29	0.96	1.27	0.93	1.27	0.99
Er	5.91	3.19	2.28	2.76	2.47	2.74	2.44	2.70
Tm	0.63	0.41	0.42	0.28	0.46	0.39	0.33	0.38
Yb	4.47	2.95	2.06	1.62	2.63	1.87	2.49	2.83
Lu	0.61	0.34	0.21	0.31	0.43	0.24	0.24	0.33
Hf	6.52	6.35	3.36	7.20	7.26	5.85	5.30	6.26
Ta	3.63	4.95	2.93	3.34	3.51	2.58	2.41	3.29
Pb	6.03	3.19	2.59	2.50	2.54	2.06	1.65	4.15
Th	22.10	6.41	4.01	4.89	4.71	3.62	4.28	5.30
U	2.16	1.69	1.40	1.29	1.27	0.96	0.95	1.41
Al	32.65	35.34	33.56	33.76	33.68	34.34	33.79	33.27
CCPI	77.26	67.44	79.79	74.48	76.47	78.90	80.14	73.74

Full dataset of major and trace elemental compositions of glass shards from the AND-2A core, continued

Sample Model Age (Ma)	650.67-A 17.46	650.67-A2 17.46	650.67-D 17.46	650.67-C 17.46	650.67-B 17.46	650.67-G 17.46	650.67-O 17.46	650.67-M 17.46
SiO <sub>2</sub>	45.70	45.70	44.55	45.28	45.65	45.77	47.69	47.11
TiO <sub>2</sub>	3.59	3.59	3.74	3.81	4.55	3.74	3.43	3.17
Al <sub>2</sub> O <sub>3</sub>	16.02	16.02	14.80	14.66	14.64	16.54	13.54	13.96
FeO	9.92	9.92	11.37	10.20	12.56	9.91	8.98	9.84
MnO	0.14	0.14	0.26	0.16	0.20	0.17	0.14	0.17
MgO	6.09	6.09	5.27	6.51	4.99	5.20	8.24	6.96
CaO	11.10	11.10	11.43	11.99	9.14	9.83	14.40	12.66
Na <sub>2</sub> O	3.87	3.87	4.20	3.70	3.71	4.21	2.57	3.35
K <sub>2</sub> O	1.79	1.79	1.73	1.86	1.86	2.26	1.27	1.33
P <sub>2</sub> O <sub>5</sub>	0.96	0.96	0.93	0.87	1.05	1.13	0.65	0.64
SO <sub>2</sub>	-0.05	-0.05	-0.02	-0.01	-0.01	-0.04	-0.04	-0.04
Cl	0.07	0.07	0.11	0.06	0.11	0.08	0.03	0.06
SrO	-0.16	-0.16	-0.14	-0.14	-0.10	-0.13	-0.15	-0.14
BaO	0.08	0.08	0.00	0.01	0.10	0.16	0.05	-0.02
Total	99.12	99.12	98.24	98.95	98.45	98.85	100.79	99.06
Mg-no.	52.25	52.25	45.26	53.24	41.47	48.34	62.09	55.79
ne	8.81	8.81	12.92	10.59	1.94	9.53	3.27	5.72
di	22.36	22.36	27.94	28.97	17.04	17.67	36.21	31.90
ol	4.31	4.31	2.08	2.76	4.89	4.26	3.37	3.59
Q	0.00	0.00	0.00	0.00	0.00	0.00	0.00	0.00
hy	0.00	0.00	0.00	0.00	0.00	0.00	0.00	0.00
Li	6.14	<1.26	<0.00	5.90	6.81	7.52	2.28	3.61
Be	<6.25	<0.00	<0.00	<0.00	<4.94	<0.00	<0.00	7.13
B	<7.89	13.84	15.54	29.90	14.95	10.23	<10.33	26.79
Sc	29.70	29.75	25.56	33.30	23.44	20.63	37.64	28.43
Ti	18563.75	20226.04	22354.77	19723.40	23241.04	18419.12	21110.29	18301.33
V	267.94	297.14	344.39	316.83	325.01	225.54	342.80	302.61
Cr	137.65	82.50	23.36	101.04	20.24	66.87	83.18	69.20
Co	27.78	34.09	42.95	34.33	36.04	28.22	46.12	40.52
Ni	46.44	51.04	24.10	43.44	17.99	19.84	96.46	67.51
Zn	88.09	99.35	114.43	78.44	112.85	72.03	98.89	100.57
Rb	28.62	32.77	40.15	37.23	32.95	40.59	31.40	30.14
Sr	1005.78	914.48	757.71	745.47	635.31	856.28	865.00	729.62
Y	25.87	29.35	31.91	29.17	32.33	25.86	29.13	24.40
Zr	228.04	266.68	260.97	252.07	339.91	302.86	305.88	260.60
Nb	63.69	64.57	76.82	58.21	67.90	68.01	58.53	54.82
Cs	0.25	0.30	0.29	0.49	0.37	0.26	0.38	0.39
Ba	406.70	425.73	493.44	459.51	406.97	467.86	393.30	327.23
La	53.92	55.75	57.50	50.92	63.05	55.33	56.11	45.80
Ce	100.03	109.56	110.65	92.79	113.70	109.94	100.54	90.43
Pr	11.46	13.03	12.21	10.78	15.42	12.72	12.39	11.19
Nd	45.09	55.12	55.79	50.09	62.85	55.23	50.02	50.80
Sm	9.28	9.71	8.56	7.28	15.86	7.34	9.96	10.79
Eu	2.83	2.91	3.93	2.93	3.72	2.40	3.78	3.02
Gd	6.89	9.13	10.48	8.99	8.63	5.83	9.04	5.46
Tb	0.41	1.22	1.31	1.28	1.41	1.05	1.62	0.90
Dy	5.12	6.09	5.87	8.11	7.52	4.87	5.46	4.66
Ho	0.90	1.18	1.65	1.28	1.25	0.66	0.84	1.06
Er	3.13	1.12	2.74	2.42	4.08	2.96	3.22	2.89
Tm	0.26	0.38	0.57	0.33	0.39	0.34	0.20	0.35
Yb	2.55	2.48	2.83	3.01	3.87	2.73	2.97	2.06
Lu	0.21	0.41	0.42	0.41	0.49	0.18	0.20	0.51
Hf	4.84	5.92	5.84	4.63	6.03	9.29	7.83	6.29
Ta	3.17	3.43	4.40	3.22	4.45	3.93	3.06	3.26
Pb	2.58	3.21	2.48	3.02	2.50	2.43	1.77	2.49
Th	4.70	5.41	6.16	4.85	5.18	4.78	5.26	4.91
U	1.16	1.48	1.45	1.84	1.36	1.62	1.62	1.33
Al	34.49	34.49	30.93	34.80	34.76	34.70	35.92	34.11
CCPI	73.87	73.87	73.71	75.05	75.92	70.00	81.76	78.21

Full dataset of major and trace elemental compositions of glass shards from the AND-2A core, continued

Sample Model Age (Ma)	650.67-P 17.46	650.67-Q 17.46	650.67-K 17.46	650.67-J 17.46	650.67-E 17.46	650.67-I 17.46	650.67-1 17.46	654.85-A 17.48
SiO <sub>2</sub>	45.41	46.19	45.40	47.11	45.67	48.73	45.41	45.13
TiO <sub>2</sub>	3.59	3.34	4.33	3.33	3.59	3.71	3.99	3.88
Al <sub>2</sub> O <sub>3</sub>	15.67	16.60	13.53	14.19	15.39	14.78	15.18	15.30
FeO	11.28	9.51	14.22	10.32	10.35	11.50	11.35	10.74
MnO	0.17	0.16	0.21	0.16	0.24	0.23	0.21	0.18
MgO	6.75	5.98	5.01	6.27	6.44	4.41	5.48	5.67
CaO	11.47	11.15	10.56	12.19	11.80	8.50	9.95	11.26
Na <sub>2</sub> O	3.17	4.10	3.46	3.23	3.34	4.18	3.96	3.94
K <sub>2</sub> O	1.05	1.91	1.31	1.49	1.39	2.02	1.77	1.87
P <sub>2</sub> O <sub>5</sub>	0.70	0.83	0.72	0.71	0.98	1.57	1.28	0.94
SO <sub>2</sub>	-0.01	-0.01	0.09	-0.02	-0.01	0.02	-0.06	-0.01
Cl	0.06	0.10	0.06	0.06	0.06	0.07	0.08	0.13
SrO	-0.15	-0.14	-0.12	-0.12	-0.08	-0.05	-0.14	-0.16
BaO	0.15	0.08	-0.02	-0.03	0.07	0.19	-0.01	0.05
Total	99.31	99.80	98.75	98.89	99.23	99.86	98.44	98.92
Mg-no.	51.61	52.87	38.60	52.01	52.59	40.63	46.24	48.52
ne	3.31	11.00	2.80	3.79	4.88	0.00	5.63	10.37
di	21.81	22.87	24.98	29.26	23.70	13.20	18.43	25.32
ol	7.57	3.94	4.56	3.35	5.18	3.54	5.35	2.60
Q	0.00	0.00	0.00	0.00	0.00	0.00	0.00	0.00
hy	0.00	0.00	0.00	0.00	0.00	3.18	0.00	0.00
Li	4.64	4.97	9.23				3.22	5.97
Be	4.93	<9.56	<6.03				11.11	<0.00
B	11.00	25.56	<8.78				19.60	14.20
Sc	29.16	30.97	37.53				23.93	31.23
Ti	18162.64	18562.32	25593.13				18857.89	22818.16
V	277.43	263.54	384.92				240.87	299.92
Cr	93.95	84.75	<6.66				44.05	73.95
Co	37.08	34.49	48.81				27.93	33.54
Ni	38.86	43.94	3.98				19.79	38.43
Zn	94.37	98.57	180.11				87.88	128.44
Rb	17.82	40.92	23.37				30.31	37.24
Sr	659.68	846.83	670.56				729.92	812.61
Y	22.86	27.38	27.69				26.71	22.43
Zr	209.76	296.93	245.19				241.99	303.05
Nb	43.40	64.24	42.49				52.19	67.70
Cs	0.34	0.43	0.35				0.06	0.28
Ba	252.48	437.37	671.76				439.96	405.01
La	35.11	53.20	43.01				51.21	55.85
Ce	70.86	100.93	80.01				102.81	103.36
Pr	9.11	11.97	10.39				12.27	11.79
Nd	38.84	50.55	43.88				54.22	40.98
Sm	8.24	11.71	10.65				9.18	10.63
Eu	2.17	3.17	3.48				3.92	3.14
Gd	5.29	7.13	8.25				8.14	9.29
Tb	0.81	1.07	0.99				1.19	1.17
Dy	4.88	6.14	6.96				4.44	6.98
Ho	0.66	0.94	1.48				0.81	1.21
Er	2.90	3.84	3.64				2.46	3.22
Tm	0.28	0.26	0.50				0.40	0.61
Yb	2.58	2.10	1.17				2.85	0.69
Lu	0.24	0.20	0.46				0.38	0.54
Hf	4.74	9.08	5.96				4.08	5.76
Ta	2.15	3.72	2.83				3.27	3.85
Pb	1.65	2.76	3.59				1.29	3.12
Th	3.13	5.33	3.59				3.95	5.99
U	1.12	1.82	1.00				0.78	1.62
Al	34.76	34.09	31.08	33.48	34.08	33.65	34.27	33.16
CCPI	81.02	72.07	80.10	77.83	78.01	71.98	74.61	73.85

Full dataset of major and trace elemental compositions of glass shards from the AND-2A core, continued

Sample Model Age (Ma)	654.85-A2 17.48	654.85-Q 17.48	654.85-G 17.48	654.85-B 17.48	654.85-H 17.48	654.85-J 17.48	654.85-I 17.48	654.85-K 17.48
SiO <sub>2</sub>	45.13	45.27	46.63	46.84	46.57	48.23	45.70	45.61
TiO <sub>2</sub>	3.88	4.47	3.26	3.13	3.71	3.92	3.46	4.12
Al <sub>2</sub> O <sub>3</sub>	15.30	14.38	14.27	13.71	16.24	15.22	15.08	14.99
FeO	10.74	12.14	10.26	10.13	10.92	11.36	10.13	11.75
MnO	0.18	0.16	0.15	0.18	0.20	0.21	0.21	0.22
MgO	5.67	5.56	6.75	6.93	4.51	4.43	5.78	5.81
CaO	11.26	10.73	13.12	13.18	8.12	8.96	11.82	10.71
Na <sub>2</sub> O	3.94	3.78	3.14	3.00	4.59	4.04	3.55	3.59
K <sub>2</sub> O	1.87	1.76	1.42	1.37	2.71	2.07	1.55	1.54
P <sub>2</sub> O <sub>5</sub>	0.94	1.15	0.65	0.57	1.67	1.29	0.72	1.01
SO <sub>2</sub>	-0.01	-0.01	-0.02	0.03	-0.05	0.02	0.06	0.01
Cl	0.13	0.08	0.06	0.05	0.14	0.07	0.09	0.07
SrO	-0.16	-0.15	-0.17	-0.15	-0.15	-0.14	-0.19	-0.18
BaO	0.05	0.05	0.02	-0.03	0.01	0.13	0.13	0.15
Total	98.92	99.36	99.55	98.93	99.18	99.80	98.09	99.39
Mg-no.	48.52	44.94	53.99	54.96	42.39	41.02	50.45	46.87
ne	10.37	6.10	6.30	5.16	7.57	0.47	7.31	4.32
di	25.32	23.30	32.40	33.89	11.04	15.19	27.32	21.41
ol	2.60	3.22	3.17	3.31	6.16	4.45	2.65	5.01
Q	0.00	0.00	0.00	0.00	0.00	0.00	0.00	0.00
hy	0.00	0.00	0.00	0.00	0.00	0.00	0.00	0.00
Li	11.16	4.26	6.17	2.90	6.29	7.30	5.60	3.52
Be	<0.00	<2.00	<0.00	4.32	<0.00	3.54	6.60	<3.45
B	19.12	16.31	33.06	5.50	<4.49	45.22	13.86	11.72
Sc	33.64	29.62	28.85	35.23	16.63	16.85	28.16	24.82
Ti	22317.60	27014.93	16036.27	18448.37	21793.16	20583.63	21269.34	22794.54
V	305.70	380.87	259.35	309.48	198.94	231.06	296.86	296.70
Cr	72.29	85.89	137.31	213.60	<4.06	<3.67	27.70	99.17
Co	42.68	40.73	37.93	40.06	27.77	24.04	37.74	35.74
Ni	37.88	28.85	72.36	62.91	6.92	6.02	33.29	33.93
Zn	95.31	110.86	71.29	96.14	95.08	137.33	113.27	115.20
Rb	37.77	31.99	36.72	21.82	52.68	36.18	32.11	27.54
Sr	858.55	794.16	602.34	648.91	927.68	802.53	705.72	820.80
Y	28.60	35.73	23.65	24.21	38.02	39.07	29.18	25.75
Zr	317.59	343.39	264.47	241.26	369.38	367.04	291.19	267.80
Nb	67.25	75.18	44.33	47.33	105.52	77.08	57.71	64.78
Cs	0.28	0.25	0.53	0.40	0.71	0.26	0.37	0.30
Ba	437.01	410.87	339.92	296.76	696.05	436.12	357.25	348.27
La	55.32	63.20	37.26	39.49	84.39	67.71	49.73	50.85
Ce	106.10	125.36	71.09	81.59	160.04	152.46	91.45	96.81
Pr	13.65	15.02	8.92	10.92	16.55	17.83	10.93	12.61
Nd	51.97	63.85	39.53	44.58	73.79	74.26	50.86	53.17
Sm	10.55	11.96	8.61	9.02	11.30	13.82	7.91	8.37
Eu	3.36	4.39	2.25	2.83	4.16	4.22	3.76	4.49
Gd	6.09	10.31	6.81	6.67	9.47	10.87	5.85	7.22
Tb	1.29	1.26	0.85	1.00	1.23	1.57	0.98	1.30
Dy	5.90	7.65	4.39	3.62	6.38	8.91	5.38	7.80
Ho	0.92	1.31	1.03	0.99	1.42	1.75	1.21	0.99
Er	1.88	3.04	2.29	2.97	3.55	3.17	2.21	2.20
Tm	0.21	0.54	0.25	0.50	0.66	0.40	0.58	0.29
Yb	2.56	2.92	2.04	2.25	3.92	2.58	3.89	1.94
Lu	0.34	0.27	0.32	0.25	0.37	0.47	0.41	0.39
Hf	6.70	8.52	5.29	4.72	9.67	9.22	6.39	4.47
Ta	4.29	3.87	2.52	3.03	5.30	4.49	3.84	3.20
Pb	2.49	2.60		1.61	3.25	3.73	2.22	2.53
Th	6.38	5.03	3.96	4.11	7.89	7.39	5.15	3.64
U	1.43	1.78	1.00	1.10	2.29	1.94	1.24	1.14
Al	33.16	33.52	33.44	33.91	36.23	33.32	32.29	33.93
CCPI	73.85	76.17	78.85	79.61	67.87	72.10	75.72	77.39

Full dataset of major and trace elemental compositions of glass shards from the AND-2A core, continued

Sample Model Age (Ma)	654.85-L 17.48	654.85-C 17.48	<b>654.85-D 17.48</b>	654.85-P 17.48	654.85-F 17.48	661.67-D 17.52	661.67-E 17.52	661.67-F 17.52
SiO <sub>2</sub>	49.89	46.63	<b>64.53</b>	46.57	47.64	45.99	46.74	44.97
TiO <sub>2</sub>	3.61	4.14	<b>0.56</b>	3.44	3.79	4.01	3.54	3.72
Al <sub>2</sub> O <sub>3</sub>	14.79	15.00	<b>13.32</b>	14.54	14.81	14.83	15.42	15.20
FeO	11.67	11.79	<b>6.58</b>	10.30	11.85	11.21	10.25	10.76
MnO	0.19	0.20	<b>0.26</b>	0.18	0.24	0.15	0.22	0.16
MgO	3.98	4.87	<b>0.07</b>	6.21	4.42	5.74	5.96	6.60
CaO	8.33	8.62	<b>1.40</b>	12.33	9.03	10.96	11.09	11.50
Na <sub>2</sub> O	3.97	3.69	<b>0.11</b>	2.98	4.03	4.01	3.61	3.36
K <sub>2</sub> O	2.33	2.06	<b>1.73</b>	1.53	2.25	1.72	1.98	1.27
P <sub>2</sub> O <sub>5</sub>	1.25	0.99	<b>0.05</b>	0.70	1.33	1.00	0.99	0.94
SO <sub>2</sub>	0.04	0.02	<b>0.00</b>	0.02	0.08	0.00	-0.01	0.02
Cl	0.09	0.09	<b>0.13</b>	0.04	0.09	0.22	0.07	0.08
SrO	-0.12	-0.18	<b>-0.17</b>	-0.18	-0.16	-0.15	-0.16	-0.19
BaO	0.08	0.05	<b>-0.06</b>	0.08	-0.06	-0.01	0.07	0.11
Total	100.10	97.99	<b>88.52</b>	98.69	99.34	99.68	99.75	98.50
Mg-no.	37.83	42.43	<b>1.76</b>	51.82	39.94	47.71	50.91	52.25
ne	0.00	0.54	<b>0.00</b>	3.14	2.46	7.97	6.07	5.00
di	14.18	14.91	<b>0.00</b>	28.42	16.63	24.55	22.91	23.06
ol	0.07	5.62	<b>0.00</b>	3.25	4.92	3.17	4.36	5.93
Q	0.00	0.00	<b>56.74</b>	0.00	0.00	0.00	0.00	0.00
hy	6.66	0.00	<b>6.79</b>	0.00	0.00	0.00	0.00	0.00
Li	9.37	22.94		8.63	9.10	7.79	10.07	1.22
Be	<0.00	<4.29		<0.00	<0.00	<0.00	<0.00	<2.84
B	<4.70	<5.65		28.53	12.03	<3.40	7.37	26.91
Sc	16.45	15.39		33.97	22.20	28.72	25.58	30.89
Ti	18696.52	22532.56		18278.23	20595.25	23754.71	21033.42	20844.08
V	201.32	255.74		296.42	220.95	328.27	280.90	296.64
Cr	<5.10	6.29		72.50	<4.29	73.07	97.76	145.61
Co	26.37	28.75		36.19	24.42	40.30	31.95	32.84
Ni	0.58	9.33		43.96	7.65	29.34	35.20	53.42
Zn	121.01	168.32		128.35	126.25	104.72	121.91	105.12
Rb	44.87	30.04		30.20	33.41	32.91	28.58	21.34
Sr	650.68	721.17		722.49	714.65	858.67	838.57	799.71
Y	38.70	36.17		26.71	44.13	27.69	29.37	25.07
Zr	373.98	381.20		276.81	382.61	306.79	287.09	235.30
Nb	69.52	80.12		53.78	66.54	71.27	63.29	48.91
Cs	0.54	0.19		0.34	0.43	0.37	0.24	0.11
Ba	528.58	478.40		323.65	500.64	459.99	441.35	322.93
La	67.08	64.26		46.94	69.75	61.78	56.27	43.97
Ce	134.94	117.08		89.31	132.66	122.57	103.27	84.21
Pr	15.67	14.52		10.82	16.63	15.49	12.19	11.09
Nd	71.07	69.72		46.11	71.29	56.26	47.53	49.02
Sm	12.15	10.90		10.12	14.37	10.78	11.04	7.27
Eu	4.05	4.25		2.18	4.15	4.42	4.64	2.98
Gd	12.83	10.69		5.55	9.19	8.99	10.03	9.15
Tb	2.33	1.92		1.13	1.58	1.11	1.27	1.40
Dy	8.39	8.25		5.76	9.74	6.42	7.01	4.91
Ho	1.84	1.90		1.17	1.68	1.46	1.38	0.77
Er	5.07	<b>4.73</b>		2.62	4.65	3.53	<b>2.34</b>	2.19
Tm	<b>0.71</b>	0.23		0.38	<b>0.61</b>	0.48	<b>0.35</b>	<b>0.36</b>
Yb	<b>4.31</b>	0.92		2.52	<b>3.41</b>	1.52	<b>1.11</b>	<b>1.80</b>
Lu	<b>0.61</b>	<b>0.65</b>		0.38	<b>0.56</b>	0.51	<b>0.18</b>	<b>0.46</b>
Hf	9.02	11.23		8.78	9.19	8.18	8.24	4.61
Ta	3.92	5.38		2.94	4.96	4.07	3.99	3.27
Pb	3.42	2.93			3.09	2.98	2.65	1.71
Th	7.30	6.40		4.67	5.40	4.87	4.80	4.02
U	1.63	1.71		1.40	1.53	1.40	1.52	1.02
Al	33.93	36.03	54.23	33.58	33.80	33.25	35.06	34.64
CCPI	71.31	74.33	78.30	78.54	72.16	74.75	74.36	78.94

Full dataset of major and trace elemental compositions of glass shards from the AND-2A core, continued

Sample Model Age (Ma)	661.67-G 17.52	661.67-H 17.52	661.67-N 17.52	661.67-M 17.52	661.67-L 17.52	661.67-J 17.52	661.67-I 17.52	661.67-P 17.52
SiO <sub>2</sub>	48.18	44.33	49.61	51.36	45.70	45.89	46.71	46.41
TiO <sub>2</sub>	3.31	4.67	3.48	2.90	3.94	3.71	3.16	3.75
Al <sub>2</sub> O <sub>3</sub>	16.94	15.73	14.65	15.82	14.97	15.29	13.75	14.92
FeO	10.14	11.21	11.12	10.10	11.07	10.49	10.20	10.73
MnO	0.22	0.21	0.21	0.22	0.17	0.16	0.14	0.19
MgO	4.09	5.33	4.03	3.39	5.89	5.90	8.11	5.89
CaO	8.07	11.02	8.09	7.17	10.73	11.00	12.22	11.07
Na <sub>2</sub> O	4.36	4.05	3.71	4.03	3.59	3.69	3.01	3.60
K <sub>2</sub> O	2.85	1.95	2.58	2.51	1.59	1.64	1.08	1.45
P <sub>2</sub> O <sub>5</sub>	1.44	1.18	1.55	1.05	1.04	0.90	0.59	0.98
SO <sub>2</sub>	-0.01	-0.02	0.02	-0.01	0.00	-0.04	-0.03	0.02
Cl	0.15	0.11	0.08	0.12	0.06	0.06	0.07	0.07
SrO	-0.11	-0.16	-0.14	-0.15	-0.16	-0.16	-0.16	-0.17
BaO	0.10	0.18	0.12	0.04	0.09	0.04	0.03	0.13
Total	99.73	99.78	99.12	98.54	98.67	98.56	98.87	99.02
Mg-no.	41.81	45.88	39.25	37.47	48.69	50.07	58.63	49.46
ne	4.79	11.12	0.00	0.00	4.27	6.09	2.94	3.59
di	9.98	22.61	11.74	9.00	21.56	23.05	29.04	22.95
ol	5.83	2.65	0.00	0.00	4.76	4.11	7.49	4.34
Q	0.00	0.00	0.97	1.71	0.00	0.00	0.00	0.00
hy	0.00	0.00	7.89	7.91	0.00	0.00	0.00	0.00
Li	6.15	8.99	7.14	9.74	2.79	11.20	1.44	6.64
Be	<0.00	13.32	12.39	<0.00	7.79	<0.00	<2.40	<2.71
B	<3.64	75.80	42.10	11.23	42.28	27.60	19.00	20.64
Sc	12.33	28.70	16.63	14.49	26.65	32.12	25.39	29.97
Ti	18610.61	25986.96	19919.89	16150.91	21479.32	20998.65	17225.54	22890.76
V	166.83	316.09	208.28	140.15	302.67	337.45	267.34	314.57
Cr	5.56	36.54	<3.31	<3.65	76.45	119.82	236.10	93.35
Co	18.33	36.06	23.26	13.99	39.26	33.72	40.08	34.14
Ni	5.56	24.60	2.82	<0.36	29.17	48.79	82.99	37.52
Zn	84.92	116.23	128.56	128.19	120.73	139.72	81.16	116.56
Rb	59.19	42.14	45.15	44.58	27.67	27.83	18.14	33.60
Sr	1015.06	888.80	730.76	759.42	743.07	857.38	649.01	826.37
Y	34.98	30.12	42.37	41.47	26.77	27.08	23.06	28.33
Zr	401.91	257.21	407.83	457.30	269.11	306.93	220.47	294.15
Nb	112.58	71.27	83.35	97.82	59.49	67.11	41.83	68.74
Cs	0.52	0.42	0.50	0.34	0.28	0.25	0.28	0.37
Ba	730.97	558.48	494.38	538.67	406.07	435.97	262.23	477.70
La	93.91	62.15	74.65	77.90	52.23	55.06	36.56	58.73
Ce	178.14	114.24	151.97	152.39	102.80	105.31	72.25	115.51
Pr	20.00	13.77	17.21	17.43	12.56	13.58	9.56	14.85
Nd	76.36	54.48	76.60	69.26	54.75	52.56	41.13	53.78
Sm	11.01	10.74	17.05	15.09	10.40	10.72	10.14	12.74
Eu	3.51	3.04	4.61	3.69	3.38	3.43	3.28	4.21
Gd	10.09	6.92	11.39	11.97	8.13	7.79	5.99	8.64
Tb	1.32	1.50	1.42	1.63	1.13	1.50	0.94	1.50
Dy	6.71	5.10	8.81	8.16	5.37	6.36	4.63	7.41
Ho	1.41	1.41	1.86	1.60	0.89	1.22	1.26	1.17
Er	3.67	1.66	4.15	5.12	3.61	2.52	2.30	2.96
Tm	0.36	0.38	0.64	0.69	0.41	0.31	0.17	0.64
Yb	3.08	1.42	2.47	2.75	3.77	2.31	2.25	2.88
Lu	0.27	0.32	0.50	0.80	0.25	0.83	0.27	0.27
Hf	8.40	4.38	9.79	9.79	5.01	6.69	3.50	9.49
Ta	5.88	3.88	5.02	6.25	3.09	4.37	2.41	4.38
Pb	3.93	3.90	4.14	2.90	2.80	3.54	1.43	3.42
Th	7.83	4.90	7.61	8.51	4.77	5.62	3.82	5.86
U	1.95	1.39	2.01	2.29	1.50	1.48	0.95	1.52
Al	35.83	32.57	35.93	34.52	34.32	33.92	37.63	33.34
CCPI	66.36	73.37	70.66	67.39	76.58	75.48	81.75	76.73

Full dataset of major and trace elemental compositions of glass shards from the AND-2A core, continued

Sample Model Age (Ma)	661.67-A 17.52	661.67-B 17.52	721.67-H 18.19	721.67-I 18.19	721.67-A 18.19	721.67-B 18.19	721.67-C 18.19	721.67-C2 18.19
SiO <sub>2</sub>	46.18	<b>50.12</b>	<b>6.91</b>	45.27	46.59	44.59	46.43	46.43
TiO <sub>2</sub>	3.95	<b>1.16</b>	<b>1.06</b>	3.22	3.26	4.37	3.79	3.79
Al <sub>2</sub> O <sub>3</sub>	15.10	<b>25.21</b>	<b>2.06</b>	13.33	16.86	14.93	15.54	15.54
FeO	10.66	<b>3.93</b>	<b>15.88</b>	9.40	8.76	12.08	11.46	11.46
MnO	0.17	<b>0.11</b>	<b>16.70</b>	0.26	0.17	0.18	0.20	0.20
MgO	5.54	<b>1.96</b>	<b>11.04</b>	7.35	5.95	5.54	4.99	4.99
CaO	10.50	<b>13.65</b>	<b>8.18</b>	13.94	13.40	10.43	9.43	9.43
Na <sub>2</sub> O	3.80	<b>3.42</b>	<b>0.46</b>	3.41	3.63	3.60	3.82	3.82
K <sub>2</sub> O	1.64	<b>0.61</b>	<b>0.21</b>	1.83	1.26	1.59	1.66	1.66
P <sub>2</sub> O <sub>5</sub>	0.96	<b>0.30</b>	<b>0.14</b>	0.83	0.78	1.10	1.40	1.40
SO <sub>2</sub>	0.00	<b>-0.01</b>	<b>-0.01</b>	-0.01	-0.04	0.00	0.04	0.04
Cl	0.09	<b>0.02</b>	<b>0.06</b>	0.08	0.06	0.06	0.08	0.08
SrO	-0.15	<b>-0.10</b>	<b>-0.42</b>	-0.17	-0.12	-0.18	-0.15	-0.15
BaO	0.02	<b>-0.01</b>	<b>0.01</b>	0.00	0.05	0.04	0.14	0.14
Total	98.45	<b>100.36</b>	<b>62.28</b>	98.74	100.60	98.33	98.83	98.83
Mg-no.	48.09	<b>47.04</b>	<b>55.35</b>	58.25	54.77	44.98	43.71	43.71
ne	4.62	<b>0.53</b>	<b>4.16</b>	13.34	8.87	4.79	0.98	0.98
di	21.64	<b>10.67</b>	<b>0.00</b>	38.79	28.06	20.34	14.11	14.11
ol	3.59	<b>0.00</b>	<b>2.42</b>	1.26	1.69	4.66	6.59	6.59
Q	0.00	<b>0.00</b>	<b>0.00</b>	0.00	0.00	0.00	0.00	0.00
hy	0.00	<b>0.00</b>	<b>0.00</b>	0.00	0.00	0.00	0.00	0.00
Li	7.79			4.41	<0.00	6.22	5.81	4.29
Be	<0.00			5.36	<0.00	<0.00	<0.00	8.70
B	<3.40			6.07	14.56	<2.83	<2.09	5.03
Sc	28.72			30.05	34.03	26.34	24.32	23.25
Ti	23754.71			22613.39	22937.20	23280.63	22151.65	21712.62
V	328.27			309.05	317.38	314.62	225.63	230.93
Cr	73.07			39.35	170.32	26.75	15.02	30.96
Co	40.30			39.60	37.05	36.04	32.28	26.61
Ni	29.34			19.32	57.53	24.33	18.76	13.58
Zn	104.72			100.74	125.24	114.50	118.41	132.69
Rb	32.91			57.34	33.92	31.28	32.51	32.72
Sr	858.67			1144.60	979.03	725.79	898.80	877.53
Y	27.69			31.04	29.06	27.65	43.72	39.52
Zr	306.79			341.77	288.22	282.38	334.03	342.28
Nb	71.27			106.96	72.61	61.20	72.02	69.00
Cs	0.37			0.68	0.45	0.18	0.52	0.29
Ba	459.99			806.39	435.00	431.15	1161.95	1167.65
La	61.78			87.86	56.83	52.26	71.98	70.97
Ce	122.57			151.52	108.14	102.07	144.44	136.56
Pr	15.49			16.82	14.00	12.85	16.74	18.23
Nd	56.26			65.92	46.72	55.52	72.17	73.92
Sm	10.78			13.05	12.60	9.66	14.71	15.81
Eu	4.42			3.91	3.98	4.41	5.00	4.74
Gd	8.99			8.40	8.12	9.45	11.36	10.53
Tb	1.11			1.35	1.35	1.49	1.26	1.97
Dy	6.42			7.63	7.61	7.97	8.74	10.20
Ho	1.46			1.59	<b>0.96</b>	1.10	1.12	1.53
Er	3.53			4.73	4.15	<b>1.73</b>	5.36	2.97
Tm	<b>0.48</b>			<b>0.33</b>	0.41	0.47	0.58	<b>0.54</b>
Yb	1.52			3.73	3.54	<b>1.74</b>	4.09	2.19
Lu	<b>0.51</b>			<b>0.32</b>	0.36	<b>0.36</b>	0.62	<b>0.39</b>
Hf	8.18			7.54	<b>5.13</b>	7.35	9.44	8.03
Ta	4.07			5.54	4.65	3.93	4.66	4.27
Pb	2.98				<b>13.21</b>	2.92	3.07	2.52
Th	4.87				10.19	5.18	4.02	5.54
U	1.40				2.64	1.88	1.72	1.44
Al	33.42	13.07	56.55	34.60	29.73	33.69	33.44	33.44
CCPI	74.85	59.35	97.59	76.19	75.08	77.24	75.02	75.02

Full dataset of major and trace elemental compositions of glass shards from the AND-2A core, continued

Sample	721.67-D 18.19	721.67-E 18.19	721.67-F 18.19	721.67-L 18.19	721.67-K 18.19	740.89-A 18.29	740.89-B 18.29	740.89-C 18.29
SiO <sub>2</sub>	<b>1.86</b>	48.52	45.03	44.62	43.40	<b>57.64</b>	47.20	42.37
TiO <sub>2</sub>	<b>0.00</b>	3.79	3.99	3.98	5.00	<b>0.42</b>	2.98	4.88
Al <sub>2</sub> O <sub>3</sub>	<b>0.45</b>	15.10	15.58	15.59	14.35	<b>12.77</b>	16.32	13.77
FeO	<b>26.53</b>	11.29	11.34	11.90	12.84	<b>5.96</b>	10.18	12.98
MnO	<b>1.04</b>	0.21	0.18	0.19	0.19	<b>0.08</b>	0.21	0.22
MgO	<b>20.30</b>	4.32	6.44	6.19	6.15	<b>4.02</b>	3.95	5.23
CaO	<b>6.53</b>	8.22	10.81	11.25	11.52	<b>3.27</b>	7.32	10.54
Na <sub>2</sub> O	<b>0.26</b>	3.95	3.49	3.37	3.12	<b>1.80</b>	4.43	3.45
K <sub>2</sub> O	<b>0.08</b>	2.44	1.39	1.53	1.15	<b>0.80</b>	2.40	1.45
P <sub>2</sub> O <sub>5</sub>	<b>0.07</b>	1.30	0.73	0.69	0.82	<b>0.55</b>	1.34	2.27
SO <sub>2</sub>	<b>-0.01</b>	-0.03	-0.02	0.03	0.06	<b>0.67</b>	0.04	0.14
Cl	<b>0.06</b>	0.13	0.05	0.08	0.05	<b>0.74</b>	0.09	0.05
SrO	<b>-0.53</b>	-0.16	-0.21	-0.18	-0.18	<b>-0.04</b>	-0.08	-0.06
BaO	<b>0.04</b>	0.03	-0.06	-0.01	-0.01	<b>0.05</b>	0.12	0.12
Total	<b>56.68</b>	99.10	98.76	99.22	98.47	<b>88.73</b>	96.49	97.42
Mg-no.	<b>57.71</b>	40.54	50.32	48.13	46.06	<b>54.57</b>	40.86	41.81
ne	<b>1.99</b>	0.00	5.51	7.05	4.06	<b>0.00</b>	3.20	1.87
di	<b>0.00</b>	13.07	21.19	23.05	24.76	<b>0.00</b>	8.33	16.50
ol	<b>-10.77</b>	4.31	6.22	5.68	3.85	<b>0.00</b>	7.39	5.43
Q	<b>0.00</b>	0.00	0.00	0.00	0.00	<b>32.52</b>	0.00	0.00
hy	<b>0.00</b>	1.40	0.00	0.00	0.00	<b>18.50</b>	0.00	0.00
Li	10.80	5.83		<0.44			6.39	4.98
Be	<2.86	<0.00		<0.00			4.58	20.64
B	<2.01	<2.38		3.48			19.64	20.42
Sc	19.14	26.34		26.88			6.88	23.76
Ti	20820.61	22209.65		29179.29			8027.37	26638.06
V	210.68	298.79		405.71			62.35	301.94
Cr	3.80	83.61		36.44			<4.63	8.79
Co	22.38	39.00		49.29			9.70	33.69
Ni	1.97	43.48		40.04			<0.72	3.12
Zn	142.67	103.33		104.95			43.65	133.99
Rb	48.21	25.33		21.76			39.77	24.06
Sr	680.03	775.71		824.46			438.48	1066.00
Y	44.99	26.38		24.28			19.00	39.03
Zr	491.42	266.06		235.43			241.96	263.70
Nb	102.88	55.88		45.79			41.31	58.06
Cs	0.53	0.28		0.19			0.46	0.25
Ba	623.02	319.99		262.18			408.37	554.12
La	87.67	46.48		41.48			37.18	66.95
Ce	163.07	89.12		82.51			71.75	135.96
Pr	21.20	10.03		9.54			8.39	18.27
Nd	78.50	48.39		44.03			35.51	84.15
Sm	12.61	9.21		8.88			6.14	14.66
Eu	5.03	2.77		3.22			1.77	6.98
Gd	12.25	6.40		7.81			3.99	11.47
Tb	2.21	1.02		1.11			0.70	1.71
Dy	11.67	4.99		4.83			3.55	8.97
Ho	1.60	1.08		0.97			0.70	1.56
Er	4.99	2.80		2.85			1.76	5.34
Tm	0.71	0.41		<b>0.37</b>			0.26	0.69
Yb	<b>3.10</b>	2.28		<b>2.10</b>			1.61	<b>3.37</b>
Lu	<b>0.27</b>	<b>0.30</b>		0.42			0.21	<b>0.51</b>
Hf	10.83	6.75		5.59			5.59	8.23
Ta	5.98	3.12		2.75			2.12	3.25
Pb	3.82	1.68		1.75			5.42	2.49
Th	8.49	4.23		3.63			4.09	3.50
U	1.95	1.23					1.11	1.30
Al	75.02	35.72	35.40	34.56	33.26	48.69	35.04	32.28
CCPI	99.28	70.96	78.46	78.70	81.66	79.31	67.42	78.80

Full dataset of major and trace elemental compositions of glass shards from the AND-2A core, continued

Sample Model Age (Ma)	740.89-E 18.29	740.89-F 18.29	740.89-G 18.29	740.89-H 18.29	740.89-H2 18.29	740.89-J 18.29	740.89-L 18.29	<b>740.89-S 18.29</b>
SiO <sub>2</sub>	44.50	43.56	42.79	41.54	41.54	41.59	44.50	<b>60.34</b>
TiO <sub>2</sub>	2.92	3.96	4.37	5.16	5.16	4.87	3.11	<b>0.87</b>
Al <sub>2</sub> O <sub>3</sub>	17.01	15.29	15.16	12.71	12.71	15.00	16.73	<b>12.37</b>
FeO	9.13	10.79	11.79	15.17	15.17	12.40	9.10	<b>8.86</b>
MnO	0.17	0.20	0.20	0.23	0.23	0.18	0.17	<b>0.37</b>
MgO	5.05	5.73	6.14	5.05	5.05	6.13	5.89	<b>0.23</b>
CaO	10.12	11.44	10.79	11.37	11.37	11.36	11.33	<b>1.12</b>
Na <sub>2</sub> O	4.27	3.87	3.43	3.40	3.40	2.98	3.84	<b>0.49</b>
K <sub>2</sub> O	2.05	1.48	1.39	1.10	1.10	1.24	1.65	<b>1.67</b>
P <sub>2</sub> O <sub>5</sub>	0.81	0.77	1.44	1.03	1.03	0.85	0.75	<b>0.16</b>
SO <sub>2</sub>	0.03	0.10	0.07	0.10	0.10	0.08	0.06	<b>0.03</b>
Cl	0.09	0.07	0.05	0.04	0.04	0.07	0.06	<b>0.13</b>
SrO	-0.12	-0.15	-0.09	-0.16	-0.16	-0.10	-0.12	<b>-0.10</b>
BaO	0.16	0.13	0.11	0.10	0.10	0.09	0.16	<b>0.03</b>
Total	96.18	97.21	97.62	96.83	96.83	96.75	97.24	<b>86.57</b>
Mg-no.	49.65	48.63	48.15	37.25	37.25	46.86	53.58	<b>4.38</b>
ne	13.06	11.21	5.43	7.01	7.01	6.01	11.11	<b>0.00</b>
di	19.65	26.24	18.45	28.39	28.39	22.66	22.76	<b>0.00</b>
ol	4.29	2.49	6.42	2.63	2.63	4.83	4.25	<b>0.00</b>
Q	0.00	0.00	0.00	0.00	0.00	0.00	0.00	<b>50.46</b>
hy	0.00	0.00	0.00	0.00	0.00	0.00	0.00	<b>10.75</b>
Li	13.78	3.90	6.26	5.36	5.49	1.72	3.52	
Be	3.88	<0.00	<2.07	<2.34	5.92	10.89	<3.33	
B	32.44	65.25	27.80	8.33	15.19	19.68	21.59	
Sc	22.65	31.55	22.57	32.00	38.88	25.26	26.32	
Ti	15752.67	21312.49	20865.99	26403.94	27602.63	25035.75	17247.32	
V	232.22	334.84	255.70	416.76	423.19	347.85	249.03	
Cr	90.44	80.02	88.43	47.03	39.16	69.99	95.89	
Co	32.00	33.35	34.22	43.65	45.53	40.57	31.02	
Ni	33.05	30.25	34.11	14.32	13.71	33.42	50.12	
Zn	87.22	74.86	84.29	108.84	111.09	103.56	78.90	
Rb	61.51	33.19	30.74	22.03	20.90	20.77	35.23	
Sr	770.03	697.13	821.06	571.44	584.67	793.30	787.18	
Y	26.15	28.29	24.99	27.00	30.27	20.90	25.40	
Zr	253.28	232.05	233.54	232.04	233.95	224.62	244.02	
Nb	69.57	63.13	48.06	41.57	45.56	45.19	64.42	
Cs	1.59	0.38	0.27	0.28	0.31	0.26	0.40	
Ba	560.39	377.97	533.33	325.68	328.80	252.88	420.55	
La	53.37	46.81	45.02	37.74	40.73	38.34	46.49	
Ce	103.69	90.22	90.80	75.69	78.27	76.13	90.92	
Pr	11.52	10.55	11.60	8.97	9.90	9.43	9.83	
Nd	47.25	48.22	52.22	42.38	44.43	43.19	43.08	
Sm	8.41	8.37	10.33	8.55	8.65	7.93	7.80	
Eu	3.51	3.06	3.85	3.16	3.72	3.02	2.38	
Gd	7.95	7.96	8.78	7.95	8.84	7.01	5.62	
Tb	0.91	1.19	0.90	1.08	1.25	1.32	0.86	
Dy	5.59	6.59	5.20	7.40	7.17	4.19	4.75	
Ho	1.01	1.21	0.94	1.20	1.28	0.84	0.94	
Er	2.35	2.87	2.40	2.39	2.53	1.51	3.01	
Tm	0.41	0.47	0.34	0.31	0.32	0.18	0.47	
Yb	2.18	3.40	2.62	3.14	2.72	1.51	2.07	
Lu	0.28	0.42	0.32	0.38	0.35	0.42	0.41	
Hf	6.13	4.29	4.85	5.13	5.17	5.68	6.15	
Ta	3.75	3.53	2.63	2.47	2.57	2.49	3.29	
Pb	6.61	2.50		2.04	1.79	2.30	2.76	
Th	5.79	3.91	3.47	3.65	3.81	3.49	4.70	
U	1.86	1.33	0.97	0.97	1.14	0.82	1.40	
Al	33.03	32.01	34.63	29.39	29.39	33.93	33.21	54.18
CCPI	69.16	75.54	78.82	81.82	81.82	81.46	73.21	80.82

Full dataset of major and trace elemental compositions of glass shards from the AND-2A core, continued

Sample Model Age (Ma)	740.89-U 18.29	740.89-W 18.29	740.89-Z 18.29	740.89-A1 18.29	740.89-F1 18.29	742.00-D 18.29	742.00-A 18.29	742.00-E 18.29
SiO <sub>2</sub>	45.72	41.66	42.48	45.01	42.78	43.07	45.70	42.43
TiO <sub>2</sub>	2.97	4.98	5.00	3.12	4.39	4.65	3.45	4.75
Al <sub>2</sub> O <sub>3</sub>	16.67	14.14	13.54	16.52	14.95	14.06	15.92	13.95
FeO	10.62	12.80	13.28	9.97	12.03	12.96	10.92	12.82
MnO	0.24	0.22	0.22	0.18	0.22	0.22	0.24	0.25
MgO	3.69	5.58	5.20	5.43	6.40	5.28	3.96	5.45
CaO	7.56	10.74	10.24	10.64	11.97	9.95	8.73	10.68
Na <sub>2</sub> O	5.05	3.20	3.76	4.49	3.23	4.03	4.65	3.41
K <sub>2</sub> O	3.18	1.26	1.39	1.74	1.19	1.33	2.39	1.38
P <sub>2</sub> O <sub>5</sub>	1.47	0.62	2.15	0.97	0.98	2.48	1.10	1.60
SO <sub>2</sub>	0.04	0.08	0.15	0.07	0.10	0.13	0.06	0.14
Cl	0.19	0.04	0.05	0.08	0.06	0.06	0.12	0.05
SrO	-0.06	-0.10	-0.07	-0.09	-0.09	-0.04	-0.10	-0.10
BaO	0.18	0.17	0.16	0.11	0.08	0.13	0.10	0.13
Total	97.51	95.38	97.55	98.21	98.30	98.31	97.22	96.96
Mg-no.	38.26	43.73	41.10	49.28	48.70	42.06	39.27	43.11
ne	14.22	6.08	3.35	13.31	7.27	3.14	10.60	3.94
di	11.89	24.55	17.42	21.64	24.83	13.92	17.03	20.05
ol	5.93	3.13	5.02	4.57	4.75	6.94	3.73	4.80
Q	0.00	0.00	0.00	0.00	0.00	0.00	0.00	0.00
hy	0.00	0.00	0.00	0.00	0.00	0.00	0.00	0.00
Li	5.24	6.64		4.97	2.85		6.50	3.25
Be	3.27	<0.00		<2.73	<1.99		<3.12	4.52
B	25.93	40.71		20.26	20.85		8.24	12.30
Sc	13.92	22.81		17.07	29.62		19.53	23.67
Ti	16215.19	18680.12		11093.04	19562.45		12878.93	20004.49
V	144.67	291.77		157.92	278.33		164.95	253.14
Cr	8.60	32.49		47.12	105.85		10.46	5.25
Co	19.93	32.07		20.67	35.73		17.50	26.72
Ni	6.14	21.69		21.37	40.49		12.56	7.54
Zn	81.99	64.19		52.54	75.42		73.63	117.97
Rb	78.30	36.60		25.16	20.12		54.11	18.33
Sr	1054.48	598.26		973.36	648.80		445.95	704.58
Y	30.24	19.18		17.59	20.73		23.96	25.17
Zr	431.58	220.39		155.16	189.37		259.87	190.66
Nb	131.88	34.33		46.63	38.35		61.11	38.89
Cs	0.92	0.44		0.24	0.24		0.76	0.14
Ba	823.72	292.47		419.97	235.41		521.96	310.40
La	107.12	30.28		39.25	34.18		52.82	40.17
Ce	172.76	57.29		69.04	66.17		91.92	80.89
Pr	19.17	7.03		8.42	8.55		9.89	9.97
Nd	69.48	31.18		30.22	39.83		38.66	47.99
Sm	11.35	6.16		4.90	8.38		6.02	9.20
Eu	3.68	1.89		2.68	2.91		2.82	3.88
Gd	8.03	4.96		4.38	6.86		5.51	6.88
Tb	1.16	0.61		0.52	0.86		0.84	1.25
Dy	6.60	3.56		3.66	5.21		5.23	6.69
Ho	1.14	0.80		0.71	0.76		1.08	1.37
Er	3.06	2.09		2.10	2.86		1.80	2.26
Tm	0.54	0.16		0.23	0.40		0.39	0.42
Yb	2.85	2.21		1.36	2.56		2.68	3.58
Lu	0.39	0.19		0.26	0.35		0.30	0.27
Hf	8.24	5.09		2.48	3.98		5.66	5.17
Ta	7.09	2.06		2.63	2.36		3.32	2.45
Pb	5.44	8.24		1.32	1.83		6.01	2.87
Th	14.16	3.03		3.51	2.96		5.26	3.38
U	3.21	0.94		0.90	0.78		1.46	1.22
Al	35.27	32.90	32.02	32.14	33.32	32.11	32.18	32.63
CCPI	63.46	80.48	78.20	71.20	80.66	77.30	67.88	79.23

Full dataset of major and trace elemental compositions of glass shards from the AND-2A core, continued

Sample Model Age (Ma)	742.00-G 18.29	742.00-F 18.29	742.00-H 18.29	742.00-J 18.29	742.00-M 18.29	742.00-N 18.29	742.00-N2 18.29	742.00-O 18.29
SiO <sub>2</sub>	40.41	44.22	45.41	44.14	44.84	44.86	44.86	45.11
TiO <sub>2</sub>	4.34	4.36	3.17	3.58	2.78	3.53	3.53	2.73
Al <sub>2</sub> O <sub>3</sub>	12.44	13.92	16.31	15.63	16.11	16.10	16.10	16.09
FeO	11.95	11.62	10.00	10.62	8.52	9.71	9.71	9.24
MnO	0.24	0.24	0.20	0.20	0.16	0.24	0.24	0.20
MgO	4.83	4.86	3.45	4.98	5.78	4.69	4.69	5.74
CaO	8.90	9.21	7.62	9.91	11.54	9.73	9.73	11.07
Na <sub>2</sub> O	2.81	3.81	5.05	3.94	3.82	4.62	4.62	3.99
K <sub>2</sub> O	1.52	1.64	2.83	1.92	1.66	2.14	2.14	1.63
P <sub>2</sub> O <sub>5</sub>	1.98	1.32	1.46	0.81	0.75	0.92	0.92	0.74
SO <sub>2</sub>	0.15	0.12	0.07	0.15	0.05	0.06	0.06	0.02
Cl	0.20	0.05	0.16	0.10	0.09	0.11	0.11	0.14
SrO	-0.12	-0.11	-0.13	-0.13	-0.14	-0.12	-0.12	-0.15
BaO	0.12	0.42	0.08	0.11	0.03	0.16	0.16	0.10
Total	89.75	95.68	95.69	95.94	95.99	96.74	96.74	96.65
Mg-no.	41.88	42.72	38.09	45.52	54.72	46.29	46.29	52.58
ne	0.00	2.38	12.24	9.37	10.86	13.17	13.17	10.94
di	13.16	17.92	12.38	20.59	25.25	20.94	20.94	23.81
ol	0.00	4.03	4.08	3.98	3.39	2.17	2.17	4.85
Q	0.36	0.00	0.00	0.00	0.00	0.00	0.00	0.00
hy	9.41	0.00	0.00	0.00	0.00	0.00	0.00	0.00
Li	3.27		6.39	4.83	4.25	5.15	5.15	8.00
Be	<2.42		<0.00	<0.00	2.19	<4.14	<4.14	6.88
B	3.84		4.87	12.79	<3.41	13.49	13.49	19.78
Sc	24.39		23.29	29.06	23.43	27.84	27.84	26.96
Ti	23399.73		18085.72	13339.28	16839.26	19575.20	19575.20	13407.35
V	283.98		246.39	227.49	236.47	276.18	276.18	234.18
Cr	26.87		79.48	74.59	90.26	84.17	84.17	116.06
Co	28.23		28.42	28.28	26.02	29.21	29.21	31.66
Ni	20.78		26.85	38.81	26.94	29.09	29.09	34.71
Zn	101.04		87.14	70.90	67.73	91.43	91.43	83.22
Rb	23.97		36.38	42.42	49.30	50.40	50.40	47.02
Sr	694.41		653.84	678.59	643.98	754.20	754.20	542.44
Y	28.33		26.25	23.35	25.85	34.66	34.66	23.16
Zr	229.25		257.83	202.43	247.06	294.45	294.45	201.83
Nb	44.48		67.14	56.02	71.10	84.11	84.11	57.82
Cs	0.20		0.35	0.79	0.63	0.55	0.55	0.65
Ba	2618.80		420.46	412.45	469.26	498.35	498.35	409.69
La	48.04		51.79	41.65	51.01	64.84	64.84	43.36
Ce	94.60		95.07	78.13	95.93	120.77	120.77	79.20
Pr	11.67		10.95	8.69	10.61	13.80	13.80	8.42
Nd	53.81		42.73	34.10	42.96	53.51	53.51	33.39
Sm	10.78		8.15	6.41	7.44	10.24	10.24	6.97
Eu	5.47		2.92	2.52	2.46	3.20	3.20	2.21
Gd	7.77		6.86	5.49	4.96	8.06	8.06	6.46
Tb	1.40		0.95	0.99	0.96	1.06	1.06	0.81
Dy	5.90		5.77	4.56	5.56	6.66	6.66	4.83
Ho	1.09		0.92	0.88	0.89	1.23	1.23	0.93
Er	2.76		2.37	1.86	2.90	3.95	3.95	2.44
Tm	0.40		0.38	0.22	0.40	0.47	0.47	0.36
Yb	1.76		3.03	2.46	2.09	4.56	4.56	1.89
Lu	0.49		0.40	0.27	0.36	0.59	0.59	0.36
Hf	4.59		5.91	4.68	5.30	7.42	7.42	4.40
Ta	3.15		3.43	2.97	3.86	3.92	3.92	2.96
Pb	2.10		2.06	11.11	4.40	5.89	5.89	29.63
Th	3.96		5.43	4.77	5.36	9.93	9.93	5.64
U	1.03		1.23	1.38	1.60	2.29	2.29	1.41
Al	35.16	33.29	33.14	33.23	32.61	32.24	32.24	32.87
CCPI	79.49	75.14	63.04	72.70	72.29	68.06	68.06	72.73

Full dataset of major and trace elemental compositions of glass shards from the AND-2A core, continued

Sample Model Age (Ma)	742.00-S 18.29	742.00-T 18.29	742.00-D1 18.29	742.00-F1 18.29	742.00-H1 18.29	763.52-A 18.41	763.52-J 18.41	763.52-Y 18.41
SiO <sub>2</sub>	<b>59.68</b>	44.89	43.40	45.85	43.39	45.03	<b>61.04</b>	<b>40.70</b>
TiO <sub>2</sub>	<b>0.88</b>	3.15	3.95	3.72	3.67	3.29	<b>0.71</b>	<b>3.10</b>
Al <sub>2</sub> O <sub>3</sub>	<b>12.04</b>	16.22	16.83	14.86	15.68	16.47	<b>10.43</b>	<b>10.61</b>
FeO	<b>8.37</b>	10.39	9.19	11.38	10.84	9.12	<b>8.17</b>	<b>16.13</b>
MnO	<b>0.37</b>	0.19	0.16	0.24	0.24	0.15	<b>0.38</b>	<b>0.32</b>
MgO	<b>0.22</b>	5.25	5.44	4.26	5.18	6.50	<b>0.13</b>	<b>15.33</b>
CaO	<b>1.13</b>	10.57	11.38	8.13	10.61	12.16	<b>0.72</b>	<b>6.90</b>
Na <sub>2</sub> O	<b>1.28</b>	4.06	4.50	4.06	4.28	3.86	<b>0.90</b>	<b>2.93</b>
K <sub>2</sub> O	<b>1.94</b>	1.65	2.23	2.04	1.76	1.40	<b>1.49</b>	<b>1.44</b>
P <sub>2</sub> O <sub>5</sub>	<b>0.06</b>	0.71	1.05	1.53	0.94	0.67	<b>0.08</b>	<b>0.97</b>
SO <sub>2</sub>	<b>0.06</b>	0.07	0.03	0.11	0.06	0.03	<b>0.04</b>	<b>0.07</b>
Cl	<b>0.17</b>	0.10	0.14	0.09	0.13	0.07	<b>0.23</b>	<b>0.07</b>
SrO	<b>-0.07</b>	-0.06	-0.10	-0.05	-0.13	-0.05	<b>-0.10</b>	<b>-0.16</b>
BaO	<b>0.05</b>	0.07	0.18	0.33	0.13	0.05	<b>-0.04</b>	<b>0.05</b>
Total	<b>86.17</b>	97.25	98.38	96.53	96.77	98.76	<b>84.18</b>	<b>98.43</b>
Mg-no.	<b>4.50</b>	47.39	51.36	40.05	45.99	55.96	<b>2.72</b>	<b>62.90</b>
ne	<b>0.00</b>	10.47	18.94	1.19	13.62	11.62	<b>0.00</b>	<b>9.28</b>
di	<b>0.00</b>	21.93	24.63	11.76	23.30	26.20	<b>0.00</b>	<b>13.10</b>
ol	<b>0.00</b>	4.72	2.16	6.39	3.30	3.73	<b>0.00</b>	<b>35.54</b>
Q	<b>43.31</b>	0.00	0.00	0.00	0.00	0.00	<b>51.89</b>	<b>0.00</b>
hy	<b>9.72</b>	0.00	0.00	0.00	0.00	0.00	<b>10.08</b>	<b>0.00</b>
Li	8.57	6.50		4.30				
Be	8.23	<3.03		<3.18				
B	2.40	15.32		5.83				
Sc	26.86	25.91		25.88				
Ti	17230.16	16735.36		18067.40				
V	265.24	227.96		274.46				
Cr	63.45	52.90		70.42				
Co	32.35	31.26		32.82				
Ni	27.76	47.29		26.27				
Zn	86.58	60.70		84.05				
Rb	34.32	52.45		36.42				
Sr	686.71	806.59		753.26				
Y	28.64	27.43		30.29				
Zr	237.95	258.11		211.74				
Nb	61.93	66.35		65.87				
Cs	0.42	0.49		0.41				
Ba	393.83	512.03		531.92				
La	46.38	54.24		50.46				
Ce	84.37	96.49		95.59				
Pr	9.83	10.80		10.92				
Nd	41.87	49.01		47.30				
Sm	9.52	7.65		9.11				
Eu	2.83	3.08		2.87				
Gd	5.91	8.04		8.28				
Tb	0.98	1.11		0.83				
Dy	4.84	5.60		5.92				
Ho	0.87	0.91		1.24				
Er	2.84	2.48		2.14				
Tm	0.31	0.33		0.37				
Yb	1.84	3.07		2.22				
Lu	0.27	0.27		0.39				
Hf	4.06	5.63		6.01				
Ta	3.59	3.78		3.77				
Pb	3.23	15.73		2.18				
Th	5.27	5.96		4.91				
U	1.51	1.41		1.38				
Al	<b>47.27</b>	32.04	32.59	34.09	31.78	33.03	50.11	63.05
CCPI	72.74	73.26	68.51	71.96	72.61	74.79	77.63	87.81

Full dataset of major and trace elemental compositions of glass shards from the AND-2A core, continued

Sample Model Age (Ma)	763.52-R 18.41	763.52-S 18.41	763.52-Q 18.41	763.52-U 18.41	763.52-V 18.41	763.52-X 18.41	763.52-B1 18.41	763.52-C1 18.41
SiO <sub>2</sub>	46.52	<b>60.05</b>	45.03	45.43	42.76	43.26	46.81	<b>45.64</b>
TiO <sub>2</sub>	3.25	<b>0.80</b>	2.96	3.46	3.73	3.96	2.68	<b>2.66</b>
Al <sub>2</sub> O <sub>3</sub>	16.05	<b>12.52</b>	16.83	16.41	16.13	15.38	17.49	<b>18.12</b>
FeO	10.46	<b>7.09</b>	9.00	10.25	10.71	11.51	8.71	<b>8.20</b>
MnO	0.30	<b>0.30</b>	0.16	0.22	0.23	0.23	0.19	<b>0.21</b>
MgO	3.57	<b>0.29</b>	5.22	4.65	5.33	5.13	4.74	<b>2.83</b>
CaO	7.70	<b>1.03</b>	10.55	8.83	11.21	10.82	9.44	<b>6.36</b>
Na <sub>2</sub> O	4.62	<b>1.04</b>	4.43	4.50	4.48	4.16	4.53	<b>2.15</b>
K <sub>2</sub> O	2.71	<b>1.65</b>	1.79	2.19	2.06	1.94	2.43	<b>3.41</b>
P <sub>2</sub> O <sub>5</sub>	1.02	<b>0.11</b>	0.82	1.10	0.88	0.87	0.70	<b>1.13</b>
SO <sub>2</sub>	0.05	<b>0.04</b>	0.04	0.05	0.06	0.09	0.04	<b>0.03</b>
Cl	0.12	<b>0.08</b>	0.09	0.11	0.11	0.10	0.12	<b>0.18</b>
SrO	-0.10	<b>-0.08</b>	-0.12	-0.11	-0.10	-0.08	-0.11	<b>-0.13</b>
BaO	0.09	<b>-0.01</b>	0.13	0.15	0.14	0.10	0.09	<b>0.14</b>
Total	96.35	<b>84.91</b>	96.93	97.23	97.71	97.47	97.86	<b>90.94</b>
Mg-no.	37.85	<b>6.68</b>	50.85	44.71	46.99	44.28	49.27	<b>38.08</b>
ne	8.37	<b>0.00</b>	13.04	9.53	19.03	14.28	12.08	<b>0.00</b>
di	13.71	<b>0.00</b>	21.53	15.21	26.14	25.14	17.85	<b>0.00</b>
ol	4.28	<b>0.00</b>	3.57	5.01	2.11	2.50	4.26	<b>0.00</b>
Q	0.00	<b>48.56</b>	0.00	0.00	0.00	0.00	0.00	<b>5.25</b>
hy	0.00	<b>7.80</b>	0.00	0.00	0.00	0.00	0.00	<b>9.46</b>
Li	9.11		7.52	14.89	2.35	5.05	8.47	
Be	<0.00		4.25	<2.87	<0.00	<2.32	5.79	
B	43.89		41.84	16.46	12.51	4.87	38.28	
Sc	18.00		21.10	18.41	17.59	30.45	22.17	
Ti	16423.55		12291.56	13233.25	12570.08	20020.63	13869.31	
V	182.68		182.62	182.19	193.02	304.27	209.69	
Cr	10.20		128.14	182.08	17.05	75.03	54.30	
Co	22.03		23.78	23.59	22.11	33.45	25.75	
Ni	11.16		31.59	19.15	21.95	43.46	32.65	
Zn	85.50		60.12	66.99	51.06	81.12	57.62	
Rb	56.23		55.84	62.17	31.54	37.06	56.01	
Sr	588.95		648.93	522.72	944.07	664.63	616.82	
Y	30.95		21.70	27.68	18.64	33.17	29.24	
Zr	362.60		224.16	335.96	133.35	245.69	314.07	
Nb	95.55		63.12	64.06	50.62	65.18	71.88	
Cs	0.61		0.62	1.08	0.40	0.41	0.74	
Ba	639.84		515.68	434.31	449.36	509.25	510.38	
La	73.14		46.24	54.30	35.55	53.55	60.24	
Ce	127.54		78.39	93.06	64.54	96.24	100.90	
Pr	14.77		9.04	10.77	7.94	11.11	11.24	
Nd	59.48		37.45	47.24	30.55	45.02	43.17	
Sm	8.87		6.35	8.58	4.49	10.02	7.66	
Eu	2.44		2.47	2.31	2.34	3.70	2.50	
Gd	6.86		4.67	6.40	4.88	7.01	6.52	
Tb	1.21		0.68	0.89	0.65	1.01	0.92	
Dy	5.58		4.29	5.01	2.88	6.40	6.45	
Ho	1.29		0.72	1.16	0.77	1.36	1.04	
Er	3.20		1.67	3.22	2.19	2.77	3.04	
Tm	0.31		0.33	0.47	<b>0.13</b>	0.52	0.42	
Yb	2.34		2.04	2.68	2.82	4.07	1.81	
Lu	0.64		0.35	0.32	<b>0.28</b>	0.61	0.43	
Hf	7.94		4.62	6.43	4.58	5.37	7.71	
Ta	5.10		3.22	3.87	2.71	4.08	4.06	
Pb	3.54		7.97	6.97	1.68	2.07	9.04	
Th	7.41		5.77	7.24	4.15	5.21	8.43	
U	2.14		1.56	1.85	1.15	1.71	2.09	
Al	33.78	48.35	31.88	33.90	32.02	32.08	33.92	42.31
CCPI	65.71	73.31	69.55	69.03	71.06	73.18	65.91	66.48

Full dataset of major and trace elemental compositions of glass shards from the AND-2A core, continued

Sample Model Age (Ma)	763.52-D1 18.41	763.52-D1-2 18.41	763.52-E1 18.41	763.52-F1 18.41	763.52-F1-2 18.41	763.52-G1 18.41	764.44-A 18.41	764.44-A2 18.41
SiO <sub>2</sub>	46.06	46.06	44.03	45.09	45.09	44.80	43.54	43.54
TiO <sub>2</sub>	3.01	3.01	3.48	3.35	3.35	3.26	3.89	3.89
Al <sub>2</sub> O <sub>3</sub>	16.60	16.60	16.17	15.81	15.81	16.75	15.91	15.91
FeO	9.60	9.60	9.72	10.70	10.70	9.19	10.59	10.59
MnO	0.17	0.17	0.15	0.24	0.24	0.18	0.20	0.20
MgO	5.56	5.56	5.55	4.51	4.51	4.90	4.46	4.46
CaO	10.30	10.30	11.70	9.71	9.71	9.96	9.57	9.57
Na <sub>2</sub> O	4.15	4.15	4.07	4.45	4.45	4.91	4.80	4.80
K <sub>2</sub> O	1.82	1.82	1.84	2.25	2.25	2.18	2.32	2.32
P <sub>2</sub> O <sub>5</sub>	0.87	0.87	0.71	0.91	0.91	1.12	1.20	1.20
SO <sub>2</sub>	0.07	0.07	0.10	0.06	0.06	0.05	0.09	0.09
Cl	0.10	0.10	0.11	0.11	0.11	0.13	0.13	0.13
SrO	-0.10	-0.10	-0.10	-0.13	-0.13	-0.09	-0.11	-0.11
BaO	0.16	0.16	0.07	0.19	0.19	0.15	0.09	0.09
Total	98.37	98.37	97.58	97.22	97.22	97.49	96.67	96.67
Mg-no.	50.80	50.80	50.44	42.90	42.90	48.73	42.87	42.87
ne	9.33	9.33	14.72	12.58	12.58	15.91	15.83	15.83
di	19.55	19.55	27.01	21.21	21.21	20.25	20.35	20.35
ol	5.50	5.50	1.63	3.32	3.32	2.77	1.94	1.94
Q	0.00	0.00	0.00	0.00	0.00	0.00	0.00	0.00
hy	0.00	0.00	0.00	0.00	0.00	0.00	0.00	0.00
Li	0.60	3.01	6.58	8.98	8.78	12.03	1.82	8.68
Be	4.03	<0.00	<0.00	<3.74	8.09	8.43	4.56	<0.00
B	7.35	7.93	<5.99	7.43	22.70	10.36	8.66	3.58
Sc	27.86	21.55	28.42	26.26	24.07	18.23	26.81	25.78
Ti	15621.34	16574.03	14259.20	17534.62	17241.76	13644.61	21367.12	18802.10
V	223.11	234.69	240.60	258.83	254.78	184.31	271.13	249.86
Cr	95.76	86.92	61.22	53.45	49.84	35.62	21.51	24.65
Co	28.67	30.02	28.09	28.11	29.83	25.79	25.59	25.95
Ni	31.53	33.07	28.24	15.65	17.59	23.68	22.36	18.24
Zn	81.52	82.82	53.64	89.74	92.75	44.74	96.17	74.73
Rb	38.61	39.77	46.29	44.74	46.64	59.25	58.62	56.43
Sr	659.41	740.61	561.60	612.78	626.75	644.05	760.47	645.39
Y	26.28	27.81	24.31	31.82	30.77	24.24	36.74	33.22
Zr	254.82	273.05	223.71	293.39	287.81	267.70	321.61	291.28
Nb	74.99	76.45	47.51	84.27	80.23	71.02	97.61	81.16
Cs	0.40	0.37	0.65	0.45	0.49	0.62	0.81	0.67
Ba	467.04	496.26	441.21	562.41	524.82	569.82	609.99	582.38
La	53.29	56.78	39.06	61.03	59.68	51.64	70.64	63.24
Ce	96.44	102.91	65.20	108.52	104.49	91.09	127.92	109.50
Pr	11.15	10.74	7.77	12.73	11.71	10.10	14.72	11.97
Nd	45.62	47.66	32.89	51.08	50.37	39.47	57.16	49.59
Sm	8.80	8.90	5.86	10.35	9.67	7.00	12.15	10.15
Eu	2.45	3.38	2.06	3.07	3.08	2.47	3.92	3.29
Gd	6.53	7.24	6.53	9.53	7.99	5.61	9.67	8.74
Tb	0.91	1.08	0.93	1.25	1.17	0.75	1.34	1.10
Dy	5.81	6.29	5.07	5.96	6.04	5.30	7.98	7.02
Ho	1.24	1.33	1.00	1.04	1.15	1.09	1.40	1.53
Er	2.47	2.12	2.66	3.16	2.47	2.21	3.51	3.08
Tm	0.49	0.25	0.32	0.44	0.46	0.35	0.35	0.44
Yb	2.96	1.88	1.77	3.70	3.30	2.50	3.43	2.69
Lu	0.43	0.42	0.32	0.36	0.35	0.26	0.39	0.45
Hf	5.83	6.55	5.17	5.79	7.45	6.20	8.16	6.08
Ta	3.77	3.84	2.76	4.92	4.83	3.72	4.93	4.65
Pb	2.21	2.34	5.64	2.70	3.12	6.36	4.79	4.03
Th	5.86	5.88	4.33	7.27	6.99	6.08	7.37	6.05
U	1.78	1.80	1.08	1.85	1.60	1.61	2.54	1.70
Al	33.79	33.79	31.91	32.29	32.29	32.26	32.05	32.05
CCPI	71.74	71.74	72.07	69.43	69.43	66.53	67.89	67.89

Full dataset of major and trace elemental compositions of glass shards from the AND-2A core, continued

Sample Model Age (Ma)	764.44-B 18.41	764.44-E 18.41	764.44-Z 18.41	764.44-G 18.41	764.44-H 18.41	764.44-I 18.41	764.44-P 18.41	764.44-N 18.41
SiO <sub>2</sub>	<b>45.28</b>	43.54	43.15	43.93	44.49	45.66	44.33	43.58
TiO <sub>2</sub>	<b>3.08</b>	3.85	4.64	3.53	4.03	3.32	3.81	3.97
Al <sub>2</sub> O <sub>3</sub>	<b>16.02</b>	15.33	13.01	15.62	15.88	15.91	16.21	15.53
FeO	<b>9.41</b>	10.85	13.15	11.52	10.72	11.12	10.83	11.20
MnO	<b>0.23</b>	0.21	0.29	0.27	0.19	0.27	0.19	0.22
MgO	<b>3.33</b>	4.81	4.88	4.46	4.24	3.80	4.35	4.75
CaO	<b>7.41</b>	9.96	9.51	9.63	8.93	8.15	8.64	9.91
Na <sub>2</sub> O	<b>2.18</b>	4.51	4.24	4.68	4.95	5.11	4.89	4.61
K <sub>2</sub> O	<b>2.92</b>	2.11	1.66	2.24	2.48	2.72	2.30	2.01
P <sub>2</sub> O <sub>5</sub>	<b>1.33</b>	0.91	2.20	1.06	1.14	1.24	1.10	1.01
SO <sub>2</sub>	<b>0.06</b>	0.10	0.13	0.06	0.08	0.06	0.06	0.10
Cl	<b>0.14</b>	0.10	0.07	0.12	0.10	0.16	0.12	0.11
SrO	<b>-0.12</b>	-0.09	-0.03	-0.10	-0.14	-0.11	-0.12	-0.10
BaO	<b>0.14</b>	0.13	0.04	0.15	0.19	0.01	0.07	0.05
Total	<b>91.41</b>	96.32	96.94	97.15	97.28	97.41	96.78	96.96
Mg-no.	<b>38.70</b>	44.15	39.83	40.85	41.38	37.85	41.74	43.07
ne	<b>0.00</b>	14.85	5.52	15.47	14.79	14.15	13.72	14.54
di	<b>2.49</b>	23.45	17.83	21.33	18.94	16.35	16.65	22.16
ol	<b>0.00</b>	2.04	5.12	3.72	1.94	4.19	3.57	2.43
Q	<b>4.50</b>	0.00	0.00	0.00	0.00	0.00	0.00	0.00
hy	<b>10.24</b>	0.00	0.00	0.00	0.00	0.00	0.00	0.00
Li	3.82		8.50	5.78	5.36		8.17	
Be	<2.84		<0.00	3.36	<0.00		15.31	
B	<3.49		20.25	8.56	9.04		14.95	
Sc	26.64		16.94	19.66	10.87		28.48	
Ti	20144.23		13764.41	16501.37	9832.47		20078.52	
V	286.52		186.97	217.16	106.99		266.63	
Cr	44.56		22.58	12.29	17.22		31.47	
Co	30.41		26.67	23.59	15.31		28.68	
Ni	35.17		14.56	17.54	5.85		33.50	
Zn	81.48		60.35	74.78	40.54		82.34	
Rb	36.55		48.58	51.70	52.31		39.22	
Sr	735.87		496.15	553.92	399.12		647.34	
Y	29.12		25.06	27.82	19.93		34.82	
Zr	233.74		231.16	266.73	252.26		270.46	
Nb	74.03		64.07	69.45	53.51		70.55	
Cs	0.53		0.45	0.50	0.68		0.51	
Ba	543.95		474.00	579.93	467.10		502.33	
La	54.52		43.98	54.05	44.54		54.77	
Ce	102.66		87.39	96.95	76.25		103.79	
Pr	11.93		9.69	11.07	8.32		12.13	
Nd	52.21		42.57	45.97	33.08		51.19	
Sm	10.81		6.95	8.95	5.70		11.77	
Eu	2.61		2.55	2.65	1.90		2.86	
Gd	6.88		7.10	7.93	4.84		9.68	
Tb	1.37		0.81	0.96	0.73		1.23	
Dy	6.86		5.58	5.33	3.12		7.32	
Ho	1.26		1.09	1.22	0.72		1.44	
Er	3.71		2.76	2.23	1.67		3.04	
Tm	<b>0.36</b>		0.35	0.34	0.27		0.47	
Yb	<b>2.95</b>		2.99	2.97	1.83		<b>2.90</b>	
Lu	<b>0.45</b>		0.35	0.26	0.29		<b>0.39</b>	
Hf	6.34		5.82	6.55	5.15		9.40	
Ta	3.80		3.25	3.60	2.68		3.94	
Pb	1.91		7.26	4.95	5.46		3.27	
Th	5.48		5.69	5.37	5.48		5.69	
U	1.26		1.40	1.49	1.48		1.61	
Al	39.48	32.35	32.23	31.90	32.62	32.93	32.98	31.77
CCPI	71.39	70.29	75.35	69.78	66.84	65.57	67.85	70.70

Full dataset of major and trace elemental compositions of glass shards from the AND-2A core, continued

Sample Model Age (Ma)	764.44-O 18.41	764.44-Q 18.41	764.44-R 18.41	764.44-W 18.41	764.44-X 18.41	764.44-Y 18.41	764.44-Z 18.41
SiO <sub>2</sub>	44.17	43.22	43.31	45.18	42.21	44.87	42.98
TiO <sub>2</sub>	4.05	4.10	4.09	3.28	4.31	3.45	3.48
Al <sub>2</sub> O <sub>3</sub>	15.32	15.24	16.03	15.36	15.69	15.76	16.11
FeO	11.41	10.88	10.77	10.53	10.52	8.96	9.85
MnO	0.25	0.18	0.18	0.20	0.23	0.24	0.12
MgO	3.95	4.87	4.33	5.06	4.70	5.54	5.82
CaO	9.01	10.53	9.44	9.72	10.20	11.39	11.73
Na <sub>2</sub> O	5.14	4.35	5.14	4.33	4.80	3.78	3.89
K <sub>2</sub> O	2.58	2.02	2.50	1.90	2.17	1.75	1.68
P <sub>2</sub> O <sub>5</sub>	1.30	1.01	1.28	0.98	1.35	0.77	0.68
SO <sub>2</sub>	0.04	0.04	0.07	0.05	0.07	-0.04	-0.03
Cl	0.11	0.10	0.14	0.10	0.14	0.09	0.09
SrO	-0.10	-0.09	-0.10	-0.14	-0.10	-0.13	-0.10
BaO	0.19	0.10	0.17	0.16	0.05	0.07	0.00
Total	97.39	96.54	97.35	96.71	96.32	96.48	96.50
Mg-no.	38.17	44.38	41.74	46.16	44.35	52.44	51.32
ne	16.72	14.36	18.92	10.00	18.19	9.87	14.65
di	20.68	24.55	20.66	20.62	22.31	25.34	26.66
ol	1.32	1.27	1.45	4.72	1.73	2.36	2.62
Q	0.00	0.00	0.00	0.00	0.00	0.00	0.00
hy	0.00	0.00	0.00	0.00	0.00	0.00	0.00
Li	7.79	4.13	12.00				
Be	12.64	<3.17	27.00				
B	25.49	8.27	<3.39				
Sc	20.82	23.92	22.25				
Ti	20564.73	17530.12	20652.95				
V	232.13	254.01	253.29				
Cr	21.82	44.45	16.33				
Co	27.07	27.73	24.49				
Ni	10.96	16.84	14.12				
Zn	122.58	75.20	102.75				
Rb	53.50	39.62	52.81				
Sr	631.50	653.78	719.01				
Y	39.95	28.19	30.97				
Zr	322.25	242.13	258.72				
Nb	105.13	70.08	95.27				
Cs	0.28	0.40	0.62				
Ba	589.80	490.70	629.22				
La	74.87	48.97	68.47				
Ce	127.78	90.45	114.21				
Pr	15.03	11.17	13.81				
Nd	56.97	42.74	52.52				
Sm	11.33	9.08	8.45				
Eu	3.14	2.18	3.40				
Gd	5.42	7.99	6.69				
Tb	1.32	0.86	0.90				
Dy	9.40	4.62	6.36				
Ho	1.47	1.12	1.51				
Er	4.63	3.25	3.19				
Tm	0.32	0.55	0.67				
Yb	2.08	2.65	2.52				
Lu	0.63	0.60	0.41				
Hf	5.35	4.43	9.06				
Ta	5.06	3.66	4.16				
Pb	3.50	4.06	2.62				
Th	9.31	4.84	7.10				
U	2.38	1.42	2.10				
Al	31.57	31.66	31.87	33.14	31.42	32.45	32.44
CCPI	66.57	71.21	66.41	71.46	68.60	72.39	73.79